

## Quantitative magnetic resonance techniques in epilepsy

**Citation for published version (APA):**

Jansen, J. F. A. (2007). *Quantitative magnetic resonance techniques in epilepsy*. [Phd Thesis 1 (Research TU/e / Graduation TU/e), Biomedical Engineering]. Technische Universiteit Eindhoven.  
<https://doi.org/10.6100/IR626203>

**DOI:**

[10.6100/IR626203](https://doi.org/10.6100/IR626203)

**Document status and date:**

Published: 01/01/2007

**Document Version:**

Publisher's PDF, also known as Version of Record (includes final page, issue and volume numbers)

**Please check the document version of this publication:**

- A submitted manuscript is the version of the article upon submission and before peer-review. There can be important differences between the submitted version and the official published version of record. People interested in the research are advised to contact the author for the final version of the publication, or visit the DOI to the publisher's website.
- The final author version and the galley proof are versions of the publication after peer review.
- The final published version features the final layout of the paper including the volume, issue and page numbers.

[Link to publication](#)

**General rights**

Copyright and moral rights for the publications made accessible in the public portal are retained by the authors and/or other copyright owners and it is a condition of accessing publications that users recognise and abide by the legal requirements associated with these rights.

- Users may download and print one copy of any publication from the public portal for the purpose of private study or research.
- You may not further distribute the material or use it for any profit-making activity or commercial gain
- You may freely distribute the URL identifying the publication in the public portal.

If the publication is distributed under the terms of Article 25fa of the Dutch Copyright Act, indicated by the "Taverne" license above, please follow below link for the End User Agreement:

[www.tue.nl/taverne](http://www.tue.nl/taverne)

**Take down policy**

If you believe that this document breaches copyright please contact us at:

[openaccess@tue.nl](mailto:openaccess@tue.nl)

providing details and we will investigate your claim.

**Quantitative Magnetic Resonance  
Techniques in Epilepsy**

Financial support for the publication of this thesis was kindly provided by het Van Leersum Fonds, het Nationaal Epilepsie Fonds, Kempenhaeghe Sector for Research and Development, Kodak, and the CODICE research group.

A catalogue record is available from the Library Eindhoven University of Technology  
ISBN: 978-90-386-0976-8

Copyright © 2007 by JFA Jansen, all rights reserved.

Cover design: Paul Verspaget  
Printed by: Universiteitsdrukkerij Technische Universiteit Eindhoven  
Layout: Ine Kengen

# Quantitative Magnetic Resonance Techniques in Epilepsy

PROEFSCHRIFT

ter verkrijging van de graad van doctor aan de  
Technische Universiteit Eindhoven, op gezag van de  
Rector Magnificus, prof.dr.ir. C.J. van Duijn, voor een  
commissie aangewezen door het College voor  
Promoties in het openbaar te verdedigen  
op donderdag 7 juni 2007 om 16.00 uur

door

Jacobus Franciscus Antonius Jansen

geboren te Oirschot



Dit proefschrift is goedgekeurd door de promotor:

prof.dr. K. Nicolay

Copromotoren:

dr.ir. W.H. Backes

en

dr. M.E. Kooi

*You can know the name of a bird in all the languages of the world, but when you're finished, you'll know absolutely nothing whatever about the bird... So let's look at the bird and see what it's doing – that's what counts. I learned very early the difference between knowing the name of something and knowing something.*

"What is Science?", Richard Phillips Feynman 1966

*We doen ons best, zei hij lang geleden, we bouwen een vliegtuig om het geheim te zien, maar dan kom je erachter dat er geen geheim is, alleen een vliegtuig. En dat is mooi.*

Joe Speedboot, Tommy Wieringa 2005

## Cover Illustration

Vincent van Gogh (1853-1890), *The Starry Night (La Nuit Etoilée)* (1889). Oil on canvas, 29x36 ¼" © 2007. Digital image, Courtesy of the Museum of Modern Art, New York / Scala, Florence. Acquired through the Lillie P. Bliss Bequest 472.19.

Vincent van Gogh suffered from attacks accompanied with visual and auditory hallucinations as well as a mood disorder aggravated by stress. His illness may have been worsened by his chronic use of absinthe, brandy, turpentine, and camphor. In May 1889 van Gogh was confined voluntarily in an asylum for epilepsy and mental disorders in Saint-Rémy-de-Provence (France). He was under the care of doctor Peyron, who thought that Vincent was suffering from some type of epilepsy, likely because that asylum was especially for patients with seizures. Also, the doctor's definition of epilepsy was so extended that he stated that van Gogh's last attack lasted two months. However, today the diagnosis of epilepsy requires spontaneous attacks, rather than reactions to a drug or to withdrawal from a drug. Therefore, van Gogh did probably not have epilepsy (Hughes, 2005).

In mid June 1889, a period with many episodes, van Gogh painted *The Starry Night*. The painting depicts the eastern predawn sky as he saw it from his room at Saint-Rémy-de-Provence at about 4 AM on June 19th, 1889 (Harris, 2002). *The Starry Night* has become a visionary image with its network of pulsating stars above the village surrounded by wheat fields and an olive grove. Venus is depicted near the cyprus tree on the left. The waning moon, with its aureole, is painted on the right. Although the sky is in turmoil, the overall effect of the painting is an invigorating calmness.

Harris, J.C., 2002. *The Starry Night (La Nuit Etoilee)*. *Arch Gen Psychiatry* 59, 978-979.

Hughes, J.R., 2005. A reappraisal of the possible seizures of Vincent van Gogh. *Epilepsy Behav* 6, 504-510.

## Contents

1.	Introduction	9
<b>Part I</b>	<b>Development and Validation of Quantitative MR</b>	19
2.	<sup>1</sup> H-MR spectroscopy of the brain: absolute quantification of metabolites	21
3.	Reproducibility of quantitative cerebral T2 relaxometry, diffusion tensor imaging, and <sup>1</sup> H magnetic resonance spectroscopy at 3.0 Tesla	51
4.	Enhanced signal detection in neuroimaging by means of regional control of the global false discovery rate	73
<b>Part II:</b>	<b>Clinical applications of Quantitative MR in epilepsy</b>	103
5.	Multimodal MR reveals secondarily generalized seizure related abnormalities at 1.5 T	105
6.	Seizure related cognitive deterioration is associated with increased prefrontal fMRI activation	127
7.	Soluble telencephalin is a marker for frontotemporal dysfunction in epilepsy as revealed by fMRI	145
8.	Quantitative MR at 3.0 T of patients with cryptogenic localization related epilepsy: a preliminary investigation of neuronal correlates of cognitive impairment	153
9.	Functional MRI reveals declined prefrontal cortex activation in epilepsy patients on topiramate therapy	172
<b>Part III:</b>	<b>Preclinical application of Quantitative MR in epilepsy</b>	184
10.	Multimodal brain MR in a developmental rat model of early-life febrile seizures	186
11.	General discussion and Conclusions	206
	Summary	213
	Samenvatting	217
	Dankwoord	221
	List of publications	225
	Curriculum vitae	227



# Chapter 1

**Introduction**

## Introduction

### Epilepsy

Epilepsy is one of the most common neurological disorders worldwide. Affecting 1-2% of the population at some point in their lives and requiring considerable medical care, it also is a major economical issue (Sander et al., 1987). Epilepsy, a symptom of abnormal brain function, is a chronic brain disorder characterized by unprovoked recurrent seizures that give rise to episodes of abnormal neuronal activity in the central nervous system. According to the International League Against Epilepsy and the International Bureau for Epilepsy (Fisher et al., 2005), an epileptic seizure is a transient occurrence of signs and symptoms due to excessive or abnormally synchronous neuronal activity in the brain. During a seizure, neurons fire abnormally frequent causing various alterations in behavior and possible control thereof. Brain disorders with an enduring predisposition to generate epileptic seizures and the neurobiological, cognitive, psychological, and social consequences of this condition are called epilepsy. The definition of epilepsy requires the occurrence of at least one unprovoked epileptic seizure (Fisher et al., 2005). Seizures are thought to arise from discharging lesions in the cerebral cortex (Adams et al., 1997). The behavioral expressions of a seizure are determined by the normal functions of the region of the cortex in which neurons fire abnormally and include various stereotyped alterations in consciousness, behavior, emotion, motor function or sensation. The classification of epileptic seizures is based on the proposal by the commission Classification and Terminology of the ILAE (1981; 1985; 1989). In this proposal, seizures are classified according to seizure type and electroencephalography (EEG) characteristics. First epileptic seizures are defined as partial or generalized. During partial seizures the first clinical and EEG changes indicate that activation of neurons starts in one cerebral hemisphere. A partial seizure is sub-classified based of whether or not consciousness is impaired during the seizure. When consciousness is impaired it concerns complex partial seizures, while otherwise one refers to simple partial seizures. Both simple and complex partial seizures can further develop into secondarily generalized seizures. If both cerebral hemispheres are involved in seizure induction, the seizures are called generalized. Epilepsy syndromes can be classified according to the underlying etiology as idiopathic (not associated with lesions) or symptomatic (consequence of a known or suspected disorder of the brain) epilepsy.

## MRI in epilepsy

Magnetic resonance imaging (MRI) enables a detailed view of the fine structure of the living brain, and is important for the identification of the etiology and the localization of seizure origin (Kuzniecky et al., 2004). Common etiologies of epilepsy detected by MRI include cerebrovascular lesions, brain tumors, traumatic scar formation, and abnormal brain development. Structural imaging provides static anatomical information, and has already a significant impact in clinical research and practice. It offers rich in vivo data rapidly and safely, and has a role in establishing diagnosis, deciding on treatment, monitoring treatment effects, and investigating pathological processes. Various types of high resolution T1- and T2-weighted images have become a standard tool in epilepsy diagnostics, as they provide excellent anatomical detail of the brain, strong gray/white matter contrast, and high sensitivity to pathological changes in local water content. Pathological processes are therefore most often

**Table 1.1.** Changes in magnetic resonance derived quantities following seizures

MR modality	Quantity	Acute change	Possible attribution	Chronic Change	Possible attribution
<b>T1-weighted</b>	Local volume	Increase	Edema, cortical dysplasia	Atrophy	Neuronal cell loss
<b>T2-relaxometry</b>	T2 relaxation time	Increase	Cell edema / blood-brain-barrier disruption	Increase	Gliosys or cell loss
<b>Diffusion</b>	ADC	Increase	Cytotoxic cell edema	Increase	Gliosys or cell loss
	ADC	Decrease	Vasogenic cell edema	Increase	Gliosys or cell loss
	FA	Decrease	Cell edema, loss of fibres	Increase ?	Sprouting ?
<b>Proton MRS</b>	NAA	Decrease	Decreased mitochondrial function	Decrease	Neuronal loss
	tCr	Unknown	Changes in cell energy status	Decrease	Cell dysfunction or loss?
	Cho	Increase	Increased membrane turnover	Decrease	Cell dysfunction or loss?
	mI	Decrease	Osmolyte changes	Decrease	Gliosys
	Lactate	Increase	Anaerobic metabolism	Normalization	-
<b>Functional MRI</b>	Neuronal activation	Decrease	Dysfunction	Decrease / Increase	Permanent dysfunction or reorganization

T1, longitudinal relaxation time; T2, transverse relaxation time; ADC, apparent diffusion coefficient; FA, fractional anisotropy; NAA, N-acetyl-aspartate; tCr, total creatine; Cho, choline; and mI, myo-inositol. Adapted from (Briellmann et al., 2005)



described in terms of T1 and T2 signal characteristics. An example of the possibilities of MRI is its ability to identify the hippocampus and its characteristic structure which is paramount for assessing atrophy in hippocampal sclerosis in patients with mesio-temporal lobe epilepsy. Similarly, accurate visualization of the cortex is important for the diagnosis of cortical dysplasia. The radiological detection of pathologies often consists of: (i) visual analysis for localization, (ii) identifying alterations in signal intensity on T1- or T2- weighted images, and (iii) detailed morphological analysis of structure, which can demonstrate changes in size and appearance that correlate with underlying pathological conditions.

### **Quantitative MR**

Structural MRI has been established for over a decade as a superior research and clinical modality for anatomical imaging, by enabling a non-invasive procedure to detect the potential causes of epileptic seizures and to study the macrostructural effects of epilepsy on the human brain. Lately, MRI has been demonstrating the potential of tracing the links between tissue function, microstructure, and metabolism in both normal and diseased brain states. These new quantitative magnetic resonance (MR) techniques are still improving, and provide the opportunity to investigate cerebral damage in various fundamentally different ways. As definitions of quantitative imaging are varied and often broad and will always be arbitrary to a certain extent, we refer to quantitative MR in the sense Paul Tofts described (Tofts, 2003). As opposed to conventional structural MR imaging, in which images are visually interpreted in a qualitative way, for quantitative MR, raw data first require processing with the intention to (eventually) obtain clinically relevant quantities.

Quantitative MR techniques are potentially more sensitive than conventional structural MRI, as (i) these techniques provide the opportunity to investigate tissue in various fundamentally different ways, and (ii) in the essential data processing steps, relevant features can be enhanced by special techniques such as noise suppression and artifact removal. Since quantitative MR often enables expressing contrast in terms of physical quantities, it is more objective and thus less susceptible to differences between MR methods from different vendors of MR systems (e.g. using different pulse sequences). Therefore it can be applied to compare results from longitudinal studies with serial assessments, or from different MR systems and research institutes.

Not the conventional structural MRI techniques, used to determine etiology or to detect the seizure focus, but the following quantitative MR techniques have a prominent role in this thesis, as they enable the detection of abnormalities at the macroscopic water content (T2 relaxometry), micro-

structural (diffusion weighted imaging), metabolic (spectroscopy), and functional (functional MRI) level.

#### *T2 relaxometry*

T2 relaxometry is a quantitative technique, which provides an objective measurement of tissue characteristics, as the transverse relaxation time (T2) is a physical property of the tissue, which mainly reflects the (relatively) free water content. Abnormalities on T2 maps usually reflect altered water content, possibly associated with neuronal or axonal loss, gliosis, demyelination, or oedema (Larsson et al., 1989).

#### *Diffusion Weighted Imaging*

Diffusion Weighted Imaging (DWI) is a relatively new MR technique that allows the measurement of water self diffusivity (Schaefer et al., 2000). Since freedom of motion of water molecules is hindered by interactions with other molecules and cellular barriers, water molecule diffusion abnormalities can reflect changes of tissue organization at the cellular level (e.g. increase of extra-cellular space due to cell death). These micro-structural changes affect the (hindered) motion of water molecules, and consequently alter the water diffusion properties and thus the MR signal. Apart from deriving a measure for the average extent of molecular motion that is affected by cellular organization and integrity (Apparent Diffusion Coefficient, ADC), it is also possible using Diffusion Tensor Imaging (DTI) to measure the preferred direction of molecular motion, which provides information on the degree of alignment of cellular structures within fiber tracts, as well as their structural integrity (fractional anisotropy, FA).

#### *Spectroscopy*

<sup>1</sup>H-MR Spectroscopy (<sup>1</sup>H-MRS) is a technique which enables quantification of in vivo metabolite concentrations of the brain, thus offering a window on cell metabolism (Ross et al., 2001). Three major metabolites that are commonly observed are: N-acetyl-aspartate (NAA), which is indicative of neuronal integrity, choline (Cho), of which increased concentrations can act as a malignancy (i.e. tumor) marker, and creatine (Cr), playing a vital role in energy metabolism (Govindaraju et al., 2000). With chemical shift imaging (CSI) it is possible to measure the distribution of metabolites throughout the brain, by simultaneously recording spectra from multiple adjoining spatial regions (i.e. voxels) (Brown et al., 1982).

### *Functional MRI*

Functional magnetic resonance imaging (fMRI) is the use of MRI to measure the hemodynamic response related to neural activity in the brain (Nair, 2005). It provides the opportunity to accurately localize brain activation and to investigate to which extent neuronal regions activate in response to cognitive tasks, in terms of oxygenation changes of the draining blood. It can show whether the activation pattern is altered due to a certain clinical conditions.

### **Quantitative MR and epilepsy**

As quantitative MR techniques are potentially more sensitive and image other tissue properties than conventional structural MRI, these techniques enable examining certain relatively subtle aspects of epilepsy that go beyond the identification of seizure focus. In this thesis we explored in a clinical setting how the cognitive consequences of epilepsy may be reflected in altered MR tissue characteristics. Furthermore, in a preclinical setting it was investigated whether neurological abnormalities, possibly linked with epileptogenesis and thus with epilepsy, could be detected using quantitative MR.

#### *MR of epilepsy and cognition*

Behavioral or cognitive dysfunction is frequently observed in patients with epilepsy and represents an important challenge in treating these patients (Cole et al., 2002). A number of factors influence the behavioral and cognitive impact of epilepsy, including the etiology of the epilepsy, the epilepsy syndrome in question, seizure-related factors (i.e. semiology) and side-effects of antiepileptic drugs (Kwan et al., 2001; Jokeit et al., 2004). The location of the epileptic focus is also an important determinant of the extent and nature of cognitive deficits, as brain regions mediating certain cognitive functions may be disrupted (Meador, 2002). Characteristics, such as duration and number of seizures that describe the chronicity of epilepsy are most likely related to the worsening of the mental status. However, the exact nature of the brain-behavior relationship, i.e. what neuronal mechanisms and changes thereof underlie the cognitive and behavioral changes, still remains to be elucidated. As studies employing multimodal quantitative MR can provide microstructural, functional and biochemical information on the affected brain tissue, a better understanding of the underlying pathologic mechanisms may be obtained.

#### *MR of epileptogenesis*

Epilepsy generally develops over a defined time period, and therefore should not be seen only as a random succession of seizures but as a continuous process. Current understanding of human epileptic processes enables the

classification of three successive phases (Pitkanen et al., 1998). First, the brain usually functions normally, but either after a specific developmental sequence or in response to some form of injury (e.g. trauma or hypoxia), a new state develops in which the neuronal circuits become hyperexcitable, which leads to spontaneous recurrent seizures. This process is called epileptogenesis. Between the initial insult and the eventual emergence of epilepsy a latent period of varying length usually exists. A dynamic and evolving process takes place during this latent period, which may progressively alter neuronal excitability, establishes critical interconnections, and may require critical structural changes before the first clinical seizure appears (Mcnamara, 1999). Various experimental models of epilepsy have been used to mimic different aspects of the epileptic process and temporal stages of epileptogenesis (Cole et al., 2002). Rats have been the most widely exploited experimental animal for modeling epilepsy and epileptogenesis. Experimental animal models are crucial to develop a better understanding of the pathophysiology of epilepsy and the mechanisms linked to the development of epilepsy. Quantitative MR would very much add to this field of research by enabling noninvasive assessment of epileptogenesis in a serial manner. Longitudinal investigations allow to follow the development of lesions to eventual epileptic foci, and thus to define which brains are at risk to present epileptic seizures. The use of quantitative MR may be essential in such investigations as (i) processes involved in epileptogenesis are likely to be subtle, and therefore hard to detect at an early stage of development with conventional structural MRI, and (ii) monitoring is most objective when brain tissue changes over time rely on comparisons of quantitative parameters.

## **Thesis outline**

This thesis addresses the application of quantitative magnetic resonance techniques to epilepsy related abnormalities of metabolism, microstructures and brain function. The research project was aimed at developing and validating quantitative MR techniques (spectroscopy, diffusion, relaxometry, and functional MRI) with clinical diagnostic value. The main focus was on data acquisition and processing, and the application of this multi-modal MR approach in both preclinical and clinical epilepsy settings. The clinical research was mainly aimed at obtaining a better understanding of particularly the cognitive adverse events of epilepsy (either due to medication or due to seizures), by finding possible neuronal correlates. In the preclinical investigations, the emphasis was on the detection of neurological abnormalities, visible on quantitative MR, possibly linked with epileptogenesis and thus with epilepsy. For these purposes, a number of studies were designed and performed. This thesis presents the description of the methods applied and the main results that were obtained.

*The thesis is divided in three parts:*

*Part I: Development and validation*

Part I concerns the development and validation of diagnostic quantitative MR techniques particularly useful in clinical epilepsy research.

Chapter 2 describes a thorough review on absolute quantification of metabolites using spectroscopy, which can substantially improve the diagnostic utility of spectroscopy. Chapter 3 concerns a clinically relevant reproducibility study of several quantitative MR techniques (spectroscopy, diffusion and relaxometry) which was performed on a 3.0 Tesla MR system. A newly developed statistical image analysis method, which offers considerably increased sensitivity for the detection of subtle signal changes in images of several neurological MR applications (diffusion and fMRI) is described in chapter 4.

*Part II: Clinical applications*

Part II concerns the application of the various quantitative MR techniques in a clinical setting with patients with epilepsy.

Quantitative MR (T2 relaxation, diffusion, spectroscopy, and functional MRI) at 1.5 T and neuropsychological assessment was performed in a group of patients with localization related epilepsy and secondarily generalized tonicoclonic seizures to study cognitive deterioration. Chapter 5 relates to the investigation of the effect of these seizures on microstructural and metabolic changes in brain tissue characteristics. In chapter 6 possible functional reorganizations of memory due to secondarily generalized tonicoclonic seizures are described. In chapter 7 it is investigated whether the presence of a certain marker for neuronal damage in blood serum (telencephalin) correlates with abnormal brain activity during a memory task. Chapter 8 discusses preliminary results from a study investigating whether quantitative MR abnormalities detected at 3.0 Tesla appear more profound in epilepsy patients with than without (determined) cognitive decline. In chapter 9 it is investigated whether the antiepileptic drug topiramate, which is known to induce cognitive impairment, also caused changes in activation patterns on functional MRI at 1.5 Tesla during a cognitive language task.

*Part III: Preclinical research*

Part III concerns the application of the various quantitative MR techniques in an experimental epileptogenesis rodent model.

In chapter 10, a quantitative MR study of an experimental epileptogenesis model for febrile convulsions is described. Neonatal rats were subjected to a hyperthermia treatment, which is known to be linked with the later

development of epilepsy. Using quantitative MR it was investigated whether microstructural and metabolic changes in brain tissue could be found.

Chapter 11 concludes with a general discussion, reviewing the results of the various studies that have been described, and putting them into a single comprehensive framework. Main conclusions are drawn and future prospects are discussed.

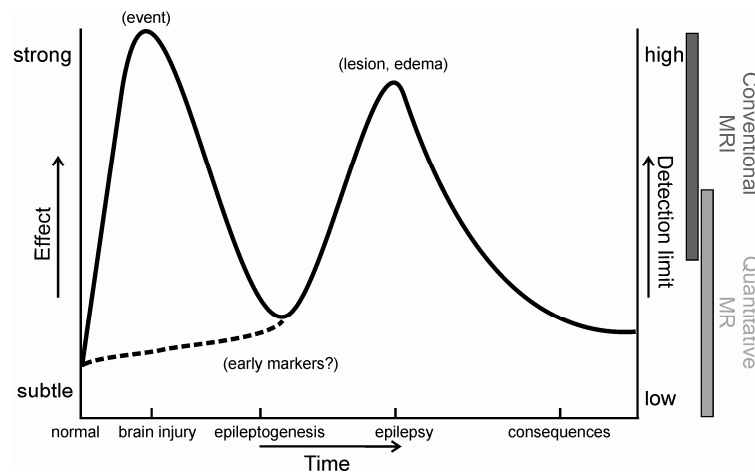


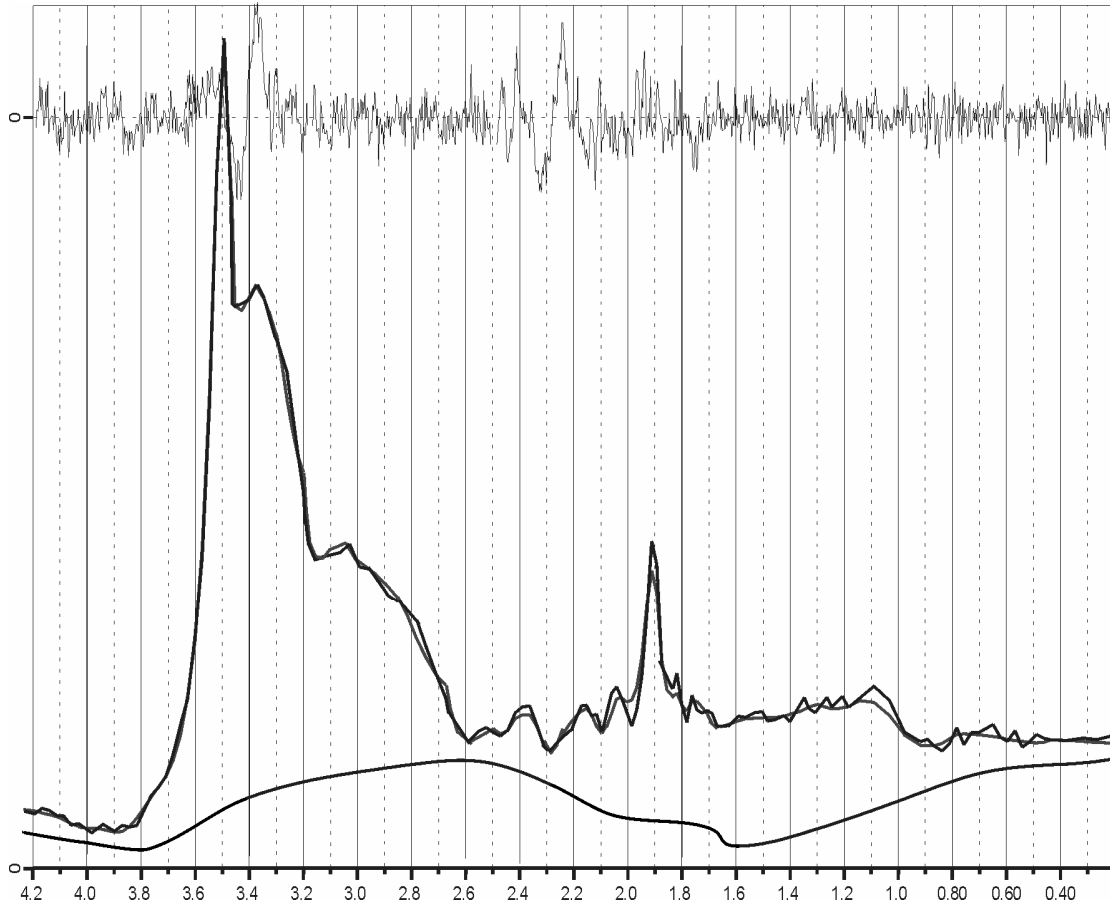
**Figure 1.1.** Scheme presenting the possibilities of quantitative MR relative to conventional MRI for detecting subtle cerebral effects during the development of epilepsy. In response to some form of injury (e.g. trauma or hypoxia) strong effects may be detected by both conventional and quantitative MR techniques. Alternatively, after a specific abnormal developmental period (dotted line, subtle or no MR response) epileptogenesis is initiated. This process takes place during a latent period and usually might be too subtle to be detected with conventional MRI; quantitative MR on the contrary might provide sufficient sensitivity to detect early markers of epileptogenesis. When the first clinical seizures appear, strong MR effects (e.g. seizure induced edema, or epileptogenic lesions) might be detected using both forms of MR. As the epilepsy progresses, quantitative MR might also be able to detect the subtle effects related to the (cognitive) consequences of epilepsy (e.g. due to seizures or medication).

## References

- Adams, R.D., Victor, M., Ropper, A.H. (1997) Principles of neurology, New York, McGraw-Hill, Health Professions Division.
- Brown, T.R., Kincaid, B.M., Ugurbil, K., 1982. NMR chemical shift imaging in three dimensions. Proc Natl Acad Sci U S A 79, 3523-3526.
- Briellmann, R.S., Wellard, R.M., Jackson, G.D., 2005. Seizure-associated abnormalities in epilepsy: evidence from MR imaging. *Epilepsia* 46, 760-766.
- Cole, A.J., Koh, S., Zheng, Y., 2002. Are seizures harmful: what can we learn from animal models? *Prog Brain Res* 135, 13-23.
- Fisher, R.S., van Emde Boas, W., Blume, W., et al., 2005. Epileptic seizures and epilepsy: definitions proposed by the International League Against Epilepsy (ILAE) and the International Bureau for Epilepsy (IBE). *Epilepsia* 46, 470-472.
- Govindaraju, V., Young, K., Maudsley, A.A., 2000. Proton NMR chemical shifts and coupling constants for brain metabolites. *NMR Biomed* 13, 129-153.
- ILAE, 1981. Proposal for revised clinical and electroencephalographic classification of epileptic seizures. From the Commission on Classification and Terminology of the International League Against Epilepsy. *Epilepsia* 22, 489-501.
- ILAE, 1985. Proposal for classification of epilepsies and epileptic syndromes. Commission on Classification and Terminology of the International League Against Epilepsy. *Epilepsia* 26, 268-278.
- ILAE, 1989. Proposal for revised classification of epilepsies and epileptic syndromes. Commission on Classification and Terminology of the International League Against Epilepsy. *Epilepsia* 30, 389-399.
- Jokeit, H., Schacher, M., 2004. Neuropsychological aspects of type of epilepsy and etiological factors in adults. *Epilepsy Behav* 5 Suppl 1, S14-20.
- Kuzniecky, R., Jackson, G.D. (2004) *Magnetic Resonance in Epilepsy: Neuroimaging. Techniques*, Academic Press.
- Kwan, P., Brodie, M.J., 2001. Neuropsychological effects of epilepsy and antiepileptic drugs. *Lancet* 357, 216-222.
- Larsson, H.B., Frederiksen, J., Petersen, J., et al., 1989. Assessment of demyelination, edema, and gliosis by in vivo determination of T1 and T2 in the brain of patients with acute attack of multiple sclerosis. *Magn Reson Med* 11, 337-348.
- McNamara, J.O., 1999. Emerging insights into the genesis of epilepsy. *Nature* 399, A15-22.
- Meador, K.J., 2002. Cognitive outcomes and predictive factors in epilepsy. *Neurology* 58, S21-26.
- Nair, D.G., 2005. About being BOLD. *Brain Res Brain Res Rev* 50, 229-243.
- Pitkanen, A., Halonen, T., 1998. Prevention of epilepsy. *Trends Pharmacol Sci* 19, 253-255.
- Ross, B., Bluml, S., 2001. Magnetic resonance spectroscopy of the human brain. *Anat Rec* 265, 54-84.
- Sander, J.W., Shorvon, S.D., 1987. Incidence and prevalence studies in epilepsy and their methodological problems: a review. *J Neurol Neurosurg Psychiatry* 50, 829-839.
- Schaefer, P.W., Grant, P.E., Gonzalez, R.G., 2000. Diffusion-weighted MR imaging of the brain. *Radiology* 217, 331-345.
- Tofts, P. (2003) *Quantitative MRI of the brain measuring changes caused by disease*, Chichester, West Sussex; Hoboken, N.J., John Wiley & Sons Ltd.

## Part I

### Development and Validation of Quantitative MR







# Chapter 2

**<sup>1</sup>H-MR spectroscopy of the brain: absolute quantification of metabolites**

**Jansen JFA, Backes WH, Nicolay K, and Kooi ME**

*Published in: Radiology 240 (2): 318-332, 2006*

**Abstract**

<sup>1</sup>H Magnetic Resonance Spectroscopy (<sup>1</sup>H-MRS) enables non-invasive in vivo quantification of metabolite concentrations in the brain. Currently, metabolite concentrations are most often presented as ratios, e.g. relative to creatine, rather than as absolute concentrations. Despite of the success of this approach, it has recently been suggested that relative quantification may introduce substantial errors, and can lead to misinterpretation of spectral data and erroneous metabolite values. The present review discusses relevant methods to obtain absolute metabolite concentrations on a clinical MRI system using single voxel spectroscopy or chemical shift imaging. Important methodological aspects in an absolute quantification strategy are addressed, including radiofrequency coil properties, calibration procedures, spectral fitting methods, cerebrospinal fluid content correction, macromolecule suppression, and spectral editing. Techniques to obtain absolute concentrations are now available and can be successfully applied in clinical practice. Although the present review is focused on <sup>1</sup>H-MRS of the brain, a large part of the methodology described can be applied to other tissues as well.

## Introduction

$^1\text{H}$ -MR-Spectroscopy ( $^1\text{H}$ -MRS) enables non-invasive quantification of in vivo metabolite concentrations in the brain. It has proved to be a powerful addition to the clinical assessment tools for numerous pathologies, including epilepsy, multiple sclerosis, stroke, cancer, and metabolic diseases (Ross et al., 2001). In nuclear Magnetic Resonance (MR), the total area under a metabolite resonance in a  $^1\text{H}$ -MR spectrum is directly proportional to the concentration of the metabolite. Currently, metabolite concentrations are usually expressed as ratios (relative quantification), rather than as absolute concentrations. Ratios can be useful in clinical diagnosis to characterize pathological tissue. For example, it has been successfully applied for the diagnosis of cancer (Alger et al., 2000), leukaemia (Chu et al., 2003), epilepsy (Vermathen et al., 2003), dementia (Rai et al., 1999), and multiple sclerosis (Ruiz-Pena et al., 2004). A locally obtained reference data set with normal ratios for healthy tissue can be used for most clinical purposes, while in focal pathologies, a reference spectrum can be acquired from the patient's contralateral brain region. The use of signal ratios has the great advantage that it is very easy to implement, as it does not require extra scan time and time-consuming postprocessing. Furthermore, a number of problems, e.g. due to partial volume effects arising from different amounts of cerebrospinal fluid (CSF) in the selected volumes can be largely avoided. In addition, ratios are in some cases more sensitive in terms of detecting changes (e.g. when one metabolite increases and another decreases) and can be more accurate than absolute concentrations, due to specific characteristics of the analysis computer program applied (Kanowski et al., 2004).

However, if a change is observed in the ratio of metabolite peaks it remains uncertain which metabolite concentration actually changes. This information can only be obtained from absolute concentrations. Absolute quantification (AQ, also referred to as absolute quantitation) implies that concentrations are expressed in biochemical units, such as mmol per kg wet weight. Furthermore, when spectroscopic results are to be compared in an interdisciplinary context (e.g. with biochemically derived concentrations), ratios or arbitrary units might not be appropriate.

Since many factors need to be considered to obtain reliable absolute concentrations with  $^1\text{H}$ -MRS, it is hard for a newcomer to comprehend all aspects and potential pitfalls concerned with AQ and to decide what method to use. The latest reviews on absolute quantification were written several years ago (Tofts et al., 1988; Cady, 1992; Henriksen, 1995; Kreis, 1997), when AQ was more or less considered to be a basic research tool. However, several groups have recently published clinical trials incorporating AQ. These include studies of patients with Alzheimer's disease (Stoppe et al., 2000), epilepsy (Simister

et al., 2002; Mueller et al., 2003; Savic et al., 2004), multiple sclerosis (Hetherington et al., 1996; Fernando et al., 2004), leukoencephalopathy (Auer et al., 2001b), amyotrophic lateral sclerosis (Pohl et al., 2001), and cancer (Auer et al., 2001a). Furthermore, the reviews published so far have mainly focused on single voxel spectroscopy, whereas spectra simultaneously recorded from multiple adjoining spatial regions (chemical shift imaging, CSI) find increasing use in many clinical trials (Hetherington et al., 1996; Mclean et al., 2000; Simister et al., 2002; Mueller et al., 2003). In addition, new developments such as spectral editing, macromolecule suppression, tissue segmentation, and quantitative analysis of spectra with dedicated software can aid in the absolute quantification of brain metabolites. This review will address the implementation of these new developments in absolute quantification strategies.

### **Advantages and disadvantages of absolute metabolite concentrations**

In relative quantification, which yields concentrations expressed as ratios, one of the metabolite peaks measured is used as the concentration standard, and serves as the denominator of the peak ratios. As a result, the total number of quantifiable metabolites is decreased by one. Furthermore, alterations in the peak ratio do not necessarily reflect a change in the concentration of the numerator. The alteration may be caused by changes in the concentration of either the numerator or the denominator or both, or may merely be due to changes in relaxation behavior. The assumption that the concentration of certain reference metabolites (e.g. total creatine, tCr; or choline, Cho) remains constant may be incorrect under normal conditions as well as in many pathological states. It has, for example, been shown in patients with temporal lobe epilepsy (Connelly et al., 1994) that the temporal lobe ipsilateral to the seizure focus displays a significant increase in tCr and Cho and a similar finding has been reported in patients with frontal lobe epilepsy (Lundbom et al., 2001). Furthermore, even the temporal lobe contralateral to the seizure focus exhibits increased tCr and Cho concentrations, albeit not significantly (Connelly et al., 1994). Additionally, if patients have global metabolic defects, comparisons with contralateral brain regions (which are assumed to be metabolically normal) may not be feasible (Mathews et al., 1995; Chang et al., 1997). In addition to causing possibly ambiguous interpretation, clear evidence has recently been provided that relative quantification may introduce larger errors than AQ (Schirmer et al., 2000; Li et al., 2003). Two independent <sup>1</sup>H-MRS studies on healthy volunteers using single voxel spectroscopy (Schirmer et al., 2000) and CSI (Li et al., 2003) have shown that metabolite ratios exhibit higher coefficients of variation (up to 1.6-fold) than absolute quantified concentrations of individual metabolites. Furthermore, a CSI study among patients with temporal lobe epilepsy (Simister et al., 2002) reported that metabolite ratios

were less sensitive to abnormalities than absolute values. It is therefore advisable to obtain concentrations expressed in standard units (such as mmol per kg wet weight) by applying AQ.

However one should realize that AQ requires more time than relative quantification, and one only can benefit from AQ if all additional referencing steps are executed properly, otherwise unwanted additional errors may be introduced.

## **Theoretical background**

### **Characteristics of the radiofrequency coil**

Radiofrequency (RF)-coils are used to transmit the excitative ( $B_1$ ) field, and to detect the resulting signal. In case of clinical brain  $^1\text{H}$ -MRS, the patient's head is positioned within the head coil, which is used as a receive coil, while either the head or the body coil acts as the transmit coil. With a dedicated pulse sequence such as PRESS (Bottomley, 1987) or STEAM (Frahm et al., 1987) a spectrum can be obtained from a single well-defined spatial volume (single voxel spectroscopy) to detect metabolites. Alternatively, multiple spectra can be obtained simultaneously from multiple adjoining spatial regions (CSI; also referred to as magnetic resonance spectroscopic imaging, MRSI) (Brown et al., 1982; Maudsley et al., 1983). The transmit coil should generate RF pulses with sufficient power to penetrate into all tissue regions of interest. The requirements for signal reception are generally similar to those for transmission. The penetration of the RF pulses of the transmit coil and the signal-to-noise ratio (SNR) from the receive coil are strongly dependent on the coil loading, which is determined by the electrical conductivity and the volume of the object near the coil. Variations in the size and tissue composition of the head positioned in the RF-coil affect the amount of RF energy getting into and the amount of signal detected from the volume-of-interest. This is one of the reasons why prior to starting a measurement, the electrical characteristics of the RF-coil are optimized in order to obtain the most efficient performance.

### **Characteristics of MR spectra**

A water-suppressed brain  $^1\text{H}$ -MR spectrum typically displays a number of signals, corresponding to several brain metabolites. These signals are characterized by one or more peaks with a certain resonance frequency, linewidth (full width of the peak at half its maximum height), lineshape (e.g. Lorentzian or Gaussian), phase, and area. The peaks are separated due to differences in resonance frequency, which are caused by the difference in chemical environment of the different nuclei. The molecular structure of a particular metabolite is reflected by a typical peak pattern. The peak areas are

directly proportional to the number of nuclei that contribute to them and to the concentration of the metabolite to which the nuclei belong. However, the peak areas are also influenced by other factors, including T1 and T2 relaxation times.

### **Quantification of $^1\text{H}$ -MR spectra**

Generally, the quantification procedure is divided into two steps. The first step is to determine accurate peak areas for the relevant metabolites. In the second step, peak areas are converted into metabolite concentrations using careful calibration to which the metabolite signals are referenced.

### **Definitions of concentration**

Different quantification strategies lead to different concentration standards. Two definitions of concentration are commonly used: (i) molarity: number of moles of metabolite per liter tissue water (mmol/L) and (ii) molality: number of moles of metabolite per kilogram of tissue water (mmol/kg tissue water). In principle, molal concentrations can be converted into molar concentrations (Kreis et al., 1993) using a conversion that requires knowledge of the specific brain tissue density.

### **Comparison of in vivo $^1\text{H}$ -MRS with other quantification methods**

Most alternative quantification methods can only be performed in vitro, following brain autopsy. These methods include high-pressure liquid chromatography (HPLC) and high field ( $> 7\text{T}$ )  $^1\text{H}$ -MRS. Whereas in vivo  $^1\text{H}$ -MRS can only detect metabolites with a concentration of the order of mM, both HPLC and high field  $^1\text{H}$ -MRS can detect concentrations in the  $\mu\text{M}$  range. However, several metabolites, including NAA and phosphocreatine are generally detected at lower concentrations by in vitro methods (up to 10% reduction) (Huppi et al., 1995; Fatouros et al., 2000), due to their rapid degradation in the brain tissue samples immediately after autopsy (Battistuta et al., 2001; Bottomley et al., 2001). The assessment of metabolites that are not subject to degradation yields similar concentrations in both in vivo and in vitro methods (Burri et al., 1990). Typical metabolite concentrations in parietal white matter obtained with in vivo  $^1\text{H}$ -MRS are  $9.6 \pm 3.0$  for N-acetylaspartate (NAA),  $7.0 \pm 2.0$  for tCr,  $1.8 \pm 0.5$  for Cho, and  $5.2 \pm 3.3$  mmol per kg wet weight for myo-inositol (Ins) (De Graaf et al., 2001).

### **Quantification strategies**

In this section, the most widely used quantification strategies for in vivo  $^1\text{H}$ -MRS are described. The relative merits and drawbacks of each approach are

indicated in Table 2.1. The schematic setup for the brain and calibration measurement for each case is shown in Figure 2.1.

**Table 2.1.** Relative merits and drawbacks of quantification strategies\*

	Extra scan time for patient	Extra scan time after patient scan	Preparation time†	Ease of use	Accuracy
<b>Internal endogenous marker</b>	+	+	+	+	-
<b>External reference</b>	-	+	0	-	0
<b>Replace and match method</b>	+	-	-	-	+
<b>Water signal reference</b>	-	+	+	0	0
<b>Principle of Reciprocity</b>	0	+	-	-	+

\* - indicates a serious drawback of the strategy, 0 indicates a neutral aspect, and + indicates a merit.

† Preparation time includes the preparation of phantoms and validation of the strategy.

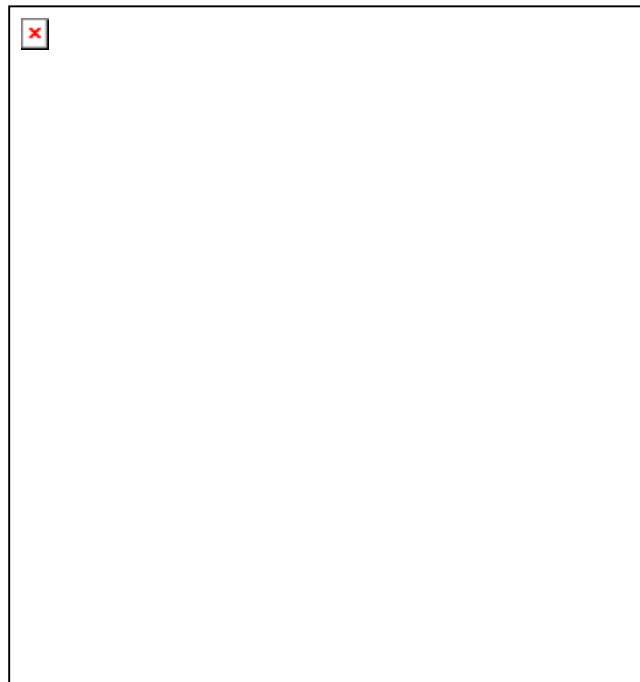


**Figure 2.1.** Schematic view illustrating the experimental setup of the calibration strategies used for the quantification of cerebral metabolite concentrations. The figures on the left show the setup for the brain examination, while the figures on the right refer to the calibration measurement. (a) Internal endogenous marker, water signal reference method, and principle of reciprocity. (b) External reference method. (c) Replace and match method. VOI = spectroscopic volume of interest.



## Relative quantification

### *Internal endogenous marker*

One of the simplest approaches is to use one of the measured peaks, originating from an endogenous metabolite, as a concentration standard (Figure 2.1a). Peak ratios (possibly corrected for factors such as relaxation) are converted into concentrations using a literature value of the reference metabolite, whose concentration is supposed to be invariant. Commonly used reference metabolites are NAA, tCr, and Cho. Although this method allows direct comparison with other biochemical measurements, it is essentially a relative quantification method and shares all previously mentioned possible merits and drawbacks.

## Absolute quantification

### *External reference method*

A vial with known reference solution and relaxation properties is positioned near or inside the RF-coil (Figure 2.1b) (Roth et al., 1989). Immediately after the acquisition of the *in vivo* spectrum, a reference spectrum from the calibration sample is obtained, with the patient's head still inside the coil. The reference scan can also be made simultaneously with the acquisition of patient data (Alger et al., 1993). An option to account for possible  $B_1$  inhomogeneity is to measure (Webb et al., 1992) or to simulate (Li et al., 1995) the  $B_1$  field distribution of the RF-coil used. It is important to realize that the external vial might introduce substantial distortions of the  $B_0$  field homogeneity, which will complicate shimming (adjustment of the homogeneity of the local magnetic field) and water suppression.

### *Replace and match method*

The basic principle of the replace and match strategy is to replace the human subject by a phantom, which simulates (human) tissue as closely as possible, and to match the coil load to equal the load obtained previously *in vivo* (Figure 2.1c) (Buchli et al., 1993; Duc et al., 1998). Then, a calibration measurement is performed, which is identical with respect to all scanner settings, e.g. the pulse sequence and the size and position of the volume-of-interest (VOI). The phantom usually contains a solution that mimics the electrical conductivity of human tissue. Fine adjustment of the coil load can be made by placing the phantom further inside or outside the coil or by inserting a small bottle containing saline. It is important that the load is accurately matched, because it is usually not possible to eliminate the effect of a difference in load using a post-hoc correction factor (Duc et al., 1998). Unfortunately, the matching of the load by maneuvering a phantom is not always straightforward

and can be time-consuming. Furthermore, the  $B_1$  distribution through a phantom is often considerably different from that in the human head. Therefore, simply matching the conductivity and overall load might be insufficient, because the human head has structures of varying resistance that alter electric current paths.

#### *Water signal reference method*

Several research groups have used tissue water as an internal standard (Thulborn et al., 1983; Barker et al., 1993; Christiansen et al., 1993; Ernst et al., 1993; Kreis et al., 1993; Danielsen et al., 1994; Knight-Scott et al., 2003). After the in vivo measurement, from the same voxel the signal from unsuppressed tissue water is recorded, which serves as an endogenous concentration reference (Figure 2.1a). It is best to record the unsuppressed water spectra under identical conditions as the metabolite spectra, which can be achieved by detuning or switching off the water-suppression RF-pulses. The use of pure CSF (recorded from a voxel that only contains CSF) as a water reference to obtain molar concentrations is inadvisable, since it is usually impossible to position a voxel of sufficiently large size in CSF only (e.g. ventricles). Alternatively, the water content can be derived from proton density weighted images (Brooks et al., 1999; Schuff et al., 2001). The obtained metabolite concentrations in molal units (mmol/kg tissue water), can be converted into molar concentration (mmol/kg wet weight) using the density of brain tissue (Kreis et al., 1993). Because the determination of brain density and brain water content can be quite elaborate, one usually applies a literature value. However, one has to be cautious since several pathologies are known to affect the water content. For instance, it has been determined for pathologies such as multiple sclerosis (Helms, 2001; Laule et al., 2004), brain tumors (Grasso et al., 2002), and hydrocephalus (Grasso et al., 2002) that the brain water content can be increased up to 12%, 50%, and 120%, respectively.

#### *Principle of Reciprocity*

From the principle of reciprocity (POR) (Hoult et al., 1976; Grasso et al., 2002) it can be deduced that (if the coil is a combined transmit-receive coil) the external voltage needed to produce a certain  $B_1$  field at a given location is inversely related to the voltage induced in the same RF-coil by a predefined  $B_1$  field. The calibration strategy (also referred to as phantom replacement strategy) that is based on this notion involves the determination of the local  $B_1$  field at the VOI, by measuring the voltage amplitude ( $V_{\max}$ ) required to obtain the maximum signal response (Figure 2.1a). Absolute standard units can then be obtained by dividing the recorded in vivo MR signals through the voltage  $V_{\max}$ , and by performing additional calibration measurements with a

solution of known concentration (Michaelis et al., 1993; Soher et al., 1996; Helms, 2000; Kreis et al., 2001; Kreis et al., 2002). The principle of reciprocity applies only to transmit-receive coils. For MR-systems with a receive-only coil an alternative approach based on the same principle has been designed utilizing the transmit-receive capabilities of the body coil (Jost et al., 2005).

#### *Institutional units*

In this quantification approach, one of the above absolute reference methods is used, but the final calibration to standard units is not performed. Therefore, this method shares the robustness of the applied absolute quantification strategy, but it is only useful for diagnostic comparison within one institution.

### **Important considerations for absolute quantification**

#### *Echo time and repetition time*

When the repetition time TR of a pulse sequence is relatively short (generally shorter than 5 times the longitudinal relaxation time T1), the magnetization cannot totally recover before the following excitation, which leads to a reduction of the signal (i.e. signal saturation). Typical T1 relaxation times for several metabolites, measured at 1.5 T are  $1430 \pm 165$  for NAA,  $1330 \pm 199$  for Cho,  $1460 \pm 270$  for tCr, and  $1140 \pm 308$  ms for Ins (Kreis et al., 1993; Ethofer et al., 2003; Rutgers et al., 2003). Using these values, a repetition time of 2000 ms will lead to a decrease of the NAA signal of approximately 25%, whereas a repetition time of 7000 ms causes a reduction of only 0.7%. As the T1 relaxation times of most metabolites are not the same, the acquired signal intensity of each resonance should be corrected separately for partial saturation. Therefore, the usage of long repetition times is advisable since it reduces systematic errors caused by T1 signal saturation, even though this increases the scan duration. The usage of short echo times (e.g. TE < 20 ms) minimizes signal losses caused by T2 relaxation. Typical T2 relaxation times for several metabolites, recorded at 1.5 T are  $422 \pm 48$  for NAA,  $356 \pm 35$  for Cho,  $214 \pm 23$  for tCr, and  $200 \pm 20$  ms for Ins (Kreis et al., 1993; Brooks et al., 1999; Rutgers et al., 2003). The reduction of the NAA signal will be approximately 21% if an echo time of 100 ms is used, while the signal loss will only be approximately 5% with an echo time of 20 ms (the effect of varying echo times is indicated in Table 2.2). In contrast, macromolecules (compounds with a high effective molecular weight) have very short T2 relaxation times (T2 < 50 ms at 2.1T (Behar et al., 1994)) so that using even the shortest TE leads to large signal reduction. For instance, an echo time of 20 ms will lead to a reduction of the

**Table 2.2.** Reduction of metabolite peak areas as function of echo time\*

Echo time (ms)	N-acetylaspartate (T2 = 420 ms (Kreis et al., 1993))	Macromolecules (T2 = 50 ms (Behar et al., 1994))
20	4.6	33.0
30	6.9	45.1
50	11.2	63.2
130	26.5	92.6
260	46.0	99.4

\*Reduction is given in percentage (%) with respect to a hypothetical echo time of 0 ms.

macromolecule signal of approximately 30%. On the other hand, spectra acquired with long echo times (TE > 150 ms) benefit from a less complicated appearance (mainly resonances from uncoupled spins remain visible, i.e. the singlets from NAA, tCr, and Cho), improved water suppression and a flatter baseline (due to the signal reduction of components with short T2 relaxation times such as water and MM, respectively). In all these cases, signal intensities of each resonance have to be properly corrected for T2 relaxation. However, accurate determination of T1 and T2 relaxation times is usually too time-consuming to be performed for every patient (Kreis et al., 2005). Unfortunately sometimes one cannot resort to using average values of a patient group, since relaxation times may be influenced by pathologies, and by the severity of a specific pathology. For example, for diseases such as stroke (Walker et al., 2004), amyotrophic lateral sclerosis (Hanstock et al., 2002), low-grade and high-grade gliomas (Isobe et al., 2002) the T2 relaxation times of NAA can be reduced up to 42%, 22%, 38%, and 43%, respectively.

#### *Receiver gain instability*

In any quantification strategy, which requires an additional calibration measurement of a phantom, this measurement should be recorded with exactly the same amplifier gain settings as the in vivo measurement to prevent systematic errors. Therefore, a calibration experiment is preferably performed immediately after the in vivo experiment. However, if time restrictions prevent this measurement, one has to monitor the receiver stability on a regular basis, since it is not easily corrected for afterwards. An assessment of receiver gain stability can be performed by measuring the background noise level in a region of the spectrum downfield from the water resonance, where no signals are expected (Soher et al., 1996). The background noise level should exhibit minimal variations if the spectrometer has good long-term stability (Hoult et al., 1976).

### *Compartmentation*

As *in vivo* MR is performed on tissue at a macroscopic level, various brain compartments (grey matter, white matter, blood, CSF or lesions) with different metabolite concentrations might contribute to the metabolite signal measured. It is hard to determine the 'true' concentration level of a metabolite in a specific, homogeneous tissue. For example, metabolite concentrations that are uncorrected for CSF contribution are generally underestimated, since CSF hardly contains  $^1\text{H}$ -MRS detectable metabolites (Lynch et al., 1993). Therefore, several tissue segmentation approaches have been proposed, which all rely on differences in relaxation properties, as determined from a separate MRI measurement. These include methods using calculated T1 or T2 value images (Hetherington et al., 1996) or spectra in which the T2 decay of water is measured as a function of TE (Ernst et al., 1993; Helms, 2003). However, since pathologies may affect relaxation times, one should always carefully interpret results from any segmentation procedure.

### *MR visibility*

Not all metabolite molecules equally contribute to the MR signal from a certain VOI. For example, creatine has an invisible metabolite pool (2.5%) that is bound to macromolecular structures and therefore has a low mobility, which results in very short T2 relaxation times and thus broad resonances, which can be unobservable in conventional MR spectra (Kruiskamp et al., 1999). A larger underestimation (up to 10% for creatine (Kruiskamp et al., 2001) and 30% for lactate (Kotitschke et al., 1994)) of the true concentration can be caused by magnetization transfer effects, if a water suppression technique such as presaturation is used. However, most metabolites are not susceptible to magnetization transfer effects and show a signal change only slightly above the limits of experimental error (Leibfritz et al., 2001). Furthermore, in most measurement methods, magnetization transfer effects can generally be avoided.

## **Data analysis**

In this section, the most important methods of data analysis will be described and the merits and drawbacks of each analysis method are shown in Table 2.3. The actual quantification can be performed either in the time (Vanhamme et al., 2001) or frequency domain (Mierisova et al., 2001). In the time domain, the MR signal is represented as a function of recording time, whereas in the frequency domain the signal is represented as a function of resonance frequency. The time-dependent signal can be converted into its equivalent frequency representation by applying Fourier transformation. Theoretically, there are no differences between the two domains (Abildgaard

et al., 1988) but the data are always presented in the frequency domain, since this enables direct (visual) interpretation.

**Table 2.3.** Relative merits and drawbacks of data analysis procedures\*

	Preparation time	Sensitivity to baseline imperfections	Ease of use	Accuracy
<b>Integration</b>	+	-	+	-
<b>Peak fitting</b>	+	-	+	-
<b>Peak fitting with Prior Knowledge</b>	0	0	0	0
<b>Peak fitting with metabolite basis set</b>	-	+	-	+

\* - indicates a serious drawback of the procedure, 0 indicates a neutral aspect, and + indicates a merit.

### Integration

The traditional procedure to determine the area of a certain peak in the frequency domain is integration. The operator selects a frequency range, which preferably contains only one peak, followed by numerical integration. As only the total area under a resonance corresponds to the real peak intensity, and the contribution beyond the lower and upper integration boundaries is neglected, the peak area will be underestimated (possibly up to 40% (Meyer et al., 1988)). Therefore, integration is an adequate method only if the resonances are well separated without any baseline fluctuations. Unfortunately this is rarely the case, since most in vivo spectra suffer significantly from spectral overlap and baseline fluctuations. Therefore, the area can hardly be attributed to one single resonance, and additionally, the baseline will lead to an unknown contribution.

### Peak fitting

In this approach, all important peaks are initially selected, and a coarse estimation of the resonance frequency, linewidth, and peak intensity is performed, either by the operator or by an algorithm. Subsequently, a fit is performed by a least-squares optimization algorithm, which iteratively fits all peaks to a lineshape model function, so that the fitted spectrum resembles the experimental spectrum as closely as possible (Nelson et al., 1987). In general, this method proves to be fairly robust with respect to spectral overlap. However, if the actual lineshapes deviate significantly from Gaussian or Lorentzian model functions, the algorithm will not be able to fit the peaks accurately. To avoid this problem, other lineshapes have occasionally been used, of which the Voigt profile is the most common (Marshall et al., 1997). However, the use of a Voigt profile introduces more degrees of freedom in the fitting procedure, which can lead to ambiguous results.

## Prior Knowledge

This method allows the incorporation of prior knowledge about the metabolites that contribute to the  $^1\text{H}$ -MRS signal (De Graaf et al., 1990a). All known signal parameters, such as relative frequencies, amplitude ratios, scalar coupling and phases of resonances that are characteristics of a certain metabolite, can be implemented as constraints in the fitting routine. Prior knowledge is the only way of enhancing the accuracy of fitted model parameters for a given dataset, by reducing the number of degrees of freedom. The calculation time is also reduced. An example of a method that enables incorporation of prior knowledge is AMARES (Vanhamme et al., 1997).

### *Metabolite basis set based advanced prior knowledge*

A decade ago, algorithms were proposed (De Graaf et al., 1990a; Provencher, 1993) that implement a strategy where the maximum of prior knowledge is utilized. The methods are based on the assumption that there are only a limited number of  $^1\text{H}$ -MRS-detectable metabolites present in the human brain, which have already been identified and analyzed in earlier studies. The approach aims to individually determine the exact response of all metabolites possibly present to a specific pulse sequence. One has to take into account the type of scanner, static magnet ( $B_0$ ) field, pulse sequence, echo time, and repetition time, as well as the pH, ion composition, and temperature of the solution in which the individual metabolites are dissolved. In this way, the prior knowledge of each metabolite, such as chemical shifts, signal intensity (influenced by relaxation effects), amplitude ratios, splitting patterns, and J evolution is known. The in vivo MR spectra are then analyzed as a linear combination of the separately recorded in vitro spectra of the individual metabolites. There are two commonly used approaches for obtaining a basis set: simulation and in vitro measurement. In the simulation approach (Govindaraju et al., 2000; Ratiney et al., 2004), the response is numerically simulated, based on the molecular and quantum mechanical characteristics of each metabolite (Graveron-Demilly et al., 1993; Young et al., 1998). The in vitro approach (Pfeuffer et al., 1999) requires that for each metabolite a spectrum is acquired with exactly the same conditions (e.g. pulse sequence and timing parameters) as those used during the in vivo measurements. The advantage of the simulation approach is that, as long as the exact molecular structure is known, each metabolite can be included, whereas the in vitro approach requires carefully prepared metabolite phantoms. The advantage of the in vitro approach is that, as long as the phantoms are adequately prepared, the response of the metabolites in the in vitro measurement will be identical to the response of the metabolites in the in vivo  $^1\text{H}$ -MRS study. The high information content of  $^1\text{H}$ -MRS spectra leads to an advantage regarding the fitting accuracy because

overlapping resonances at one chemical shift position can be directly related to other non-overlapping resonances from the same metabolite. Currently used computer software includes: the metabolite basis set fitting program LCModel (Provencher, 1993) possibly incorporating the molecular simulation library GAMMA (Young et al., 1998), the quantification package jMRUI (Naressi et al., 2001) (which includes the quantum mechanical simulation algorithm NMR-SCOPE (Graveron-Demilly et al., 1993) and the metabolite basis set fitting routine QUEST (Ratiney et al., 2004)), and the algorithm TDFDFit (Slotboom et al., 1998). A detailed description (In 'T Zandt et al., 2001) and a critical assessment (Kanowski et al., 2004) of both AMARES and LCModel can be found elsewhere. Examples of LCModel output and TDFDFit output are given in Figure 2.2 and Figure 2.3, respectively. One should note that the T1 and/or T2 relaxation times are not always the same in the in vitro and in vivo situations, and different resonances within the same metabolite might have different relaxation times. For example, the methylene-protons of creatine ( $^2\text{CH}_2$ ), which resonate around 3.90 ppm display shorter T1 and T2 relaxation times (31% for T1 and 28% for T2, measured at 3T) than the methyl-protons of creatine ( $\text{N}(\text{CH}_3)$ ), which resonate around 3.03 ppm (Traber et al., 2004). Therefore, in pathologies, which are known to affect relaxation times, the in vitro prior knowledge cannot always be applied to the in vivo  $^1\text{H}$ -MRS spectra, which may lead to systematic errors (see above). In that case, a separate relaxation measurement would be favorable.

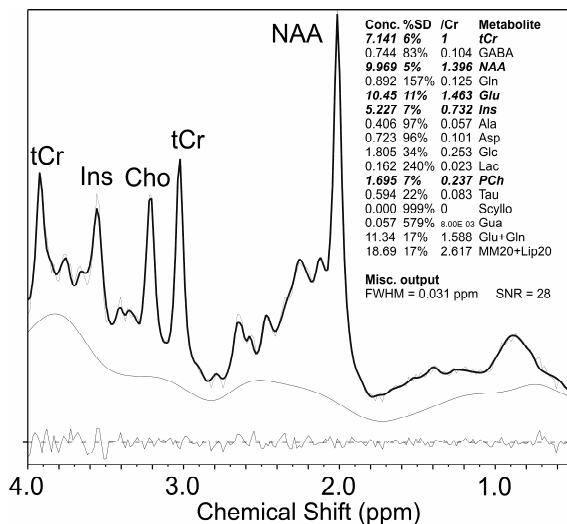


**Figure 2.2.** LCModel (Version 6.1-4) analysis output of a PRESS localized  $^1\text{H}$ -MRS spectra obtained from a healthy adult subject, recorded at 1.5T (Philips Intera, Philips Medical Systems). The spectra were recorded from the occipital lobe, using the following experimental parameters: TE = 23 ms, TR = 2 s, 128 averages, 8  $\text{cm}^3$  voxel size. The in vivo spectrum (thin upper curve) has been estimated with the LCModel output (thick upper curve), and the difference of the spectra is plotted at the bottom. Above the difference spectrum, the baseline spline estimate, as determined by LCModel, is displayed. The inserted table at the right displays the estimated metabolite concentrations and the Cramer Rao minimum variance bounds. NAA = N-acetylaspartate, tCr, = total creatine, Cho = choline, and Ins = myo-inositol.



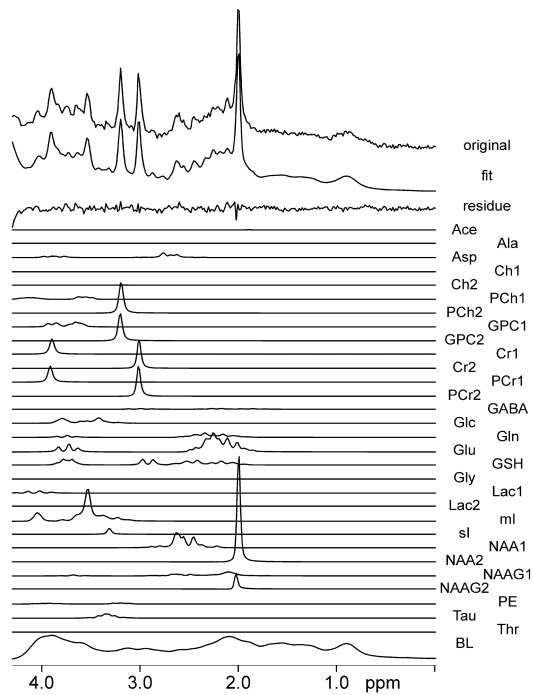


**Figure 2.3.** Fit results for a PRESS localized  $^1\text{H}$ -MRS spectrum, from white matter in the centrum semiovale of a 18 year old control subject using parameterized fitting with the metabolite basis set fitting algorithm TDFDfit. It was recorded at 1.5T (Signa, General Electric, Milwaukee, WI), using the following experimental parameters: TE = 20 ms, TR = 3 s, 128 averages,  $16\text{ cm}^3$  voxel size. The top contains the experimental spectrum, its fit and the residuals. Below, the individual components are displayed that add up to the best fit (used abbreviations are from (Hofmann et al., 2002)). Some metabolites were split into two spectra, providing the freedom of differential  $T_2$ 's for different protons within the same molecule. The baseline spectrum has been obtained from a saturation recovery experiment. (Courtesy of R. Kreis (Hofmann et al., 2002). Reprinted with permission of Wiley-Liss, Inc., a subsidiary of John Wiley & Sons, Inc.)

## Important considerations for data analysis

### *Quantification accuracy*

It is important to study and report the error estimates of the quantification method. Most fitting routines present the so-called Cramer Rao minimum variance bounds (CRMVB), which reflect the theoretical standard of precision for the model parameter estimates obtained from the data (Cavassila et al., 2001). The parameter estimation must not contain systematic errors (e.g. incorrect prior knowledge), which may lead to underestimated errors. It is important to realize that the CRMVB provide a measure of quality of the spectral fit, and do not necessarily reflect the quality of the original data. Furthermore, SNR degradation and increases in linewidth, which may lead to systematic errors, may not necessarily be reflected in CRMVB estimates (Kreis et al., 2003).

### Macromolecules

Macromolecules (MM) are compounds with a relatively high molecular weight, including proteins and polypeptides. Due to their lower mobility, MM

generally have a short T2 and are thus characterized by broad spectral lines in  $^1\text{H}$ -MRS. MM are the main contributors to the fluctuating baseline that generally hinders accurate quantification of small metabolites. Some MM resonances even overlap completely with sharp metabolite resonances, and can therefore not even be accounted for with conventional  $^1\text{H}$ -MRS (Behar et al., 1993; Behar et al., 1994). Several methods can be used to separate the MM-baseline from the wanted metabolite signal. The best way to eliminate MM contamination is to use acquisition schemes, which exploit the different relaxation properties of MM and small metabolites. Removal based on T1 relaxation can be achieved by so-called inversion recovery (Behar et al., 1994) or saturation recovery (Hofmann et al., 2001) sequences (Figure 2.4), whereas removal based on T2 relaxation can be obtained by increasing the echo time TE

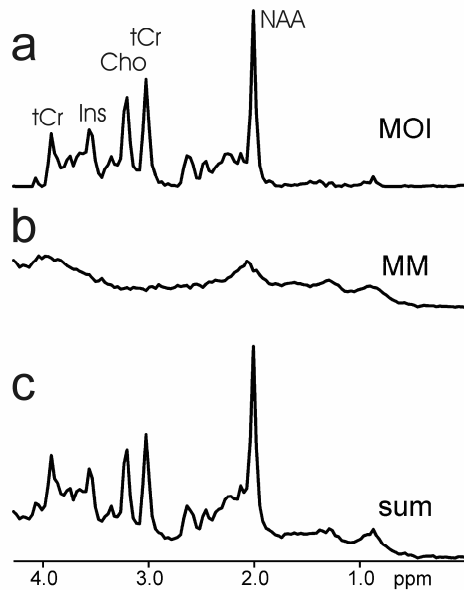


**Figure 2.4.** PRESS localized  $^1\text{H}$ -MRS spectra obtained from a healthy adult, recorded at 1.5T (Signa, General Electric, Milwaukee, WI). The spectra were recorded from the centrum semiovale, using the following experimental parameters: TE 20 ms, TR 6s, 128 averages, 12  $\text{cm}^3$  voxel size. (a) metabolites only spectrum, (b) MM only spectrum and (c) their sum spectra calculated from a series of saturation recovery spectra (Courtesy of R. Kreis, (Hofmann et al., 2001). Reprinted with permission of Wiley-Liss, Inc., a subsidiary of John Wiley & Sons, Inc.). NAA = N-acetylaspartate, tCr, = total creatine, Cho = choline, and Ins = myo-inositol, MOI = Metabolites of interest.

(Kreis et al., 1993). Alternatively, a pure metabolite spectrum can be obtained by subtracting an MM spectrum (similarly obtained exploiting the relaxation differences) from the in vivo acquired spectrum (Kassem et al., 2003). Unfortunately, the in vivo determination of the exact values of relaxation times for both MM and metabolites is complicated and time-consuming. Furthermore, both metabolites and MM do not necessarily display a narrow distribution of relaxation times, which means that a removal based on relaxation times will not always perform well. During post-processing, the MM signal can be estimated using a spline or polynomial function, which can be subtracted from the original spectrum, to improve the baseline (Provencher, 1993). However, since this approach relies on an estimation, it is not flawless. Recently, it has become popular to include the MM-baseline in the fitting routine (Pfeuffer et al., 1999;

Auer et al., 2001a; Mader et al., 2001). In the LCModel approach it is possible to extend the metabolite basis set with an MM spectrum. Since the macromolecular contribution to *in vivo* spectra cannot be simulated with simple model solutions, one has to determine the MM-baseline experimentally. Both inversion recovery (Pfeuffer et al., 1999) and saturation recovery (Hofmann et al., 2002) have been used to obtain MM-baseline spectra, which were averaged over several subjects and then parameterized to be included in the basis set. The incorporation of MM into the basis set generally improves the quantification accuracy and precision (Seeger et al., 2003). MM themselves have been the subject of recent research (Behar et al., 1994; Mader et al., 2002). It has been reported that several pathologies, such as stroke (Graham et al., 2001), brain tumors (Seeger et al., 2003), and multiple sclerosis (Mader et al., 2001), show an altered MM profile. For example, stroke (Graham et al., 2001) and multiple sclerosis (Mader et al., 2001) can cause the signal occurring from the MM resonance at 1.3 ppm to increase by 86% and 60%, respectively. Therefore, one should always carefully consider the incorporation of MM spectra in the basis set when such a pathology is concerned.

### **Motion**

Physiologic motion can have a large effect upon  $^1\text{H}$ -MRS quantification (Felblinger et al., 1998). For example, repeated small body motions or pulsatile cerebral motion (e.g. due to cardiac activity), can substantially affect the characteristics of the MR signal, even with motion-compensated  $^1\text{H}$ -MRS sequences. These effects may include an increase in linewidth, reduced peak intensities, a diminished quality of water suppression, or a doubling of all peaks. Moreover, if quantification is based on the summed signal of reference scans of the unsuppressed water peak, motion-induced phase effects can cause a substantial overestimation of metabolite concentrations, a problem that can be circumvented by storing and phasing all spectra individually (Felblinger et al., 1998). For CSI studies that include subcutaneous lipid signals, which have an enhanced sensitivity to subject motion, an in-plane motion correction can be applied (Haupt et al., 1998). The reduction of motion effects in  $^1\text{H}$ -MRS has been achieved in several studies (e.g. using cardiac triggering (Felblinger et al., 1998) or postprocessing (Helms et al., 2001)).

### **VOI shape and location**

In the process of spectral quantification, one should always keep in mind that the true spatial voxel profile might deviate from a perfect rectangular profile. The voxel dimensions are in principle identical for all resonances; however, the voxel position is dependent on the chemical shift of individual resonances. When a slice-selective gradient is applied to a volume containing

metabolites with different chemical shifts, there will be a displacement of the sensitive volume for each resonance of the metabolite. The displacement is regulated by the bandwidth of the RF pulse for voxel selection (De Graaf et al., 2001). For example, the methyl protons of NAA and the methylene protons of tCr are separated by 1.90 parts per million (ppm), or 122 Hz at 1.5 T. Usage of a RF bandwidth of 2000 Hz and a voxel size of 2 x 2 x 2 cm results in a displacement of the two voxels of 1.22 mm, which results in an overlap of the two voxels of 82.8%. Chemical shift artifacts can be reduced by increasing the bandwidth of the slice-selective RF pulses and, to keep the same voxel dimensions, by increasing the strength of slice-selective gradients. Obviously, safety margins should not be exceeded. It should be noted that CSI does not suffer from the chemical shift artifact for the spatial phase-encoding gradients, which are applied in the absence of RF pulses. However, if the CSI study involves the pre-selection of a VOI (e.g. to exclude skull lipids) then the position of that VOI is again subject to the chemical shift artifact, while the CSI voxels within the VOI are not shifted with respect to each other. CSI data is also influenced by the point spread function, which will be treated in the section entitled 'Sequence Specific Issues'.

### **Lineshape and eddy currents**

Very often, the obtained lineshape of signals from metabolites significantly deviates from ideal Lorentzian lineshape. If left uncorrected, these lineshape deviations severely complicate peak fitting. Generally, lineshape deviations are caused by variations in  $B_0$ , such as magnetic field inhomogeneities and eddy currents. Rapid switching of magnetic field gradients (which occurs in every localization pulse sequence) induces time-varying eddy currents in the magnetic cryostat, and as a result the magnetic field is transiently distorted. Several methods have been developed to correct irregular lineshapes, including the QUALITY deconvolution (De Graaf et al., 1990b) and eddy current correction (ECC) procedure (Klose, 1990). These correction methods use a single reference peak that was affected by the same distortions. The unsuppressed water signal, acquired using the same spoiler gradients as the metabolite spectrum, is usually used for that purpose.

### **Water suppression**

As indicated above, water suppression pulses might saturate parts of the metabolite spectrum, and can thus influence the measured concentration of several metabolites (a reduction of up to 21% has been reported (Hsu et al., 1998)). Numerical calculations can be employed for accurate corrections for these effects (Hsu et al., 1998). In addition, the residual water signal that is still present in water-suppressed spectra can significantly degrade the performance

of metabolite fitting routines. Therefore it is advisable to eliminate the unwanted water signal with a high pass filter (Marion et al., 1989) or an algorithm such as the Hankel Lanczos Singular Values Decomposition filter (HLSVD) (De Beer et al., 1992) prior to data analysis (Figure 2.5).

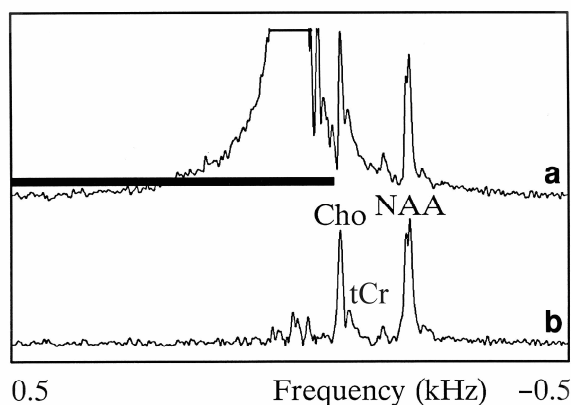


**Figure 2.5.** Water removal by HLSVD. (a) In vivo CSI  $^1\text{H}$ -MRS spectrum obtained from the brain of a healthy adult. The region indicated by the horizontal black bar contains the water peak. The peaks of interest, indicated by Cho, Cr, and NAA are disturbed by right tail of the water peak. (b) Spectrum after subtraction of the water components, as retrieved and quantified by HLSVD in the region of the black bar. Components outside the region of the black bar are not affected by the procedure. (Courtesy of R. de Beer, (De Beer et al., 1992). Reprinted with permission of Springer Science and Business Media)

## Sequence specific issues

### Spectral editing

Lately, several clinical studies have been performed using the spectral editing approach (Mueller et al., 2001; Chang et al., 2003). Spectral editing enables detection of metabolites that are hard to detect using conventional  $^1\text{H}$ -MRS techniques because they are present in lower concentrations and their resonance peaks overlap with other more abundant metabolites (Trabesinger et al., 2003). Using a specifically designed acquisition scheme that allows selective recording of only signals from desired metabolite(s), the information content of the acquired signal is reduced. Preferably, only peaks of the desired metabolite(s) remain in the spectrum, while the other metabolites are eliminated. Among the metabolites that are the target of the spectral editing approach are gamma-aminobutyric acid, glutamine, lactate, and glutathione.

It is important that the pulse sequence is carefully optimized and that the specificity of the editing procedure is critically assessed. If unwanted signals remain in the final spectrum, simple peak fitting will not suffice, and one could resort to the advanced prior knowledge approach (Terpstra et al., 2003).

## Chemical shift imaging

Quantification of CSI data generally requires extra considerations, as CSI data can be different from single voxel data in some aspects. For example, CSI data usually have a lower SNR since these suffer from field inhomogeneities (due to the large VOI). Additionally, CSI data also suffer from artifacts like imperfect water suppression and lipid contamination. On the other hand, the spatial information of CSI offers several opportunities to improve postprocessing and analysis. Knowledge on the spatial dependence of parameters may present extra information on prior knowledge or constraints. For instance, the notion that voxel-to-voxel variations in metabolite concentrations can be expected to change smoothly, can be used to set constraints on the limits of these variations (Soher et al., 1998).

Not all AQ strategies are necessarily compatible with CSI data. For example, it is often too time-consuming to obtain fully relaxed water reference scans with the same resolution (Ebel et al., 2001). A commonly used referencing scheme for CSI is the time-efficient reciprocity principle (Soher et al., 1996; Mclean et al., 2000). An absolute reference can also be obtained by proton density weighted MRI (Alger et al., 1993).

### *Point Spread Function*

Quantification of CSI data is complicated by the point spread function (PSF), which describes the spread of signal from each voxel to surrounding voxels. The PSF originates from Fourier transformation of a signal sampled in the time domain at a limited number of discrete points. Although the PSF influences all Fourier transformed data, in CSI the effect may become prominent since CSI data are generally acquired with a relatively low spatial resolution, corresponding to a small number of phase-encoding increments. The PSF, and therefore the spatial resolution, can be improved by applying apodization functions in the spatial frequency or k-space domain (Ernst et al., 1987). One approach is to apply different k-space sampling schemes to improve the PSF and SNR (Maudsley et al., 1994; Hugg et al., 1996). Another approach is k-space weighting during signal acquisition, which also gives a better SNR (Kuhn et al., 1996). In CSI of the brain, the PSF effect will typically lead to contamination of  $^1\text{H}$  spectra of voxels within the brain by intense extracranial lipid signals. K-space weighting or applying apodization functions to improve the PSF is usually insufficient in this case, and therefore other methods to prevent lipid signals from contaminating brain spectra are used, such as outer volume suppression. Other methods reduce lipid contamination in post-acquisition processing (Haupt et al., 1996). In an absolute quantification strategy co-registered MR images are generally used for tissue segmentation (T1 or T2 weighted (Hetherington et al., 1996)) or water referencing (proton density

weighted MRI (Alger et al., 1993; Schuff et al., 2001)). It is important to note that apodization filters, used to improve the PSF of the metabolite spectra, should also be applied to the MRI data that are used for the segmentation procedure.

#### *Fully automated spectral analysis*

Analysis of spectra from large CSI data sets is time-consuming, and because usually only spectra from a few selected voxels are analyzed, the complete data set is often under-utilized. Therefore, automated methods have been developed (Soher et al., 1998; Young et al., 1998; Ebel et al., 2001) that enable analysis of large numbers of spectra and that are relatively insensitive to the low SNR and spectral distortions commonly associated with in vivo CSI. Furthermore, the introduction of a standardized processing and analysis protocol makes comparisons between different studies possible.

### **Quality Assessment**

Generally speaking, spectra with a large linewidth, low SNR or obvious artifacts (i.e. signal contributions from outside the VOI, phase distortions, and technical failures) should be discarded. Additionally, in studying certain pathologies, it is important to establish the limits of metabolite concentrations that represent abnormality. To obtain reliable absolute concentrations for the assessment of pathological changes, it is necessary to take both the data acquisition and the data processing methods into account. The overall reproducibility depends on the variability upon immediate repetition of a scan, the intra-individual variability upon re-examination of the same subject in a subsequent scan, and the inter-individual variability. The achievable overall reproducibility figures for the absolute quantification of NAA, tCr, Cho, and Ins have been published for single voxel spectroscopy, with ranges from 7 to 16% (Schirmer et al., 2000; Hofmann et al., 2002), and for CSI, with ranges from 5 to 21% (Wiedermann et al., 2001; Chard et al., 2002). Therefore, to detect pathology, the deviation from normal values should be larger than the reproducibility of that particular measurement.

#### **Signal-to-noise ratio**

The SNR can be used as a measure in the rejection of spectra (e.g. generally, the SNR should be at least 4). The SNR is usually defined in frequency domain as the ratio of the highest metabolite peak intensity to the standard deviation of the noise amplitude in a metabolite-free part of the spectrum (Ernst et al., 1987). The SNR can be improved by increasing the VOI size and the number of averages. However, increasing the VOI size generally degrades the lineshape,

increases the linewidth, and may decrease the sensitivity to detect pathology, while increasing the number of averages adds to the acquisition time.

### **Linewidth**

The linewidth is commonly defined as the full width of the peak at half its maximum height (FWHM) in the frequency domain (Ernst et al., 1987). A small linewidth generally implies a high spectral resolution, which will improve the quality of the fitting routines. Better shimming, using a smaller VOI size and choosing a VOI at sufficient distance from tissue interfaces can improve the resolution. It has been recommended that the FWHM should always be treated as a covariate in the statistical analysis, to correct for single-subject inter-session variations (Schirmer et al., 2000).

### **Criteria for rejection of data**

In a recent, insightful review (Kreis, 2004), Kreis has proposed the following acceptance criteria for spectral data and their fitting results: (i) the FWHM of the metabolites should be less than 0.1 ppm; (ii) the CRMVB should be smaller than 50%; (iii) the fitting residual should not contain unexplained features; and (iv) the spectra should not contain artifacts (e.g. doubled peaks or asymmetric lineshapes).

### **Conclusions & Future perspectives**

The implementation of AQ in a clinical routine has been greatly facilitated by the development of calibration strategies and the availability of spectral fitting routines. This is a beneficial progress, since AQ has an added value for  $^1\text{H}$ -MRS quantification. Furthermore, the introduction of phased array coils (Natt et al., 2005) and higher field strengths ( $>1.5$  T) (Srinivasan et al., 2004) has been proven to be advantageous with regard to SNR, quantification precision, reproducibility, and detection sensitivity. However, in order to obtain reliable absolute concentrations, one has to consider potential complicating factors, both with respect to the data acquisition and data processing method. For example, relaxation effects in data acquisition can either be corrected for or eliminated, whereas data fitting is complicated by factors such as MM contribution. Nevertheless, most of these problems have been critically addressed and can be taken into account in a satisfying manner. AQ is available and can improve the diagnostic utility of  $^1\text{H}$ -MRS procedures. Therefore further progress in the development of automated spectral analysis methods and databases of normal regional and age-dependent metabolite concentrations has to be encouraged to make the AQ procedures more easily applicable in clinical routine.



## References

- Abildgaard, F., Gesmar, H., Led, J.J., 1988. Quantitative-analysis of complicated nonideal fourier-transform NMR-spectra. *Journal of Magnetic Resonance* 79, 78-89.
- Alger, J.R., Cloughesy, T.F. (2000) Structural and functional imaging of cerebral neoplasia. IN Mazziotto, J. C., Toga, A. W. & Frackowiak, R. S. J. (Eds.) *Brain mapping: the disorders*. San Diego, Academic Press.
- Alger, J.R., Symko, S.C., Bizzi, A., et al., 1993. Absolute quantitation of short TE brain 1H-MR spectra and spectroscopic imaging data. *J Comput Assist Tomogr* 17, 191-199.
- Auer, D.P., Gossel, C., Schirmer, T., et al., 2001a. Improved analysis of 1H-MR spectra in the presence of mobile lipids. *Magn Reson Med* 46, 615-618.
- Auer, D.P., Schirmer, T., Heidenreich, J.O., et al., 2001b. Altered white and gray matter metabolism in CADASIL: a proton MR spectroscopy and 1H-MRSI study. *Neurology* 56, 635-642.
- Barker, P.B., Soher, B.J., Blackband, S.J., et al., 1993. Quantitation of proton NMR spectra of the human brain using tissue water as an internal concentration reference. *NMR Biomed* 6, 89-94.
- Battistuta, J., Bjartmar, C., Trapp, B.D., 2001. Postmortem degradation of N-acetyl aspartate and N-acetyl aspartylglutamate: an HPLC analysis of different rat CNS regions. *Neurochem Res* 26, 695-702.
- Behar, K.L., Ogino, T., 1993. Characterization of macromolecule resonances in the 1H NMR spectrum of rat brain. *Magn Reson Med* 30, 38-44.
- Behar, K.L., Rothman, D.L., Spencer, D.D., et al., 1994. Analysis of macromolecule resonances in 1H NMR spectra of human brain. *Magn Reson Med* 32, 294-302.
- Bottomley, P.A. (1987) Selective volume method for performing localized NMR spectroscopy. US.
- Bottomley, P.A., Weiss, R.G., 2001. Noninvasive localized MR quantification of creatine kinase metabolites in normal and infarcted canine myocardium. *Radiology* 219, 411-418.
- Brooks, J.C., Roberts, N., Kemp, G.J., et al., 1999. Magnetic resonance imaging-based compartmentation and its application to measuring metabolite concentrations in the frontal lobe. *Magn Reson Med* 41, 883-888.
- Brown, T.R., Kincaid, B.M., Ugurbil, K., 1982. NMR chemical shift imaging in three dimensions. *Proc Natl Acad Sci U S A* 79, 3523-3526.
- Buchli, R., Boesiger, P., 1993. Comparison of methods for the determination of absolute metabolite concentrations in human muscles by 31P MRS. *Magn Reson Med* 30, 552-558.
- Burri, R., Bigler, P., Straehl, P., et al., 1990. Brain development: 1H magnetic resonance spectroscopy of rat brain extracts compared with chromatographic methods. *Neurochem Res* 15, 1009-1016.
- Cady, E., 1992. Determination of absolute concentrations of metabolites from NMR spectra. *NMR Basic Principles and Progress* 26, 249-281.
- Cavassila, S., Deval, S., Huegen, C., et al., 2001. Cramer-Rao bounds: an evaluation tool for quantitation. *NMR Biomed* 14, 278-283.
- Chang, L., Cloak, C.C., Ernst, T., 2003. Magnetic resonance spectroscopy studies of GABA in neuropsychiatric disorders. *J Clin Psychiatry* 64 Suppl 3, 7-14.
- Chang, L., Ernst, T., Tornatore, C., et al., 1997. Metabolite abnormalities in progressive multifocal leukoencephalopathy by proton magnetic resonance spectroscopy. *Neurology* 48, 836-845.
- Chard, D.T., McLean, M.A., Parker, G.J., et al., 2002. Reproducibility of in vivo metabolite quantification with proton magnetic resonance spectroscopic imaging. *J Magn Reson Imaging* 15, 219-225.

- Christiansen, P., Henriksen, O., Stubgaard, M., et al., 1993. In vivo quantification of brain metabolites by 1H-MRS using water as an internal standard. *Magn Reson Imaging* 11, 107-118.
- Chu, W.C., Chik, K.W., Chan, Y.L., et al., 2003. White matter and cerebral metabolite changes in children undergoing treatment for acute lymphoblastic leukemia: longitudinal study with MR imaging and 1H MR spectroscopy. *Radiology* 229, 659-669.
- Connelly, A., Jackson, G.D., Duncan, J.S., et al., 1994. Magnetic resonance spectroscopy in temporal lobe epilepsy. *Neurology* 44, 1411-1417.
- Danielsen, E.R., Henriksen, O., 1994. Absolute quantitative proton NMR spectroscopy based on the amplitude of the local water suppression pulse. Quantification of brain water and metabolites. *NMR Biomed* 7, 311-318.
- de Beer, R., van Ormondt, D., 1992. Analysis of NMR data using time domain fitting procedures. *NMR Basic Principles and Progress* 26, 201-248.
- de Graaf, A.A., Bovee, W.M., 1990a. Improved quantification of in vivo 1H NMR spectra by optimization of signal acquisition and processing and by incorporation of prior knowledge into the spectral fitting. *Magn Reson Med* 15, 305-319.
- de Graaf, A.A., van Dijk, J.E., Bovee, W.M., 1990b. QUALITY: quantification improvement by converting lineshapes to the Lorentzian type. *Magn Reson Med* 13, 343-357.
- de Graaf, R.A., Rothman, D., 2001. In vivo detection and quantification of scalar coupled (1)H NMR resonances. *Concepts in Magnetic Resonance* 13, 32-76.
- Duc, C.O., Weber, O.M., Trabesinger, A.H., et al., 1998. Quantitative 1H MRS of the human brain in vivo based on the stimulation phantom calibration strategy. *Magn Reson Med* 39, 491-496.
- Ebel, A., Soher, B.J., Maudsley, A.A., 2001. Assessment of 3D proton MR echo-planar spectroscopic imaging using automated spectral analysis. *Magn Reson Med* 46, 1072-1078.
- Ernst, R.R., Bodenhausen, G., Wokaun, A. (1987) *Principles of nuclear magnetic resonance in one and two dimensions*, Oxford, Oxford University Press.
- Ernst, T., Kreis, R., Ross, B.D., 1993. Absolute quantitation of water and metabolites in the human brain. I. compartments and water. *J Magn Reson B* 102, 1-8.
- Ethofer, T., Mader, I., Seeger, U., et al., 2003. Comparison of longitudinal metabolite relaxation times in different regions of the human brain at 1.5 and 3 Tesla. *Magn Reson Med* 50, 1296-1301.
- Fatouros, P.P., Heath, D.L., Beaumont, A., et al., 2000. Comparison of NAA measures by MRS and HPLC. *Acta Neurochir Suppl* 76, 35-37.
- Felblinger, J., Kreis, R., Boesch, C., 1998. Effects of physiologic motion of the human brain upon quantitative 1H-MRS: analysis and correction by retro-gating. *NMR Biomed* 11, 107-114.
- Fernando, K.T., McLean, M.A., Chard, D.T., et al., 2004. Elevated white matter myo-inositol in clinically isolated syndromes suggestive of multiple sclerosis. *Brain* 127, 1361-1369.
- Frahm, J., Merboldt, K.D., Hanicke, W., 1987. Localized proton spectroscopy using stimulated echoes. *J Magn Reson* 72, 502-508.
- Govindaraju, V., Young, K., Maudsley, A.A., 2000. Proton NMR chemical shifts and coupling constants for brain metabolites. *NMR Biomed* 13, 129-153.
- Graham, G.D., Hwang, J.H., Rothman, D.L., et al., 2001. Spectroscopic assessment of alterations in macromolecule and small-molecule metabolites in human brain after stroke. *Stroke* 32, 2797-2802.
- Grasso, G., Alafaci, C., Passalacqua, M., et al., 2002. Assessment of human brain water content by cerebral bioelectrical impedance analysis: a new technique and its application to cerebral pathological conditions. *Neurosurgery* 50, 1064-1072; discussion 1072-1064.
- Graveron-Demilly, D., Diop, A., Briguet, A., et al., 1993. Product-operator algebra for strongly coupled spin systems. *J Magn Reson A* 101, 233-239.
- Hanstock, C.C., Cwik, V.A., Martin, W.R., 2002. Reduction in metabolite transverse relaxation times in amyotrophic lateral sclerosis. *J Neurol Sci* 198, 37-41.

- Haupt, C.I., Kiefer, A.P., Maudsley, A.A., 1998. In-plane motion correction for MR spectroscopic imaging. *Magn Reson Med* 39, 749-753.
- Haupt, C.I., Schuff, N., Weiner, M.W., et al., 1996. Removal of lipid artifacts in <sup>1</sup>H spectroscopic imaging by data extrapolation. *Magn Reson Med* 35, 678-687.
- Helms, G., 2000. A precise and user-independent quantification technique for regional comparison of single volume proton MR spectroscopy of the human brain. *NMR Biomed* 13, 398-406.
- Helms, G., 2001. Volume correction for edema in single-volume proton MR spectroscopy of contrast-enhancing multiple sclerosis lesions. *Magn Reson Med* 46, 256-263.
- Helms, G., 2003. T2-based segmentation of periventricular paragraph sign volumes for quantification of proton magnetic paragraph sign resonance spectra of multiple sclerosis lesions. *Magma* 16, 10-16.
- Helms, G., Piringer, A., 2001. Restoration of motion-related signal loss and line-shape deterioration of proton MR spectra using the residual water as intrinsic reference. *Magn Reson Med* 46, 395-400.
- Henriksen, O., 1995. In vivo quantitation of metabolite concentrations in the brain by means of proton MRS. *NMR Biomed* 8, 139-148.
- Hetherington, H.P., Pan, J.W., Mason, G.F., et al., 1996. Quantitative <sup>1</sup>H spectroscopic imaging of human brain at 4.1 T using image segmentation. *Magn Reson Med* 36, 21-29.
- Hofmann, L., Slotboom, J., Boesch, C., et al., 2001. Characterization of the macromolecule baseline in localized (<sup>1</sup>H)-MR spectra of human brain. *Magn Reson Med* 46, 855-863.
- Hofmann, L., Slotboom, J., Jung, B., et al., 2002. Quantitative <sup>1</sup>H-magnetic resonance spectroscopy of human brain: Influence of composition and parameterization of the basis set in linear combination model-fitting. *Magn Reson Med* 48, 440-453.
- Hoult, D.I., Richards, R.E., 1976. The signal-to-noise ratio of the nuclear magnetic resonance experiment. *J Magn Reson* 24, 71-85.
- Hsu, A.C., Gregory, C.D., 1998. Offset-dependent partial saturation in binomial solvent suppression sequences. *J Magn Reson* 131, 46-53.
- Hugg, J.W., Maudsley, A.A., Weiner, M.W., et al., 1996. Comparison of k-space sampling schemes for multidimensional MR spectroscopic imaging. *Magn Reson Med* 36, 469-473.
- Huppi, P.S., Fusch, C., Boesch, C., et al., 1995. Regional metabolic assessment of human brain during development by proton magnetic resonance spectroscopy in vivo and by high-performance liquid chromatography/gas chromatography in autopsy tissue. *Pediatr Res* 37, 145-150.
- in 't Zandt, H., van Der Graaf, M., Heerschap, A., 2001. Common processing of in vivo MR spectra. *NMR Biomed* 14, 224-232.
- Isobe, T., Matsumura, A., Anno, I., et al., 2002. Quantification of cerebral metabolites in glioma patients with proton MR spectroscopy using T2 relaxation time correction. *Magn Reson Imaging* 20, 343-349.
- Jost, G., Harting, I., Heiland, S., 2005. Quantitative single-voxel spectroscopy: the reciprocity principle for receive-only head coils. *J Magn Reson Imaging* 21, 66-71.
- Kanowski, M., Kaufmann, J., Braun, J., et al., 2004. Quantitation of simulated short echo time <sup>1</sup>H human brain spectra by LCModel and AMARES. *Magn Reson Med* 51, 904-912.
- Kassem, M.N., Bartha, R., 2003. Quantitative proton short-echo-time LASER spectroscopy of normal human white matter and hippocampus at 4 Tesla incorporating macromolecule subtraction. *Magn Reson Med* 49, 918-927.
- Klose, U., 1990. In vivo proton spectroscopy in presence of eddy currents. *Magn Reson Med* 14, 26-30.
- Knight-Scott, J., Haley, A.P., Rossmiller, S.R., et al., 2003. Molality as a unit of measure for expressing <sup>1</sup>H MRS brain metabolite concentrations in vivo. *Magn Reson Imaging* 21, 787-797.

- Kotitschke, K., Schnackerz, K.D., Dringen, R., et al., 1994. Investigation of the  $^1\text{H}$  NMR visibility of lactate in different rat and human brain cells. *NMR Biomed* 7, 349-355.
- Kreis, R., 1997. Quantitative localized ( $^1\text{H}$ ) MR spectroscopy for clinical use. *J Progress NMR* 31, 155-195.
- Kreis, R., 2004. Issues of spectral quality in clinical  $^1\text{H}$ -magnetic resonance spectroscopy and a gallery of artifacts. *NMR Biomed* 17, 361-381.
- Kreis, R., Boesch, C. (2003) Bad spectra can be better than good spectra. *Proc. Intl. Soc. Mag. Reson. Med.* Toronto, Ontario, Canada.
- Kreis, R., Ernst, T., Ross, B.D., 1993. Absolute quantitation of water and metabolites in the human brain. II. metabolite concentrations. *J Magn Reson B* 102, 9-19.
- Kreis, R., Hofmann, L., Kuhlmann, B., et al., 2002. Brain metabolite composition during early human brain development as measured by quantitative in vivo  $^1\text{H}$  magnetic resonance spectroscopy. *Magn Reson Med* 48, 949-958.
- Kreis, R., Slotboom, J., Hofmann, L., et al., 2005. Integrated data acquisition and processing to determine metabolite contents, relaxation times, and macromolecule baseline in single examinations of individual subjects. *Magn Reson Med* 54, 761-768.
- Kreis, R., Slotboom, J., Pietz, J., et al., 2001. Quantitation of localized ( $^{31}\text{P}$ ) magnetic resonance spectra based on the reciprocity principle. *J Magn Reson* 149, 245-250.
- Kruiskamp, M.J., de Graaf, R.A., van der Grond, J., et al., 2001. Magnetic coupling between water and creatine protons in human brain and skeletal muscle, as measured using inversion transfer ( $^1\text{H}$ -MRS. *NMR Biomed* 14, 1-4.
- Kruiskamp, M.J., de Graaf, R.A., van Vliet, G., et al., 1999. Magnetic coupling of creatine/phosphocreatine protons in rat skeletal muscle, as studied by ( $^1\text{H}$ -magnetization transfer MRS. *Magn Reson Med* 42, 665-672.
- Kuhn, B., Dreher, W., Norris, D.G., et al., 1996. Fast proton spectroscopic imaging employing k-space weighting achieved by variable repetition times. *Magn Reson Med* 35, 457-464.
- Laule, C., Vavasour, I.M., Moore, G.R., et al., 2004. Water content and myelin water fraction in multiple sclerosis. A T2 relaxation study. *J Neurol* 251, 284-293.
- Leibfritz, D., Dreher, W., 2001. Magnetization transfer MRS. *NMR Biomed* 14, 65-76.
- Li, B.S., Wang, H., Gonen, O., 2003. Metabolite ratios to assumed stable creatine level may confound the quantification of proton brain MR spectroscopy. *Magn Reson Imaging* 21, 923-928.
- Li, S., Williams, G.D., Frisk, T.A., et al., 1995. A computer simulation of the static magnetic field distribution in the human head. *Magn Reson Med* 34, 268-275.
- Lundbom, N., Gaily, E., Vuori, K., et al., 2001. Proton spectroscopic imaging shows abnormalities in glial and neuronal cell pools in frontal lobe epilepsy. *Epilepsia* 42, 1507-1514.
- Lynch, J., Peeling, J., Auty, A., et al., 1993. Nuclear magnetic resonance study of cerebrospinal fluid from patients with multiple sclerosis. *Can J Neurol Sci* 20, 194-198.
- Mader, I., Seeger, U., Karitzky, J., et al., 2002. Proton magnetic resonance spectroscopy with metabolite nulling reveals regional differences of macromolecules in normal human brain. *J Magn Reson Imaging* 16, 538-546.
- Mader, I., Seeger, U., Weissert, R., et al., 2001. Proton MR spectroscopy with metabolite-nulling reveals elevated macromolecules in acute multiple sclerosis. *Brain* 124, 953-961.
- Marion, D., Ikura, M., Bax, A., 1989. Improved solvent suppression in one- and two-dimensional NMR spectra by convolution of time-domain data. *J Magn Reson* 84, 425-430.
- Marshall, I., Higinbotham, J., Bruce, S., et al., 1997. Use of Voigt lineshape for quantification of in vivo  $^1\text{H}$  spectra. *Magn Reson Med* 37, 651-657.
- Mathews, V.P., Barker, P.B., Blackband, S.J., et al., 1995. Cerebral metabolites in patients with acute and subacute strokes: concentrations determined by quantitative proton MR spectroscopy. *AJR Am J Roentgenol* 165, 633-638.

- Maudsley, A.A., Hilal, S.K., Perman, W.H., et al., 1983. Spatially resolved high resolution spectroscopy by "four-dimensional" NMR. *J Magn Reson* 51, 147-152.
- Maudsley, A.A., Matson, G.B., Hugg, J.W., et al., 1994. Reduced phase encoding in spectroscopic imaging. *Magn Reson Med* 31, 645-651.
- McLean, M.A., Woermann, F.G., Barker, G.J., et al., 2000. Quantitative analysis of short echo time (1)H-MRSI of cerebral gray and white matter. *Magn Reson Med* 44, 401-411.
- Meyer, R.A., Fisher, M.J., Nelson, S.J., et al., 1988. Evaluation of manual methods for integration of in vivo phosphorus NMR spectra. *NMR Biomed* 1, 131-135.
- Michaelis, T., Merboldt, K.D., Bruhn, H., et al., 1993. Absolute concentrations of metabolites in the adult human brain in vivo: quantification of localized proton MR spectra. *Radiology* 187, 219-227.
- Mierisova, S., Ala-Korpela, M., 2001. MR spectroscopy quantitation: a review of frequency domain methods. *NMR Biomed* 14, 247-259.
- Mueller, S.G., Laxer, K.D., Suhy, J., et al., 2003. Spectroscopic metabolic abnormalities in mTLE with and without MRI evidence for mesial temporal sclerosis using hippocampal short-TE MRSI. *Epilepsia* 44, 977-980.
- Mueller, S.G., Trabesinger, A.H., Boesiger, P., et al., 2001. Brain glutathione levels in patients with epilepsy measured by in vivo (1)H-MRS. *Neurology* 57, 1422-1427.
- Naressi, A., Couturier, C., Devos, J.M., et al., 2001. Java-based graphical user interface for the MRUI quantitation package. *Magma* 12, 141-152.
- Natt, O., Bezkorovaynyy, V., Michaelis, T., et al., 2005. Use of phased array coils for a determination of absolute metabolite concentrations. *Magn Reson Med* 53, 3-8.
- Nelson, S.J., Brown, T.R., 1987. A method for automatic quantification of one-dimensional spectra with low signal-to-noise ratio. *J Magn Reson* 75, 229-243.
- Pfeuffer, J., Tkac, I., Provencher, S.W., et al., 1999. Toward an in vivo neurochemical profile: quantification of 18 metabolites in short-echo-time (1)H NMR spectra of the rat brain. *J Magn Reson* 141, 104-120.
- Pohl, C., Block, W., Karitzky, J., et al., 2001. Proton magnetic resonance spectroscopy of the motor cortex in 70 patients with amyotrophic lateral sclerosis. *Arch Neurol* 58, 729-735.
- Provencher, S.W., 1993. Estimation of metabolite concentrations from localized in vivo proton NMR spectra. *Magn Reson Med* 30, 672-679.
- Rai, G.S., McConnell, J.R., Waldman, A., et al., 1999. Brain proton spectroscopy in dementia: an aid to clinical diagnosis. *Lancet* 353, 1063-1064.
- Ratiney, H., Coenradie, Y., Cavassila, S., et al., 2004. Time-domain quantitation of 1H short echo-time signals: background accommodation. *Magma* 16, 284-296.
- Ross, B., Bluml, S., 2001. Magnetic resonance spectroscopy of the human brain. *Anat Rec* 265, 54-84.
- Roth, K., Hubesch, B., Meyerhoff, D.J., et al., 1989. Noninvasive quantitation of phosphorus metabolites in human-tissue by NMR-spectroscopy. *Journal of Magnetic Resonance* 81, 299-311.
- Ruiz-Pena, J.L., Pinero, P., Sellers, G., et al., 2004. Magnetic resonance spectroscopy of normal appearing white matter in early relapsing-remitting multiple sclerosis: correlations between disability and spectroscopy. *BMC Neurol* 4, 8.
- Rutgers, D.R., Kingsley, P.B., van der Grond, J., 2003. Saturation-corrected T 1 and T 2 relaxation times of choline, creatine and N-acetyl aspartate in human cerebral white matter at 1.5 T. *NMR Biomed* 16, 286-288.
- Savic, I., Osterman, Y., Helms, G., 2004. MRS shows syndrome differentiated metabolite changes in human-generalized epilepsies. *Neuroimage* 21, 163-172.
- Schirmer, T., Auer, D.P., 2000. On the reliability of quantitative clinical magnetic resonance spectroscopy of the human brain. *NMR Biomed* 13, 28-36.

- Schuff, N., Ezekiel, F., Gamst, A.C., et al., 2001. Region and tissue differences of metabolites in normally aged brain using multislice 1H magnetic resonance spectroscopic imaging. *Magn Reson Med* 45, 899-907.
- Seeger, U., Klose, U., Mader, I., et al., 2003. Parameterized evaluation of macromolecules and lipids in proton MR spectroscopy of brain diseases. *Magn Reson Med* 49, 19-28.
- Simister, R.J., Woermann, F.G., McLean, M.A., et al., 2002. A short-echo-time proton magnetic resonance spectroscopic imaging study of temporal lobe epilepsy. *Epilepsia* 43, 1021-1031.
- Slotboom, J., Boesch, C., Kreis, R., 1998. Versatile frequency domain fitting using time domain models and prior knowledge. *Magn Reson Med* 39, 899-911.
- Soher, B.J., van Zijl, P.C., Duyn, J.H., et al., 1996. Quantitative proton MR spectroscopic imaging of the human brain. *Magn Reson Med* 35, 356-363.
- Soher, B.J., Young, K., Govindaraju, V., et al., 1998. Automated spectral analysis III: application to in vivo proton MR spectroscopy and spectroscopic imaging. *Magn Reson Med* 40, 822-831.
- Srinivasan, R., Vigneron, D., Sailasuta, N., et al., 2004. A comparative study of myo-inositol quantification using LCmodel at 1.5 T and 3.0 T with 3 D 1H proton spectroscopic imaging of the human brain. *Magn Reson Imaging* 22, 523-528.
- Stoppe, G., Bruhn, H., Pouwels, P.J., et al., 2000. Alzheimer disease: absolute quantification of cerebral metabolites in vivo using localized proton magnetic resonance spectroscopy. *Alzheimer Dis Assoc Disord* 14, 112-119.
- Terpstra, M., Henry, P.G., Gruetter, R., 2003. Measurement of reduced glutathione (GSH) in human brain using LCModel analysis of difference-edited spectra. *Magn Reson Med* 50, 19-23.
- Thulborn, K.T., Ackerman, J.H., 1983. Absolute molar concentrations by NMR in inhomogeneous B1. A scheme for analysis of in vivo metabolites. *J Magn Reson* 55, 357-371.
- Tofts, P.S., Wray, S., 1988. A critical assessment of methods of measuring metabolite concentrations by NMR spectroscopy. *NMR Biomed* 1, 1-10.
- Traber, F., Block, W., Lamerichs, R., et al., 2004. 1H metabolite relaxation times at 3.0 tesla: Measurements of T1 and T2 values in normal brain and determination of regional differences in transverse relaxation. *J Magn Reson Imaging* 19, 537-545.
- Trabesinger, A.H., Meier, D., Boesiger, P., 2003. In vivo 1H NMR spectroscopy of individual human brain metabolites at moderate field strengths. *Magn Reson Imaging* 21, 1295-1302.
- Vanhamme, L., Sundin, T., Hecke, P.V., et al., 2001. MR spectroscopy quantitation: a review of time-domain methods. *NMR Biomed* 14, 233-246.
- Vanhamme, L., van den Boogaart, A., Van Huffel, S., 1997. Improved method for accurate and efficient quantification of MRS data with use of prior knowledge. *J Magn Reson* 129, 35-43.
- Vermathen, P., Laxer, K.D., Schuff, N., et al., 2003. Evidence of neuronal injury outside the medial temporal lobe in temporal lobe epilepsy: N-acetylaspartate concentration reductions detected with multisection proton MR spectroscopic imaging--initial experience. *Radiology* 226, 195-202.
- Walker, P.M., Ben Salem, D., Lalande, A., et al., 2004. Time course of NAA T2 and ADC(w) in ischaemic stroke patients: 1H MRS imaging and diffusion-weighted MRI. *J Neurol Sci* 220, 23-28.
- Webb, P., Spielman, D., Macovski, A., 1992. Inhomogeneity correction for in vivo spectroscopy by high-resolution water referencing. *Magn Reson Med* 23, 1-11.
- Wiedermann, D., Schuff, N., Matson, G.B., et al., 2001. Short echo time multislice proton magnetic resonance spectroscopic imaging in human brain: metabolite distributions and reliability. *Magn Reson Imaging* 19, 1073-1080.
- Young, K., Govindaraju, V., Soher, B.J., et al., 1998. Automated spectral analysis I: formation of a priori information by spectral simulation. *Magn Reson Med* 40, 812-815.



# Chapter 3

**Reproducibility of quantitative cerebral T2 relaxometry, diffusion tensor imaging, and  $^1\text{H}$  magnetic resonance spectroscopy at 3.0 Tesla**

**Jansen JFA, Kooi ME, Kessels AGH, Nicolay K, and Backes WH**

*Accepted for Investigative Radiology 42: 2007*



## **Abstract**

### **Objectives**

The reproducibility of quantitative cerebral T2 relaxometry, Diffusion Tensor Imaging, and <sup>1</sup>H Magnetic Resonance Spectroscopic Imaging was assessed on a clinical 3.0 T MR system.

### **Materials and Methods**

Repeated measurements in 10 healthy volunteers were used to establish the reproducibility of quantitative measures derived from different quantitative MR techniques, namely the T2 relaxation time, the apparent diffusion coefficient (ADC), the fractional anisotropy (FA), and metabolite concentrations of N-acetyl-aspartate (NAA), total creatine (tCr), choline (Cho) and myo-inositol (mI). Results were compared with previously reported reproducibility measures from 1.5 T.

### **Results**

The coefficient of variation (CV) was  $\leq 1.6\%$  for T2,  $\leq 1.6\%$  for ADC, and  $\leq 5.3\%$ , for FA in the cerebrum. For metabolites the CV was  $\leq 8.0\%$  in the frontal lobe and  $\leq 20.4\%$  in the temporal lobe.

### **Conclusions**

The reproducibility of quantitative brain MR at 3.0 T is better than or at least comparable to the reproducibility at 1.5 T.

## Introduction

In quantitative magnetic resonance imaging (MRI) of the human brain, the measured magnetic resonance (MR) contrasts are converted into physical quantities with metrical units. Quantitative MR has already been shown to have great clinical utility in identifying age- and disease-related abnormalities at a regional and global brain level (Inglese et al., 2004). Unlike conventional structural MRI (i.e. T1 and T2 weighted imaging), used to visually detect abnormalities of brain tissue, quantitative MR techniques such as T2 relaxometry, diffusion tensor imaging (DTI), and proton MR spectroscopy ( $^1\text{H-MRS}$ ), may be more sensitive to micro-structural (T2, DTI) and metabolic changes ( $^1\text{H-MRS}$ ) in brain tissue. Therefore, quantitative MR provides the opportunity to investigate cerebral damage in various fundamentally different ways (Tofts, 2003). Moreover, as quantitative MR enable expressing contrast in terms of physical quantities, it is less susceptible to differences between MR methods from different vendors of MR systems (e.g. using different pulse sequences) and could therefore be applied to compare results across different MR systems or research institutes.

### T2 relaxometry

T2 relaxometry is a quantitative technique, which provides an objective measurement of tissue characteristics, as the T2 or transverse relaxation time is a physical property of the tissue, which mainly reflects the (relatively) free water content. Previous studies using voxelwise determination, or so-called mapping, of the T2 relaxation time in neurological diseases have demonstrated variations in T2 in a number of diseases (Larsson et al., 1989; Pitkanen et al., 1996). Abnormalities on T2 maps usually reflect altered water content, possibly associated with neuronal or axonal loss, gliosis, demyelination, and oedema. For example, in patients with epilepsy, the hippocampal T2 relaxation time is increased due to gliosis, compared with controls (Pitkanen et al., 1996). However, as oedema (e.g. due to seizures) is also associated with increased T2 values, an increase in T2 does not necessarily co-localize with the specific pathology (Katz et al., 1992). Furthermore, in acute multiple sclerosis (MS) lesions, T2 relaxation times initially increase as a result of inflammation and oedema. As the oedema resolves, but before significant demyelination and axonal loss occurs, values rapidly decrease (Larsson et al., 1989). It has also been shown that T2 relaxometry is more sensitive to detect pathology than visual assessment of T2 weighed images (Okujava et al., 2002).

### **Diffusion Tensor Imaging**

Diffusion Tensor Imaging (DTI) is a relatively new MR technique that allows the measurement of water self diffusivity (Schaefer et al., 2000). Since freedom of motion of water molecules is hindered by interactions with other molecules and cellular barriers, DTI abnormalities can reflect changes of tissue organization at the cellular level (e.g. increase of extra-cellular space due to cell death). These micro-structural changes affect the hindered motion of water molecules, and consequently alter the water diffusion properties and thus the MR signal. Apart from deriving a measure for the average molecular motion that is affected by cellular organization and integrity (Apparent Diffusion Coefficient, ADC), it is also possible to measure the degree of alignment of cellular structures within fiber tracts, as well as their structural integrity (fractional anisotropy, FA). For example in multiple sclerosis, white matter lesions are characterized by an increased diffusivity and a more isotropic diffusion, which is reflected by elevated ADC values, and decreased FA values, compared to healthy tissue, respectively (Castriota-Scanderbeg et al., 2003). It has recently been shown that the usage of a fractional anisotropy index as a single measure for the mean tissue anisotropy in certain brain regions of interest represents a robust and observer independent measure for the comparative assessment of white matter integrity (Deppe et al., 2007).

### **Spectroscopy**

<sup>1</sup>H-MR-Spectroscopy (<sup>1</sup>H-MRS) is a non-invasive analytical technique which enables quantification of in vivo metabolite concentrations in the brain, thus offering a window on cell metabolism (Ross et al., 2001). Four major metabolites that are commonly observed are: N-acetyl-aspartate (NAA), which is indicative of neuronal integrity, choline (cho), which can act as a malignancy marker, total creatine (tcr), indicative of the energy metabolism, and myo-inositol (ml), which functions as an osmolyte and is thought to indicate ongoing myelin damage (Govindaraju et al., 2000). Using chemical shift imaging (CSI), in which spectra are simultaneously recorded from multiple adjoining spatial regions (i.e. voxels), it is also possible to measure the distribution of metabolites throughout the brain (Brown et al., 1982). Techniques to determine the metabolite concentrations in metric units (mmol per kg wet weight), so-called absolute quantification, are currently available and can improve the diagnostic utility of <sup>1</sup>H-MRS procedures (Jansen et al., 2006).

### **Reproducibility**

It is important to study and report the reproducibility of quantitative MR methods, as changes associated with a certain pathology, progression of

disease, advancing age, or intervention can only be detected when the deviation from normal values are larger than the reproducibility of that particular measurement. Therefore, knowing the reproducibility limits in terms of physical quantities provides information to which extent measured tissue values can be classified as normal or abnormal. Reproducibility is defined as the extent to which repeated measurements on the same subject are in agreement (Tofts, 2003). In contrast to conventional structural imaging techniques, quantitative MR allows one to report the reproducibility in quantitative terms as well.

3.0 T clinical systems are currently commercially available, and seem to improve (quantitative) neuroradiological brain applications with respect to 1.5 T (Frayne et al., 2003; Sicotte et al., 2003; Biswas et al., 2005; Nielsen et al., 2006; Orbach et al., 2006). However, surprisingly little information regarding the reproducibility of several quantitative brain MR techniques is currently available. As most reproducibility studies of quantitative MR were performed at 1.5 T so far, we set out to assess the reproducibility of several distinct quantitative MR techniques of the brain on a clinical 3.0 T MR system. The MR research protocol used consisted of T2 relaxometry, DTI, and CSI. In this work, repeated measurements in 10 healthy volunteers were used to establish the reproducibility of the different quantitative MR techniques. To our knowledge, this is the first study to report these reproducibility measures for T2 relaxometry, DTI, and CSI at 3.0 T.

## Materials and Methods

### Subjects

Ten young healthy adults between 23 and 28 years of age (7 males, 3 females, mean age  $26 \pm 2$ ) were included. The volunteers were imaged on two separate days with a 3.0-Tesla whole-body unit (Philips Achieva [software release 1.5.4.0], Philips Medical Systems, Best, The Netherlands). Data acquisition was conducted within the guidelines of the local institutional review boards overseeing human research, and every study participant provided written informed consent. Image acquisition was conducted over a 2 month period, and scan sessions for every subject were separated by at most 29 days (mean period  $15 \pm 10$  days).

### Image acquisition

Each scan session consisted of an imaging part of 50 minutes (using an 8 channel receive-only head coil suitable for parallel imaging (sensitivity encoding (SENSE))) and a spectroscopy part of 40 minutes (using a quadrature

transmit receive head coil), which were separated by a break of 10 minutes. Total scan time was 90 minutes.

### **MR Imaging**

For every subject, the following images were acquired using the SENSE head coil. For anatomic reference, first a T1-weighted three-dimensional (3D) turbo field echo (TFE) was acquired with the following parameters: repetition time (TR) 9.91 ms, echo time (TE) 4.6 ms, inversion time (TI) 3 s, flip angle 8°, matrix 256x256x160, field of view (FOV) 256x256x160 mm<sup>3</sup>, 1 mm adjacent coronal slices, scan time 12 minutes. For T2 quantification a 3D dual-echo turbo spin echo (TSE-Dual) was performed, using the following parameters: TR 2500 ms, TE<sub>1</sub> 10 ms, TE<sub>2</sub> 110 ms, matrix 256x256x100, FOV 256x256x200 mm<sup>3</sup>, 2.0 mm adjacent coronal slices, acceleration (i.e. SENSE reduction) factor 1.5 in the left-right direction, k-space segmentation 6 shots per image, scan time 10 minutes. DTI images were obtained with a single shot echo planar imaging spin echo (EPI-SE) sequence, using the following parameters: b-values 0 and 800 s/mm<sup>2</sup>, TR 6600 ms, TE 62 ms, 15 gradient directions for diffusion sensitization (gradient overplus on), matrix 128x128x66, FOV 256x256x132 mm<sup>3</sup>, 2 mm adjacent transverse slices, acceleration factor 2.5 in the anterior-posterior direction, scan time 10 minutes.

### **Proton MR spectroscopic imaging**

The following measurements were acquired using a transmit receive head coil: For anatomical reference, a T1-weighted 3D turbo field echo (TFE) was performed with the following parameters: TR 9.3 ms, TE 4.6 ms, TI 3 s, flip angle 8°, matrix 256x256x60, FOV 256x256x120 mm<sup>3</sup>, 2 mm adjacent transverse slices, and k-space segmentation 200 shots per slice. Using the Multiplanar Reconstruction software available on the MRI scanner, the obtained transverse images were transformed into coronal and sagittal orientations to facilitate an optimal positioning of the spectroscopic imaging slices.

Two slices were selected for spectroscopic imaging, one accommodated in the temporal and one in the frontal lobe, respectively. The following parameters were used: 20x20 voxels per slice, FOV 256x256 mm<sup>2</sup>, slice thickness 20 mm, TR 2.0 s, TE 30 ms, a nominal voxel size of 3.3 ml, echo acquisition half echo, scan time 12 min per slice. Localization and water suppression was achieved with point-resolved spatially localized spectroscopy (PRESS) and chemical shift selective suppression (CHESS), respectively. Lipid signals from the skull base and from the retro-orbital space were eliminated by polygonal outer volume presaturation using 10 'multiple regional saturation technique' slabs of 5 cm thickness. Localized automated shimming was performed based on a B<sub>0</sub> map using first and second order shim corrections. The spectroscopic imaging slice

through the temporal lobe was selected angulated along the long anterior-posterior axis of the hippocampus, covering both hippocampi, extending from the anterior temporal lobe to the parieto-occipital sulcus (Figure 3.1a). The PRESS box size was chosen to obtain optimal water suppression in 8 x 6 voxels. The frontal slice was oriented just above both lateral ventricles, parallel to the line from the rostrum to the splenium of the corpus callosum, extending from the frontal lobe to the parieto-occipital sulcus (Figure 3.1b). Here the PRESS box was placed to yield 8 x 8 optimally water-suppressed voxels.

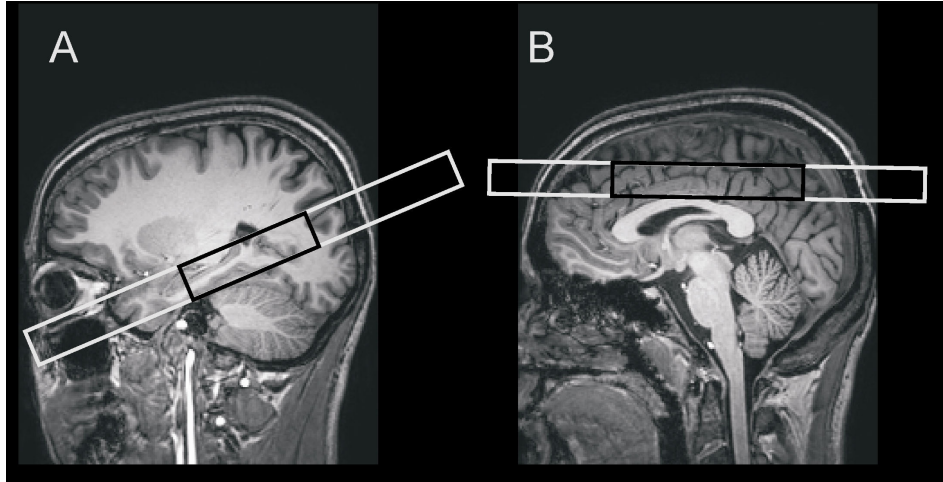


**Figure 3.1.** Orientation of the (A) temporal and (B) frontal spectroscopic imaging slice overlaid on sagittal T1-weighted images of the brain. The field of view and the PRESS box are indicated in white and black, respectively.

### Image analysis

Unless otherwise described, image processing was performed using customized software in Matlab (The Mathworks, Natick, MA, USA), based on SPM2 software routines (Wellcome Department of Cognitive Neurology, London, UK).

### T2 and cerebrospinal fluid quantification

*T*<sub>2</sub>. The *T*<sub>2</sub> was calculated (in ms) on a voxel-by-voxel basis using the signal intensities of the images obtained at the two echo times, using the following equation (Woermann et al., 1998):

$$T2 = \frac{TE_2 - TE_1}{\ln\left(\frac{SI_1}{SI_2}\right)} \quad [3.1]$$

Where  $TE_1$  is the first echo time of 22 ms, and  $TE_2$  is the second echo time of 110 ms,  $SI_1$  and  $SI_2$  are the signal intensities corresponding to  $TE_1$  and  $TE_2$ , respectively.

*Cerebrospinal fluid.* A percentile volume cerebrospinal fluid (CSF) map was calculated by attributing voxels individually to a CSF percentage ( $\lambda_{CSF}$ ) on a scale of 0-100 %. The  $\lambda_{CSF}$  was based on the T2 value of the voxel as calculated from the TSE-dual images. For this, the T2 relaxation rate (i.e.  $1/T2$ ) was assumed to be a fractional volume weighted sum of CSF ( $T2 > 2500$  ms) and uniform brain tissue ( $T2 < 110$  ms):  $1/T2 = \lambda_{CSF} / T2_{CSF} + (1 - \lambda_{CSF}) / T2_{tissue}$ . For large T2 values (i.e.  $T2 \geq 2500$  ms),  $\lambda_{CSF}$  was set to 100%. We were mainly interested in the reproducibility quantitative MR measures of tissue, therefore tissue was segmented from CSF by applying the threshold  $\lambda_{CSF} \leq 5\%$ . The T2-map was spatially transformed into common coordinates along with the spatial normalization procedure of the  $TE_2$  image into the standard brain space defined by the Montreal Neurological Institute (MNI) T2 template. This approach facilitated analysis of various separate brain regions through masks.

### ADC and FA quantification

The ADC and FA map were calculated using the diffusion software available on the MRI scanner. In short, using the averaged images acquired at  $b = 0$  and  $b = 800$  s/mm<sup>2</sup>, 15 images directional sensitive ADCs can be calculated, each being the sum of three elements of the diffusion tensor. The diffusion tensor was subsequently diagonalized, yielding eigenvalues  $\lambda_1$ ,  $\lambda_2$ , and  $\lambda_3$ , as well as eigenvectors that define the corresponding orthogonal diffusion directions. Based on the eigenvalues from the tensor, FA and mean ADC (i.e. the average ADC of the three eigenvalues) were calculated on a voxel-by-voxel basis, according to the following formulas:

$$\langle ADC \rangle = \sqrt[3]{\lambda_1 \cdot \lambda_2 \cdot \lambda_3} \text{ and}$$

$$FA = \sqrt{\frac{3}{2}} \sqrt{\frac{(\lambda_1 - \bar{\lambda})^2 + (\lambda_2 - \bar{\lambda})^2 + (\lambda_3 - \bar{\lambda})^2}{\lambda_1^2 + \lambda_2^2 + \lambda_3^2}} \quad [3.2]$$

$$\text{where } \bar{\lambda} = \frac{\lambda_1 + \lambda_2 + \lambda_3}{3}$$

FA was expressed as percent and ADC was expressed in units of  $10^{-6}$  mm<sup>2</sup>/s. The FA- and ADC-maps were spatially normalized along with the normalization procedure of the  $b=0$  image into the space defined by the MNI T2 template.

## Metabolite quantification

For both slices, the metabolite spectra within the PRESS box were analyzed using the LCModel software package (Version 6.1-4), which analyzes the in vivo MR spectra as a linear combination of the separately recorded in vitro spectra of the individual metabolites (Provencher, 1993). The metabolite basis set (PRESS, TE 30 ms, 3.0 T) was kindly provided by Dr. Provencher (Provencher, 1993). For absolute quantification, the calibration strategy based on the principle of reciprocity was used (Soher et al., 1996). In short, from the principle of reciprocity it can be deduced that for a combined transmit-receive coil the external voltage needed to produce a certain  $B_1$  field at a given location is inversely related to the voltage induced in the same RF-coil by a predefined  $B_1$  field. Practically, the coil loading of a certain subject in the coil is related to the intensity of a measured peak. Therefore the difference in the coil loading for each measurement for every subject can be corrected by using the 'relative coil load', a parameter that can be obtained for each experiment. The precise relationship between the 'relative coil load' and the signal intensity was assessed using phantom experiments of varying NaCl concentrations. Metabolite concentrations were corrected for cerebrospinal fluid (CSF) contribution, using the CSF-map calculated from the T2-map.

Of each spectrum, the parts per million (ppm) range included for analysis was 0.5-3.85 ppm. Although LCModel generates estimates for a total of 16 metabolites, only those for choline-containing compounds (Cho), total creatine (tCr), mI and NAA were subsequently used in the statistical analysis. The Cramer-Rao minimum variance was calculated as an estimate of the error in metabolite quantification. Metabolite estimates were excluded from analysis, if the Cramer-Rao minimum variance exceeded the 20% range. Furthermore, voxels were only included in the analysis procedure if at least 5 volunteers displayed reliable spectra in those voxels. Metabolite concentrations were determined in institutional units, but calibrated such, that the average NAA value was 9.6 mmol per kg wet weight, to allow comparison with other studies (Jansen et al., 2006).

## Accuracy

Accuracy, or systematic error, was assessed using phantoms at 25 °C and additional MR sequences, not using fast imaging principles, and therefore not suited for the clinical practice, but ideal for phantom experiments. For T2 and DTI, an one liter phantom containing an aqueous 0.2 mM  $MnCl_2$  solution was examined using the standard protocol, extended (using the same geometry) with a spin echo (SE) experiment using 6 echoes (echo times: 30, 60, 90, 120, 150, and 180 ms) for T2 quantification (scan time: 150 minutes), and a DTI SE experiment using 30 gradient directions for diffusion sensitization (gradient overplus off) and 3 b-values (0, 1000, and 2000  $s/mm^2$ , scan time: 300 minutes).



The T2 map was calculated using a nonlinear monoexponential fit, whereas the ADC and FA map were calculated using the MR diffusion software at the scanner. For analysis, a region of interest (ROI) was positioned within the phantom of approximately  $4 \times 4 \times 2 \text{ cm}^3$  on the calculated T2-, ADC- and FA-map. Statistics (mean and SD) were derived from the values within the ROI. For spectroscopy, an 0.5 l phantom containing 10.0 mM NAA, 7.0 mM tCr, 4.9 mM mL, and 1.9 Cho (phosphate buffer, pH = 7.2, 0.2 mM  $\text{MnCl}_2$  for T1 shortening) was placed in transmit receive head coil together with a one liter saline bottle for approximate load matching, and examined using the standard CSI sequence.

### Statistical analysis

Statistical calculations were performed in SPSS 12.0.1 (SPSS Inc., Chicago, IL). Descriptive statistical analysis of the T2-, ADC-, and FA-maps was performed on various cerebral regions, using masks created with WFU-Pickatlas (Maldjian et al., 2003). Investigated regions in the cerebrum were the frontal and temporal lobe, and the entire cerebrum. To enable comparison with previous reproducibility studies on 1.5 T, we derived descriptive statistics in two different manners.

- (i) Median method. For each mask (for the T2-, ADC-, and FA-maps) and slice (for the spectroscopy), the median value was chosen to represent all voxels within that region, and used to derive descriptive statistics of that region.
- (ii) Voxel-wise method. Descriptive statistics were derived on a voxel-by-voxel basis, and then summarized per region by calculating the median.

Among several statistical methods available to define the precision of a measurement technique, the coefficient of variation (CV), the repeatability coefficient (RC) and the intraclass correlation coefficient (ICC) were chosen as measures of precision.

**CV.** Following the methods of Bland and Altman, the CV was estimated by calculating the overall mean within-subject standard deviation ( $SD_{ws}$ ) of a given measurement and dividing it by the mean measurement value for all subjects (Bland et al., 1986; Bland et al., 1996). However, the CV has major limitations as a measure of precision, the most important of which is the dependence on the magnitude of the measured value. Therefore, a single value for CV not necessarily describes the true precision.

**RC.** The RC is defined as  $1.95 * \sqrt{2} * SD_{ws}$ , and provides an indication of the minimum detectable biological difference (Bland et al., 1986; Bland et al., 1996). The difference between two measurements for the same subject is expected to be less than the RC in 95% of observations. The assumptions inherent in the RC are that there should be no systematic bias

between replicated measurements and no relation between the  $SD_{ws}$  of the replicated measurements and the mean. These assumptions were checked using a one sample t-test, and by calculating the rank correlation coefficient (Kendall's tau), respectively.

**ICC.** An intraclass correlation coefficient was calculated, using a one-way random model. The ICC considers both the within-subject variance arising from measurement error (plus any biological variation over time), and variance arising from the difference between subjects (Tofts, 2003), according to  $ICC = SD_{bs}^2 / (SD_{bs}^2 + SD_{ws}^2)$ , where  $SD_{bs}$  represents between-subjects standard deviation. The ICC can be thought of as being the fraction of the total variance that is attributed to true biological variation instead of measurement error.

The reproducibility values; CV, RC and ICC, include changes resulting from repositioning and real biological changes during the time between two scans.

To correct for not perfectly matched voxels between the two scan sessions, due to variability in the outcomes of the normalization procedure, the T2-, ADC-, and FA-maps were smoothed using a Gaussian kernel with a full width half maximum (FWHM) value of 6 mm data for visualization and descriptive statistics. This is in agreement with clinical practice, where a neuroradiologist does not examine brain images on a pixel level, but rather on a pixel cluster level. To illustrate the effect of smoothing, the T2 map of one volunteer was smoothed using FWHM values of 0, 6, and 10 mm. To visualize which regions of the brain display the worst reproducibility, the CV was calculated on a voxel-by-voxel basis for each MR contrast.

## Results

### Quality

Visual inspection of all T2-, ADC- and FA maps did not reveal substantial image artifacts; therefore we were confident that the obtained maps were of good quality. For the CSI, out of a total of 480 voxels from the temporal slice of all volunteers, 155 voxels were rejected based on their too high Cramer-Rao minimum variance estimate for NAA (for at least one session). For the frontal slice, 79 out of a total of 640 voxels were discarded.

### Accuracy

Using the TSE-Dual sequence an average T2 of  $42.0 \pm 0.8$  ms was obtained for the 0.2 mM  $MnCl_2$  phantom, whereas the SE sequence with six echoes yielded  $40.9 \pm 0.4$  ms (in accordance with T2 values of 0.2 mM  $MnCl_2$  described by Tofts (Tofts, 2003)), a small difference of less than 3%. The standard DTI-TSE sequence yielded an average ADC of  $2200 \pm 40 \cdot 10^{-6}$  mm<sup>2</sup>/s (in accordance with

ADC values of water at 25 °C, as described by de Graaf (De Graaf, 1998)), whereas the DTI-SE with three b values sequence yielded  $2270 \pm 40 \cdot 10^{-6} \text{ mm}^2/\text{s}$ , a difference of 3%. For FA, the DTI-TSE sequence yielded  $5 \pm 2\%$  for the DTI-TSE and  $4 \pm 2\%$  for the DTI-SE experiment (close to 0%, as one does not expect anisotropy in a homogeneous aqueous phantom). The obtained concentrations from the phantom CSI experiment were 10.3, 7.1, 5.4, and 1.9 mM for NAA, tCr, mI, and Cho, respectively. This yields a difference of less than 3% for NAA, tCr, and Cho. The difference for mI was 10%, which can be explained by the relative low intensity of mI peaks. As most quantitative measurements did not reveal a systematic bias larger than 3%, we are confident of the validity of the quantitative methods applied.

Figure 3.2 A-C,E-H illustrate the agreement of the quantitative measurements within the frontal lobe, obtained from one subject in two separate scan sessions, through scatter plots for the T2, ADC, FA, NAA, tCr, Cho, and mI values. Furthermore, in Figure 3.2D the effect of smoothing data on a T2-map using various Gaussian kernel sizes (0, 6, and 10 mm) is shown. With increasing smoothness, the whole distribution shifts to somewhat higher T2 values, and the distribution of voxels becomes narrower.

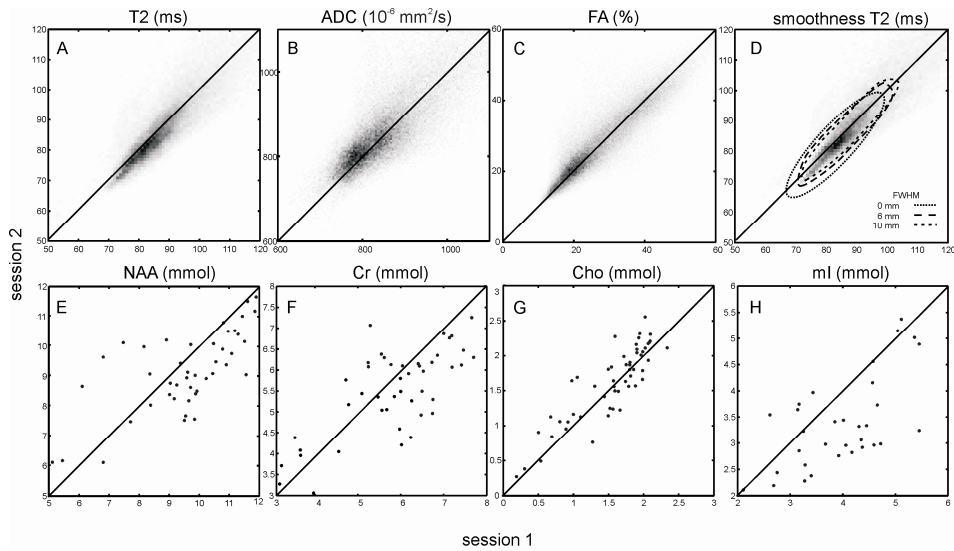


**Figure 3.2.** Scatter plots of the (A) T2, (B) ADC, (C) FA, (E) NAA, (F) tCr, (G) Cho, and (H) mI values within the frontal lobe, obtained from one subject at 2 separate scan sessions. (D) The effect of smoothing the T2 data using a Gaussian kernel with different full width half maximum (FWHM) values. Overlaid on a scatter plot from T2 data smoothed with a FWHM of 10 mm, are dotted lines that illustrate the approximate 95% confidence interval regions, for a FWHM of 0, 6, and 10 mm, respectively.

**Table 3.1.** Descriptive statistics of reproducibility measures, derived from median values per region

Technique	Measured quantity	Cerebral region	Average median session 1*	Average median session 2*	CV (%)	RC*	ICC
TSE-Dual	T2	Frontal	83.2	82.2	1.6	3.7	0.27
		Temporal	84.0	85.1	1.1	2.6	0.70
		Cerebrum	84.1	83.5	1.1	2.6	0.48
DTI	ADC	Frontal	820	816	1.6	36	0.74
		Temporal	840	834	1.5	35	0.73
		Cerebrum	827	825	1.4	32	0.74
	FA	Frontal	34.6	35.5	3.7	3.6	0.68
		Temporal	29.6	31.4	5.3	4.5	0.46
		Cerebrum	31.8	32.8	3.0	2.7	0.73
CSI	NAA	Frontal	11.5	10.9	8.0	2.5	0.28
		Temporal	8.9	9.4	7.5	1.9	0.44
	tCr	Frontal	7.0	6.7	7.4	1.4	0.51
		Temporal	5.9	6.3	7.6	1.3	0.49
	Cho	Frontal	1.9	1.9	7.0	0.4	0.35
		Temporal	1.6	1.6	12.6	0.6	0.00
	mI	Frontal	3.9	3.6	7.8	0.8	0.55
		Temporal	4.3	4.1	20.4	2.4	0.52

Note-

CV indicates coefficient of variation, RC, repeatability coefficient, ICC, intraclass correlation coefficient, TSE-Dual, dual-echo turbo spin echo, DTI, diffusion tensor imaging, CSI, chemical shift imaging, T2, transverse relaxation time (ms), ADC, apparent diffusion coefficient ( $10^{-6}$  mm<sup>2</sup>/s), FA, fractional anisotropy (%), NAA, N-acetyl-aspartate, tCr, total creatine, Cho, choline-containing compounds, mI, myo-inositol, (all in mmol per kg wet weight).

\* in units of the MR measured quantity.

Table 3.1 and 3.2 display the reproducibility characteristics for each quantitative measure using the ‘median method’ and the ‘voxel-wise method’, respectively. Included in the table are the mean values per session, the CV, the RC and the ICC. For all modalities, the values measured per session were not significantly different (one sample t-test,  $P > 0.1$ ), and no relation between the  $SD_{ws}$  of the replicated measurements and the mean was observed (Kendall’s tau  $< 0.6$ ,  $P > 0.06$ , i.e. no significant bias). For all measured quantities, the obtained values lie within the expected range as measured in previous studies at 3.0T. The average T2 within the cerebrum for white and gray matter combined was 78-84 ms, which is in accordance with the T2s derived by Stanisiz et al. of 69 and 99 ms for white matter and gray matter, respectively (Stanisiz et al., 2005). The average ADC and FA values measured within the cerebrum were 786-827  $\cdot 10^{-6}$  mm<sup>2</sup>/s and 31.8-37.9%, respectively, which was in agreement with values obtained from the thalamus by Huisman and coworkers, who found 717  $\cdot 10^{-6}$  mm<sup>2</sup>/s and 33.3%, respectively (Huisman et al., 2006). Values for NAA, tCr, Cho and mI were 8.8-11.5, 6.0-7.0, 1.6-1.9, and 3.7-4.3 mmol per kg wet

weight, in accordance with values from reference (Jansen et al., 2006), that describes 9.6, 7.0, 1.8, and 5.3 mmol per kg wet weight, respectively (note that the average NAA concentration was set to 9.6 mmol per kg wet weight).

**Table 3.2.** Descriptive statistics of reproducibility measures, derived on a voxel-wise basis, and averaged per region.

Technique	Measured quantity	Cerebral region	Average median session 1*	Average median session 2*	CV (%)	RC*	ICC
TSE-Dual	T2	Frontal	79.0	77.5	3.9	8.5	0.59
		Temporal	78.6	80.2	4.7	10.4	0.61
		Cerebrum	79.4	78.3	4.3	9.5	0.56
DTI	ADC	Frontal	784	781	3.2	69	0.70
		Temporal	800	804	3.5	78	0.75
		Cerebrum	786	786	3.4	74	0.73
	FA	Frontal	38.3	39.0	6.4	6.9	0.75
		Temporal	35.2	35.7	6.7	6.6	0.86
		Cerebrum	37.4	37.9	6.5	6.7	0.80
CSI	NAA	Frontal	11.5	11.0	13.8	4.1	0.28
		Temporal	8.8	9.4	16.1	4.2	0.19
	tCr	Frontal	7.0	6.7	14.3	2.8	0.28
		Temporal	6.0	6.3	18.9	3.1	0.04
	Cho	Frontal	1.9	1.9	13.8	0.8	0.26
		Temporal	1.6	1.6	27.3	1.1	0.00
	mI	Frontal	3.9	3.7	17.2	1.9	0.18
		Temporal	4.3	4.1	30.4	3.8	0.18

Note-

See Table 3.1

### Descriptive statistics for reproducibility

The median method yielded CVs of  $\leq 1.6\%$  for T2,  $\leq 1.6\%$  for ADC, and  $\leq 5.3\%$ , for FA in the cerebral cortex. For metabolites the CV was  $\leq 8.0\%$  for the metabolites in the frontal lobe and  $\leq 20.4\%$  in the temporal lobe. The CVs for the metabolites in the frontal lobe were highly similar, whereas the CVs for the temporal lobe range from 7.5%(NAA)-20.4%(mI).

The CVs as calculated through the voxelwise method were approximately 2 times higher than those from the median method. The ICCs for the T2-, ADC- and FA-maps lie within the range from 0.27 to 0.74. The ICCs for the metabolites were worse and ranged from 0.00 to 0.55. The ICCs for the voxelwise method were comparable or better for the T2-, ADC- and FA-maps, but worse for the metabolites, compared with the median method.

### Regions with unfavorable reproducibility characteristics.

In Figure 3.3A-C, the areas that display high CV values for the T2, ADC and FA measures are projected on a transverse T1-weighted slice. It is important to note that for these figures, no voxels were excluded based on high  $\lambda_{\text{CSF}}$  values, otherwise all non-highlighted voxels might have an ambiguous origin, since either their CV values could be low, or their  $\lambda_{\text{CSF}}$  could be too high.

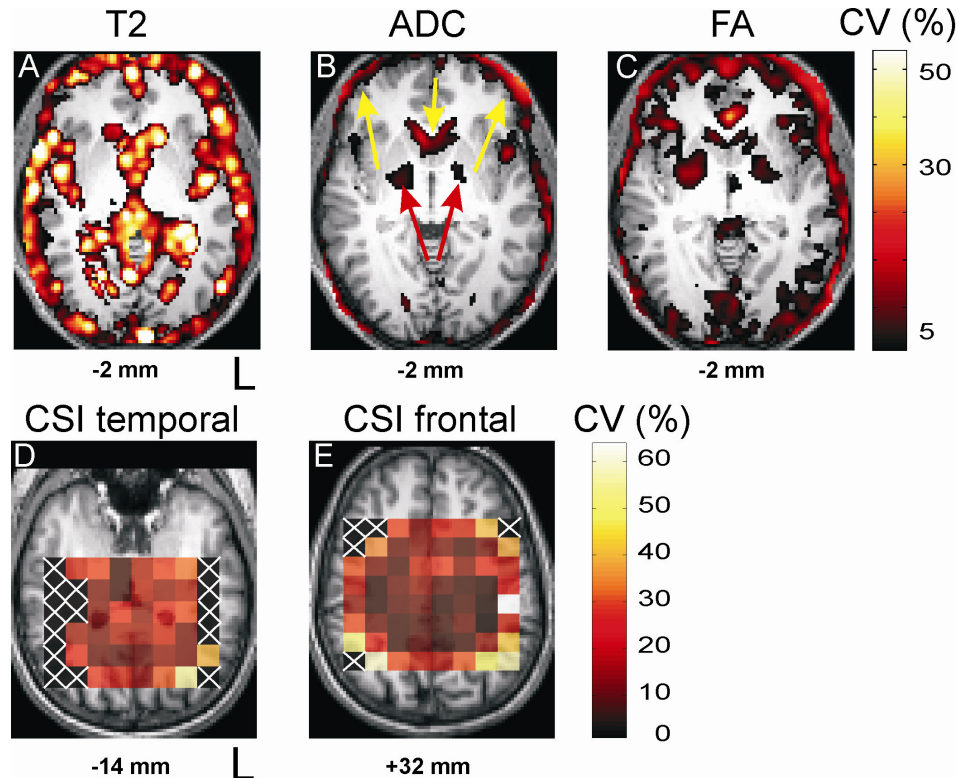


**Figure 3.3.** Regions with unfavorable reproducibility characteristics, expressed using their coefficient of variation (CV). For the (A) T2, (B) ADC, and (C) FA, voxels with a CV > 10% are overlaid on transverse T1-weighted images of the brain. A description of the arrows can be found in the text. (D) and (E) display for all voxels the CV characteristics of the NAA quantification in the temporal and frontal slice, respectively. Voxels that did not fulfill the quality control criteria are marked with white crosses.

Slice positions are given in approximate stereotaxic Talairach z-coordinates.

Several regions display less favorable reproducibility characteristics (expressed by high CV values). Most of these regions (indicated with yellow arrows in Figure 3.3B) display a large variability in CSF content (e.g. near the dorsal horn of the lateral ventricle). The areas (indicated with red arrows in Figure 3.3B) that display less favorable reproducibility characteristics, which are

not related to different CSF contributions, are part of the basal ganglia, anterior to the thalamus, which includes the head of the caudate nucleus, the putamen, and the internal capsule. The amount of voxels with a high CV value increases from ADC, FA to T2. In Figure 3.3D and 3E the CV per voxel is visualized overlaid on oblique transverse T1-weighted images, for the temporal and frontal slice, respectively. Voxels with less favorable reproducibility characteristics, expressed either by high CV values, or low quality characteristics (indicated by white crosses), for both slices were found lateral, close to the skull.

## Discussion

In this study, the reproducibility was assessed of three different quantitative brain MR techniques at 3.0 T, namely T2 relaxometry, Diffusion Tensor Imaging, and Spectroscopic imaging. The CV observed in the cerebrum was  $\leq 1.6\%$  for T2,  $\leq 1.6\%$  for ADC, and  $\leq 5.3\%$ , for FA. In the frontal lobe the CV for metabolites was  $\leq 8.0\%$  and  $\leq 20.4\%$  in the temporal lobe.

### Regional differences

For the T2-, ADC-, and FA-maps, there were no obvious differences in reproducibility characteristics between the selected regions. The most notable differences in reproducibility between regions were observed in the CSI experiment, where the frontal lobe displayed far better characteristics than the temporal lobe. The selected slice in the temporal lobe is close to the tissue-bone interface and air cavities near the skull base. This causes an increased B0 inhomogeneity, which complicates shimming and water suppression, leading to a decreased quality of spectra. As nearly all of the lateral voxels within the temporal slice did not fulfill the quality control criteria (see Figure 3.3D), it might be better to decrease the size of the PRESS box (e.g. to 6 x 6 voxels), in order to improve the quality of the other voxels.

As the total area of metabolites with the largest peaks in the  $^1\text{H}$  MR spectra generally can be estimated most accurately, it is not surprising that NAA, tCr and Cho, that all have a prominent peak, display smaller CV values than mI, which has only small peaks. Furthermore, the fitting of the mI peaks, in contrast to the other peaks, is hampered by the variability of the baseline in close proximity to the peak from residual water.

### Unfavorable regions

The voxels that have large CV values for the T2-map (Figure 3.3A) all have (partial) contribution from the CSF. As the dual spin echo technique used to obtain T2-maps was specifically aimed at determining reliable T2 values for

cerebral tissue, the TE values (22 and 110 ms) used are rather short compared to the T2 relaxation time of CSF (>2500 ms). To determine an appropriate estimate of the T2 for CSF would require longer echo times, and preferably more than just two echoes. Therefore the calculated T2 of CSF containing voxels is inaccurate, which results in high CV values for those voxels. The ADC (Figure 3.3B) and FA (Figure 3.3B) display similar regions with high CV values. The brain regions close to the CSF spaces (i.e. ventricles and pericortex) display large CV values due to the highly variable size of CSF containing compartments throughout the volunteer population. This was confirmed by high between-subject variance in these regions (data not shown).

A reason for the fact that the part of the basal ganglia, which is not close to CSF spaces, also displays high CV values, might be explained by the high levels of iron within the basal ganglia (Brooks et al., 1989). At 3.0 T these iron deposits lead to substantial magnetic susceptibility artifacts, which influence the quality of T2-weighted images in these regions. Therefore, as both the DTI and dual spin echo technique yield T2-weighted images, the reproducibility in the iron rich basal ganglia is weak. This was confirmed by high within-subject variance in these regions and by a visual assessment of the non-normalized images (data not shown). This is important to consider when the region of interest investigated for a certain pathology lies within the basal ganglia.

### Smoothing

The appearance of the T2 scatter plot (Figure 3.2D) changes with increasing smoothing parameters in two ways: (i) it shifts towards higher T2 values, and (ii) it has a more narrow distribution. These effects can be explained as follows:

Since smoothing mixes the values of spatially nearby voxels, the resulting values are a combination of the original value and a certain contribution of nearby voxels. The general increase of tissue T2 values is due to the influence of spatially nearby CSF voxels, which have high T2 values. Due to smoothing, voxel values furthermore were averaged in a weighted manner, which narrows the distribution of the voxel values (i.e. spatial noise suppression).

### Comparisons with reproducibility studies at 1.5 T

Most reproducibility studies were performed on 1.5 T. The majority of the measured variation is of biological origin (due to the differences between subjects), and will be present at any field strength. The stability at 3.0 T is likely to improve slightly, as instrumental contributions to the variations are compensated by a higher signal-to-noise ratio and smaller voxel sizes. Furthermore, spectroscopic quantification might benefit from an increase in chemical shift dispersion. However, due to increased magnetic field (B0 and B1) inhomogeneities within the tissue spectral linewidths increase. Therefore, there



might not be a substantial gain in spectral resolution as theoretically might be expected (Ugurbil et al., 2003).

Okujava and coworkers (Okujava et al., 2002) investigated the reproducibility of T2-maps obtained from fast spin dual echo measurements in five healthy volunteers, who were imaged twice at 1.5 T. Their ROI included the hippocampus, and statistics were derived from the average T2 values within the ROI. They reported results in coefficients of reliability, that correspond to  $2 \times CV$  values. The CV for the temporal region, calculated from the reported coefficient of reliability, was 1.8%. The CV we determined for the temporal region was 1.1%. Larsson et al (Larsson et al., 1992) determined RCs for a ROI in the frontal white matter in T2 maps obtained with a multi echo sequence of 15 echoes, in 10 patients with MS scanned twice at 1.5 T. The RC in frontal white matter was 18 ms. We determined a RC within the frontal region of 3.7 ms. Therefore, regarding T2 measurements on healthy young volunteers, 3.0 T seems better than (or at least as good as) 1.5 T.

A study with healthy subjects that investigated the reproducibility of the trace of the diffusion tensor (trace is approximately  $3 \times ADC$ ) and FA values, was performed by Pfefferbaum et al (Pfefferbaum et al., 2003). Ten healthy volunteers were imaged twice on 1.5 T (single shot EPI, matrix 128x128, 4 mm slice thickness, 6 diffusion-sensitizing directions). A single region analysis of the corpus callosum revealed a CV of 2.6% and 1.9% for the trace and FA, respectively. As we found 1.4% and 3.0% for ADC and FA, respectively, the reproducibility of DTI at 3.0 T is comparable to 1.5 T. They also reported voxel-by-voxel analysis results of the whole cerebrum, which yielded a CV of 0.9% for the trace value and 1.2% and for the FA value. Unfortunately it is not clear what exact procedure was used to generate the latter statistics, therefore a comparison with our results remains difficult.

A few studies have reported descriptive reproducibility statistics of CSI measurements with short spin echo times. Chard et al (Chard et al., 2002) examined the CV of the relevant metabolites on one subject that underwent a total of nine scan sessions at 1.5T (TR 3.0 s, TE 30 ms, a nominal voxel size of 2.3 ml). They reported a CV of 11.4% for NAA, 9.9 % for Cr, 12.3 % for Cho, and 18.5 % for mI. Wiedermann and coworkers (Wiedermann et al., 2001) determined the reproducibility of multi-slice CSI in 10 healthy subjects, scanned twice at 1.5T (TR 1.8 s, TE 25 ms, a nominal voxel size of 0.9 ml). In frontal gray matter, they observed a CV of 11%, 12%, 27%, and 23% for NAA, tCr, Cho and mI, respectively. Also included were ICC values: 0.91, 0.91, <0.50, and 0.61 for NAA, tCr, Cho and mI, respectively.

In the frontal lobe, we report CVs of 8%, 7.5%, 7%, and 8% for NAA, tCr, Cho and mI, respectively. Although the CVs we found for all metabolites are more favorable, the ICC values look worse.

In summary, the reproducibility at 3.0 T, as expressed through the CV or the RC, seems to be better than (or at least similar to) the reproducibility at 1.5 T, as determined by other groups. For CSI the ICC seems to be weaker, but it is important to note that due to the homogeneous nature of the group of volunteers group in the current study, the ICC for all quantitative measures is relatively low, compared to a heterogeneous population of patients with degenerative brain disorders. In a patient population, the ICC is expected to be higher than observed in this study, as the variation in measured values in such patients will be larger. Furthermore, when diagnosing individual patients, who are expected to have only a subtle MR visible response to a certain treatment, the most important parameter is the repeatability (derived from the within-subject standard deviation), as this is the smallest biological change that can reliably be detected. Here the ICC might have little value. Therefore, in clinical studies, inter-hemispheric comparisons are often made to determine cerebral pathology, which could be a particularly useful solution for methods that display large between-subject variability.

To attribute the observed differences in reproducibility purely to the different field strength is not correct. There are several methodological differences related to the acquisition techniques and the statistical methods used between the reproducibility studies at 1.5 T and our study at 3.0T. For example, for the CSI measurement, the following pulse sequence characteristics are very important: echo time, voxel volume, localization scheme, and acquisition time. Therefore these results should be considered in light of the different techniques and the different statistical methods used to derive descriptive statistics. In order to explore this issue further, both techniques should have to be compared using the same statistical analysis.

#### **Different methods to calculate descriptive statistics**

Most studies on reproducibility did not describe in detail how the descriptive statistical analyses were performed, but most likely, the 'median method' was used. In this method, for each region, the median value is used to derive descriptive statistics of that region. The alternative is the voxel-wise method, where descriptive statistics are obtained on a voxel-by-voxel basis and then summarized per region by calculating the median. The median method generally yields better CVs and reproducibility coefficients. However, it is questionable whether this method yields accurate descriptive statistics for one region, as the spatial resolution of the acquired data is decreased drastically by taking only one value to represent a certain region. Moreover, neuroradiologists analyse brain images of patients with potential pathologies by scanning for abnormalities on a pixel (or pixel cluster) level, and compare each 'spot' with the surrounding or contralateral tissue. Analogous to the median method, in that case the neuroradiologist would only include average (or median) values

for whole regions to assess the manifestation of pathology within that region. Therefore it is better to use the voxel-wise method, as the spatial resolution of the method is preserved throughout the calculation procedure, and it gives a better estimate of the reproducibility on a small scale.

### **Comparison with epilepsy pathology**

To illustrate the applicability of the current reproducibility results, we related the CVs and RCs derived using the voxelwise method from our work to 'pathological' values associated with epilepsy from the literature. An increase of 20 ms for the T2 was observed at 3.0 T by Briellmann et al (Briellmann et al., 2004) in the hippocampus ipsilateral to the seizure focus in patients with refractory epilepsy, compared with healthy volunteers. The RC of the T2 of the temporal region for our study was 10.4 ms, thus the T2 difference should be easily detected in single patients with the T2 relaxometry method at 3.0 T we used. Kimiwada and coworkers (Kimiwada et al., 2006) reported from a 1.5T study that the FA values are 9% lower in the hippocampus for children with partial epilepsy, compared with healthy children. Furthermore, ADC values were increased with  $80 \cdot 10^{-6} \text{ mm}^2/\text{s}$ , though not significantly. We found RCs within the temporal lobe of  $78 \cdot 10^{-6} \text{ mm}^2/\text{s}$  and 6.6% for ADC and FA, respectively. This suggests that at 3.0T the ADC results could have been significant. Capizzano et al. observed at 1.5 T a decrease of 27.3% and 18.5% of NAA concentration in the hippocampus ipsilateral and contralateral, respectively, of patients with epilepsy compared with a healthy control group (Capizzano et al., 2002). As we found a CV of 16.1% for NAA in the temporal region, both differences should be detected reliably at 3.0 T. Since the response to (drug) treatment in neurological diseases such as epilepsy may be rather subtle, one can only speculate whether the obtained reproducibility characteristics (despite the general improvement with respect to 1.5 T) are sufficient for adequate treatment monitoring.

### **Conclusion**

Despite increased magnetic field inhomogeneities within the tissue at 3.0 T, the reproducibility of quantitative brain MR at 3.0 T seems to be better than or at least comparable to the reproducibility at 1.5 T, as determined by other groups.

## References

- Biswas, J., Nelson, C.B., Runge, V.M., et al., 2005. Brain tumor enhancement in magnetic resonance imaging: comparison of signal-to-noise ratio (SNR) and contrast-to-noise ratio (CNR) at 1.5 versus 3 tesla. *Invest Radiol* 40, 792-797.
- Bland, J.M., Altman, D.G., 1986. Statistical methods for assessing agreement between two methods of clinical measurement. *Lancet* 1, 307-310.
- Bland, J.M., Altman, D.G., 1996. Measurement error. *Bmj* 313, 744.
- Briellmann, R.S., Syngneniotis, A., Fleming, S., et al., 2004. Increased anterior temporal lobe T2 times in cases of hippocampal sclerosis: a multi-echo T2 relaxometry study at 3 T. *AJNR Am J Neuroradiol* 25, 389-394.
- Brooks, D.J., Luthert, P., Gadian, D., et al., 1989. Does signal-attenuation on high-field T2-weighted MRI of the brain reflect regional cerebral iron deposition? Observations on the relationship between regional cerebral water proton T2 values and iron levels. *J Neurol Neurosurg Psychiatry* 52, 108-111.
- Brown, T.R., Kincaid, B.M., Ugurbil, K., 1982. NMR chemical shift imaging in three dimensions. *Proc Natl Acad Sci U S A* 79, 3523-3526.
- Capizzano, A.A., Vermathen, P., Laxer, K.D., et al., 2002. Multisection proton MR spectroscopy for mesial temporal lobe epilepsy. *AJNR Am J Neuroradiol* 23, 1359-1368.
- Castriota-Scanderbeg, A., Fasano, F., Hagberg, G., et al., 2003. Coefficient D(av) is more sensitive than fractional anisotropy in monitoring progression of irreversible tissue damage in focal nonactive multiple sclerosis lesions. *AJNR Am J Neuroradiol* 24, 663-670.
- Chard, D.T., McLean, M.A., Parker, G.J., et al., 2002. Reproducibility of in vivo metabolite quantification with proton magnetic resonance spectroscopic imaging. *J Magn Reson Imaging* 15, 219-225.
- De Graaf, R.A. (1998) *In vivo NMR spectroscopy: principles and techniques*, Chichester; New York, Wiley.
- Deppe, M., Duning, T., Mohammadi, S., et al., 2007. Diffusion-Tensor Imaging at 3T: Detection of White Matter Alterations in Neurological Patients on the Basis of Normal Values. *Invest Radiol* 42, xxx-xxx.
- Frayne, R., Goodyear, B.G., Dickhoff, P., et al., 2003. Magnetic resonance imaging at 3.0 Tesla: challenges and advantages in clinical neurological imaging. *Invest Radiol* 38, 385-402.
- Govindaraju, V., Young, K., Maudsley, A.A., 2000. Proton NMR chemical shifts and coupling constants for brain metabolites. *NMR Biomed* 13, 129-153.
- Huisman, T.A., Loenneker, T., Barta, G., et al., 2006. Quantitative diffusion tensor MR imaging of the brain: field strength related variance of apparent diffusion coefficient (ADC) and fractional anisotropy (FA) scalars. *Eur Radiol* 16, 1651-1658.
- Inglese, M., Ge, Y., 2004. Quantitative MRI: hidden age-related changes in brain tissue. *Top Magn Reson Imaging* 15, 355-363.
- Jansen, J.F., Backes, W.H., Nicolay, K., et al., 2006. <sup>1</sup>H MR spectroscopy of the brain: absolute quantification of metabolites. *Radiology* 240, 318-332.
- Katz, A., Marks, D., Spencer, S., 1992. Focal brain MRI findings: transient signal changes secondary to seizures. *Neurology* 42, 206.
- Kimiwada, T., Juhasz, C., Makki, M., et al., 2006. Hippocampal and thalamic diffusion abnormalities in children with temporal lobe epilepsy. *Epilepsia* 47, 167-175.
- Larsson, H.B., Christiansen, P., Zeeberg, I., et al., 1992. In vivo evaluation of the reproducibility of T1 and T2 measured in the brain of patients with multiple sclerosis. *Magn Reson Imaging* 10, 579-584.

- Larsson, H.B., Frederiksen, J., Petersen, J., et al., 1989. Assessment of demyelination, edema, and gliosis by in vivo determination of T1 and T2 in the brain of patients with acute attack of multiple sclerosis. *Magn Reson Med* 11, 337-348.
- Maldjian, J.A., Laurienti, P.J., Kraft, R.A., et al., 2003. An automated method for neuroanatomic and cytoarchitectonic atlas-based interrogation of fMRI data sets. *Neuroimage* 19, 1233-1239.
- Nielsen, K., Rostrup, E., Frederiksen, J.L., et al., 2006. Magnetic resonance imaging at 3.0 tesla detects more lesions in acute optic neuritis than at 1.5 tesla. *Invest Radiol* 41, 76-82.
- Okujava, M., Schulz, R., Ebner, A., et al., 2002. Measurement of temporal lobe T2 relaxation times using a routine diagnostic MR imaging protocol in epilepsy. *Epilepsy Res* 48, 131-142.
- Orbach, D.B., Wu, C., Law, M., et al., 2006. Comparing real-world advantages for the clinical neuroradiologist between a high field (3 T), a phased array (1.5 T) vs. a single-channel 1.5-T MR system. *J Magn Reson Imaging* 24, 16-24.
- Pfefferbaum, A., Adalsteinsson, E., Sullivan, E.V., 2003. Replicability of diffusion tensor imaging measurements of fractional anisotropy and trace in brain. *J Magn Reson Imaging* 18, 427-433.
- Pitkanen, A., Laakso, M., Kalviainen, R., et al., 1996. Severity of hippocampal atrophy correlates with the prolongation of MRI T2 relaxation time in temporal lobe epilepsy but not in Alzheimer's disease. *Neurology* 46, 1724-1730.
- Provencher, S.W., 1993. Estimation of metabolite concentrations from localized in vivo proton NMR spectra. *Magn Reson Med* 30, 672-679.
- Ross, B., Bluml, S., 2001. Magnetic resonance spectroscopy of the human brain. *Anat Rec* 265, 54-84.
- Schaefer, P.W., Grant, P.E., Gonzalez, R.G., 2000. Diffusion-weighted MR imaging of the brain. *Radiology* 217, 331-345.
- Sicotte, N.L., Voskuhl, R.R., Bouvier, S., et al., 2003. Comparison of multiple sclerosis lesions at 1.5 and 3.0 Tesla. *Invest Radiol* 38, 423-427.
- Soher, B.J., van Zijl, P.C., Duyn, J.H., et al., 1996. Quantitative proton MR spectroscopic imaging of the human brain. *Magn Reson Med* 35, 356-363.
- Stanisz, G.J., Odobina, E.E., Pun, J., et al., 2005. T1, T2 relaxation and magnetization transfer in tissue at 3T. *Magn Reson Med* 54, 507-512.
- Tofts, P. (2003) *Quantitative MRI of the brain measuring changes caused by disease*, Chichester, West Sussex; Hoboken, N.J., John Wiley & Sons Ltd.
- Ugurbil, K., Adriany, G., Andersen, P., et al., 2003. Ultrahigh field magnetic resonance imaging and spectroscopy. *Magn Reson Imaging* 21, 1263-1281.
- Wiedermann, D., Schuff, N., Matson, G.B., et al., 2001. Short echo time multislice proton magnetic resonance spectroscopic imaging in human brain: metabolite distributions and reliability. *Magn Reson Imaging* 19, 1073-1080.
- Woermann, F.G., Barker, G.J., Birnie, K.D., et al., 1998. Regional changes in hippocampal T2 relaxation and volume: a quantitative magnetic resonance imaging study of hippocampal sclerosis. *J Neurol Neurosurg Psychiatry* 65, 656-664.

# Chapter 4

**Enhanced signal detection in  
neuroimaging by means of regional  
control of the global false discovery rate**

**Langers DRM, Jansen JFA, and Backes WH**

*Provisionally accepted by Neuroimage*

## Abstract

In the context of neuroimaging experiments, it is essential to account for the multiple comparisons problem when thresholding statistical mappings. Various methods are in use to deal with this issue, but they differ in their signal detection power for small- and large-scale effects. In this paper we comprehensively describe a new method that is based on control of the false discovery rate (FDR). Our method increases sensitivity by exploiting the spatially clustered nature of neuroimaging effects. This is achieved by using a sliding window technique, in which FDR-control is first applied at a regional level. Thus, a new statistical map that is related to the regionally achieved FDR is derived from the available voxelwise  $P$ -values. On the basis of receiver operating characteristic (ROC) curves, thresholding based on this map is demonstrated to have better discriminatory power than conventional thresholding based on  $P$ -values. Secondly, it is shown that the resulting maps can be thresholded at a level that results in control of the global FDR. By means of statistical arguments and numerical simulations under widely varying conditions, our method is validated, characterized, and compared to some other common voxel-based methods (uncorrected thresholding, Bonferroni correction, and conventional FDR-control). It is found that our method shows considerably higher sensitivity as compared to conventional FDR-control, while still controlling the achieved FDR at the same level or better. Finally, our method is applied to two diverse neuroimaging experiments to assess its practical merits, resulting in substantial improvements as compared to the other methods.

## Introduction

In neuroimaging studies, it is often desirable to reveal and map structural or functional characteristics of the brain on a detailed scale. This generally means that analyses are carried out at the level of individual volume elements (voxels). However, because the total number of considered voxels is usually enormous, the use of common statistical thresholds to assess the significance of effects in individual voxels would result in an unacceptably large number of voxels for which the null-hypothesis, that no effects are present, is falsely rejected (i.e., the number of false positive voxels). For instance, using a threshold  $p = 0.05$ , a significant effect would be detected on average in fifty voxels for every thousand voxels in the volume of interest, even if no effect is truly present in any voxel. Because the number of voxels that has to be taken into consideration can run into the hundreds of thousands, the amount of false positives could easily outnumber the amount of true positives, and results would be largely based on chance. Therefore, the use of such simple statistical tests is generally unacceptable.

This ‘multiple comparisons problem’ can be remedied by the use of a stricter statistical threshold. As a result, the proportion of voxels for which an effect is falsely detected is reduced, increasing the specificity and the reliability of the results. However, an inevitable disadvantage is that the probability for the detection of voxels with true effects will also decrease, thus reducing the sensitivity of the analysis. In literature, various methods have been proposed to find a compromise in this situation, by optimizing signal detection while still controlling some measure for the error rate (Logan et al., 2004).

A common method is to adjust the threshold such that the probability for the presence of any false positives in the entire volume (the familywise error rate, FWE) is kept below some upper limit  $\alpha$  (Nichols et al., 2003). A distinction can be made between methods with weak and strong error control. For weak error control, the chance of falsely rejecting one or more null-hypotheses is bounded by a specified level  $\alpha$  if the null-hypothesis holds *everywhere*; for strong error control, the chance of falsely rejecting one or more null-hypotheses is bounded by a specified level  $\alpha$  for *any subset* of the voxels for which the null-hypothesis holds. The essential difference is that methods with strong control have the ability to localize effects, while methods with weak control only assess if effects are present anywhere in the volume.

A simple and common approach that provides strong control of the FWE is offered by the Bonferroni correction: if tests are performed on a large number  $N$  of voxels, an FWE bound  $\alpha$  can be achieved for the entire volume by applying a stricter threshold  $p = \alpha/N$  to each individual voxel. However, the Bonferroni correction is quite stringent and often considered too conservative. Better methods have been described (Holm, 1979; Hochberg, 1988), but analyses on neuroimaging data usually benefit little from such improvements because of the



large proportion of voxels without significant effects. Also, in practice, spatial correlations may exist between neighboring voxels, requiring the use of more refined techniques like Gaussian field theory or resampling methods in order to make accurate statistical inferences (Nichols et al., 2003; Worsley, 2005).

Some alternative methods are also based on FWE-based error control, but test the significance of effects in clusters or regions of interest as a whole instead of in individual voxels. Because this reduces the total number of tests, and because neuroimaging effects are usually clustered in nature, such cluster- and set-level inferences are generally more powerful than voxel-level inferences. However, such inferences are less regionally specific because they cannot be made at the level of individual voxels and only apply to an entire cluster or set of clusters. Various methods have been proposed that compromise between sensitivity and regional specificity in different ways (Worsley et al., 1995; Friston et al., 1996; Poline et al., 1997; Heller et al., 2006), some of which offer the potential to detect both weak but extensive diffuse effects and strong but confined focal effects at the same time.

A completely different approach to error control in neuroimaging experiments is provided by relatively new developments that are not based on FWE, but that limit the false discovery rate (FDR) (Benjamini et al., 1995; Genovese et al., 2002; Laird et al., 2005; Singh et al., 2006). The FDR is the proportion of incorrect rejections of the null-hypothesis among the total number of rejections, or in other words the proportion of false positives among all the positives. This error measure addresses the issue that it is often permissible for the null-hypothesis to be falsely rejected in some voxels, as long as these constitute a negligible fraction in comparison with the total number of voxels for which the null-hypothesis is rejected. This is for instance the case if one is interested in large-scale spatial patterns in the brain, or if summary values are calculated over the detected regions (e.g., the mean level, spatial extent, or lateralization index of neural effects).

FDR-controlling procedures are claimed to be more powerful, and FDR-control has been predicted to overtake FWE-control as the most common measure to limit the number of false positives (Nichols et al., 2003). Current FDR-related methods can be advantageous over FWE-related methods especially if true positive regions comprise many voxels and constitute a notable proportion of the total volume of interest. In such cases, a fair number of false positives can be allowed without much affecting the overall outcome, leading to tolerant statistical thresholds and improved sensitivity.

In this paper we present an extension to Benjamini's FDR-controlling method that is based on regional analyses to exploit the generally clustered nature of true neuroimaging effects. Our method will be substantiated and validated, and we will show that our method usually results in better sensitivity than Benjamini's original method while it is still possible to achieve identical

global control of the FDR. In particular, our method provides enhanced sensitivity to large brain volumes with weak effects while still imposing strong thresholds on small isolated foci, similar to cluster- and set-level inferences in FWE-related methods. Our method will be tested and compared to other commonly used methods using numerical simulations. Furthermore, to assess the practical feasibility and benefits, the new method will be applied to two distinct neuroimaging experiments that employ diffusion weighted imaging (DWI) and functional magnetic resonance imaging (fMRI) to focus on local structural and functional changes in the brain, respectively.

## Theory

In this paper, an uppercase notation (i.e.,  $P$  and  $Q$ ) will be used to denote statistics that are attained in individual voxels, while a lowercase notation (i.e.,  $p$  and  $q$ ) will be used to indicate the thresholds that are imposed on the corresponding maps. Furthermore, regarding FDR-control, an explicit distinction will be made between global and regional bounds by means of subscripts (i.e.,  $q_{\text{global}}$  and  $q_{\text{regional}}$ ).

### False discovery rate

The FDR is defined as the proportion of false positives ( $N_{\text{FP}}$ ) among the total number of positives ( $N_{\text{P}}$ ),

$$\text{FDR} \equiv \frac{N_{\text{FP}}}{N_{\text{P}}}. \quad [4.1]$$

Of course, in practice it is unknown which positives are false and which are true. Nevertheless, in a seminal paper (Benjamini et al., 1995), an elegant procedure was demonstrated (henceforth referred to as B-H FDR-control) that controls the globally attained FDR in the sense that its expectation value will lie below some upper limit  $q_{\text{global}}$  that can be freely specified beforehand ( $0.0 < q_{\text{global}} < 1.0$ ). Note that the FDR may exceed  $q_{\text{global}}$  in some actual realization of an experiment, but averaged over many experiments it will be bounded by  $q_{\text{global}}$ .

The probability that a certain experimental outcome is expected to occur by chance, given the null-hypothesis that no effects are truly present, is conventionally denoted by  $P$ . If  $P$  is sufficiently small, the null-hypothesis is rejected.  $P$ -values are assumed to be derived from experimental neuroimaging data for all voxels individually (e.g., by Student's  $T$ -tests, ANOVA Chi-square tests, permutation tests, etc.). For a total of  $N$  voxels being tested, B-H FDR-control starts by ordering the  $P$ -values of all voxels from smallest to largest

$$0 < P_1 \leq P_2 \leq \dots \leq P_i \leq \dots \leq P_N < 1, \quad [4.2]$$

and by determining the voxel with the largest (sorted) index  $i$  for which

$$P_i \cdot N \leq q_{\text{global}} \cdot i. \quad [4.3]$$

The method prescribes that the value  $P_i$  should be used to threshold all  $P$ -value data (i.e.,  $p = P_i$ ) in order to obtain an FDR that is bounded by  $q_{\text{global}}$  on average. The procedure is illustrated graphically in Figure 4.3.1a by plotting the left and right hand sides of the inequality in Eq. 4.3 as a function of  $i$  (Genovese et al., 2002).

The meaning of Eq. 4.3 can be understood intuitively. Its left hand side ( $P_i \cdot N$ ) provides an estimate of the number of false positives that would occur if the null-hypothesis actually holds for all  $N$  voxels and if the value  $P_i$  is used as the statistical threshold. The right hand side ( $q_{\text{global}} \cdot i$ ) represents the number of false positive voxels that we are willing to tolerate, since there are  $i$  voxels that will be declared significant because their  $P$ -values do not exceed  $P_i$ , and a fraction  $q_{\text{global}}$  of this total number of positives is allowed to be false. Eq. 4.3 thus succinctly expresses that the expected number of false positives should not exceed a fraction  $q_{\text{global}}$  of the total number of positives. While this requirement can potentially be satisfied by a range of values  $P_i$ , the procedure aims at finding the most tolerant threshold (i.e., the largest  $P_i$ ) that still does.

Actually, it has been shown that Eq. 4.3 holds only under some restrictive technical conditions. In order to achieve general validity, a multiplicative constant that depends on  $N$  can be introduced in Eq. 4.3. Because the mentioned conditions are reasonably satisfied for neuroimaging data (Genovese et al., 2002), this factor will be ignored in this paper.

### Regional FDR-control

The described procedure has the disadvantage that the resulting threshold  $p$  on the map of  $P$ -values quickly tends to become stricter if the spatial region under consideration is enlarged (i.e., if extra voxels for which the null-hypothesis is valid are added to the analysis). As more voxels without true effects are included, there is more potential for false positives to arise while the number of true positives does not increase. Consequently, thresholds need to be chosen more strictly to guarantee the expected FDR to lie below the desired  $q_{\text{global}}$ . Therefore, the method will become less sensitive.

In practice, neural effects will be clustered in certain brain regions. Although statistically justifiable, it seems somewhat unreasonable that such regions should become less detectable if other remote and potentially irrelevant brain areas are included into the analysis. This problem may potentially be overcome by subdividing the entire brain volume into a number of regions, and by applying B-H FDR-control to each such region separately. By choosing the size of the regions smaller than the size of the entire volume of interest, the sensitivity can be enhanced. Also, the analysis can be extended to larger portions of the brain without decreasing sensitivity, by increasing the number of regions but not their size.

When the entire volume is parceled into adjacent non-overlapping regions, artifacts can arise along their boundaries. Because in each region a different threshold  $p$  will be employed, the detected clusters might be clipped along these boundaries and would no longer accurately represent the actual shape of true positive regions. To overcome this, a ‘sliding window’ or ‘searchlight’ technique may be used (Kriegeskorte et al., 2006). For each voxel, an individual threshold is determined by applying the B-H FDR-controlling procedure to a suitable region centered on the voxel, and only the centered voxel is thresholded at the resulting threshold  $p$ . For other voxels, other surrounding regions are taken into account, although they may partially overlap.

The method can be further generalized to not just include all voxels in a discrete region centered on the voxel and exclude all voxels outside this region, but to allow for a continuous weighting to be applied to all surrounding voxels. Hence, voxels that are close to the voxel under consideration will strongly affect the calculation of its threshold, while distant voxels will have a smaller effect. For that purpose, a weight  $w_{jk}$  can be assigned to any voxel  $k$  relative to the centered voxel of interest  $j$  (the indices  $k$  and  $j$  are uniquely defined by the sorting of  $P$ -values according to Eq. 4.2). Without loss of generality, we will assume that the weights  $w_{jk}$  are normalized such that  $w_{jj} = 1$ . We suggest to use unit-amplitude weighting functions that monotonically decrease to zero as a function of the Euclidean distance between pairs of voxels (e.g., a Gaussian).

Modifying Eq. 4.3 in straightforward fashion to accommodate these voxel-dependent weights, the largest index  $i$  should now be determined for which

$$P_i \cdot \sum_{k=1}^N w_{jk} \leq q_{\text{regional}} \cdot \sum_{k=1}^i w_{jk} . \quad [4.4]$$

The above equation is equivalent to Eq. 4.3 if  $w_{jk} = 1$  for all voxels  $k$  inside the region surrounding the voxel of interest  $j$ , and  $w_{jk} = 0$  for all voxels outside this region. However, Eq. 4.4 offers the additional possibility to use continuously valued weightings. This should further reduce discretization artifacts as a result of the choice of the shape of the region.

Because the threshold that is derived from Eq. 4.4 is used for assessing the significance of effects in one voxel only (namely, the centered voxel of interest  $j$ ), the algorithm can be reformulated in a more convenient way. The range of values of  $q_{\text{regional}}$  for which the null-hypothesis can be rejected in the centered voxel  $j$ , is that for which

$$q_{\text{regional}} \geq Q_j \equiv \min_{i \geq j} \frac{P_i \cdot \sum_{k=1}^N w_{jk}}{\sum_{k=1}^i w_{jk}} . \quad [4.5]$$

The notation  $Q_j$  is introduced for this critical value for  $q_{\text{regional}}$  because it is an experimentally derived voxel-dependent statistic. In other words, the null-hypothesis is rejected for a voxel  $j$  if and only if  $Q_j$ , as calculated for that particular voxel according to the above equation, does not exceed the imposed regional FDR threshold  $q_{\text{regional}}$ . The role of  $Q_j$  with respect to  $q_{\text{regional}}$  is comparable to the role of  $P_j$  with respect to the  $P$ -value threshold  $p$ . By formulating the criterion in terms of a threshold for  $Q_j$ , computations need only be carried out a single time. Once the  $Q$ -value map is known, the presence of effects can easily be determined in all voxels for any bound on the regional FDR that is desired.

If the calculated  $Q$ -values of all voxels are ordered from smallest to largest

$$0 < Q_1 \leq Q_2 \leq \dots \leq Q_m \leq \dots \leq Q_N < 1, \quad [4.6]$$

then the number of detected positives  $N_P$  will equal the value of the largest index  $m$  for which  $Q_m$  does not exceed  $q_{\text{regional}}$ .

### Global FDR-control

Since B-H FDR-control bounds the average FDR below the level  $q_{\text{regional}}$  in all individual regions, it results in a regional type of error control, which may be difficult to interpret. Because in practice it is often desirable to control an error measure for the entire volume of interest, the correspondingly achieved global FDR needs to be estimated. In our approach, we will first estimate the global FDR in the two limiting cases where true positives are either [i] densely distributed throughout the entire volume, or [ii] absent or sparse. Next, the resulting expressions will be combined to obtain a more general formula.

*Case [i].* If true positives are dense, most regions can be expected to contain true positives. Since the expected regional density of false positives on average nowhere exceeds a fraction  $q_{\text{regional}}$  of the regional density of all positives, as guaranteed by the B-H FDR-controlling procedure, also the total number of false positives in the entire volume should not exceed a fraction  $q_{\text{regional}}$  of the total number of positives. As a first approximation, this suggests that regional error control automatically implies global error control in this case.

In practice, performance may be affected by edge effects. True positives that are located in the center of the imaging volume are included in the regional FDR analysis of many surrounding voxels, and therefore will induce the detection of false positives in many regional applications of the B-H FDR-controlling procedure. Contrariwise, true positive voxels near the edge of the imaging volume will contribute to fewer regions, and will therefore result in less additional false positives in the entire volume. As a result, the achieved global FDR can exceed the desired bound if the density of true positives is larger in the center of the imaging volume than at the edges. This can be corrected for by suitably weighting individual positives according to the

volume of the surrounding regions. As explained in more detail in Appendix I, this results in an estimated number of false positives in the entire volume according to

$$N_{\text{FP}} \leq \sum_{j=1}^N \frac{q_{\text{regional}} \cdot \sum_{k=1}^{N_p} w_{jk}}{\sum_{k=1}^N w_{jk}}. \quad [4.7]$$

Here, summations are carried out according to the index ordering in Eq. 4.6, and  $N_p$  equals the known number of positive voxels for which  $Q_m$  is smaller than  $q_{\text{regional}}$ .

*Case [ii].* The validity of Eq. 4.7 breaks up if the null hypothesis is valid for all voxels, and true effects are absent. Since B-H FDR-control displays weak error control, the probability of finding false positives in any particular single region will not exceed the imposed threshold  $q_{\text{regional}}$ . Yet, because typically there are many independent regions, the chances of finding false positives anywhere in the entire volume may become much larger than  $q_{\text{regional}}$ . In other words, a multiple comparisons correction needs to be performed on the basis of the effective number of independent regions.

In appendix II it is substantiated that, if the null hypothesis is valid for all voxels, the average total number of false positives in the entire volume can be approximated by

$$N_{\text{FP}} \leq \frac{q_{\text{regional}}}{1 - q_{\text{regional}}} \cdot \sum_{j=1}^N \frac{\frac{1}{2} + \frac{1}{2} \sum_{k \in C_j} w_{jk}}{\sum_{k=1}^N w_{jk}}. \quad [4.8]$$

This equation takes the smoothness of the data into account by means of the summation in the numerator that is restricted to a correlated element  $C_j$  ('corel'). We define the corel of a centered voxel  $j$  as the equivalent surrounding volume of voxels for which the signal is correlated with the centered voxel (e.g., due to smoothing). This resembles the concept of a 'resel' which arises in Gaussian field theory. Inside such a corel, the statistical  $P$ -value and  $Q$ -value maps vary smoothly. In this paper,  $C_j$  will be identified with a sphere that is centered on the voxel  $j$ , with a diameter that equals the full width at half maximum (FWHM) of the point spread function of the data.

*Combined cases [i] & [ii].* If true positives are distributed throughout the volume, Eq. 4.7 will approximate the number of false positives. If no true positives are present in the volume, Eq. 4.7 underestimates the number of false positives, but Eq. 4.8 should be used. In practice, true positives will usually be present in only some of the regions. As a result, an intermediate number of false

positives will usually be present. In any case, the total number of false positives will be smaller than the sum of both expressions.

$$N_{\text{FP}} \leq q_{\text{regional}} \cdot \sum_{j=1}^N \frac{1}{1 - q_{\text{regional}} \left( \frac{1}{2} + \frac{1}{2} \sum_{k \in C_j} w_{jk} \right) + \sum_{k=1}^{N_P} w_{jk}}. \quad [4.9]$$

If  $q_{\text{regional}}$  is chosen equal to  $Q_m$  (for some  $m$ ), then it follows from Eq. 4.6 that the number of positives  $N_P$  will equal  $m$ . The requirement that the number of false positives (bounded according to Eq. 4.9) should not exceed a fraction  $q_{\text{global}}$  of the total number of positives that is actually found, will now be met if

$$Q_m \cdot \sum_{j=1}^N \frac{1}{1 - Q_m \left( \frac{1}{2} + \frac{1}{2} \sum_{k \in C_j} w_{jk} \right) + \sum_{k=1}^m w_{jk}} \leq q_{\text{global}} \cdot m. \quad [4.10]$$

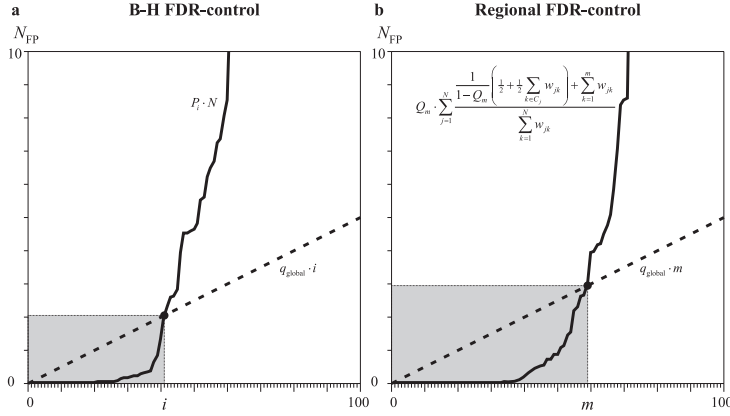


**Figure 4.1.** FDR-control. Exemplary plots were derived from a single numerical simulation with default parameters ( $N = 9216$ ,  $q_{\text{global}} = 0.05$ ; see Materials and Methods), and are shown for (a) B-H FDR-control, and (b) regional FDR-control. The estimated number of false positives ( $N_{\text{FP}}$ ) is plotted as a function of the index  $i$  or  $m$  (solid line; see the left hand sides of Eqs. 3 & 10, respectively). The line through the origin with slope  $q_{\text{global}}$  represents the maximum acceptable number of false positives (dashed line; see the right hand sides of Eqs. 3 & 10, respectively). The thresholding level follows from the largest index  $i$  or  $m$  for which the estimated number of false positives does not exceed the maximum acceptable number. Null-hypotheses are rejected for tests whose  $P$ - or  $Q$ -values are at or below this threshold. In the figure, this corresponds with the voxels for which the data points lie in the grayed area to the lower left of the intersection of the curves. Typically, less voxels with significant effects can be detected by means of B-H FDR-control than by means of regional FDR-control (41 and 59, respectively, in this example). At the same time, the global FDR is bounded at the same level.

This daunting inequality can now be used to determine a suitable threshold that will control the global FDR below a desired level  $q_{\text{global}}$ . Similar to the role of Eq. 4.3 in B-H FDR-control, the largest  $m$  should be determined for which Eq. 4.10 holds, and the corresponding value  $Q_m$  should be used to threshold the  $Q$ -value mapping that was derived from Eq. 4.5. The procedure is illustrated graphically in Figure 4.1b by plotting the left and right hand sides of the inequality in Eq. 4.10 as a function of  $m$ . The appearance and interpretation of this figure is highly similar to that of Figure 4.1a.

In summary, our proposed method firstly comprises the calculation of voxelwise  $Q$ -values according to Eq. 4.5, on the basis of the attained  $P$ -values for the individual voxels and a weighting function  $w_{jk}$  for pairs of voxels. Secondly, the presence of significant effects can be determined while controlling the global FDR by thresholding these  $Q$ -values at a level that is derived from Eq. 4.10.

In the Supplementary Materials, an implementation of the complete procedure is provided in the MatLab language (The MathWorks Inc.). Since the method uses only basic arithmetic functions and sorting, it should be straightforward to port the procedure to any other preferred programming language or data processing environment.

## Materials and Methods

### Simulations

Numerical simulations with artificially generated neuroimaging data were performed in the MatLab programming environment while varying a number of configuration parameters, to assess the validity and test the performance of our proposed method in a controlled manner, and to compare its results with those of some frequently used other voxel-based methods.

A 3D data matrix was filled with normally distributed pseudo-random noise. The default dimensions of the volume were  $24 \times 24 \times 16$ . To model spatial correlations, the noise was smoothed by convolution with an isotropic Gaussian kernel. The kernel function's default FWHM was infinitesimal, effectively performing no smoothing by default. A constant signal was added to a centrally positioned block of voxels with default dimensions  $4 \times 4 \times 4$ . The ratio of the signal magnitude to the standard deviation of the noise in the image (i.e., the signal-to-noise ratio, SNR) equaled 4.0 by default. Next, two-tailed  $P$ -values were calculated for each voxel on the basis of normal distribution statistics, and the corresponding  $Q$ -value maps were derived using Eq. 4.5.

Receiver operating characteristic (ROC) curves were determined by varying the thresholds for the  $P$ - and  $Q$ -value maps in the range 0.0-1.0. All simulation parameters were set to their default values, except for the SNR,



which was varied from 1.0 to 4.0. Per SNR setting, simulations were repeated 100 times, and the results were averaged.

Four methods were used to threshold the simulation outcomes and determine which voxels contained significant signal: [i] uncorrected  $P$ -value thresholding, [ii] Bonferroni-corrected FWE-control (Nichols et al., 2003), [iii] B-H FDR-control (Benjamini et al., 1995), and [iv] regional FDR-control (this paper). Default thresholds were set at  $p = 0.05$  (for uncorrected thresholding and FWE-control) and  $q_{\text{global}} = 0.05$  (for B-H and regional FDR-control).

Simulation parameters that were varied included the dimensions of the entire volume (range:  $12 \times 12 \times 8$  to  $48 \times 48 \times 32$ ), the FWHM of the noise smoothing kernel (range: infinitesimal to 4.0), the size of the central signal block (range:  $0 \times 0 \times 0$  to  $16 \times 16 \times 16$ ), the SNR in the block (range: 2.0 to 6.0), and the thresholds  $p$  and  $q_{\text{global}}$  (range: 0.01 to 0.20). For regional FDR-control, the default weighting function  $w_{jk}$  was a Gaussian function centered on the voxel of interest with an isotropic FWHM size of 4.0 voxels. Additional simulations were performed with alternative isotropic functions, with profiles that were either uniform or according to a parabolic Welch window. The FWHM size of the regional weighting function was varied from infinitesimally small to infinitely large.

Per setting, simulations were repeated 500 times. The four methods' average sensitivities (SEN), specificities (SPE), familywise error (FWE) rates, and global false discovery rates (FDR) were determined.

### Experiment I (DWI)

Thirteen healthy subjects (aged 23-57 years, median 26) and one patient with epilepsy (female, 25 y, cryptogenic localization-related epilepsy, right frontal focus) were included. Whole cerebrum imaging was performed with a clinical 1.5-T MRI system (Philips Intera, Philips Medical Systems), which was equipped with a standard quadrupolar head receiver coil. The protocol included a 3D  $T_1$ -weighted fast field-echo sequence (TR 11 ms, TE 3.5 ms, flip angle  $90^\circ$ , matrix  $256 \times 256$ , 150 contiguous slices,  $3.5 \times 3.5 \times 3.5$  mm<sup>3</sup> sized voxels), a dual-echo turbo spin echo sequence (TR 5211 ms, TE 11.9 ms/80 ms, matrix  $256 \times 256$ , FOV  $204 \times 112$  mm<sup>2</sup>), a diffusion weighted multi-shot echo-planar imaging (EPI) sequence (EPI-factor 31,  $b$ -values 0/400/800/1200 s/mm<sup>2</sup>, 3 orthogonal diffusion sensitizing directions, TR 2 cardiac cycles, TE 76 ms, matrix  $128 \times 128$ , FOV  $230 \times 230$  mm<sup>2</sup>,  $1.8 \times 1.8 \times 6.0$  mm<sup>3</sup> sized voxels).

All images were co-registered and spatially normalized to Talairach space (dimension  $79 \times 95 \times 69$ ,  $2 \times 2 \times 2$  mm<sup>3</sup> sized voxels) using the SPM2 software package (Wellcome Department of Cognitive Neurology). Volume maps of the apparent diffusion coefficient (ADC) were calculated by second order polynomial fitting of the direction averaged logarithmic signal intensities versus  $b$ -values. ADC maps were smoothed with a 5-mm Gaussian kernel. Mean and standard deviation ADC maps were calculated for the healthy

subject group. The preprocessed ADC data from the epilepsy patient and the entire group of healthy subjects were analyzed using a  $T$ -test model (Rugg-Gunn et al., 2001). The statistical comparisons were performed on a voxel-by-voxel basis, resulting in a statistical  $T$ -value map for the patient from which  $p$ -values were obtained for each voxel. For our thresholding method based on regional FDR-control, the weighting function  $w$  consisted of an isotropic Gaussian function with a FWHM of 20 mm.

### Experiment II (fMRI)

A functional MRI study was performed to measure the brain response to broadband auditory stimuli as a function of sound level in a subject with normal hearing. Scans were performed using a clinical 1.5-T MRI system (Philips Intera, Philips Medical Systems). Functional image volumes were acquired that covered the superior surfaces of both temporal lobes, and consisted of a dynamic series of 2.5-s single-shot  $T_2^*$ -sensitive EPI sequences with twelve 2.0-mm thick adjacent slices (TR 10 s; TE 50 ms; flip angle 90°; matrix 192×192; field of view 192×192 mm<sup>2</sup>). Six functional runs were performed, each consisting of 32 scans. A sparse scanning paradigm was used to reduce the influence of acoustic scanner noise (Hall et al., 1999). The stimuli were 2.0 s in duration and consisted of pink noise or dynamic rippled noise (Langers et al., 2003). Stimuli were presented in pairs in the silent interval between consecutive scans. The stimuli in each pair randomly differed by 3 dB in intensity, with an average intensity that was a multiple of 10 dB above the auditory threshold in a range of 0-70 dB. The subject was instructed to indicate which stimulus appeared loudest by pressing fiber-optic buttons that were held in both hands.

In the image analysis we made use of pre-processing routines from the SPM2 software package (Wellcome Department of Cognitive Neurology). The functional image volumes were realigned using 3D rigid body transformations to correct for motion effects. To improve signal-to-noise characteristics, spatial smoothing was performed using an isotropic 5-mm Gaussian kernel. For each of the functional runs, linear drifts of the scanner baseline signal were removed. Regression was performed using a general linear model that contained the intensity of the presented stimuli as a covariate to determine the rate of fMRI signal increase as a function of sound level for each voxel. The significance of effects was determined using Student's  $T$ -test statistic. The resulting statistical parametric mapping (SPM) listed  $p$ -values for all voxels and was used as input for the various thresholding methods. For our thresholding method based on regional FDR-control, the weighting functions  $w_{jk}$  consisted of isotropic Gaussian functions with a FWHM of 20 mm.

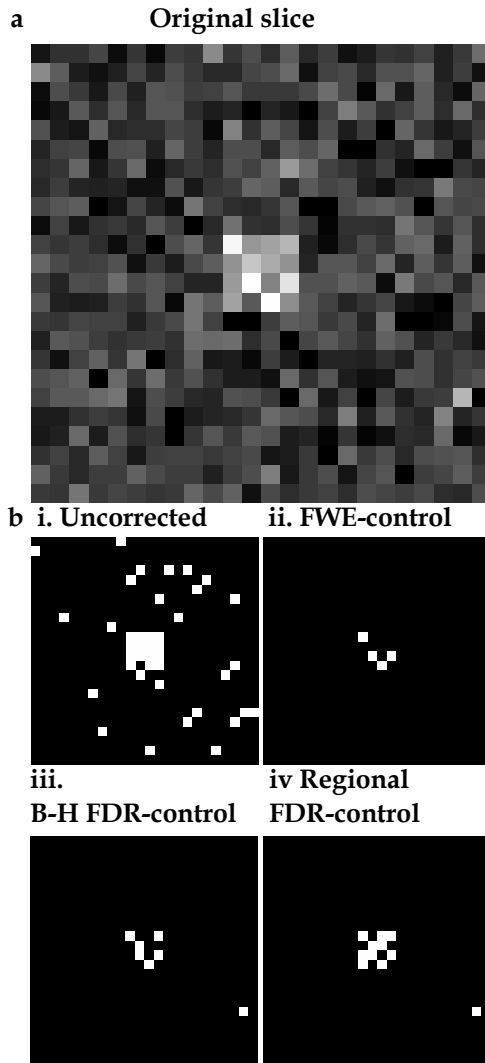


**Figure 4.2.** Simulation results. Numerical simulations were used to evaluate the performance of four thresholding methods. (a) Neuroimaging data were simulated by filling a 3D matrix with normally distributed random noise, in addition to a signal offset in a central block-shaped area (outlined). In this figure, the resulting signals in a single central slice of data are depicted using a gray value color scale. Two-tailed statistical  $P$ -values were derived that were subsequently used as input for the thresholding methods. (b) Voxels with significant effects according to the four methods are displayed in white. Using uncorrected thresholding at  $p = 0.05$ , most of the signal in the central area could be detected, but many false positives occurred outside this area. FWE-control by means of Bonferroni correction prevented the false positives from occurring at the expense of a large decrease in sensitivity. B-H FDR-control detected an intermediate number of active voxels, at the cost of a small number of false positives. Regional FDR-control achieved a similar FDR, but was able to detect a larger number of voxels with true effects.

## Results

### Simulations

Figure 4.2 illustrates simulated data using default parameter settings, along with the results that were obtained using the four different thresholding methods. Figure 4.2a displays the simulated signal in a single slice, consisting of normally distributed noise in the entire image in addition to a constant signal that is confined to the outlined central square area. In Figure 4.2b the voxels in this slice that are assessed to contain significant effects according to various

methods are highlighted. By thresholding the  $P$ -values of individual voxels at an uncorrected significance level of  $p = 0.05$ , the majority of the truly positive voxels in the central block are detected. However, a large proportion of the surrounding voxels is falsely detected as well. As a result, the false positives outnumber the true positives. By using FWE-control, the threshold is lowered such that false positives typically do not occur, at the cost of a significantly decreased sensitivity to effects inside the central block. Using this method, all positives are true, but the majority of the voxels with effects remain undetected. B-H FDR-control is able to detect an intermediate number of true positives. Although some false positives occur as well, their number is limited as compared to the total number of positives. Finally, our method based on regional FDR-control detects more true positives than B-H FDR-control, while the FDR that is achieved is similar (or better).

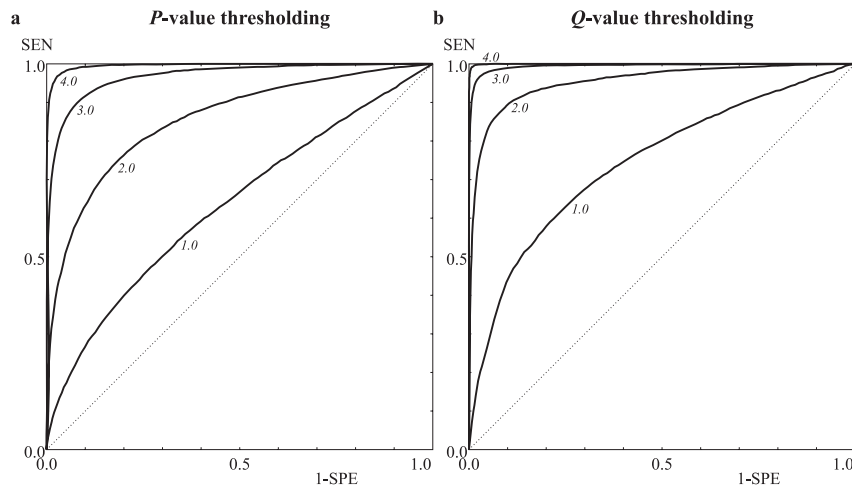


**Figure 4.3.** Receiver operating characteristic (ROC). The ROC-curves for thresholding methods based on (a)  $P$ -values and (b)  $Q$ -values were constructed by varying the thresholds  $p$  and  $q$  in a range of 0.0 to 1.0 and plotting the achieved sensitivity SEN vs. the specificity SPE. Per method, four curves are shown that correspond with simulations with signal-to-noise ratios (SNRs) that ranged from 1.0 to 4.0 (see labeling), and otherwise with default settings (see Materials and Methods). The area under the curve is a measure for the method's discriminatory power.  $Q$ -value thresholding performed substantially better than  $P$ -value thresholding.

In Figure 4.3 the ROC-curves are shown that were obtained in simulations with various SNRs, and otherwise default parameters. The areas under the curves that were based on  $P$ -value thresholding (Figure 4.3a) equaled 0.6323, 0.8548, 0.9676, and 0.9953 for SNR = 1.0, 2.0, 3.0, and 4.0 respectively. Correspondingly, the areas under the curves that were based on  $Q$ -value thresholding (Figure 4.3b) equaled 0.7432, 0.9532, 0.9938, and 0.9993. Thresholding on the basis of  $Q$ -values generally performed better than thresholding on the basis of  $P$ -values. For instance, in these simulations,

$Q$ -value thresholding at SNR = 3.0 performed similarly as  $P$ -value thresholding at SNR = 4.0, and  $Q$ -value performance at SNR = 2.0 was almost equal to  $P$ -value performance at SNR = 3.0. Therefore, in the sense of the sensitivity index ( $d'$ ) from signal detection theory, the discriminatory power of  $Q$ -value thresholding was approximately 1.4 times better than the discriminatory power of  $P$ -value thresholding at default parameter settings.

**Table 4.1.** Simulation results for various configuration parameters.

Parameters		i. Uncorrected				ii. FWE-control				iii. B-H FDR-control				iv. Regional FDR-control			
		SEN	SPE	FWE	FDR	SEN	SPE	FWE	FDR	SEN	SPE	FWE	FDR	SEN	SPE	FWE	FDR
<b>Volume size</b>	12×12×8	98	95	100	46	47	100	5	0	83	100	91	5	92	100	88	4
	16×16×12	98	95	100	71	38	100	3	0	74	100	90	5	90	100	89	4
	<u>24×24×16</u>	98	95	100	88	30	100	4	0	63	100	85	5	86	100	90	4
	32×32×24	98	95	100	95	22	100	5	0	51	100	81	5	79	100	92	5
	48×48×32	98	95	100	98	17	100	5	0	38	100	75	5	68	100	93	5
<b>Smoothness</b>	<u>0.0</u>	98	95	100	88	30	100	4	0	63	100	85	5	86	100	90	4
	1.0	98	95	100	88	30	100	5	0	63	100	87	5	86	100	92	4
	2.0	98	95	100	88	29	100	4	0	61	100	73	5	73	100	45	2
	3.0	98	95	100	88	29	100	4	1	58	100	47	5	60	100	16	2
	4.0	98	95	100	88	30	100	1	1	60	100	30	4	58	100	10	2
<b>Block size</b>	0×0×0	-	95	100	100	-	100	5	5	-	100	5	5	-	100	5	5
	1×1×1	98	95	100	100	28	100	5	4	28	100	8	6	27	100	8	6
	2×2×2	98	95	100	98	30	100	4	1	39	100	17	4	50	100	22	4
	<u>4×4×4</u>	98	95	100	88	30	100	4	0	63	100	85	5	86	100	90	4
	8×8×8	98	95	100	47	29	100	5	0	83	100	100	5	95	100	100	3
	16×16×16	98	95	100	6	29	100	2	0	96	98	100	3	97	99	100	1
<b>SNR</b>	2.0	52	95	100	93	1	100	3	3	1	100	7	4	1	100	7	4
	3.0	85	95	100	89	6	100	6	1	16	100	38	5	36	100	64	4
	<u>4.0</u>	98	95	100	88	30	100	4	0	63	100	85	5	86	100	90	4
	5.0	100	95	100	88	69	100	4	0	93	100	95	5	98	100	94	4
	6.0	100	95	100	88	93	100	5	0	99	100	96	5	100	100	94	4
<b>Threshold</b>	0.01	92	99	100	61	19	100	1	0	42	100	25	1	69	100	34	1
	0.02	95	98	100	75	23	100	3	0	51	100	50	2	78	100	61	2
	<u>0.05</u>	98	95	100	88	30	100	4	0	63	100	85	5	86	100	90	4
	0.10	99	90	100	94	35	100	12	1	71	100	99	10	91	100	100	9
	0.20	100	80	100	97	41	100	20	1	79	100	100	20	95	100	100	18

The average achieved sensitivity (SEN [%]), specificity (SPE [%]), familywise error (FWE [%]) rate and false discovery rate (FDR [%]) over 500 numerical simulations is listed for each of four thresholding methods using various simulation configurations. Default parameter values have been underlined. Parameter settings that were varied included: the volume size, the smoothness of the noise as expressed by the full width at half maximum (FWHM) of the Gaussian convolution kernel, the size of the central block with true effects, the signal-to-noise ratio (SNR) in the central block, and the globally imposed thresholds  $p$  and  $q_{\text{global}}$ .

Many configuration parameters were varied in the simulations, and the sensitivity (SEN), specificity (SPE), familywise error (FWE) rate, and false discovery rate (FDR) that were achieved on average by the four different methods were determined and listed in Table 4.1.

The uncorrected thresholding method achieved large SEN but poor SPE, FWE, and FDR. For this method, the SEN trivially depended only on the SNR and the threshold. The error measure  $1 - \text{SPE}$  was controlled at the level  $p$ , but the FWE equaled 100 % in all cases. Its FDR also depended on the size of the central signal block relative to the entire volume: better FDRs were obtained for small volumes and large blocks.

With FWE-control, the SEN improved with decreasing volume size, increasing SNR, and increasing thresholds, but was typically poor; it did not depend on the other parameters. The SPE was 100 %, while the FWE was controlled at the level  $p$ , or better. For highly correlated noise in the data, the method became conservative. The FDR was very low and further improved with increasing size of the central signal block or SNR.

Using global FDR-control, the SEN was generally considerably better than for FWE-control, for which both methods performed equally well. It also showed improvement with decreasing volume size, increasing SNR, and increasing thresholds. In addition, the SEN improved with the size of the central block. The SPE was 100 %, while the FWE varied along with the SEN, but also improved for spatially correlated data. The FDR was controlled at the imposed threshold  $q_{\text{global}}$  (except for the  $1 \times 1 \times 1$  signal block, where it was marginally exceeded).

Finally, our regional FDR-controlling method mostly showed a considerable further increase in SEN as compared to the global FDR-controlling method. Similar to the latter method, the SEN improved strongly with the size of the central signal block relative to the size of the entire volume, the SNR, as well as the threshold. In addition, the SEN suffered from spatial correlations in the noise. The SPE was again 100 %. The FWE showed comparable trends as that of global FDR-control, except that it depended oppositely and less strongly upon the volume size. The FDR was controlled at the threshold  $q_{\text{global}}$ , or better (except for the  $1 \times 1 \times 1$  signal block, where it was marginally exceeded).

For our method based on regional FDR-control, the region shape and FWHM were varied as well (Table 4.2). In these simulations, all region shapes showed optimal performance at intermediate FWHM region sizes (4.0-8.0). For the most extreme values of the FWHM (i.e.,  $1/\infty$  or  $\infty$ ), the regions become equivalent to a single voxel or the entire volume, respectively, and therefore results did not depend upon region shape. Overall, the region shapes differed little in performance. The FDR was controlled at the threshold  $q_{\text{global}}$  in all cases.

**Table 4.2.** Simulation results for various region shapes and sizes.

Region size	Spherical				Region shape				Gaussian			
					Welch							
	SEN	SPE	FWE	FDR	SEN	SPE	FWE	FDR	SEN	SPE	FWE	FDR
<u>1/∞</u>	63	100	86	5	63	100	86	5	63	100	86	5
<u>2.0</u>	77	100	92	5	73	100	92	5	78	100	91	5
<u>4.0</u>	86	100	93	5	85	100	93	5	86	100	90	4
<u>8.0</u>	89	100	89	4	87	100	92	4	82	100	90	4
<u>16.0</u>	75	100	89	4	72	100	89	5	68	100	85	4
<u>32.0</u>	57	100	87	6	62	100	86	5	63	100	83	5
<u>∞</u>	62	100	87	5	62	100	87	5	62	100	87	5

The average achieved sensitivity (SEN [%]), specificity (SPE [%]), familywise error (FWE [%]) rate and false discovery rate (FDR [%]) over 500 numerical simulations is listed for the regional FDR-control thresholding method, using varying shapes and sizes of the employed regions, and otherwise default configuration parameters. Default region shape and size are underlined. The shape of the isotropic weighting functions was either uniform over a spherical region ('Spherical'), continuous and non-zero in a finite volume according to a parabolic Welch window ('Welch'), or continuous and non-zero in an infinite volume according to a bell-shaped Gaussian window ('Gaussian'). For each type of function, the full width at half maximum (FWHM) was varied from infinitesimally small to infinitely large.

### In vivo experiments

Figure 4.4a displays abnormal ADC regions for the epilepsy patient in the right temporal lobe. Using four different thresholding methods, the significant differences in ADC values with respect to the mean of the control group as obtained from Student's *T*-test statistics, are shown overlaid on a normalized sagittal  $T_1$ -weighted MR image. Although the epileptic focus, as determined from ictal electroencephalography (EEG), was right frontal, the ADC measurement revealed right temporal abnormalities, predominantly in the superior temporal gyrus, a region close to the inferior frontal gyrus. Due to the limited spatial discriminational power of EEG, and due to the proximity of the ADC abnormalities within the superior temporal gyrus to the frontal lobe, it is not unlikely that the ictal EEG focus, characterized as right frontal, could also include the superior temporal gyrus. The uncorrected thresholding method displays noisy abnormalities that are spread over a large part of the selected slice, whereas FWE-control is not able to localize any abnormalities. Both B-H FDR-control and regional FDR-control display clearly localized abnormalities. For the latter two methods, the location of the abnormalities is identical; however, regional FDR-control yields 1.5 times more deviating voxels in this slice than B-H FDR-control.

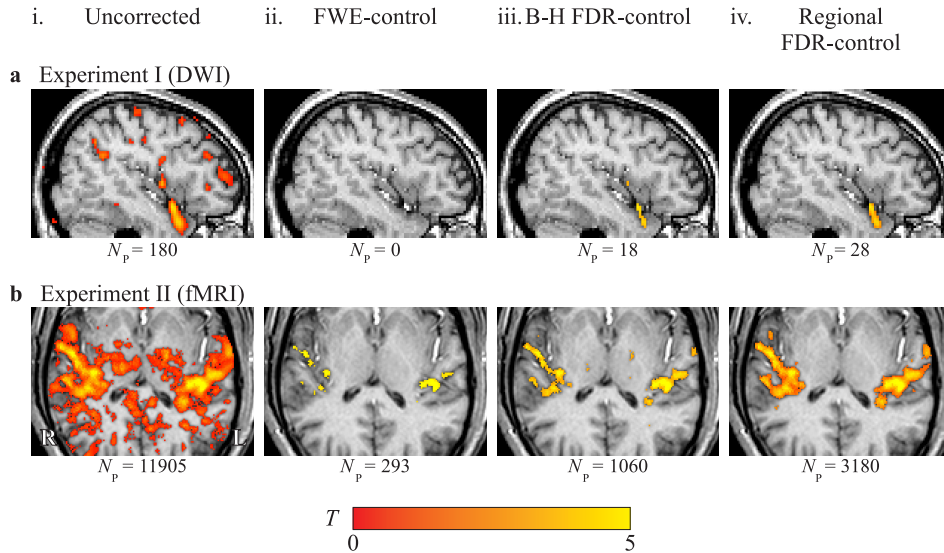


**Figure 4.4.** In vivo neuroimaging results. (a) Experiment I (DWI). Significant differences in ADC values with respect to the mean of healthy controls were determined in the right temporal lobe of an epilepsy patient using four different thresholding methods. The slice position equaled  $x = -44$  mm in Talairach coordinates. Results are overlaid on a normalized sagittal  $T_1$ -weighted MRI slice. DWI reveals temporal abnormalities in ADC values. Whereas the uncorrected thresholding method also displays noisy abnormalities spread over a large part of the selected slice, B-H FDR-control and regional FDR-control only display localized abnormalities in the right temporal region. For these latter two methods, the location of the abnormalities is identical. However, our method based on regional control detected 1.5 times more positives ( $N_p$ ) in this slice than B-H FDR-control. FWE-control is unable to localize any abnormalities. (b) Experiment II (fMRI). The four different thresholding methods were applied to the outcomes of a general linear model in a functional MRI experiment that employed auditory stimuli of varying intensity. The significance of the activation was displayed using a red-to-yellow color-code and projected on a transversal plane. Uncorrected thresholding resulted in large activation clusters, but also in apparently noisy signal detection. FWE-control by means of Bonferroni correction restricted the activation to small regions in the auditory cortex. Both methods with FDR-control generally resulted in an intermediate cluster size. Although the activation was largely confined to the temporal lobes, B-H FDR-control detected some thalamic activation whereas regional FDR-control did not. Our method based on regional control detected 3.0 times more positives ( $N_p$ ) in the volume than B-H FDR-control.

Figure 4.4b shows the results of the fMRI experiment with auditory stimulation for an individual subject. The images show a projection of all active voxels in the volume according to the various thresholding methods onto a transversal anatomical slice. The strongest activation was found bilaterally in the temporal lobe near the sites of Heschl's gyrus and Heschl's sulcus, which partly comprise the auditory cortices. For the method with uncorrected thresholding, many clusters of activation were typically detected that were distributed across the entire volume. In contrast, the use of FWE-control resulted in limited activation that was completely confined to small areas in



auditory cortex. The method based on global FDR-control showed extensive bilateral activation in the auditory cortex, as well as some small isolated clusters in the thalamus. Finally, our regional FDR-controlling method resulted in larger activation clusters in the auditory cortex as compared to global FDR-control; 3.0 times as many active voxels were detected. In contrast with other methods, other parts of the brain like the thalamus and occipital lobe did not show significant effects according to this method.

## Discussion

### Validity

In this paper, we described a new method to control the global FDR. By taking the clustered nature of neuroimaging effects into account by means of regional weightings, the sensitivity of the method is enhanced as compared to conventional (global) FDR-controlling methods. We have provided informal quantitative arguments that back up our method in the theory section and appendices, but did not prove our reasoning with mathematical rigor. To validate our method for practical purposes, a wide range of numerical simulations was therefore performed.

The simulations in Table 4.1 varied from imaging volumes without any true positives at all to volumes that were to a large degree filled with true positives, small to moderately large imaging volumes, weak to strong signals, strict to lenient thresholds, and various spatial correlation structures. In addition, many other ad hoc simulations were performed during the development of the method (e.g. with 2D imaging volumes or multiple activation clusters; results not shown). The achieved FDR was well bounded by the freely specifiable value  $q_{\text{global}}$ , and in some cases even considerably better FDRs were actually realized. The only exception that was found concerned the simulations with a  $1 \times 1 \times 1$  signal block, for which the bound was marginally exceeded. Since this occurred for B-H FDR-control in identical fashion as for regional FDR-control, we attribute this to chance. In any case, the average FDR that was achieved using regional FDR-control was always better than, or at least equal to, the FDR in B-H FDR-control. At the same time, the sensitivity was substantially enhanced in most cases. In particular, for the simulations at default settings, which seem most representative for neuroimaging experiments, the performance of our method was very good. This forms evidence for the practical validity, applicability, and usefulness of the method in a broad range of circumstances.

Spatial correlations in the data were taken into account in Eq. 4.10 by means of a summation over the correlated element  $C_j$  ('corel') to which a voxel  $j$  belongs (see Appendix II, ad [ii]). Corels were defined as spheres that were centered on the respective voxels, with diameters that equaled the FWHM of

the smoothing kernel. This is similar to suggestions by Worsley concerning resels (Worsley et al., 1995; Worsley, 2005). If smoothing is applied during the preprocessing of neuroimaging data and the corresponding kernel size is larger than the inherent smoothness of the original data, like in the analysis of our in vivo experiments, this approach can be followed as a good approximation. If no smoothing is performed, or if the inherent smoothness of the data is larger than the kernel, the corel size should be estimated from the data structure, or from prior knowledge regarding the smoothness of the data.

For smoothed data, the method was found to behave conservatively. Not only did the achieved FDR become smaller than the imposed bound, but also the sensitivity suffered. This conservative behavior on correlated data is somewhat comparable to that of Bonferroni-corrected FWE-control. In the case of regional FDR-control, this is likely caused by an overestimated corel size. This leaves room for further improvement. Nevertheless, as long as the region size exceeded the corel size in our simulations, our method still achieved higher sensitivities than B-H FDR-control. Therefore, we suggest the use of regional FWHM sizes that are larger than the corel size. Given that the corel size can be regarded as a measure of the effective spatial resolution of the data, this seems a reasonable suggestion.

### Performance

A comparison between various thresholding methods resulted in the general finding that the methods based on FWE-control, B-H FDR-control, regional FDR-control, and uncorrected thresholding (in that order) were progressively more sensitive. This came at the cost of a concurrent increase in the number of false positives, which varied from negligibly small (for FWE-control) and tolerable (for B-H and regional FDR-control) to unacceptably large (for uncorrected thresholding). The performance of the methods varied with various parameters in the simulations. Naturally, the sensitivity of all methods improved with increasing SNR in the available data and with increasingly tolerant thresholds. Also, all methods benefited from an increase in the proportion of voxels with true effects, either with respect to the achieved SEN, SPE, FWE, FDR, or a combination of these measures.

The uncorrected thresholding method and the methods based on FWE-control and B-H FDR-control by definition all achieve an identical discriminatory power according to an ROC-curve analysis. For each threshold that is employed in one of the mentioned three methods, a different but equivalent threshold can be chosen in another method that will lead to exactly the same results. That is because these methods are all based on the same type of thresholding, namely the global application of a single  $P$ -value threshold. Only the way in which this threshold is determined differs. Because ROC-curves assess performance over the entire range of thresholds, they are

insensitive to such differences. The same results will hold for any other method that controls some error measure by means of a fixed global  $P$ -value threshold.

In contrast, our method that is based on regional control of the FDR performed considerably better. In relation to SNR, the discriminatory power of our method was approximately 1.4 times better than the other methods. To achieve an equivalent improvement in performance by increasing the number of neuroimaging acquisitions, the duration of experiments would roughly have to be extended twice. Such outcomes will of course also depend on the detailed experimental configuration, but this illustrates that the potential gain in power by using  $Q$ -values instead of  $P$ -values is substantial.

Generally, a gain in sensitivity can only be realized at some cost. In this case we have made use of the clustered nature of effects in neuroimaging data. If true positives are scattered (instead of clustered) over the entire imaging volume, our method is not expected to perform better than the other methods. However, this is a very unrealistic scenario in neuroimaging experiments. Yet, even in realistic conditions, the sensitivity using regional FDR-control will only increase as compared to B-H FDR-control for those regions where the density of true positives is larger than the average global density. In contrast, in the regions where relatively few true positives occur, sensitivity can actually decrease. This can hardly be considered a disadvantage of our method relative to other types of FDR-control: the presence of single isolated positive voxels would not allow firm conclusions to be drawn about activation in a particular area anyhow. In contrast with FWE-control, FDR-control inherently allows voxels to be false, especially if many positives occur elsewhere. For practical purposes, a gain in sensitivity in the few regions that contain many true positives will therefore outweigh the decrease in sensitivity in those regions that contain little effect. In a sense, our method focuses the sensitivity to those regions of the brain where it is most advantageous. Thus, a considerable net increase in the total number of true positives that can be detected may be achieved. Also, this allows both large areas with small effects and small areas with strong effects to be detected, similar to some methods based on cluster level inferences. Moreover, our method tends to cluster any occurring false positives close to areas with true activation, which less affects the observable activation patterns.

### Choice of regions

Our proposed method controls the globally achieved FDR by imposing a suitable bound on the regional FDR. In principle, the method allows the regions to be freely chosen for each voxel individually. Also, the method supports the use of continuously weighted regions. Because of the large number of degrees of freedom in the choice of the weights  $w_{jk}$ , it is impossible to characterize our method under all imaginable circumstances. However, we evaluated various

reasonable options and showed that advantage can be taken of the clustered nature of neuroimaging data to improve the sensitivity of the analysis.

If the regions are chosen as large as possible by treating the entire imaging volume as a single region (i.e.,  $w_{jk} = 1$  for all  $j$  and  $k$ ), then Eq. 4.4 will reduce to Eq. 4.3. Also, from Eq. 4.10 it can be deduced that the imposed  $q_{\text{regional}}$  will almost equal  $q_{\text{global}}$ . Therefore, in this case our method will be slightly more conservative than, but highly similar to, B-H FDR-control. Contrariwise, if the regions are chosen as small as possible by treating each voxel as a separate region by itself (i.e.,  $w_{jk} = 1$  if  $j = k$ , and zero otherwise), then Eq. 4.5 results in  $Q_j = P_j$ . Also, Eq. 4.10 will approximate Eq. 4.3. In this case our method will again be slightly more conservative than, but very similar to, conventional global FDR-control. Therefore, for both the limiting cases of extremely large and small regions, our method reduces to a conservative version of B-H FDR-control. This is also reflected in the results for the most extreme FWHM sizes in Table 4.2, which are similar to the results for B-H FDR-control at default settings in Table 4.1. However, for intermediate choices of region sizes, our regional method typically performed much better than global FDR-control, both with regard to the achieved sensitivities (Tables 4.1 & 4.2) and the discriminatory power based on ROC-curves (Figure 4.3).

In practice, two contradictory considerations that affect the optimal choice of the region size have to be balanced. On the one hand, the sensitivity in areas of the brain that contain effects of interest will suffer from the inclusion of many distant irrelevant voxels without activation. This was the original motivation for parceling the imaging volume into regions. On the basis of this argument, regions should be taken small. On the other hand, dividing the volume into too many regions will decrease performance as a result of the implicit correction for multiple comparisons. On the basis of this latter argument, regions should be few. Intuitively, an optimum should be attained for regions that are of similar size as the scale of the activation clusters themselves. This ensures that the individual regions are large, but still to a high degree filled with true positives. This is reminiscent of the matched filter theorem, which states that the filter that will give optimum resolution of a signal from noise is a filter that is matched to the shape of the signal.

In our simulations, we observed the highest sensitivity for FWHM region sizes equal to 4.0-8.0 voxels (Table 4.2). In these simulations, the true activation consisted of a block of  $4 \times 4 \times 4$  voxels. These findings support the conclusion that as a rule of thumb optimal performance is achieved for regions of similar size as the expected activation clusters. Still, the performance of our method does not critically depend on this choice of the region size parameter, as it typically does not perform worse than B-H FDR-control for other values as well. If possible, we recommend choosing the regional FWHM equal to the typical dimensions of the structures that are expected to be activated.

The freedom to choose not only the size but also the shape of regions can potentially be further exploited to improve sensitivity. For instance, if activation is expected in a brain structure with a certain known complex morphology, non-isotropic regions could be specified that match the shape of this structure. This might be realized in a natural way by the use of digitized atlases or probability maps. Or, for example, if it is known that effects occur primarily in gray matter, the shape of the employed regions could be varied voxel by voxel to match the local orientation of the cortical surface. If symmetrical activation is expected, equivalent regions in the left and right hemispheres could be merged. Recently, Heller et al. described the advantages of a related FDR-controlling method that defines sub-regions on the basis of a clustering-algorithm that is applied to the statistical data itself (Heller et al., 2006). However, we have not explored these possibilities in this paper.

In our simulations, all regional weighting function shapes showed rotational symmetry. Our method performed well for all profiles that were explored and robustly led to improved sensitivity and valid results in all cases. For general purposes, we suggest to use isotropic regions.

### **In vivo experiments**

To judge the practical merits, our method was also applied to two diverse neuroimaging experiments that were part of ongoing research projects. In a first experiment, physiological deviations in the brain of an epilepsy patient were detected using DWI. In a second experiment, functional brain activation in response to auditory stimulation was determined using fMRI. We regard these as typical examples of practical applications, and are not aware of reasons why either of the evaluated thresholding methods should be favored by these experiments.

Our method based on regional FDR-control was always able to detect more deviant voxels (in DWI) or activation (in fMRI) than either methods based on FWE-control or B-H FDR-control could. This was in agreement with the results of the numerical simulations. At the same time, the spatial patterns of the detected effects remained coherent and confined to regions where signals could be expected. In particular, our method resulted in much less apparent noise than the method based on uncorrected thresholding, while it still recovered most of the activation that appeared to be true. In our opinion, our method never performed worse than any of the other methods, and generally led to the cleanest and most convincing results.

## Computational complexity

Our method is computationally simple in the qualitative sense that only basic arithmetic functions and sorting are used. However, its quantitative computational complexity, as with regard to the involved number of operations, is higher than for the other three methods that have been evaluated in this study. The computational complexity of uncorrected thresholding and Bonferroni correction is of the order  $O(N)$ , because  $N$  voxels'  $P$ -values need to be compared against a fixed threshold. The complexity of B-H FDR-control is  $O(N \log(N))$  because of the sorting that is involved. The complexity of our method is of the order  $O(N^2)$  because it requires a weight  $w_{jk}$  to be calculated for each pair of voxels. This means that an increase by a factor 2 in the number of voxels will result in an approximate increase by a factor 4 in calculation time. In three dimensions, an isotropic improvement in resolution by a factor 2 would result in an increase by a factor 64 in calculation time.

The thresholding of the  $Q$ -value map that corresponds with a  $24 \times 24 \times 16$  imaging volume takes approximately 40 seconds on a 2-GHz PC system. The in-vivo data required the computer to run for several hours. However, there is no need to repeat these calculations if thresholding at a different level  $q_{\text{global}}$  is required; subsequent applications of our method to the same data set is a mere  $O(N)$  process. In addition, by using a uniform spherical weighting function instead of a Gaussian function, the total duration of the calculations could be reduced by a factor two approximately, and a further gain in computing time is possible by optimizing the code for this discrete type of weighting.

Although currently the computational complexity will not be a concern for e.g. single-slice neuroimaging experiments or other experiments with small regions of interest, our method may become cumbersome for routine application to high-resolution full-brain statistical maps for purposes of initial data exploration. In such preliminary analyses, the use of sub-sampled datasets can be considered, or other thresholding methods should be used. However, the obtainable gain in sensitivity certainly justifies the application of our method to determine final results, if the FDR is the error measure of choice. Also, given the continuing increase in available computational power, such considerations are expected to be of secondary importance, and our method provides a viable alternative to the existing methods.

## Acknowledgments

The authors would like to acknowledge the contribution of the anonymous reviewers, who provided valuable comments that inspired a thorough revision of the method, which led to enormous improvements of its validity and usability. Also, we acknowledge the contribution of K. Jaspers who participated in the acquisition of the fMRI data.

## Appendices

### Appendix I

Since the B-H FDR-controlling procedure limits the average FDR below a specified level  $q_{\text{global}}$ , the total number of false positives should on average not exceed a proportion  $q_{\text{global}}$  of the total number of positives (see Eq. 4.1). Applying B-H FDR-control to continuously weighted regions, the total weight of all false positives should on average not be expected to exceed a proportion  $q_{\text{regional}}$  of the total weight of all positives.

Under the null-hypothesis, false positives are on average homogeneously distributed. Then, the probability  $P_{\text{FP},j}$  that the center voxel  $j$  of any particular region is a false positive can be estimated as the ratio of the total weight of all false positives in that region to the total weight of all voxels in that region. Because the total weight of all false positives in B-H FDR-control is estimated to be bounded at (or below) a fraction  $q_{\text{regional}}$  of the total weight of all positives, we find that

$$P_{\text{FP},j} \leq \frac{q_{\text{regional}} \cdot \sum_{k=1}^{N_p} w_{jk}}{\sum_{k=1}^N w_{jk}}. \quad [I-1]$$

The summation in the numerator is carried out over all  $N_p$  positives.

Expanding this result from a single voxel  $j$  to the entire volume, the total expected number of false positives  $N_{\text{FP}}$  that is found using our method equals the sum of these probabilities  $P_{\text{FP},j}$  over all voxels. This leads to the following bound:

$$N_{\text{FP}} = \sum_{j=1}^N P_{\text{FP},j} \leq \sum_{j=1}^N \frac{q_{\text{regional}} \cdot \sum_{k=1}^{N_p} w_{jk}}{\sum_{k=1}^N w_{jk}}. \quad [I-2]$$

Note that the B-H FDR-controlling procedure relies upon a voxel ordering according to  $P$ -values. If a voxel ordering according to  $Q$ -values is used, like in our method, a different set of voxels can be considered active, and B-H FDR-control does no longer guarantee that the achieved regional FDR is bounded by  $q_{\text{regional}}$  on that basis. However, we demonstrate in this paper that the discriminatory power of thresholding on the basis of  $Q$ -values is typically better than on the basis of  $P$ -values. In other words, an ordering on the basis of  $Q$ -values 'better separates' the true positives from the false positives. We surmise that, as a result, the average total weight of all false positives will also not exceed a proportion  $q_{\text{regional}}$  of the total weight of all positives when using a

voxel ordering on the basis of  $Q$ -values. This justifies the use of a  $Q$ -value ordering in the summations in Eq. 4.7.

## Appendix II

According to our method, a voxel  $j$  will at least be considered active if

$$\frac{P_j \cdot \sum_{k=1}^N w_{jk}}{\sum_{k=1}^j w_{jk}} \leq q_{\text{regional}} \cdot \quad \text{[II-1]}$$

Note that according to Eq. 4.5 this voxel can also be considered active if this inequality is not satisfied, provided that there is another voxel with an index  $i > j$  that satisfies the condition in Eq. 4.5. However, because these other voxels typically have smaller weights  $w_{jk}$  than the center voxel  $j$  itself, it is relatively unlikely that the inclusion of extra voxels in the denominator compensates for the accompanying increase in the  $P$ -value in the numerator. And even if such  $i$  exists, the change in the ratio on the left of Eq. 4.II-1 will typically be very small. Therefore, the above expression will form a reasonable approximation to Eq. 4.5, and we will assume that the difference can be neglected; this assumption is validated in this paper by means of various simulations.

The probability  $P_{\text{FP},j}$  that any particular voxel  $j$  is a false positive because Eq. 4.II-1 is satisfied by chance will now be estimated under the assumption that the null-hypothesis is true for all voxels.

The summation in the denominator of Eq. 4.II-1 comprises all voxels with an index smaller than, or equal to, that of the voxel  $j$  itself. Since the summations in this equation are carried out according to a  $P$ -value ordering (Eq. 4.2), this comprises all voxels with  $P$ -values smaller than (or equal to) that of the center voxel. This sum can conceptually be split up into three contributions: [i] the center voxel itself; [ii] the immediate vicinity of the center voxel; and [iii] distant voxels.

*Ad [i].* The center voxel itself is always included in the summation, and, given that the weighting functions were normalized such that  $w_{jj} = 1$ , its weight equals 1.

*Ad [ii].* We shall define the immediate vicinity of the center voxel  $j$  as the equivalent volume where the data is spatially correlated with that of the center voxel itself. We will denote this volume as a correlated element ('corel'), notated  $C_j$ , analogous to the concept of a 'resel' in Gaussian field theory. Following a similar approach as Worsley (Worsley et al., 1995; Worsley, 2005), its shape will be estimated as a sphere with a diameter equal to the FWHM of the equivalent smoothing kernel of the noise (i.e., the point spread function).

Since the  $P$ -values vary smoothly within this correlated vicinity, a  $P$ -value gradient and, perpendicularly to this gradient, an 'iso- $P$ -value plane' can be



conceived to exist. This iso- $P$ -value plane roughly divides the vicinity of the voxel into two halves, one of which will contain higher  $P$ -values as the voxel, and the other lower  $P$ -values. Therefore, the sum of the weights of all voxels in this vicinity that have  $P$ -values smaller than the center voxel, can to first order be approximated by precisely half of the total sum of the weights in the corel  $C_j$ , excluding the center voxel itself that has weight  $w_{jj} = 1$ . In symbolic notation,

$$\text{sum of weights} = \frac{1}{2} \left( \sum_{k \in C_j} w_{jk} - 1 \right).$$

Clearly, this derivation is highly informal. However, in this paper it is shown that it leads to conservative control of the FDR under the presence of spatial correlations. This can be understood by realizing that false positive voxels have low  $P$ -values, and its corel will therefore be surrounded by other corels that typically contain higher  $P$ -values. In a smoothly varying map, on average less than half of the voxels inside the corel should then have  $P$ -values below that of the center voxel.

*Ad [iii].* For distant uncorrelated voxels, the probability that their  $P$ -value does not exceed the probability  $P_j$  of the center voxel is by definition precisely equal to  $P_j$  under the null-hypothesis. Therefore, on average a fraction  $P_j$  of these voxels will have lower  $P$ -values, and their total weight can be symbolically expressed as

$$\text{sum of weights} = P_j \cdot \left( \sum_{k=1}^N w_{jk} - \sum_{k \in C_j} w_{jk} \right).$$

Now, these three contributions [i], [ii], and [iii] can be added to obtain the total expected weight of all voxels with  $P$ -values lower than or equal to  $P_j$ .

$$\sum_{k=1}^j w_{jk} = 1 + \frac{1}{2} \left( \sum_{k \in C_j} w_{jk} - 1 \right) + P_j \cdot \left( \sum_{k=1}^N w_{jk} - \sum_{k \in C_j} w_{jk} \right). \quad [\text{II-2}]$$

Substituting Eq. 4.II-2 into Eq. 4.II-1, we may derive

$$P_j \leq \frac{q_{\text{regional}}}{1 - q_{\text{regional}}} \cdot \frac{\frac{1}{2} + \frac{1}{2} \sum_{k \in C_j} w_{jk}}{\sum_{k=1}^N w_{jk} + \frac{q_{\text{regional}}}{1 - q_{\text{regional}}} \sum_{k \in C_j} w_{jk}} < \frac{q_{\text{regional}}}{1 - q_{\text{regional}}} \cdot \frac{\frac{1}{2} + \frac{1}{2} \sum_{k \in C_j} w_{jk}}{\sum_{k=1}^N w_{jk}}. \quad [\text{II-3}]$$

By definition, the probability that the statistic  $P_j$  satisfies this inequality by chance is precisely equal to the value of the right hand side expression. Returning to Eq. 4.II-1, this forms an estimate for the probability  $P_{\text{FP},j}$  that the null-hypothesis will be rejected in voxel  $j$ , turning it into a false positive.

Now, the total expected number of false positives in the entire volume  $N_{\text{FP}}$  equals the sum of the probabilities  $P_{\text{FP},j}$  for all individual voxels  $j$ . Thus,

$$N_{\text{FP}} = \sum_{j=1}^N P_{\text{FP},j} \leq \frac{q_{\text{regional}}}{1 - q_{\text{regional}}} \cdot \sum_{j=1}^N \frac{\frac{1}{2} + \frac{1}{2} \sum_{k \in C_j} w_{jk}}{\sum_{k=1}^N w_{jk}}. \quad [\text{II-4}]$$

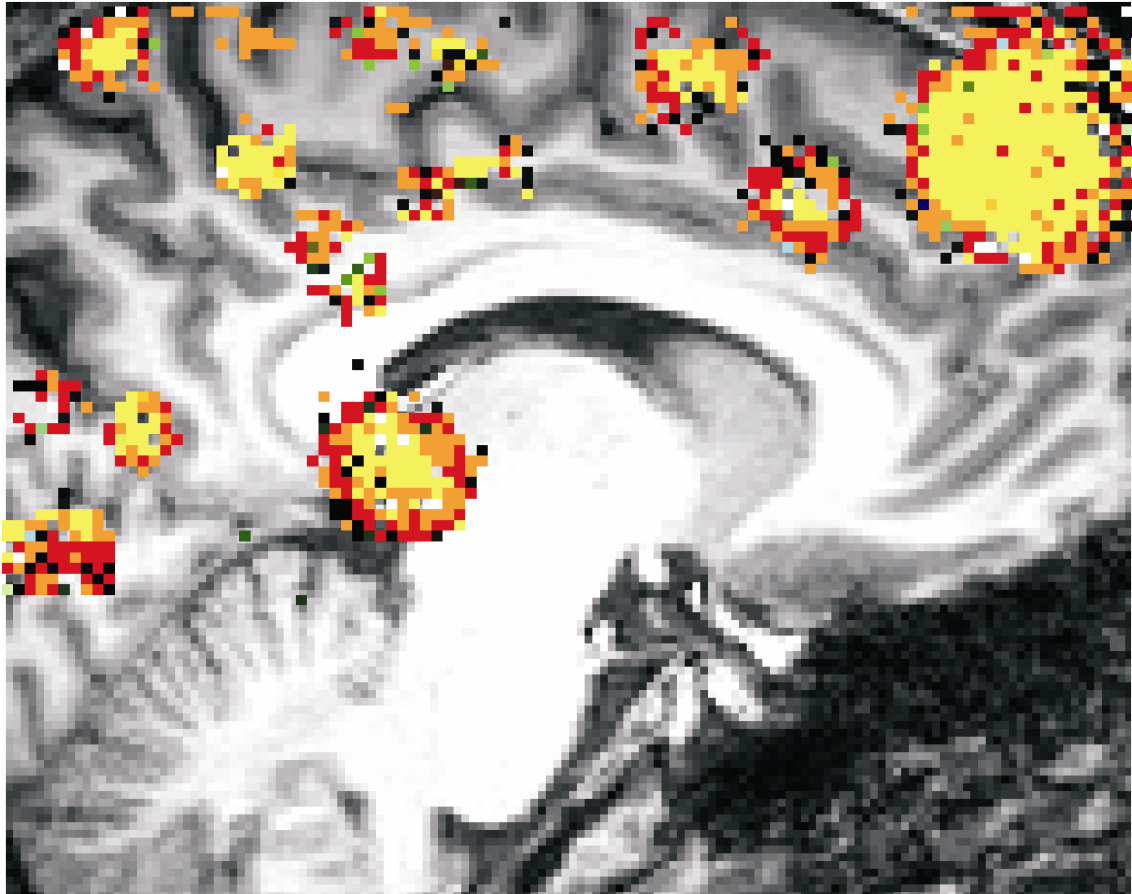
Because in this equation all summations are carried out either over all voxels, or over all voxels in a corel, the order of the summation is irrelevant and can be based on  $P$ - or  $Q$ -values alike. This justifies the use of a  $Q$ -value ordering in Eq. 4.8.

## References

- Benjamini, Y., Hochberg, Y., 1995. Controlling the false discovery rate: a practical and powerful approach. *Journal of the Royal Statistical Society, Series B, Methodological* 57, 289-300.
- Friston, K.J., Holmes, A., Poline, J.B., et al., 1996. Detecting activations in PET and fMRI: levels of inference and power. *Neuroimage* 4, 223-235.
- Genovese, C.R., Lazar, N.A., Nichols, T., 2002. Thresholding of statistical maps in functional neuroimaging using the false discovery rate. *Neuroimage* 15, 870-878.
- Hall, D.A., Haggard, M.P., Akeroyd, M.A., et al., 1999. "Sparse" temporal sampling in auditory fMRI. *Human brain mapping* 7, 213-223.
- Heller, R., Stanley, D., Yekutieli, D., et al., 2006. Cluster-based analysis of FMRI data. *Neuroimage* 33, 599-608.
- Hochberg, Y., 1988. A sharper Bonferroni procedure for multiple tests of significance. *Biometrika* 75, 800-802.
- Holm, S., 1979. A simple sequentially rejective multiple testing procedure. *Scandinavian Journal of Statistics* 6, 65-70.
- Kriegeskorte, N., Goebel, R., Bandettini, P., 2006. Information-based functional brain mapping. *Proceedings of the National Academy of Sciences of the United States of America* 103, 3863-3868.
- Laird, A.R., Fox, P.M., Price, C.J., et al., 2005. ALE meta-analysis: Controlling the false discovery rate and performing statistical contrasts. *Human Brain Mapping* 25, 155-164.
- Langers, D.R., Backes, W.H., van Dijk, P., 2003. Spectrotemporal features of the auditory cortex: the activation in response to dynamic ripples. *Neuroimage* 20, 265-275.
- Logan, B.R., Rowe, D.B., 2004. An evaluation of thresholding techniques in fMRI analysis. *Neuroimage* 22, 95-108.
- Nichols, T., Hayasaka, S., 2003. Controlling the familywise error rate in functional neuroimaging: a comparative review. *Statistical Methods in Medical Research* 12, 419-446.
- Poline, J.B., Worsley, K.J., Evans, A.C., et al., 1997. Combining spatial extent and peak intensity to test for activations in functional imaging. *Neuroimage* 5, 83-96.
- Rugg-Gunn, F.J., Eriksson, S.H., Symms, M.R., et al., 2001. Diffusion tensor imaging of cryptogenic and acquired partial epilepsies. *Brain* 124, 627-636.
- Singh, A.K., Dan, I., 2006. Exploring the false discovery rate in multichannel NIRS. *Neuroimage* 33, 542-549.
- Worsley, K.J., 2005. An improved theoretical P value for SPMs based on discrete local maxima. *Neuroimage*.
- Worsley, K.J., Poline, J.B., Vandal, A.C., et al., 1995. Tests for distributed, nonfocal brain activations. *Neuroimage* 2, 183-194.

**Part II:**

**Clinical applications of Quantitative MR in epilepsy**





# Chapter 5

**Multimodal MR reveals secondarily  
generalized seizure related  
abnormalities at 1.5 T**

**Jansen JFA, Kooi ME, Vlooswijk MCG, Majoie HJM, Reijs RP,  
Hofman PAM, Nicolay K, de Krom MCTFM, Aldenkamp AP, and  
Backes WH**

*Submitted for publication*

**Abstract**

Cognitive deterioration is a frequent observation in chronic epilepsy patients, particularly in those who have suffered a high number of secondarily generalized tonicoclonic seizures (SGTCS). Although neuropsychological evaluation frequently reveals a decline in cognitive abilities in these patients, it is unclear whether this is associated with tissue changes in the brain. In this study we investigated whether SGTCS have an effect on the outcomes of neuropsychological testing, and whether a high number of SGTCS accumulated over life is associated with microstructural and metabolic changes in brain tissue of the temporal and frontal lobes as determined by multimodal quantitative MR, comprising T2 relaxometry, diffusion weighted imaging, and <sup>1</sup>H-MR-spectroscopy. In the present study, frontal, but not temporal, MR abnormalities were found to be related to SGTCS. These findings confirm that SGTCS do have a substantial effect on both frontal brain function and on the metabolic and microstructural brain tissue characteristics. This knowledge may help to obtain a better understanding and anticipatory treatment of SGTCS-related cognitive deterioration.

## Introduction

Cognitive deterioration is a frequent clinical observation in epilepsy patients with persistent seizures (Corcoran et al., 1992; Thompson et al., 1992; Blake et al., 2000; Helmstaedter, 2002). The cognitive problems range from memory deficits and mental slowing, to sometimes even global cognitive deterioration. Also seizures, especially secondarily generalized seizures, might have an effect on cognition. In patients with a high number of secondarily generalized tonicoclonic seizures (SGTCS), cognitive deterioration has been described (Dodrill et al., 1986; Trimble, 1988; Dodrill, 2002; Stefan et al., 2002; Thompson et al., 2005), although data are sometimes contradictory (Helmstaedter et al., 1999; Kramer et al., 2006). In various preclinical and clinical studies, changes in cerebral metabolism (Jokeit et al., 1997; Tasch et al., 1999; Miller et al., 2000; Bernasconi et al., 2002) and neuronal loss (Kotloski et al., 2002) were observed shortly after SGTCS. In animal models, seizures have been shown to cause changes in protein expression, protein modification, mossy fiber sprouting, and synaptic reorganization (Beck et al., 2000), and cell loss in varying regions of the limbic system due to necrosis and apoptosis (Sass et al., 1990; Sass et al., 1992).

Previously, magnetic resonance imaging (MRI) has been applied to investigate possible structural alterations associated with seizure-related cognitive dysfunction (Hermann et al., 2007). To our knowledge, there have been no studies with conventional structural MRI (i.e. T1 and T2 weighted imaging) in which one tested whether there was a direct relation between cognitive dysfunction and structural cerebral alterations in epilepsy. Quantitative volumetric analyses revealed associations between memory deficits and volume reductions of the hippocampus (Reminger et al., 2004), cerebellum (Hermann et al., 2004), and whole cerebrum (Hermann et al., 2003). Furthermore, it was shown that temporal lobe epilepsy patients with frequent SGTCS have lower hippocampal N-acetyl-aspartate to creatine ratios (indicative of decreased neuronal integrity) than patients without SGTCS (Bernasconi et al., 2002; Lee et al., 2005). These observations raise the questions whether SGTCS are also associated with micro-structural and metabolic changes in the brain, possibly remote from the seizure focus. The population of patients with epilepsy who suffer from SGTCS is clinically heterogeneous with varying etiologies and seizure characteristics. Furthermore, in contrast to evident acute SGTCS-induced effects, chronic SGTCS-induced effects are more likely to be subtle due to the plasticity and adaptive capacities of the brain. Therefore, to detect these possible subtle structural and metabolic effects, we used multimodal quantitative MR in an inherently heterogeneous group of patients with localization-related epilepsy and secondarily generalized seizures.



In quantitative magnetic resonance (MR) of the human brain, the measured MR contrasts are converted into physical quantities with metrical units (Tofts, 2003). Compared to conventional structural MRI, used to visually detect abnormalities of brain tissue, the quantitative MR techniques used in the present study, namely T2 relaxometry, diffusion weighted imaging (DWI), and proton MR spectroscopy ( $^1\text{H}$ -MRS), may be more sensitive to micro-structural (T2, and DWI) and metabolic changes ( $^1\text{H}$ -MRS) in brain tissue. For example, quantitative MR has been successfully applied in the diagnosis of multiple sclerosis (Filippi et al., 2007), stroke (Guadagno et al., 2003), as well as in epilepsy (Duncan, 2002).

### **T2 relaxometry**

T2 relaxometry is a quantitative technique that provides an objective measurement of tissue characteristics, as the transverse relaxation time (T2) is a physical property of the tissue, which mainly reflects the (relatively) free water content (Bottomley et al., 1987). Abnormalities on T2 maps usually reflect altered water content, possibly associated with neuronal or axonal loss, gliosis, demyelination, or oedema (Larsson et al., 1989).

### **Diffusion Weighted Imaging**

Diffusion Weighted Imaging (DWI) is a relatively new MRI technique that allows the measurement of water self diffusivity (Schaefer et al., 2000). Since freedom of translational motion of water molecules is hindered by interactions with other molecules and cellular barriers, DWI abnormalities can reflect changes of tissue organization at the cellular level (e.g. the increase of extra-cellular space due to cell death will lead to less hindered water diffusion). These micro-structural changes affect the (hindered) motion of water molecules, and consequently alter the water diffusion properties and thus the MRI signal. The measured quantity is the apparent diffusion coefficient (ADC) which is measure for the average molecular motion that is affected by cellular organization and integrity.

### **Spectroscopy**

$^1\text{H}$ -MR Spectroscopy ( $^1\text{H}$ -MRS) is a technique which enables quantification of in vivo metabolite concentrations of the brain, thus offering a window on cell metabolism (Ross et al., 2001). Three major metabolites that are commonly observed are: N-acetyl-aspartate (NAA), which is indicative of neuronal integrity, choline (Cho), of which increased concentrations can act as a malignancy (i.e. tumor) marker, and total creatine (tCr), indicative of the energy metabolism (Govindaraju et al., 2000). Using chemical shift imaging (CSI), in which metabolite spectra are simultaneously recorded from multiple adjoining

spatial regions (i.e. voxels), it is possible to measure the distribution of metabolites throughout the brain (Brown et al., 1982).

In this study we investigated whether SGTCS have an effect on the outcomes of neuropsychological testing, and whether a high number of SGTCS accumulated over life is associated with microstructural and metabolic changes in brain tissue characteristics in the temporal and frontal lobes, as determined by multimodal quantitative MR.

## **Materials and Methods**

### **Subjects**

The study population included 16 patients (10 women and 6 men; mean age 40 years; range 21-59). All patients were consecutively included from the outpatient clinic for neurology of the Maastricht University Hospital. Data acquisition was conducted within the guidelines of the local institutional medical ethical committee overseeing human research, and every study participant provided written informed consent. Inclusion criteria for the study were: localization-related epilepsy with secondarily generalized seizures, no history of status epilepticus and no other underlying disease that could possibly cause cognitive decline.

The following patient data were collected: age at onset, total number of SGTCS during life-time, partial seizure frequency per month (averaged over the last six months), seizure focus, etiology, and drug load. Total number of SGTCS was calculated according to patient history and seizure diaries. Patients were divided into two groups, one group with less than 20 SGTCS (n=8), and one group with more than 20 SGTCS (n=8). Drug load was calculated by standardizing the doses of antiepileptic drugs using the ratio of prescribed daily dose to defined daily dose (Lammers et al., 1995). No SGTCS were reported in the last two weeks before MRI-scanning. Patient characteristics are listed in Table 5.1.

Additionally, fourteen healthy subjects (8 women and 6 men; mean age 35 years; range 21-60) were assessed using an identical quantitative MR protocol to investigate possible age related effects.

### **Neuropsychological testing**

All subjects underwent neuropsychological testing, including tests for intelligence, handedness, attentional functions, information processing and memory function. To test intelligence, the Wechsler Adult Intelligence Scale third edition (WAIS-III) was used. Memory function was tested using the FePsy neuropsychological testbattery (Aldenkamp et al., 1992). Based on the combined

result of these tests, a composite score was derived, comparing the actual level with the expected level, based on premorbid educational level. The resulting score was one of five categories: 1. no intellectual deterioration and no cognitive dysfunction, 2. no intellectual deterioration but signs of mental slowing, 3. no intellectual deterioration but signs of dysfunction in only one area of higher cognitive functioning (i.e. language or memory), 4. no intellectual deterioration and two impaired areas of higher cognitive function (i.e. impaired language and memory) with or without mental slowing, and 5. global intellectual deterioration.

Table 5.1.

Patient	Age (y)	Sex	Epilepsy duration (y)	Seizure focus*	Etiology	Total number of SGTCs	Partial seizure frequency (per month)	Drug load
<b>Less than 20 SGTCs</b>								
2	55	F	39	Multiple	MTS	4	2	1.2
4	24	F	15	RF	crypt	14	0	3.0
6	56	F	9	Multiple	crypt	4	0	3.7
11	40	F	34	LT	MTS, LTL	12	300	1.7
12	49	F	44	RT	crypt	2	0	0.0
13	57	M	14	Unknown	crypt	6	0	0.8
15	25	M	10	Unknown	crypt	2	0	2.4
16	21	M	9	LT	AC	1	75	2.6
<b>More than 20 SGTCs</b>								
1	23	F	1	LF	CD	32	75	1.0
3	37	F	14	LT	MTS	21	0	0.6
5	59	M	40	LF	CD	72	20	1.6
7	41	F	2	LF	APS	200	1	1.6
8	24	M	17	LT	crypt	96	0	2.0
9	31	M	27	RT	crypt	22	0	4.6
14	49	F	3	RT	crypt	21	0	0.0
10	55	F	17	LT	MTS	30	12	1.5

#### Patient demographics and characteristics

SGTCs, secondarily generalized tonicoclonic seizures; F, female; M, male; LF, left frontal; RF, right frontal; LT, left temporal; RT, right temporal; CD, cortical dysplasia; MTS, mesiotemporal sclerosis; crypt, cryptogenic; APS, anti-phospholipid syndrome; LTL, left temporal lobectomy; AC, arachnoid cyst

\* Based on the electroencephalogram

Statistical analyses were performed in SPSS (Release 12.0.1 for Windows, Chicago, SPSS Inc.). Clinical and neuropsychological data analyses were tested using the two-tailed Student's *t* tests, and differences in deterioration scores were analyzed using the non-parametric Wilcoxon/Mann-Whitney test.

## **MR Imaging**

Whole cerebrum imaging was performed with a clinical 1.5 T MRI system (Philips Intera, Philips Medical Systems, Best, The Netherlands), which was equipped with a standard quadrupolar head receiver coil. For anatomic reference, first a T1-weighted three-dimensional (3D) fast field echo (FFE) was acquired with the following parameters: repetition time (TR) 11.07 ms, echo time (TE) 3.5 ms, flip angle 90°, matrix 256x256x168, field of view (FOV) 256x130x168 mm<sup>3</sup>, 1 mm adjacent transverse slices. For T2 quantification a 3D dual-echo turbo spin echo (TSE-Dual) was performed, using the following parameters: TR 5211 ms, TE1 11.9 ms, TE2 80 ms, matrix 256x256x64, FOV 204x112.5x256 mm<sup>3</sup>, and 1.6 mm adjacent transverse slices with a gap of 0.16 mm. DWI images were obtained with a quadruple-shot echo planar imaging (EPI) sequence, using the following parameters: b-values 0, 400, 800, and 1200 s/mm<sup>2</sup>, 3 orthogonal diffusion sensitizing directions, TR 2 cardiac cycles (through cardiac triggering), TE 76 ms, gradient overplus on, matrix 128x128x28, FOV 230x230x170 mm<sup>3</sup>, and 5 mm transverse slices with a gap of 1 mm.

## **Proton MR spectroscopic imaging**

One slice was selected for spectroscopic imaging, accommodated in the frontal and parietal lobe. The slice was oriented just above both lateral ventricles, parallel to the line from the rostrum to the splenium of the corpus callosum, extending from the frontal lobe to the parieto-occipital sulcus. The following parameters were used for the spectroscopic sequence: turbo factor 3, 24x24 voxels, FOV 230x230 mm<sup>2</sup>, slice thickness 20 mm, TR 2.5 s, TE 272 ms, spectral width 1050 Hz, 256 data points, a nominal voxel size of 1.84 ml, echo acquisition mode 'maximum'. Localization and water suppression was achieved with point-resolved spatially localized spectroscopy (PRESS) and chemical shift selective suppression (CHESS), respectively. Lipid signals from the skull base and from the retro-orbital space were eliminated by polygonal outer volume presaturation using 10 'multiple regional saturation technique' slabs of 3 cm thickness.

## **Image analysis**

Unless otherwise described, image processing was performed using customized software in Matlab (The Mathworks, Natick, MA, USA), based on SPM2 software routines (Wellcome Department of Cognitive Neurology, London, UK).

## T2 and cerebrospinal fluid quantification

T2. T2 values were calculated (in ms) on a voxel-by-voxel basis using the signal intensities of the images obtained at the two echo times, using the following equation (Woermann et al., 1998):

$$T2 = \frac{TE_2 - TE_1}{\ln\left(\frac{SI_1}{SI_2}\right)} \quad [5.1]$$

Where  $TE_1$  is the first echo time of 12 ms, and  $TE_2$  is the second echo time of 80 ms,  $SI_1$  and  $SI_2$  are the signal intensities corresponding to  $TE_1$  and  $TE_2$ , respectively.

*Cerebrospinal fluid.* A percentile volume cerebrospinal fluid (CSF) map was calculated by attributing voxels individually to a pericortical CSF percentage ( $\lambda_{CSF}$ ) on a scale of 0-100 %. The  $\lambda_{CSF}$  was based on the T2 value of the voxel as calculated from the TSE-dual images. For this, the T2 relaxation rate (i.e.  $1/T2$ ) was assumed to be a fractional volume weighted sum of CSF ( $T2_{CSF} = 2200$  ms (Haacke, 1999)) and uniform brain tissue ( $T2_{tissue} = 100$  ms (Bottomley et al., 1987)):  $1/T2 = \lambda_{CSF} / T2_{CSF} + (1 - \lambda_{CSF}) / T2_{tissue}$ . For large T2 values (i.e.  $T2 \geq 2200$  ms),  $\lambda_{CSF}$  was set to 100%. The T2-map was spatially transformed into common coordinates along with the spatial normalization procedure of the TE2 image into the standard brain space defined by the Montreal Neurological Institute (MNI) T2 template. This approach facilitated analysis of various separate brain regions through masks.

## ADC quantification

Maps of the water diffusion in terms of the apparent diffusion coefficient (ADC) were calculated by second order polynomial fitting of the direction averaged logarithmic signal intensities versus b-values, according to (Maier et al., 2001; Maier et al., 2004):

$$\ln S = \ln S_0 - ADC \cdot b + \beta \cdot b^2 \quad [5.2]$$

Where  $S$  is the diffusion weighted signal intensity,  $S_0$  the non-weighted intensity,  $ADC$  the apparent diffusion coefficient,  $b$  the b-value describing the motion sensitization by the gradients, and  $\beta$  the coefficient describing the deviation from a monoexponential decay (e.g. due to the presence of water in several different water pool components).  $ADC$  was expressed in units of  $10^{-6}$  mm<sup>2</sup>/s. The ADC-map was spatially normalized along with the normalization procedure of the b=0 image into the space defined by the MNI T2 template.

### Metabolite quantification

The spectroscopic imaging metabolite spectra were analyzed using the CSX software package (P.B. Barker, D.Phil., Johns Hopkins University). The data sets were processed by two-dimensional Fourier transformation, with cosine filters in the spatial (phase-encoding) domains, and exponential line-broadening of 3 Hz, zero-filling to 2048 data points, and a high-pass convolution filter to remove the residual water signal (50 Hz band filter) in the time domain. A  $B_0$  correction was applied based on the chemical shift of NAA of 2.02 parts per million (ppm). No baseline correction was applied. Magnitude mode signals of Cho, tCr, and NAA were fitted to a Gaussian line shape using a non-linear least squares fitting (simplex) routine, and the metabolite images were reconstructed. The peak area ratios  $NAA/(Cho+tCr)$  were calculated from the uncorrected peak areas of the respective signals. Voxels with Cho, tCr, and NAA peak linewidths  $>2$  and  $<9$  Hz were included for analysis.

### Statistical analysis

As the effect of SGTCS might be different for different cerebral tissue types (e.g. neurons and axons) (Geinisman et al., 1990), we chose to examine grey matter (containing neurons) and white matter (containing axons) independently. To enable a separate analysis of grey matter and white matter, segmentation of the T1-weighted images into grey matter, white matter, and CSF was performed using SPM2. Statistical analysis of the T2-,  $\lambda$ CSF-, and ADC-maps and the 1H-MRS CSI voxels was performed on various cerebral regions, using masks created with WFU-Pickatlas (Maldjian et al., 2003). As effects related to SGTCS not necessarily localize to the same microstructural regions from patient to patient, we analyzed data more globally by averaging quantitative MR outcomes over selected regions, rather than performing a pixel by pixel analysis method. Since the presence of structural and functional brain asymmetry has been reported in morphological studies (Hugdahl, 2000), the left and right hemispheres were analyzed separately. Analysis of the imaging data was restricted to the temporal and frontal lobes (see Figure 5.1). The mean T2,  $\lambda$ CSF, ADC and  $NAA/(Cho+tCr)$  values were calculated for the selected regions.

Multiple end point testing was controlled for by first investigating in what specific regions quantitative MR alterations due to SGTCS were found. To this end,  $\lambda$ CSF, grey matter T2, and grey matter ADC MR outcomes were combined per region, since all these measures are substantially affected by changes in water content. For each region, the global null hypothesis stating that no differences exist within that region between the group with less than 20 SGTCS and the group with more than 20 SGTCS of the included MR modalities was tested using the ordinary least squares test of O'Brien and Läuter (O'Brien, 1984;

Läuter, 1996). For the combined analysis, statistical significance was calculated with two-tailed Student's *t* tests with Hochberg correction for multiple comparisons (Hochberg, 1988).

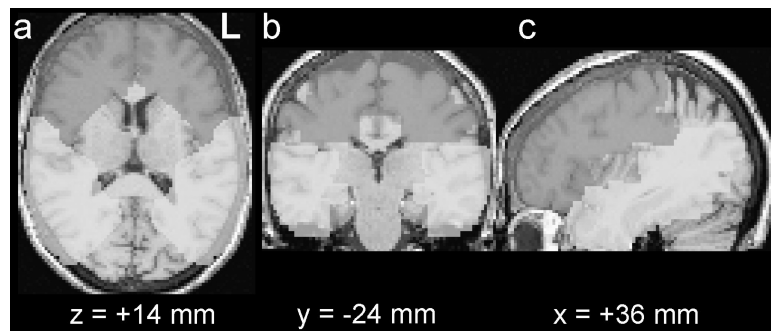


**Figure 5.1.** The employed frontal (dark grey) and temporal (light grey) masks, overlaid on spatially normalized (a) transverse, (b) coronal, and (c) sagittal T1-weighted MR images. Slice positions are given in stereotaxic Talairach coordinates.

Additionally, in a subsequent analysis per MR technique, tissue T2,  $\lambda_{\text{CSF}}$ , ADC values, and spectroscopic data of the patient group with less than 20 SGTCs were compared with those of patients with more than 20 SGTCs. For the separate modality analyses, statistical significance was calculated with two-tailed Student's *t* tests. For all statistical analyses,  $p < 0.05$  was considered significant. Results were expressed as mean  $\pm$  standard error of the mean (SEM).

### Effect of age

As the group with more than 20 SGTCs was substantially younger (11 years) than the group with less than 20 SGTCs, we performed an additional separate analysis. For this analysis, we included 14 healthy volunteers (range 21 – 60 years) that underwent the same multimodal quantitative MR protocol. Linear regression was performed to investigate possible age-dependent effects in the quantitative measurements. In a separate analysis, all quantitative data from the patients with epilepsy were corrected for age, using the coefficients obtained from these regression analyses.

## Results

### Clinical and Neuropsychological assessment

The patient group with more than 20 SGTCs displayed a significantly higher drug load (+130 %,  $p < 0.05$ ) than patients with less than 20 SGTCs. Although the age was not significantly different between the two groups

Table 5.2

	<20 SGTCs Mean (SEM)	>20 SGTCs Mean (SEM)
<b>Clinical parameters</b>		
Total number of SGTCs	6 (2) †	62 (22)
Partial seizure frequency	47 (37)	14 (9)
Age	46 (5)	35 (5)
Epilepsy duration	21 (6)	16 (4)
Drug load	1.1 (0.3) †	2.5 (0.4)
IQ	118 (5) †	94 (7)
Deterioration score	2.0 (0.4)	3.0 (0.5)
<b>Regions</b>		
<b>left frontal</b>		
T2 WM	130 (13)	102 (5)
T2 GM	155 (14)	120 (6)
$\lambda_{\text{CSF}}$	17.4 (1.2)	14.1 (1.3) ‡
ADC WM	1287 (67) †	1106 (48)
ADC GM	1408 (59) †	1228 (41)
NAA/(Cho+tCr)	0.52 (0.03)	0.55 (0.02)
<b>right frontal</b>		
T2 WM	135 (14)	103 (5)
T2 GM	160 (16) †	120 (5)
$\lambda_{\text{CSF}}$	16.5 (1.2) †	12.9 (1.1) ‡
ADC WM	1257 (68)	1077 (55)
ADC GM	1372 (62) †	1181 (43)
NAA/(Cho+tCr)	0.50 (0.04)	0.55 (0.03)
<b>left temporal</b>		
T2 WM	101 (5)	92 (2)
T2 GM	112 (6)	102 (2)
$\lambda_{\text{CSF}}$	11.3 (0.7)	9.5 (0.5)
ADC WM	1140 (70)	1005 (34)
ADC GM	1205 (76)	1080 (51)
NAA/(Cho+tCr)	0.55 (0.04)	0.65 (0.02)
<b>right temporal</b>		
T2 WM	108 (6)	97 (3)
T2 GM	122 (6)	109 (4)
$\lambda_{\text{CSF}}$	12.5 (0.9)	10.0 (1.1)
ADC WM	1172 (71)	1077 (41)
ADC GM	1244 (76)	1144 (56)
NAA/(Cho+tCr)	0.52 (0.04)	0.63 (0.03)

Clinical and quantitative MR results in patients with less than 20 SGTCs and patients with more than 20 SGTCs.

SGTCs, secondarily generalized tonicoclonic seizures; SEM, standard error of the mean; Partial seizure frequency (per month); Age (in years); Epilepsy duration (in years) T2, transverse relaxation time (in ms); WM, white matter; GM, grey matter;  $\lambda_{\text{CSF}}$ , percentage of cerebrospinal fluid (in %); ADC, apparent diffusion coefficient (in  $10^{-6} \text{ mm}^2/\text{s}$ ); NAA/(Cho+tCr), ratio of N-acetyl-aspartate to the sum of choline and total creatine concentrations.

† 2-tailed  $P < 0.05$ , ‡ 2-tailed  $P < 0.05$  (ordinary least squares test using Hochberg correction)



( $p = 0.12$ ), the group with more than 20 SGTCS is substantially younger (11 years) than the group with less than 20 SGTCS. Neuropsychological assessment revealed a significantly lower IQ (-20%,  $p < 0.05$ ) in the group with more than 20 SGTCS, and a higher (i.e. worse) deterioration score, though the latter was not statistically significant. Results are shown in Table 5.2.

### MR Quality

Visual inspection of all T2- and ADC- maps did not reveal image artifacts; therefore we were confident that the obtained maps were of good quality (Figure 5.2). For the CSI, out of a total of 1505 voxels from the selected slice of all patients, 436 voxels were rejected based on outranged linewidths for NAA, Cho, or tCr. In the frontal lobe, on average 40% of the voxels were discarded, whereas in the temporal lobe about 20% were rejected. Both patient groups displayed similar MR quality characteristics. Figure 5.3 shows an example of the selected spectroscopic imaging slice, and the spectral fit of one voxel.

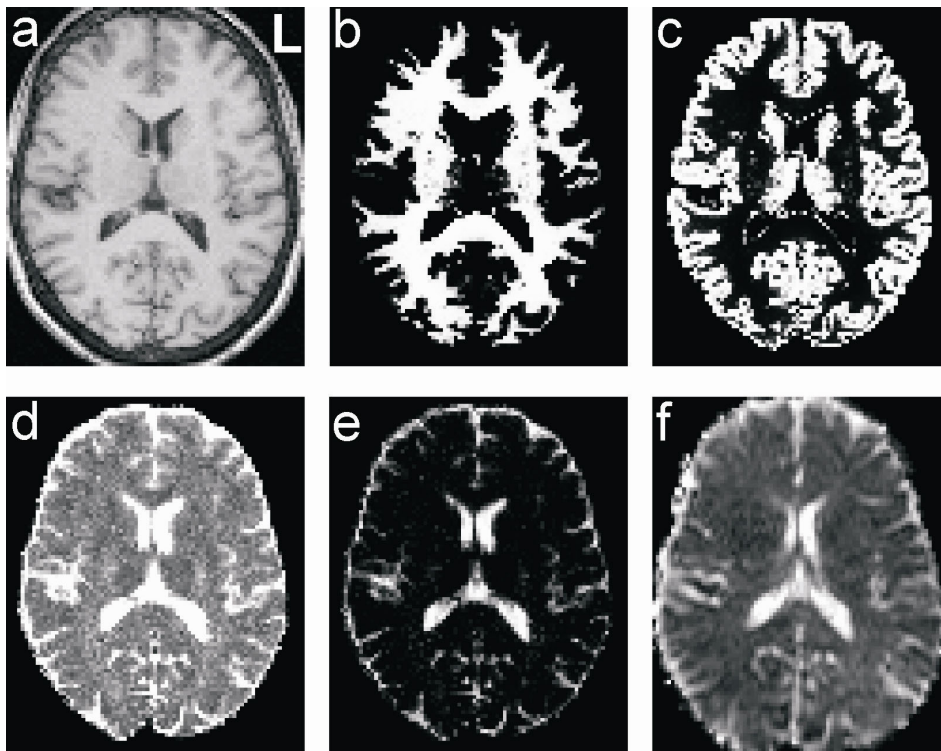


**Figure 5.2.** Spatially normalized transverse (a) T1-weighted, (b) segmented white matter, (c) segmented grey matter images, (d) T2-, (e)  $\lambda$ CSF-, and (f) ADC-maps of a patient with four secondarily generalized tonicoclonic seizures. Slice position is  $z = +14$  mm in stereotaxic Talairach coordinates.

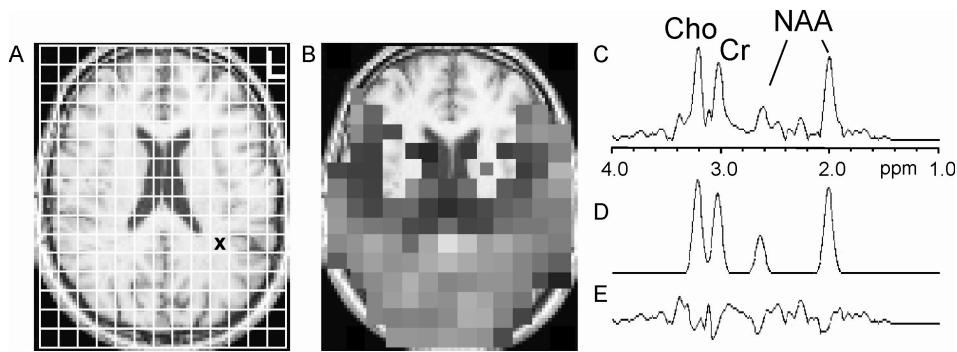


**Figure 5.3.** (a) The spectroscopic imaging grid and the (b) NAA/(Cho+tCr) map of voxels satisfying the quality control requirements of a patient with four secondarily generalized tonicoclonic seizures overlaid on an oblique normalized transverse T1-weighted image. Slice position is approximately  $z = +14$  mm in stereotaxic Talairach coordinates. (c) Original in vivo spectrum of the voxel marked with a black cross in (a), (d) Gaussian fit estimation for the main metabolites (NAA, N-acetyl-aspartate; cho, choline; and tCr, total creatine), and (e) the difference between the original spectrum and the Gaussian fit (residue).

### Quantitative MR: regional analysis

The ordinary least squares test revealed statistically significant SGTCS-related MR alterations in both left and right frontal lobe, but not in the temporal lobe. (Table 5.2)

### T2 relaxometry

In the right frontal lobe, a significantly decreased (-25%,  $p < 0.05$ ) T2 relaxation time for grey matter was observed in the group with more than 20 SGTCS. Additionally, a significantly decreased cerebrospinal fluid (-22%,  $p < 0.05$ ) content was found in this region.

### Diffusion weighted imaging

Decreased ADC values in both white (-14%,  $p < 0.05$ ) and grey matter (-13%,  $p < 0.05$ ) of the left frontal lobe were observed in the group with more than 20 SGTCS. Furthermore, a significant decrease in ADC (-14%,  $p < 0.05$ ) was noticed for the grey matter of the right frontal lobe.

Figure 5.4 illustrates a hypointense prefrontal region on both the ADC- and T2-map for a patient with 72 SGTCS compared to a patient with one SGTCS.

### $^1\text{H}$ MR spectroscopy

No significant differences in NAA/(Cho+tCr) concentrations were detected between the patient group with less than 20 SGTCS and the group with more than 20 SGTCS.

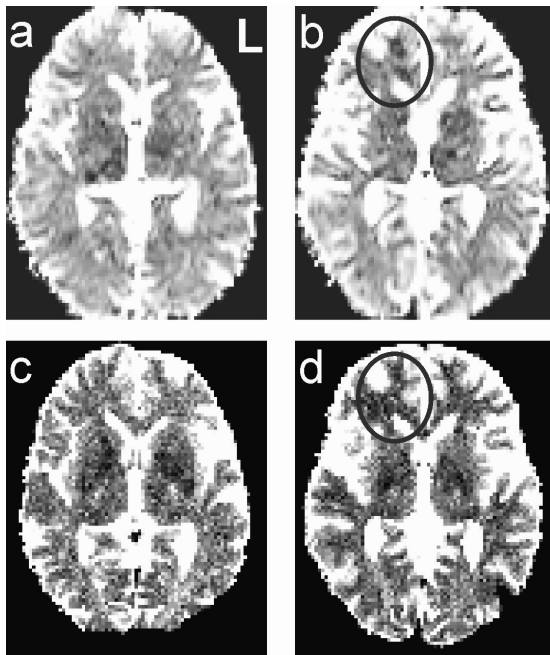


**Figure 5.4.** Transverse (a-b) ADC-maps and (c-d) T2-maps of a patient with one secondarily generalized tonicoclonic seizure (a,c) and a patient with 72 secondarily generalized tonicoclonic seizures (b,d). The black circles in (b) and (d) indicate a hypointense prefrontal region in the ADC- and T2-map, respectively, for the patient with 72 secondarily generalized tonicoclonic seizures. For both patients, the epileptic focus was left temporal. No right frontal abnormalities were observed on the conventional MRI.

Slice position is  $z = 0$  mm in stereotaxic Talairach coordinates.

### Effect of age

Linear regression of quantitative MR data from the healthy volunteers revealed significant age dependent effects for T2 (+0.8 ms/y,  $p < 0.05$ ),  $\lambda_{\text{CSF}}$  (+0.12%/y,  $p < 0.05$ ), and ADC ( $+5 \cdot 10^{-6}$  mm<sup>2</sup>/sy,  $p < 0.01$ ). NAA/(Cho+tCr) was not significantly influenced by age ( $p = 0.17$ ). A separate, age-corrected analysis of quantitative data from the patients with epilepsy revealed similar results as the analysis without age-correction, e.g. generally decreased frontal T2,  $\lambda_{\text{CSF}}$ , and ADC values due to SGTCS (data not shown).

### Discussion

In this study, the cognitive deterioration level was assessed in patients with varying numbers of SGTCS using neuropsychological testing. Also, we combined quantitative multimodal MR, comprising T2 relaxometry, DWI, and <sup>1</sup>H-MRS to assess the effect of multiple SGTCS experienced during lifetime on metabolic and microstructural cerebral tissue characteristics. A number of novel MR abnormalities were found. Regional combined multimodal analysis revealed that significant quantitative MR changes were present in the frontal lobe but not in the temporal lobe, which were related to the number of SGTCS. Furthermore, the left and right frontal lobe generally displayed lower T2

relaxation times, smaller pericortical CSF fraction and lower ADC values, in patients with more than 20 SGTCS compared to those with less than 20 SGTCS.

### **Clinical characteristics**

Clinical and neuropsychological assessment revealed lower IQ scores for patients with more than 20 SGTCS compared to patients with less than 20 SGTCS. These results are in line with earlier observations that a high number of SGTCS might be associated with cognitive deterioration (Dikmen et al., 1977; Seidenberg et al., 1981; Bourgeois et al., 1983; Dodrill, 1986; Trimble, 1988; Dodrill, 2002). Also, higher drug loads were observed for the patient group with more than 20 SGTCS. These results suggest that patients with a more severe type of epilepsy, due to many SGTCS, are receiving more antiepileptic drugs, probably because these patients are more likely to be therapy-resistant.

### **Quantitative MR: regional analysis**

The patients included in this study had varying etiologies and seizure foci. However, the heterogeneous composition of both the patient group with less than 20 SGTCS and the group with more than 20 SGTCS was highly similar (e.g. both frontal and temporal seizure foci, see Table 5.1). Therefore we argue that the influence of the focus on the observed differences between the two groups is limited, whereas the number of SGTCS is of more importance. The combined regional analysis of quantitative MR revealed predominantly frontal abnormalities. As the performance of primarily prefrontal cortex-associated executive functions, e.g. working memory, is of substantial importance for normal cognitive performance (Dikmen et al., 1977), it is most plausible to assume that the frontal lobe is involved in this cognitive dysfunction. Additionally, since the seizure focus was often not located in the frontal lobe for most patients (Table 5.1), the involvement of the frontal lobes is most likely the secondary generalization of seizures (i.e. spread). Therefore, the neuronal correlate for cognitive deterioration in patients with SGTCS might be located in the frontal or prefrontal regions.

### **Microstructural MR**

Chronic neuronal damage due to seizures is often associated with increased water content, leading to increased pericortical CSF fractions, and T2 and ADC values (Hugg et al., 1999). In this study, however, we very consistently observed the opposite effect: a high number of SGTCS was associated with decreased T2, ADC, and fractional CSF values. A possible explanation for this apparent discrepancy is that most clinical quantitative MRI epilepsy studies were focused on detecting abnormalities at or near the epileptic focus. Our method was primarily aimed at detecting general abnormalities remote from the seizure focus, therefore different mechanisms

may be underlying these abnormalities. In a recent diffusion tensor imaging study of patients with medial temporal lobe epilepsy and hippocampal sclerosis, Thivard et al (Thivard et al., 2005) also observed decreased ADC values in a region distant from the epileptic focus, e.g. the frontal lobes and the contralateral hippocampal region. Although the exact mechanism underlying this decrease was not known, it was speculated that generalization of seizures could be related to functional changes of neurons and reversible transsynaptic deafferentation (i.e. the elimination of sensory nerve impulses by injuring the sensory nerve fibers) of the contralateral temporal lobe. Moreover, it was hypothesized that the observed abnormalities would be related to neuronal dysfunction, rather than neuronal loss (Thivard et al., 2005). One can only speculate whether this explanation also holds for the SGTCS related frontal abnormalities observed in this study. The effect of SGTCS on altered MRI characteristics (i.e. T2 and ADC) was more pronounced in the grey matter than the white matter (Table 5.2). Apparently grey matter is more prone to SGTCS related alterations than white matter. We suggest that neurons (predominantly present in grey matter) are more sensitive to SGTCS-related damage than axons (predominantly present in white matter). We therefore hypothesize that the signal transduction properties of axons are more robust and less prone to increased neurotransmitter traffic than the signal reception properties of neurons.

### **Spectroscopy**

Proton MRS did not reveal any significant effects of SGTCS in this study, whereas it was previously reported that temporal lobe epilepsy patients with frequent SGTCS have lower hippocampal NAA values than patients without SGTCS (Bernasconi et al., 2002; Lee et al., 2005). In contrast to these studies, not the frequency but the number of total accumulated SGTCS over lifetime was considered for the current study. Furthermore, the selected spectroscopic imaging slice in the current study did not contain the hippocampus, therefore comparison of results should be handled with care. Unfortunately, a large part of the spectra from the frontal lobe in most patients had to be discarded based on its low quality. These voxels are close to air cavities near the skull base. This causes an increased field inhomogeneity, which complicates shimming and water suppression, leading to a decreased quality of spectra. Therefore, possible frontal spectroscopic abnormalities would have been hard to detect, due to the limited number of spectra from the frontal lobe. Future studies might benefit from improved MRI hardware and absolute quantification of metabolite concentrations (Jansen et al., 2006).

### **Limitations**

The current study has some limitations that restrict generalization of SGTCS-related cerebral abnormalities. Due to its cross-sectional design, the limited number and heterogeneous nature of patients, the observed effect cannot be unambiguously attributed to SGTCS alone. Furthermore, the group with more than 20 SGTCS is substantially younger (11 years on average) than the group with less than 20 SGTCS. However, as this difference is not significant, and as the separate age corrected analysis yielded similar results, we argue for the exclusion of an age effect. Also a significant difference in drug load between the groups was observed, which indicates that the observed differences might be purely due to higher drug loads. It is very complicated and possibly unethical to study the effect of SGTCS with lower drug load; furthermore, a high drug load is likely an ultimate consequence of the severity of the epilepsy due to the SGTCS. Even in this small population of patients with varying etiologies and seizure foci, we have been able to demonstrate a statistically significant effect of number of SGTCS on frontal abnormalities. Moreover, SGTCS are affecting intellectual functioning and probably are an important factor in cognitive decline. Possibly, in more homogeneous and larger epilepsy populations, the effects could be even more pronounced. The applied threshold of 20 SGTCS might seem somewhat arbitrary, however we found that the obtained differences between two groups of patients with epilepsy separated based on the number of SGTCS during lifetime were highly robust against considerable variation (range, 20 to 30 SGTCS) in the selected threshold of SGTCS.

### **Clinical implications**

Clinically, it has been proven difficult to substantiate that seizures can cause (permanent) brain damage, which might be responsible for cognitive decline (Vingerhoets, 2006). These days, emerging data exist from human MRI and neuropsychological studies (Sutula et al., 2003). Therefore, patients can no longer be reassured with confidence that only prolonged seizures, as in status epilepticus, can cause brain damage and/or cognitive decline, whereas repeated brief seizures do not. The results of the current study suggest that seizure control in patients with epilepsy is of major importance, as the presence of SGTCS in the human brain is associated with an adverse and widespread neurodevelopmental impact on both brain structure and function.

### **Conclusion**

In the present study, frontal, but not temporal, MR abnormalities were found to be related to SGTCS. These findings confirm that SGTCS do have a substantial effect on both frontal brain function and on the metabolic and microstructural brain tissue characteristics. This knowledge may help to obtain

a better understanding and anticipatory treatment of SGTCs-related cognitive deterioration.

### **Acknowledgements**

The authors express gratitude for the contributions of I.A.M. Westmijse and K.W. Lamberts, who participated in the development of the initial data processing routines.

P.B. Barker, D.Phil. (Johns Hopkins University) is gratefully acknowledged for providing the CSX software package.

## References

- Aldenkamp, A.P., Vermeulen, J., Alpherts, W.C.J., et al. (1992) Validity of computerized testing: patient dysfunction and complaints versus measured changes. IN Dodson, W. E. & Kinsbourne, M. (Eds.) *Assessment of cognitive function*. New York, Demos.
- Beck, H., Goussakov, I.V., Lie, A., et al., 2000. Synaptic plasticity in the human dentate gyrus. *J Neurosci* 20, 7080-7086.
- Bernasconi, A., Tasch, E., Cendes, F., et al., 2002. Proton magnetic resonance spectroscopic imaging suggests progressive neuronal damage in human temporal lobe epilepsy. *Prog Brain Res* 135, 297-304.
- Blake, R.V., Wroe, S.J., Breen, E.K., et al., 2000. Accelerated forgetting in patients with epilepsy: evidence for an impairment in memory consolidation. *Brain* 123 Pt 3, 472-483.
- Bottomley, P.A., Hardy, C.J., Argersinger, R.E., et al., 1987. A review of 1H nuclear magnetic resonance relaxation in pathology: are T1 and T2 diagnostic? *Med Phys* 14, 1-37.
- Bourgeois, B.F., Prenskey, A.L., Palkes, H.S., et al., 1983. Intelligence in epilepsy: a prospective study in children. *Ann Neurol* 14, 438-444.
- Brown, T.R., Kincaid, B.M., Ugurbil, K., 1982. NMR chemical shift imaging in three dimensions. *Proc Natl Acad Sci U S A* 79, 3523-3526.
- Corcoran, R., Thompson, P., 1992. Memory failure in epilepsy: retrospective reports and prospective recordings. *Seizure* 1, 37-42.
- Dikmen, S., Matthews, C.G., 1977. Effect of major motor seizure frequency upon cognitive-intellectual functions in adults. *Epilepsia* 18, 21-29.
- Dodrill, C.B., 1986. Correlates of generalized tonic-clonic seizures with intellectual, neuropsychological, emotional, and social function in patients with epilepsy. *Epilepsia* 27, 399-411.
- Dodrill, C.B., 2002. Progressive cognitive decline in adolescents and adults with epilepsy. *Prog Brain Res* 135, 399-407.
- Dodrill, C.B., Batzel, L.W., 1986. Interictal behavioral features of patients with epilepsy. *Epilepsia* 27 Suppl 2, S64-76.
- Duncan, J.S., 2002. MRI studies. Do seizures damage the brain? *Prog Brain Res* 135, 253-261.
- Filippi, M., Rocca, M.A., 2007. Magnetic resonance imaging techniques to define and monitor tissue damage and repair in multiple sclerosis. *J Neurol* 254 Suppl 1, I55-I62.
- Geinisman, Y., Morrell, F., deToledo-Morrell, L., 1990. Increase in the relative proportion of perforated axospinous synapses following hippocampal kindling is specific for the synaptic field of stimulated axons. *Brain Res* 507, 325-331.
- Govindaraju, V., Young, K., Maudsley, A.A., 2000. Proton NMR chemical shifts and coupling constants for brain metabolites. *NMR Biomed* 13, 129-153.
- Guadagno, J.V., Calautti, C., Baron, J.C., 2003. Progress in imaging stroke: emerging clinical applications. *Br Med Bull* 65, 145-157.
- Haacke, E.M. (1999) *Magnetic resonance imaging: physical principles and sequence design*, New York, J. Wiley & Sons.
- Helmstaedter, C., 2002. Effects of chronic epilepsy on declarative memory systems. *Prog Brain Res* 135, 439-453.
- Helmstaedter, C., Elger, C.E., 1999. The phantom of progressive dementia in epilepsy. *Lancet* 354, 2133-2134.
- Hermann, B., Seidenberg, M., 2007. Epilepsy and cognition. *Epilepsy Curr* 7, 1-6.
- Hermann, B., Seidenberg, M., Bell, B., et al., 2003. Extratemporal quantitative MR volumetrics and neuropsychological status in temporal lobe epilepsy. *J Int Neuropsychol Soc* 9, 353-362.



- Hermann, B., Seidenberg, M., Sears, L., et al., 2004. Cerebellar atrophy in temporal lobe epilepsy affects procedural memory. *Neurology* 63, 2129-2131.
- Hochberg, Y., 1988. A sharper Bonferroni procedure for multiple tests of significance. *Biometrika* 75, 800-802.
- Hugdahl, K., 2000. Lateralization of cognitive processes in the brain. *Acta Psychol (Amst)* 105, 211-235.
- Hugg, J.W., Butterworth, E.J., Kuzniecky, R.I., 1999. Diffusion mapping applied to mesial temporal lobe epilepsy: preliminary observations. *Neurology* 53, 173-176.
- Jansen, J.F., Backes, W.H., Nicolay, K., et al., 2006. 1H MR spectroscopy of the brain: absolute quantification of metabolites. *Radiology* 240, 318-332.
- Jokeit, H., Seitz, R.J., Markowitsch, H.J., et al., 1997. Prefrontal asymmetric interictal glucose hypometabolism and cognitive impairment in patients with temporal lobe epilepsy. *Brain* 120 ( Pt 12), 2283-2294.
- Kotloski, R., Lynch, M., Lauersdorf, S., et al., 2002. Repeated brief seizures induce progressive hippocampal neuron loss and memory deficits. *Prog Brain Res* 135, 95-110.
- Kramer, U., Kipervasser, S., Neufeld, M.Y., et al., 2006. Is there any correlation between severity of epilepsy and cognitive abilities in patients with temporal lobe epilepsy? *Eur J Neurol* 13, 130-134.
- Lammers, M.W., Hekster, Y.A., Keyser, A., et al., 1995. Monotherapy or polytherapy for epilepsy revisited: a quantitative assessment. *Epilepsia* 36, 440-446.
- Larsson, H.B., Frederiksen, J., Petersen, J., et al., 1989. Assessment of demyelination, edema, and gliosis by in vivo determination of T1 and T2 in the brain of patients with acute attack of multiple sclerosis. *Magn Reson Med* 11, 337-348.
- Läuter, J., 1996. Exact T and F tests for analyzing studies with multiple endpoints. *Biometrics* 52, 964-970.
- Lee, S.K., Kim, D.W., Kim, K.K., et al., 2005. Effect of seizure on hippocampus in mesial temporal lobe epilepsy and neocortical epilepsy: an MRS study. *Neuroradiology* 47, 916-923.
- Maier, S.E., Bogner, P., Bajzik, G., et al., 2001. Normal brain and brain tumor: multicomponent apparent diffusion coefficient line scan imaging. *Radiology* 219, 842-849.
- Maier, S.E., Vajapeyam, S., Mamata, H., et al., 2004. Biexponential diffusion tensor analysis of human brain diffusion data. *Magn Reson Med* 51, 321-330.
- Maldjian, J.A., Laurienti, P.J., Kraft, R.A., et al., 2003. An automated method for neuroanatomic and cytoarchitectonic atlas-based interrogation of fMRI data sets. *Neuroimage* 19, 1233-1239.
- Miller, S.P., Li, L.M., Cendes, F., et al., 2000. Medial temporal lobe neuronal damage in temporal and extratemporal lesional epilepsy. *Neurology* 54, 1465-1470.
- O'Brien, P.C., 1984. Procedures for comparing samples with multiple endpoints. *Biometrics* 40, 1079-1087.
- Reminger, S.L., Kaszniak, A.W., Labiner, D.M., et al., 2004. Bilateral hippocampal volume predicts verbal memory function in temporal lobe epilepsy. *Epilepsy Behav* 5, 687-695.
- Ross, B., Bluml, S., 2001. Magnetic resonance spectroscopy of the human brain. *Anat Rec* 265, 54-84.
- Sass, K.J., Sass, A., Westerveld, M., et al., 1992. Specificity in the correlation of verbal memory and hippocampal neuron loss: dissociation of memory, language, and verbal intellectual ability. *J Clin Exp Neuropsychol* 14, 662-672.
- Sass, K.J., Spencer, D.D., Kim, J.H., et al., 1990. Verbal memory impairment correlates with hippocampal pyramidal cell density. *Neurology* 40, 1694-1697.
- Schaefer, P.W., Grant, P.E., Gonzalez, R.G., 2000. Diffusion-weighted MR imaging of the brain. *Radiology* 217, 331-345.
- Seidenberg, M., O'Leary, D.S., Berent, S., et al., 1981. Changes in seizure frequency and test-retest scores on the Wechsler Adult Intelligence Scale. *Epilepsia* 22, 75-83.

- Stefan, H.,Pauli, E., 2002. Progressive cognitive decline in epilepsy: an indication of ongoing plasticity. *Prog Brain Res* 135, 409-417.
- Sutula, T.P., Hagen, J.,Pitkanen, A., 2003. Do epileptic seizures damage the brain? *Curr Opin Neurol* 16, 189-195.
- Tasch, E., Cendes, F., Li, L.M., et al., 1999. Neuroimaging evidence of progressive neuronal loss and dysfunction in temporal lobe epilepsy. *Ann Neurol* 45, 568-576.
- Thivard, L., Lehericy, S., Krainik, A., et al., 2005. Diffusion tensor imaging in medial temporal lobe epilepsy with hippocampal sclerosis. *Neuroimage* 28, 682-690.
- Thompson, P.J.,Corcoran, R., 1992. Everyday memory failures in people with epilepsy. *Epilepsia* 33 Suppl 6, S18-20.
- Thompson, P.J.,Duncan, J.S., 2005. Cognitive decline in severe intractable epilepsy. *Epilepsia* 46, 1780-1787.
- Tofts, P. (2003) *Quantitative MRI of the brain measuring changes caused by disease*, Chichester, West Sussex; Hoboken, N.J., John Wiley & Sons Ltd.
- Trimble, M.R., 1988. Cognitive hazards of seizure disorders. *Epilepsia* 29 Suppl 1, S19-24.
- Vingerhoets, G., 2006. Cognitive effects of seizures. *Seizure* 15, 221-226.
- Woermann, F.G., Barker, G.J., Birnie, K.D., et al., 1998. Regional changes in hippocampal T2 relaxation and volume: a quantitative magnetic resonance imaging study of hippocampal sclerosis. *J Neurol Neurosurg Psychiatry* 65, 656-664.



# Chapter 6

**Seizure related cognitive deterioration is associated with increased prefrontal fMRI activation**

**Vlooswijk MCG, Jansen JFA, Reijs RP, de Krom MCTFM, Kooi ME, Majoie HJM, Hofman PAM, Backes WH, and Aldenkamp AP**

*Submitted for publication*

**Abstract:****Introduction:**

Cognitive deterioration is a frequent comorbid disorder in epilepsy which has been associated with high seizure frequency. We examined the effect of secondarily generalized tonic-clonic seizures (SGTCS) on cognitive deterioration using neuropsychological assessment and fMRI.

**Methods:**

Sixteen patients with localization-related epilepsy of varying etiologies and SGTCS underwent extensive neuropsychological assessment. Functional MRI was performed probing the frontal and temporal lobes with two paradigms aimed at investigating speed of mental processing and working memory.

**Results:**

A high number of total lifetime SGTCS was associated with lower intelligence scores. Moreover, a trend towards cognitive decline related to the number of SGTCS was observed. A relatively increased prefrontal activation related to the number of SGTCS was demonstrated, plus a trend towards a decreased activation in the frontotemporal areas.

**Discussion:**

High numbers of SGTCS conduct to a drop in intelligence scores and altered prefrontal brain activation. A shift from frontotemporal to prefrontal activation seems to have occurred, suggesting that a functional reorganization of working memory is induced by a high number of SGTCS. It remains uncertain if this reorganization reflects a compensation mechanism, or the underlying pathological processes of cognitive deterioration.

## Introduction

In clinical experience, patients with persistent seizures are prone to deteriorate cognitively. Cognitive impairment is in fact the most frequent comorbid disorder in epilepsy (Corcoran and Thompson, 1992; Thompson and Corcoran, 1992; Blake et al., 2000; Helmstaedter, 2002). The spectrum of cognitive problems in epilepsy ranges from the frequently reported memory deficits and mental slowing, to sometimes even global cognitive deterioration. Many factors have been proposed to contribute to cognitive impairment, such as the underlying disease causing epilepsy, cognitive side-effects of antiepileptic drugs (AED) (Trimble, 1987; Ortinski and Meador, 2004; Jokeit et al., 2005), seizure-induced head trauma (Trimble, 1988; Thompson and Duncan, 2005) and ongoing interictal epileptic brain activity (Aldenkamp and Arends, 2004). Cognitive decline has been associated with status epilepticus as well (Dodrill, 1986). Also single seizures, especially secondarily generalized seizures, are thought to have an effect on cognition. In various studies, changes in metabolism (Jokeit et al., 1997; Tasch et al., 1999; Miller et al., 2000; Bernasconi et al., 2002) and neuronal loss (Kotloski et al., 2002) were observed after secondarily generalized tonic-clonic seizures (SGTCS). In patients with a high number of SGTCS, cognitive deterioration has also been described (Dodrill and Batzel, 1986; Trimble, 1988; Dodrill, 2002; Stefan and Pauli, 2002; Thompson and Duncan, 2005), although data are sometimes contradictory (Helmstaedter and Elger, 1999; Kramer et al., 2006).

Different hypotheses are proposed for the mechanisms by which such seizure induced cognitive deterioration could be produced. In animal models, seizures cause changes in protein expression, protein modification, mossy fiber sprouting and synaptic reorganization (Beck et al., 2000). Above that, cell loss in varying regions of the limbic system due to necrosis and apoptosis induced by seizures is noticed (Sass et al., 1990; Sass et al., 1992). It remains unclear, however, if these observed changes occur in either a serial or a parallel fashion (Cole, 2000) and whether they are relevant for deterioration in patients with epilepsy.

We are interested in the association between SGTCS and cognitive deterioration. Considering the global cognitive problems observed in patients with SGTCS, which are often accompanied by mental slowing and impairment in executive function (Dikmen and Matthews, 1977), it is likely to assume that the frontal lobe is involved in this cognitive dysfunction. The involvement of the frontal lobes could be explained by the secondary generalization of seizures. Therefore, the neuronal correlate for cognitive deterioration in patients with SGTCS might be located in the frontal or prefrontal regions.

Previous studies have investigated possible structural alterations associated with seizure-induced cognitive dysfunction. There have been no studies with conventional MRI which could demonstrate a relation between cognitive dysfunction and structural alterations in epilepsy. With volumetry, a

more advanced technique, associations between volume reductions of the hippocampus (Reminger et al., 2004), cerebellum (Hermann et al., 2004), and global cerebral volume reduction (Hermann et al., 2003) and memory deficits as well as poor cognitive performance have been demonstrated. Yet, another study could not establish an association between structural changes and executive function (Martin et al., 2000). However, functional changes might occur in an earlier stage than structural alterations and are possibly easier identified in epilepsy, which is a functional rather than structural disorder of the brain. Therefore, functional MRI could possibly provide a model for the development of cognitive deterioration.

Functional MRI (fMRI) enables the localization of brain activation by demonstrating a blood oxygenation level dependent (BOLD) signal during a (cognitive) paradigm. With task-related fMRI, overall differences in activation patterns between groups can be detected and localized. As the primary seizure focus and the spreading of discharges may vary strongly among patients, it is a priori unknown how seizures may alter the brain activation pattern. Ideally, one would therefore be able to investigate all parts of the brain, rather than only certain regions specifically related to a particular cognitive task. To overcome this problem, we propose to combine different cognitive paradigms which are known to activate different regions of the frontal and temporal lobe in healthy subjects.

Our goal was to investigate the effect of the number of SGTCS accumulated over life on the outcomes of neuropsychological testing and on the distribution of brain activation in the temporal and frontal lobes and foremost whether they are relevant for deterioration.

## **Methods**

### **Participants**

The study population included 16 patients (10 women and 6 men; mean age 40.4 years; range 21-59). All patients were consecutively included from the outpatient clinics for neurology of the Hospital Maastricht. All subjects gave informed consent and approval for the study by the local Medical Ethical Committee was obtained. Inclusion criteria for the study were: localisation-related epilepsy with secondarily generalized seizures, no history of status epilepticus and no other underlying disease that could possibly cause cognitive decline. The following patient data were collected: age at onset, total number of secondarily generalized seizures experienced (SGTCS) during life-time, partial seizure frequency per month (averaged over the last six months), seizure focus, etiology and drugload. Total number of SGTCS was calculated according to patient history and seizure diaries. Drugload was calculated by standardizing the doses of antiepileptic drugs using the ratio of prescribed daily dose to

defined daily dose (Lammers et al. 1995). No SGTCS were reported in the last two weeks before MRI. Patient characteristics are listed in Table 6.1.

**Table 6.1.** Patient characteristics

Patient	Age (y)	Sex	Epilepsy duration (y)	Seizure focus	Etiology	Total nr of SGTCS	Partial seizure frequency (per month)	Drugload
1	23	F	1	LF	CD	1	75	1.0
2	55	F	39	Multiple	MTS	4	2	1.2
3	37	F	14	LT	MTS	21	0	0.6
4	24	F	15	RF	crypt	14	0	3.0
5	59	M	40	LF	CD	72	20	1.6
6	56	F	9	Multiple	crypt	4	0	3.7
7	41	F	2	LF	APS	200	1	1.6
8	24	M	17	LT	crypt	96	0	2.0
9	31	M	27	RT	crypt	22	0	4.6
10	55	F	17	LT	MTS	30	12	1.5
11	40	F	34	LT	MTS, LTL	12	300	1.7
12	49	F	44	RT	crypt	2	0	0.0
13	57	M	14	Unknown	crypt	6	0	0.8
14	49	F	3	RT	crypt	21	0	0.0
15	25	M	10	Unknown	crypt	2	0	2.4
16	21	M	9	LT	AC	1	75	2.6
<b>Median</b>	40.5		14.5			17.5	0	1.6
<b>Mean</b>	40.4		18.4			33.7	28.5	1.8

F= female, M= male, LF= left frontal, RF= right frontal, LT= left temporal, RT= right temporal, CD=cortical dysplasia, MTS = mesiotemporal sclerosis, crypt = cryptogenic, APS= anti-phospholipid syndrome, LTL= left temporal lobectomy, AC= arachnoid cyst

### Neuropsychological testing

All subjects underwent extensive neuropsychological testing, including tests for intelligence, handedness, attentional functions and information processing and memory function. In order to test intelligence, the Wechsler Adult Intelligence Scale third edition (WAIS-III) was used. For handedness, the Annett Handedness Questionnaire was administered. Tests reflecting speed of information processing were the Computerized Visual Searching task (CVST) and the Binary Choice Reaction Test (BCRT). With the CVST, subjects are asked to compare a centered grid pattern with 24 surrounding patterns, one of which is identical to the target pattern. The test includes 24 trials and the outcome measure is the average search time in seconds. The BCRT is a decision task in which the subject has to react in a different way to a red square presented on the left side of the screen than to a green square on the right side. The outcome measure is the reaction time in milliseconds. Memory function was assessed by the computerized task of recognition of words and figures. Six words and four



figures are presented with a presentation time of 1s per item. After a delay of 2s, the screen shows one of these words or figures between distractors. Subjects are asked to identify the target item. The outcome measure is the number of correct answers out of 24. CVST, BCRT and the memory tests are part of the FePsy neuropsychological testbattery (Aldenkamp et al., 1991). Based on the results of these tests combined, a composite score was derived, comparing the actual level with the expected level, based on premorbid educational level. The resulting score has five categories: 1. no intellectual deterioration and no cognitive dysfunction, 2. no intellectual deterioration but signs of mental slowing, 3. no intellectual deterioration but signs of dysfunction in only one area of higher cognitive functioning (i.e. language or memory), 4. no intellectual deterioration and two impaired areas of higher cognitive function (i.e. impaired language and memory) with or without mental slowing, 5. global intellectual deterioration.

### **fMRI data acquisition**

MR imaging was performed on a 1.5-T unit (Philips Intera, Philips Medical Systems, Best, The Netherlands). Functional MRI data were acquired using a whole-brain single-shot three-dimensional (3D) blood oxygen level-dependent echo-planar imaging sequence, with repetition time 2 s, echo time 50 ms, flip angle 90°, voxel size 3.5 x 3.5 x 3.5 mm, matrix 64 x 64, 34 contiguous slices per volume, and 96 volumes per acquisition. For anatomical reference, we acquired a 3D T1-weighted fast field-echo image, with repetition time 11 ms, echo time 3.5 ms, flip angle 90°, matrix 256 x 256, 150 contiguous slices, and voxel size 3.5 x 3.5 x 3.5 mm.

### **fMRI activation paradigms**

Two experimental block paradigms were used. The Sternberg letter recognition paradigm is a choice reaction test reflecting working memory performance (Sternberg, 1966). Letters were visually presented to the patients to maintain in working memory. Subjects then responded to the presentation of single letters by pressing a button with either their right or left hand to indicate whether or not the letter was in the memorized set of letters. In the baseline condition, subjects were asked to focus on a cross-hair. The paradigm consisted of 16 blocks (memory set for 4 s followed by 13 response letters of 2 s each) alternating with 16 baseline rest condition blocks (30 s each). The memory set varied from 1 to 4 letters, presented in a random fashion with a total of four blocks for each load. The contrast between activation in baseline condition and all loads was used for further analysis. In previous studies, prefrontal and temporal areas were activated by this paradigm (Hillary et al., 2003).

The second paradigm was a covert variation of the Stroop test (Stroop, 1935). Words of colour names were presented displayed in a different colour

than the colour it actually named or in the same colour. Subjects were instructed to think of the colour in which the word was displayed. For example, the word blue was written in red letters, so the subject had to think 'red'. In the baseline condition, subjects were asked to focus on a cross-hair. This task reflects self-regulatory control processes by asking subjects to inhibit a more automatic behaviour (reading a word) to perform a less automatic one (naming of a colour). Usually, activation of the lateral prefrontal area during the Stroop paradigm is observed in healthy subjects. The paradigm comprised of six activation blocks (15 words, 2 s each) alternating with six baseline rest condition blocks (30 s each). The contrast between baseline condition and activation blocks was used for analysis. With this paradigm, activation of prefrontal areas, especially the inferior lateral prefrontal cortex, has been demonstrated in healthy adults (Marsh et al., 2006).

### **Image analysis**

Statistical analysis was performed in MATLAB (Mathworks, Natick, Massachusetts, USA) using brain activation contrasts (between task performance and baseline) according to the General Linear Model as implemented in the statistical parametric mapping (SPM) software package (SPM2) (Wellcome Department of Cognitive Neurology, London, UK). The BOLD images were realigned intraindividually to the first image in each time series on a voxel-by-voxel basis to correct for head movement. Realigned images were transformed into the standardized stereotactic reference system developed by Talairach and Tournoux (Talairach and Tournoux, 1988) and smoothed with a 6-mm Gaussian kernel.

### **Statistical analysis**

Areas with statistically significant changes in signal intensity were determined on a voxel-by-voxel basis using the Student's t-test. We selected for every patient the 5,000 most active voxels, which is approximately 1% of the brain, in a predefined region. Further analyses were performed on those 5,000 most activated voxels. The predefined region consisted of the prefrontal area (medial frontal gyrus, gyrus rectus, orbital gyrus, superior frontal gyrus, middle frontal gyrus, inferior frontal gyrus, subcallosal gyrus), frontotemporal area (superior temporal gyrus, transverse temporal gyrus, insula and part of the inferior frontal gyrus adjacent to the insula and temporal lobe), temporal area (middle temporal gyrus, mesiotemporal cortex, inferior temporal gyrus), cingulate cortex, Broca's area (Brodmann areas 44 and 45 in the inferior frontal gyrus) and Wernicke's area (Brodmann areas 22, 39 and 40). Subsequently, the relative activation level in these regions was calculated (expressed as the fraction of the 5,000 active voxels from the whole predefined region within the

specific region) in order to detect increased or decreased activity reflecting hyper- or hypoactivation, respectively. Clinical and neuropsychological data analyses were performed in SPSS for Windows (Rel. 11.5.0. 2002. Chicago: SPSS Inc.). Correlations of fMRI data, epilepsy parameters, and neuropsychological parameters were calculated with parametric (Pearson correlation) and non-parametric (Spearman correlation) statistical tools.

## Results

### Patient characteristics

Patient characteristics are described in Table 6.1.

### Neuropsychological assessment

Neuropsychological assessment measures are summarized in Table 6.2.

**Table 6.2.** Neuropsychological assessment measures

Patient	Total IQ	Verbal IQ	Performance IQ	Deterioration Score	Recognition of words (out of 24)	Recognition of figures (out of 24)	BCRT-mean reaction time (ms)	CVST - mean reaction time (s)
1	92	96	90	4	14	NA	364	9.3
2	135	136	126	2	21	NA	495	12.8
3	131	124	134	4	22	6	499	9.5
4	101	97	107	4	4	11	571	19.7
5	102	100	104	3	15	10	452	22.0
6	86	85	90	5	12	7	746	26.4
7	126	122	126	3	17	7	413	10.2
8	112	110	112	4	15	11	387	11.0
9	67	68	74	3	14	6	390	18.1
10	65	66	70	2	18	9	1799	18.9
11	120	124	112	1	20	13	444	12.4
12	112	111	112	1	20	9	416	15.3
13	115	113	116	1	18	13	395	13.4
14	124	119	126	1	18	13	469	10.1
15	111	113	107	1	21	13	419	11.0
16	101	103	98	1	19	16	401	11.7
<b>Median</b>	112	111	110	2.5				
<b>Mean(SD)</b>	106(18)	105(20)	107(18)		17 (5)	21 (30)	541(348)	14.5(5.1)

NA= not available

### *Correlation of neuropsychological findings with SGTCS*

Subjects with a higher number of total SGTCS had significantly lower IQ-measures (total IQ:  $p=0.01$ ; verbal IQ:  $p=0.01$  and performance IQ:  $p=0.01$ )

than those with a lower amount of SGTCS. A trend towards higher deterioration scores was noticed with a higher number of SGTCS ( $p=0.07$ ). No correlation was found between the remainder of neuropsychological tests and number of SGTCS experienced.

## fMRI

fMRI activation maps were analyzed using predefined brain regions. Activation patterns in these regions were compared to the number of SGTCS experienced. In the prefrontal regions, a higher activation could be observed during the Stroop paradigm ( $p=0.01$ ,  $r=0.60$ ) and a trend for higher activation was seen for the Sternberg paradigm ( $p=0.07$ ,  $r=0.46$ ) with increasing number of SGTCS experienced. In the frontotemporal region, a trend towards lower activation was observed for both Stroop and Sternberg paradigm ( $p=0.05$  and  $p=0.10$ , respectively). In the temporal regions and Broca's area, no significant correlation was found between activation patterns and number of SGTCS (Stroop  $p=0.85$  and  $p=0.25$  respectively, Sternberg  $p=0.37$  and  $p=0.57$  respectively). In the cingulate cortex, higher activation was found in the Stroop paradigm ( $p<0.01$ ;  $r=0.72$ ) but not in the Sternberg paradigm ( $p=0.33$ ). Dividing the cingulate cortex in an anterior and a posterior part, no statistically significant association was found in Stroop ( $p=0.13$  and  $p=0.09$ , respectively).

We then compared the results of the global deterioration scale with prefrontal activation patterns. No statistically significant relation could be demonstrated ( $p=0.24$  and  $p=0.19$  for Stroop and Sternberg, respectively), but data showed a trend towards higher activation in the prefrontal region for higher deterioration scores ( $r=0.46$  for Stroop and  $r=0.35$  for Sternberg) (Figure 6.1). Figure 6.2 shows an example of brain activation in the Sternberg paradigm of patient 2 with 4 lifetime SGTCS compared to patient 5 with 72 lifetime seizures.

In order to obtain a more global impression of frontal and temporal activation, the activation maps from the Sternberg and Stroop fMRI paradigms were combined according to the method of O'Brien-Lauter (O'Brien, 1984; Läuter, 1996). After combining the Z-values for both paradigms, significantly higher activation was noticed in the prefrontal region ( $p<0.01$ ,  $r=0.65$ ) (Figure 6.3) and the cingulate region ( $p=0.02$ ,  $r=0.57$ ) in relation to a higher number of SGTCS. A trend towards lower activation in the frontotemporal region was observed ( $p=0.05$ ;  $r=0.49$ ).

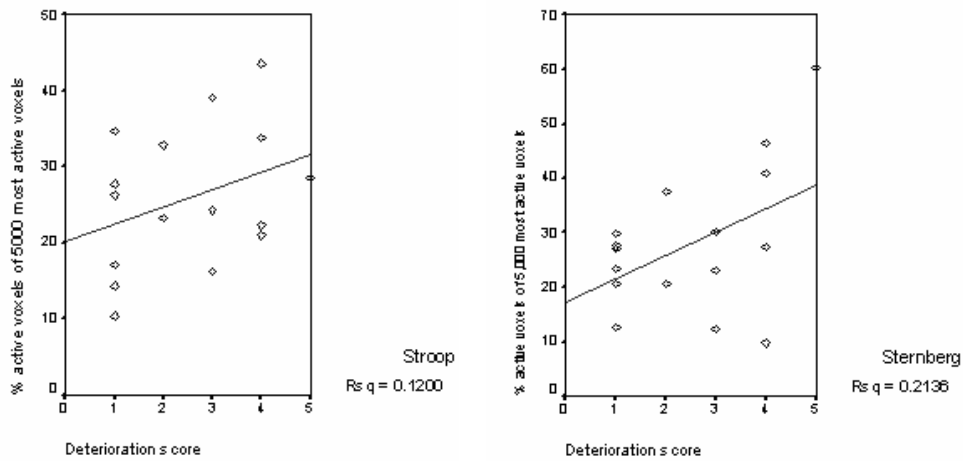


**Figure 6.1.** Relative prefrontal activation patterns for Stroop (left) and Sternberg (right) paradigms in relation to cognitive deterioration scores.

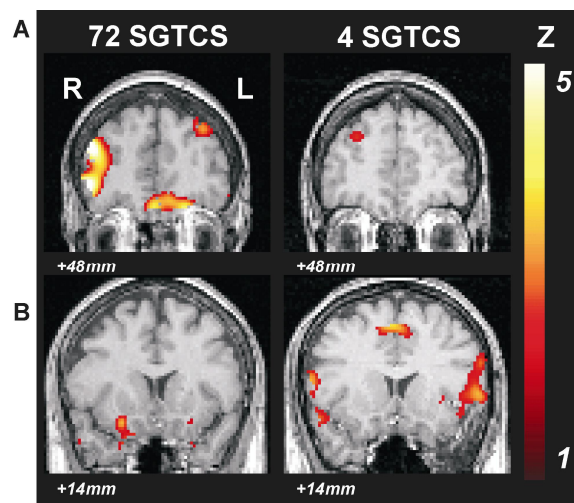


**Figure 6.2.** Coronal images of fMRI activation maps, obtained for the Sternberg paradigm overlaid on a normalized T1-weighted MR image, with left a typical patient with many SGTCs, and right a patient with few SGTCs. A) Prefrontal region, B) frontotemporal region. Slice positions are given in stereotactic Talairach y-coordinates.

In a post-hoc analysis, we focused on the prefrontal lobe by looking at the different Brodmann areas to specify the localization of the elevated activation related to a higher number of SGTCS. In the Stroop paradigm, a significantly elevated activation pattern was seen in the rostral part of the superior and the middle frontal gyri and the gyrus rectus (Brodmann areas 10,  $p=0.04$ ; and 11,  $p=0.03$ ) of the right hemisphere. In the Sternberg paradigm, a trend towards lower activation in the right dorsolateral prefrontal cortex (Brodmann area 46) was noticed ( $p=0.08$ ,  $r=0.46$ ).

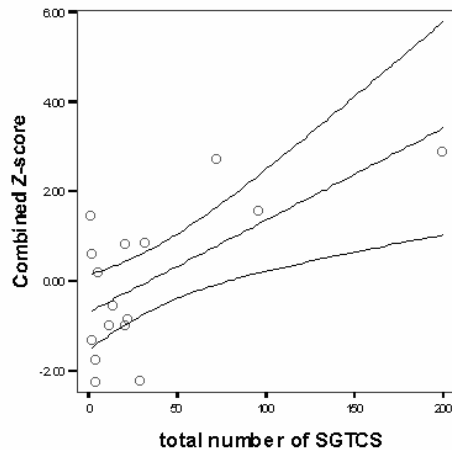


**Figure 6.3.** Relative prefrontal activation for Sternberg and Stroop combined in relation to total number of SGTCS. Lines indicate the 95% confidence interval.

## Discussion

In this study, a statistically significant correlation between number of SGTCS, experienced during life-time, and intellectual functioning as measured by the WAIS was observed. The deterioration score we used expresses a more global observation of cognitive functioning and showed a tendency to increased deterioration with a higher number of SGTCS. Possibly, due to the limited number of patients this study lacks power to reach a statistically significant association between number of SGTCS and deterioration score. However, both outcomes show a trend toward the same direction: an association between number of SGTCS and cognitive deterioration which is in line with previous studies (Rodin, 1968; Dikmen and Matthews, 1977; Seidenberg et al., 1981; Bourgeois et al., 1983; Dodrill, 1986; Trimble, 1988; Dodrill, 2002).

Moreover, we have demonstrated a relatively increased prefrontal activation related to the number of SGTCS. Furthermore, a trend towards a decreased activation in the frontotemporal areas was observed. Both paradigms used in the

current study are aimed at indicating activation of the brain areas involved in verbal working memory and speed of mental processing, more specifically, the temporal areas and the prefrontal area, especially the dorsolateral prefrontal cortex. The relative increase of activation in the prefrontal region and decrease in temporal areas, could be interpreted as a shift of activation from frontotemporal to prefrontal areas. This suggests that a functional reorganization of working memory has taken place in patients with a higher number of SGTCS.

We used the combination of two cognitive tasks to investigate the frontal and temporal lobe to detect differences in brain activation. Since the cortical spreading of seizures of varying primary seizure foci may differ strongly between patients, it was a priori unlikely to localize alterations in brain activation. Consequently, using only a single cognitive task would show different changes in brain activation patterns between epilepsy patients. Combining multiple cognitive paradigms facilitates this spatial variability and allows for a more sensitive detection of cerebral activation changes.

Previous studies have suggested different hypotheses for cerebral reorganization. It is commonly hypothesized that functional reorganization is an effect of cerebral plasticity, particularly in temporal lobe epilepsy (Beck et al., 2000; Cole, 2000). Seizures are thought to cause a cascade of molecular and genomic changes, which may be relevant for the morphologic and functional long-term changes noticed in epilepsy (Represa, 1999). Especially in patients with early-onset localisation-related epilepsies, reorganization of language and verbal memory has been suggested as an explanation for the observed increased recruitment of the homologous contralateral language areas (Carpentier et al., 2001; Berl et al., 2005).

There are two possible interpretations for the changes in activation pattern often noticed in patients with epilepsy. First, it could be a reflection of a compensatory mechanism aimed at the preservation of normal cognitive function. In patients with temporal lobe epilepsy, language reorganization due to early left temporal damage (before age of three), was not associated with verbal memory deficits. In older subjects, however, language reorganization concurred with verbal memory deficits (Helmstaedter et al., 1994). Some fMRI studies have shown marked alterations in activation patterns without altered cognitive functioning. In a study of patients with left temporal lobe epilepsy, higher interictal spiking frequency was associated with more pronounced right-sided frontal activity during speech fMRI, whereas patients performed equally as controls on a word fluency task (Janszky et al., 2006).

Alternatively, altered activation could also reflect the pathological processes underlying cognitive deterioration. Studies supporting this theory show cognitive dysfunction associated with altered activation patterns. In patients with right temporal seizure focus and left language dominance,

activation of the homologous language areas correlated inversely with verbal memory performance (Berl et al., 2005).

Whether or not the functional reorganization demonstrated in the current study is efficient to maintain a normal functioning level, remains uncertain. Neuropsychological measures indicative of mental slowing and working memory were not significantly different for patients with a high or low number of SGTCS. Nevertheless, as mentioned before, the deterioration score did show an important trend towards more cognitive deficits with a high number of SGTCS. This suggests that the functional reorganization might not be sufficient to maintain normal cognitive functioning and compensate for cognitive deficits caused by SGTCS.

The prefrontal changes observed in our study are in accordance with previous studies. In patients with depression, a similar study with fMRI and a working memory paradigm showed greater activation of the lateral prefrontal cortex and the anterior cingulate compared to healthy subjects which suggested that depressed patients needed greater activation within the same neural network to maintain a similar level of performance (Harvey et al., 2005). An fMRI study of phonological and semantic processing in left TLE patients showed increased activation in prefrontal areas without differences in accuracy compared to controls (Billingsley et al., 2001). MTLE patients who performed a verbal memory task, showed extensive activation of the left prefrontal region which was not found in healthy controls. Memory performance of patients was poor, suggesting that the altered activation reflected a dysfunction of cerebral memory processing (Dupont et al., 2000). Contrarily, a recent study showed an effective shift of spatial and figural memory to more posterior cerebral parts in patients with MTLE explained in part by a relative frontal hypoactivation (Engelsen et al., 2006).

This study has a limited number of patients, which complicates the applicability of our results. However, even in this small population of patients with varying etiologies and seizure foci, we have been able to demonstrate a statistically significant effect of number of SGTCS on prefrontal activation patterns. Moreover, SGTCS are affecting intellectual functioning and probably are an important factor in cognitive decline. Possibly, in more homogeneous and larger epilepsy populations, results could be even more notable.

The cross-sectional design of this study lacks the ability to show cognitive decline or progressive changes in activation patterns. In the future, prospective studies with test and retest intervals of a few years investigating progression of cognitive dysfunction and cerebral activation changes are needed.

To conclude, secondarily generalized seizures in frontal and temporal lobe epilepsy are associated with cognitive dysfunction. Moreover, secondarily generalized seizures are related to a relatively increased activation in the prefrontal areas as demonstrated by fMRI using two paradigms aimed at



activating regions involved in verbal working memory and speed of mental processing. It is hypothesized that a mechanism of functional reorganization underlies the change in activation patterns but does not seem to suffice in compensating for cognitive deficits caused by SGTCS. In clinical practice, it seems necessary to prevent cognitive dysfunction by proactively preventing seizures with AED or epilepsy surgery, if possible.

## References

- Aldenkamp, A., Arends, J., 2004. The relative influence of epileptic EEG discharges, short nonconvulsive seizures, and type of epilepsy on cognitive function. *Epilepsia* 45(1), 54-63.
- Aldenkamp, A.P., Vermeulen, J., Alpherts, W.C.J., Overweg, J., Van Parijs, J.A.P. and Verhoeff, N.P.L.G., 1991. Validity of computerized testing: Patient dysfunction and complaints versus measured changes. *Assessment of Cognitive Function in Epilepsy*. E. W. Dodson and M. Kinsbourne. New York, Demos, 51-68.
- Beck, H., Goussakov, I.V., Lie, A., Helmstaedter, C. and Elger, C.E., 2000. Synaptic plasticity in the human dentate gyrus. *Journal of Neuroscience* 20(18), 7080-6.
- Berl, M.M., Balsamo, L.M., Xu, B., Moore, E.N., Weinstein, S.L., Conry, J.A., Pearl, P.L., Sachs, B.C., Grandin, C.B., Frattali, C., Ritter, F.J., Sato, S., Theodore, W.H. and Gaillard, W.D., 2005. Seizure focus affects regional language networks assessed by fMRI. *Neurology* 65(10), 1604-11.
- Bernasconi, A., Tasch, E., Cendes, F., Li, L.M. and Arnold, D.L., 2002. Proton magnetic resonance spectroscopic imaging suggests progressive neuronal damage in human temporal lobe epilepsy. *Prog Brain Res* 135, 297-304.
- Billingsley, R.L., McAndrews, M.P., Crawley, A.P. and Mikulis, D.J., 2001. Functional MRI of phonological and semantic processing in temporal lobe epilepsy. *Brain* 124(Pt 6), 1218-27.
- Blake, R.V., Wroe, S.J., Breen, E.K. and McCarthy, R.A., 2000. Accelerated forgetting in patients with epilepsy: evidence for an impairment in memory consolidation. *Brain* 123 Pt 3, 472-83.
- Bourgeois, B.F., Prensky, A.L., Palkes, H.S., Talent, B.K. and Busch, S.G., 1983. Intelligence in epilepsy: a prospective study in children. *Ann Neurol* 14(4), 438-44.
- Carpentier, A., Pugh, K.R., Westerveld, M., Studholme, C., Skrinjar, O., Thompson, J.L., Spencer, D.D., Constable, R.T., 2001. Functional MRI of language processing: dependence on input modality and temporal lobe epilepsy. *Epilepsia* 42(10), 1241-54.
- Cole, A.J., 2000. Is epilepsy a progressive disease? The neurobiological consequences of epilepsy. *Epilepsia* 41 Suppl 2, S13-22.
- Corcoran, R., Thompson, P., 1992. Memory failure in epilepsy: retrospective reports and prospective recordings. *Seizure* 1(1), 37-42.
- Dikmen, S., Matthews, C.G., 1977. Effect of major motor seizure frequency upon cognitive-intellectual functions in adults. *Epilepsia* 18(1), 21-9.
- Dodrill, C.B., 1986. Correlates of generalized tonic-clonic seizures with intellectual, neuropsychological, emotional, and social function in patients with epilepsy. *Epilepsia* 27(4), 399-411.
- Dodrill, C.B., 2002. Progressive cognitive decline in adolescents and adults with epilepsy. *Prog Brain Res* 135, 399-407.
- Dodrill, C.B., Batzel, L.W., 1986. Interictal behavioral features of patients with epilepsy. *Epilepsia* 27 Suppl 2, S64-76.
- Dupont, S., Van de Moortele, P.F., Samson, S., Hasboun, D., Poline, J.B., Adam, C., Lehericy, S., Le Bihan, D., Samson, Y. and Baulac, M., 2000. Episodic memory in left temporal lobe epilepsy: a functional MRI study. *Brain* 123 ( Pt 8), 1722-32.
- Engelsen, B.A., Gramstad, A., Thomsen, T., Beneventi, H., Erslund, L., Smievoll, A.I., Lundervold, A. and Hugdahl, K., 2006. Frontoparietal activation during delayed visuospatial recall in patients with epilepsy due to hippocampal sclerosis. *Epilepsy Behav* 8(3), 565-74.
- Harvey, P.O., Fossati, P., Pochon, J.B., Levy, R., Lebastard, G., Lehericy, S., Allilaire, J.F. and Dubois, B., 2005. Cognitive control and brain resources in major depression: an fMRI study using the n-back task. *Neuroimage* 26(3), 860-9.

- Helmstaedter, C., 2002. Effects of chronic epilepsy on declarative memory systems. *Prog Brain Res* 135, 439-53.
- Helmstaedter, C., Elger, C.E., 1999. The phantom of progressive dementia in epilepsy. *Lancet* 354(9196), 2133-4.
- Helmstaedter, C., Kurthen, M., Linke, D.B. and Elger, C.E., 1994. Right hemisphere restitution of language and memory functions in right hemisphere language-dominant patients with left temporal lobe epilepsy. *Brain* 117 ( Pt 4), 729-37.
- Hermann, B., Seidenberg, M., Bell, B., Rutecki, P., Sheth, R.D., Wendt, G., O'Leary, D. and Magnotta, V., 2003. Extratemporal quantitative MR volumetrics and neuropsychological status in temporal lobe epilepsy. *J Int Neuropsychol Soc* 9(3), 353-62.
- Hermann, B., Seidenberg, M., Sears, L., Hansen, R., Bayless, K., Rutecki, P. and Dow, C., 2004. Cerebellar atrophy in temporal lobe epilepsy affects procedural memory. *Neurology* 63(11), 2129-31.
- Hillary, F.G., Chiaravalloti, N.D., Ricker, J.H., Steffener, J., Bly, B.M., Lange, G., Liu, W.C., Kalnin, A.J. and DeLuca, J., 2003. An investigation of working memory rehearsal in multiple sclerosis using fMRI. *J Clin Exp Neuropsychol* 25(7), 965-78.
- Janszky, J., Mertens, M., Janszky, I., Ebner, A. and Woermann, F.G., 2006. Left-sided interictal epileptic activity induces shift of language lateralization in temporal lobe epilepsy: an fMRI study. *Epilepsia* 47(5), 921-7.
- Jokeit, H., Kramer, G. and Ebner, A., 2005. Do antiepileptic drugs accelerate forgetting? *Epilepsy Behav* 6(3), 430-2.
- Jokeit, H., Seitz, R.J., Markowitsch, H.J., Neumann, N., Witte, O.W. and Ebner, A., 1997. Prefrontal asymmetric interictal glucose hypometabolism and cognitive impairment in patients with temporal lobe epilepsy. *Brain* 120 ( Pt 12), 2283-94.
- Kotloski, R., Lynch, M., Lauersdorf, S. and Sutula, T., 2002. Repeated brief seizures induce progressive hippocampal neuron loss and memory deficits. *Prog Brain Res* 135, 95-110.
- Kramer, U., Kipervasser, S., Neufeld, M.Y., Fried, I., Nagar, S. and Andelman, F., 2006. Is there any correlation between severity of epilepsy and cognitive abilities in patients with temporal lobe epilepsy? *Eur J Neurol* 13(2), 130-4.
- Lammers, M.W., Hekster, Y.A., Keyser, A., Meinardi, H., Renier, W.O. and van Lier, H., 1995. Monotherapy or polytherapy for epilepsy revisited: a quantitative assessment. *Epilepsia* 36(5), 440-6.
- Läuter, J., 1996. Exact T and F tests for analyzing studies with multiple endpoints. *Biometrics* 52, 964-70.
- Marsh, R., Zhu, H., Schultz, R.T., Quackenbush, G., Royal, J., Skudlarski, P. and Peterson, B.S., 2006. A developmental fMRI study of self-regulatory control. *Hum Brain Mapp*.
- Martin, R.C., Sawrie, S.M., Gilliam, F.G., Palmer, C.A., Faught, E., Morawetz, R.B. and Kuzniecky, R.I., 2000. Wisconsin Card Sorting performance in patients with temporal lobe epilepsy: clinical and neuroanatomical correlates. *Epilepsia* 41(12), 1626-32.
- Miller, S.P., Li, L.M., Cendes, F., Tasch, E., Andermann, F., Dubeau, F. and Arnold, D.L., 2000. Medial temporal lobe neuronal damage in temporal and extratemporal lesional epilepsy. *Neurology* 54(7), 1465-70.
- O'Brien, P.C., 1984. Procedures for comparing samples with multiple endpoints. *Biometrics* 40, 1079-87.
- Ortinski, P., Meador, K.J., 2004. Cognitive side effects of antiepileptic drugs. *Epilepsy Behav* 5 Suppl 1, S60-5.
- Reminger, S.L., Kaszniak, A.W., Labiner, D.M., Littrell, L.D., David, B.T., Ryan, L., Herring, A.M. and Kaemingk, K.L., 2004. Bilateral hippocampal volume predicts verbal memory function in temporal lobe epilepsy. *Epilepsy Behav* 5(5), 687-95.

- Represa, A., 1999. Molecular mechanisms of seizure-induced cerebral plasticity. *Adv Neurol* 81, 61-7.
- Rodin, E.A., 1968. *The prognosis of patients with epilepsy*. Springfield, Illinois, Thomas.
- Sass, K.J., Sass, A., Westerveld, M., Lencz, T., Novelly, R.A., Kim, J.H. and Spencer, D.D., 1992. Specificity in the correlation of verbal memory and hippocampal neuron loss: dissociation of memory, language, and verbal intellectual ability. *J Clin Exp Neuropsychol* 14(5), 662-72.
- Sass, K.J., Spencer, D.D., Kim, J.H., Westerveld, M., Novelly, R.A. and Lencz, T., 1990. Verbal memory impairment correlates with hippocampal pyramidal cell density. *Neurology* 40(11), 1694-7.
- Seidenberg, M., O'Leary, D.S., Berent, S. and Boll, T., 1981. Changes in seizure frequency and test-retest scores on the Wechsler Adult Intelligence Scale. *Epilepsia* 22(1), 75-83.
- Stefan, H. and Pauli, E., 2002. Progressive cognitive decline in epilepsy: an indication of ongoing plasticity. *Prog Brain Res* 135, 409-17.
- Sternberg, S., 1966. High-speed scanning in human memory. *Science* 153(736), 652-4.
- Stroop, J.R., 1935. Studies of interference in serial verbal reactions. *Journal of Experimental Psychology* 18(6), 643-662.
- Talairach, J., Tournoux, P., 1988. *Co-planar stereotaxic atlas of the brain. 3-D Proportional System: An Approach to Cerebral Imaging*. Thieme Medical Publishers, New York
- Tasch, E., Cendes, F., Li, L.M., Dubeau, F., Andermann, F. and Arnold, D.L., 1999. Neuroimaging evidence of progressive neuronal loss and dysfunction in temporal lobe epilepsy. *Ann Neurol* 45(5), 568-76.
- Thompson, P.J., Corcoran, R., 1992. Everyday memory failures in people with epilepsy. *Epilepsia* 33 Suppl 6, S18-20.
- Thompson, P.J., Duncan, J.S., 2005. Cognitive decline in severe intractable epilepsy. *Epilepsia* 46(11), 1780-7.
- Trimble, M.R., 1987. Anticonvulsant drugs and cognitive function: a review of the literature. *Epilepsia* 28 Suppl 3, S37-45.
- Trimble, M.R., 1988. Cognitive hazards of seizure disorders. *Epilepsia* 29 Suppl 1, S19-24.



# Chapter 7

**Soluble telencephalin is a marker for frontotemporal dysfunction in epilepsy as revealed by fMRI**

**Jansen JFA, Vlooswijk MCG, de Baets MH, de Krom MCTFM, Rieckmann P, Backes WH, Aldenkamp AP, for the SEGAED study group**

*Submitted for publication*

**Abstract**

Functional MRI (fMRI) of verbal working memory performance (Sternberg) was used to examine cortical dysfunction in 16 patients with localization-related epilepsy and secondarily generalized seizures. Additionally, blood serum concentrations of soluble telencephalin (marker for neuronal damage) were determined. In three patients (1 temporal, 2 frontal focus), telencephalin was detected. All three individuals had lower BOLD-signals in the frontotemporal region ( $p=0.015$ ), but not in the other regions ( $p>0.35$ ) compared to patients without detectable telencephalin. An association between decreased frontotemporal activation on fMRI and detectable telencephalin serum levels was demonstrated. Frontotemporal dysfunction in localization-related epilepsy might be better predicted by telencephalin than seizure focus.

Soluble telencephalin (intercellular adhesion molecule 5 (ICAM-5)) is a neuronal glycoprotein. Increased concentrations of soluble telencephalin in serum and cerebrospinal fluid have been reported in temporal lobe epilepsy and acute herpes simplex encephalitis (Rieckmann et al., 1998). Telencephalin has been suggested as a marker for neuronal damage (Guo et al., 2000).

Functional MRI (fMRI) enables the localization of brain activation by demonstrating a blood oxygenation level dependent (BOLD) signal during a (cognitive) paradigm. With fMRI, possible alterations in the functional neuroanatomy of working memory can be visualized using the Sternberg paradigm, a choice reaction time test reflecting verbal working memory performance (Manoach et al., 1997). Previous studies have demonstrated prefrontal and temporal activation using this paradigm (Hillary et al., 2003).

Temporal cortex dysfunction, which has been reported in localization-related epilepsy, can be demonstrated by decreased local activation with fMRI (Cheung et al., 2006). We investigated cortical dysfunction in 16 adult patients with localization-related epilepsy and secondarily generalized seizures using fMRI and neuropsychological assessment. Patient characteristics are listed in Table 7.1. The study was approved by the ethics committee of the Maastricht University Hospital. Both temporal and frontal seizure focus were included, since frontal seizures tend to generalize rapidly (Niedermeyer, 1998), and both seizure types are known to spread.

To detect soluble telencephalin in serum, a sensitive sandwich immunoassay with two mouse monoclonal antibodies to the extracellular domains of human telencephalin was used (Rieckmann et al., 1998). fMRI-data were acquired on a 1.5-Tesla unit (Philips Medical Systems, The Netherlands) using a whole-cerebrum single-shot threedimensional BOLD echo-planar imaging sequence. During fMRI, patients performed a covert Sternberg test in which subjects were asked to memorize visually presented letters. Subjects then indicated by pressing a button whether or not single displayed letters were in the memory set (Manoach et al., 1997; Hillary et al., 2003). Neuropsychological testing included tests for intelligence and a word recognition test from the FePsy neuropsychological battery (Aldenkamp et al., 1992).

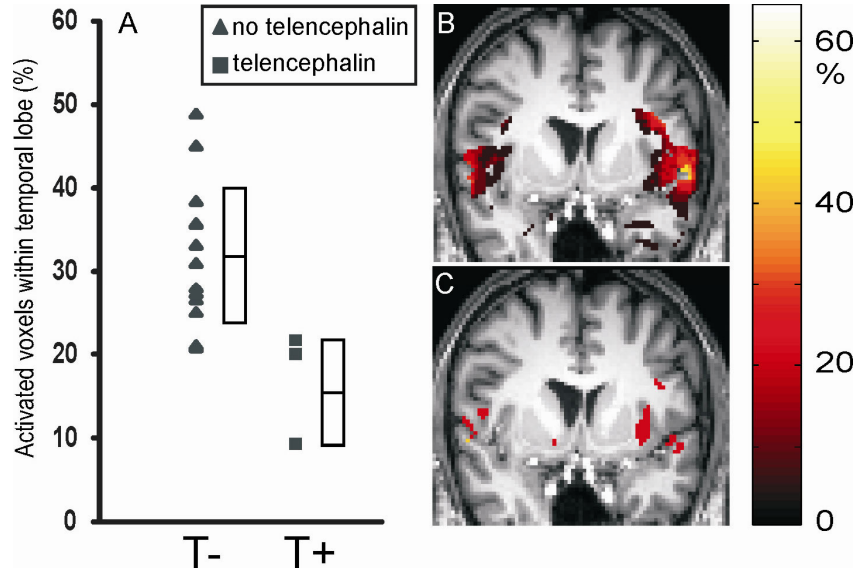
fMRI data analysis was performed in SPM2 (Wellcome Department of Cognitive Neurology, UK) and was focused on five volumes of interest covering the temporal and prefrontal cortex. The volumes of interest were the prefrontal area, frontotemporal area, cingulate cortex, Broca's and Wernicke's areas. The frontotemporal area comprised the insula extending to the superior temporal and inferior frontal cortex. The relative activation level in the volumes of interest was expressed as the fraction of the 5,000 most active voxels (approximately 1% of the cerebrum) from the temporal and prefrontal cortex.

In three patients telencephalin was detected (Table 7.1). All three individuals had lower BOLD-signals in the frontotemporal region ( $p=0.015$ ,



Mann-Whitney-U), but not in the other regions ( $p > 0.35$ ) compared to patients without detectable telencephalin (Figure 7.1). Although patients with detectable telencephalin serum levels displayed somewhat worse outcomes on neuropsychological testing, no statistical differences were found (Table 7.1).

**Figure 7.1.** (a) Relative activation of the frontotemporal cortex for the non-telencephalin group (T-; left) and telencephalin group (T+; right). Boxes show mean  $\pm$  SD. (b-c) Coronal images of fMRI activation maps obtained for the Sternberg paradigm overlaid on a spatially normalized T1-weighted MR image, for the non-telencephalin group (b) and telencephalin group (c). Activation maps show percentage of patients in which a region is activated. Slice positions are  $y = +8$  mm in stereotactic Talairach coordinates.



Previous data suggested that the appearance of soluble telencephalin in serum due to changes in cerebral telencephalin expression can be induced by both acute and chronic neurodegenerative conditions such as encephalitis (Lindsberg et al., 2002) and temporal lobe epilepsy (Rieckmann et al., 1998), respectively. In the current study, patients with localization-related epilepsy of both temporal and extratemporal origin were selected to investigate the consequences of this chronic condition on cortical function. To our knowledge, this is the first study that demonstrates an association between decreased frontotemporal activation on fMRI and detectable telencephalin serum levels.

Table 7.1.

Patient	Serum telencephalin level (ng / mL)	Age (y)	Sex	Epilepsy duration (y)	Seizure focus <sup>a</sup>	Etiology	Total nr of SGTCS	Drugload <sup>b</sup>	Total IQ	Recognition of words (out of 24)
1	2.1	23	F	1	LF	CD	1	1.0	92	14
5	36.5	59	M	40	LF	CD	72	1.6	102	15
16	8.4	21	M	9	LT	AC	1	2.6	101	19
Mean (± SD)							16 (15)	1.8 (0.8)	98 (6)	16 (3)
2	ND	55	F	39	Multiple	MTS	4	1.2	135	21
3	ND	37	F	14	LT	MTS	21	0.6	131	22
4	ND	24	F	15	RF	crypt	14	3.0	101	4
6	ND	56	F	9	Multiple	crypt	4	3.7	86	12
7	ND	41	F	2	LF	APS	200	1.6	126	17
8	ND	24	M	17	LT	crypt	96	2.0	112	15
9	ND	31	M	27	RT	crypt	22	4.6	67	14
10	ND	55	F	17	LT	MTS	30	1.5	65	18
11	ND	40	F	34	LT	MTS, LTL	12	1.7	120	20
12	ND	49	F	44	RT	crypt	2	0.0	112	20
13	ND	57	M	14	Unknown	crypt	6	0.8	115	18
14	ND	49	F	3	RT	crypt	21	0.0	124	18
15	ND	25	M	10	Unknown	crypt	2	2.4	111	21
Mean (± SD)							38 (57)	1.8 (1.4)	108 (23)	17 (5)

Patient characteristics and neuropsychological outcomes. No statistically significant differences were found between patients with detectable and patients without detectable telencephalin serum levels for total number of SGTCS, drugload, total IQ and number of correctly recognized words as determined with the Mann-Whitney-U test. a Seizure focus was determined by combining clinical semiology and EEG data. b Drugload is a quantitative assessment of total antiepileptic drug use calculated by standardizing the doses using the ratio of prescribed daily dose to defined daily dose (Lammers et al., 1995). SGTCS = secondarily generalized tonic-clonic seizures, ND = not detectable; F= female, M= male, LF= left frontal, RF= right frontal, LT= left temporal, RT= right temporal, CD=cortical dysplasia, MTS = mesiotemporal sclerosis, crypt = cryptogenic, APS= anti-phospholipid syndrome, LTL= left temporal lobectomy, AC= arachnoid cyst

Despite the limited number of patients, our results suggest that increased telencephalin levels are not a direct consequence of a temporal seizure focus, since detectable levels were found in frontal lobe epilepsy as well. Possibly, it reflects frontotemporal damage due to spread of seizures of both temporal and extratemporal origin. We hypothesize that frontotemporal dysfunction in localization-related epilepsy might be better predicted by the promising biochemical marker telencephalin than seizure focus.

## **Appendix**

Participants in SEGAED (Secondarily Generalized seizures and Deterioration)

The other participants in the study are as follows: P.A.M. Hofman, MD PhD; M.E. Kooi, PhD; H.J.M. Majoie, MD PhD; K. Nicolay, PhD; R.P. Reijs, MD

## References

- Aldenkamp, A.P., Vermeulen, J., Alpherts, W.C.J., et al. (1992) Validity of computerized testing: patient dysfunction and complaints versus measured changes. IN Dodson, W. E. & Kinsbourne, M. (Eds.) *Assessment of cognitive function*. New York, Demos.
- Cheung, M.C., Chan, A.S., Chan, Y.L., et al., 2006. Effects of illness duration on memory processing of patients with temporal lobe epilepsy. *Epilepsia* 47, 1320-1328.
- Guo, H., Tong, N., Turner, T., et al., 2000. Release of the neuronal glycoprotein ICAM-5 in serum after hypoxic-ischemic injury. *Ann Neurol* 48, 590-602.
- Hillary, F.G., Chiaravalloti, N.D., Ricker, J.H., et al., 2003. An investigation of working memory rehearsal in multiple sclerosis using fMRI. *J Clin Exp Neuropsychol* 25, 965-978.
- Lammers, M.W., Hekster, Y.A., Keyser, A., et al., 1995. Monotherapy or polytherapy for epilepsy revisited: a quantitative assessment. *Epilepsia* 36, 440-446.
- Lindsberg, P.J., Launes, J., Tian, L., et al., 2002. Release of soluble ICAM-5, a neuronal adhesion molecule, in acute encephalitis. *Neurology* 58, 446-451.
- Manoach, D.S., Schlaug, G., Siewert, B., et al., 1997. Prefrontal cortex fMRI signal changes are correlated with working memory load. *Neuroreport* 8, 545-549.
- Niedermeyer, E., 1998. Frontal lobe epilepsy: the next frontier. *Clin Electroencephalogr* 29, 163-169.
- Rieckmann, P., Turner, T., Kligannon, P., et al., 1998. Telencephalin as an indicator for temporal-lobe dysfunction. *Lancet* 352, 370-371.



# Chapter 8

**Quantitative MR at 3.0 T of patients with cryptogenic localization related epilepsy: a preliminary investigation of neuronal correlates of cognitive impairment**

**Jansen JFA, Majoie HJM, Vlooswijk MCG, Kooi ME, Hofman PAM, Nicolay K, de Krom MCTFM, Aldenkamp AP, and Backes WH**



## **Abstract**

Although cognitive dysfunction is a prevalent co-morbidity in patients with chronic epilepsy, it is not clear whether these patients display cerebral abnormalities that are related to the cognitive impairment that can be detected with in vivo magnetic resonance (MR) techniques.

This report describes the set-up of a study that aims to determine neuronal determinants of cognitive impairment in patients with chronic epilepsy. Quantitative MR, comprising T2 relaxometry, diffusion tensor imaging, and spectroscopic imaging, was applied to detect possible neuronal correlates in terms of micro-structural and metabolic abnormalities. Preliminary results of this study are discussed.



## Introduction

Decline of cognitive function is the most frequent co-morbid disorder in epilepsy, particularly in patients with localization-related (partial) epilepsy with a temporal or frontal lobe origin (Oyegbile et al., 2004). Expressions of cognitive decline may vary from memory impairment or slowing of information processing speed (in patients with frontal or temporal lobe epilepsy) to even cognitive deterioration with IQ-decline (e.g. in patients with frequent partial, secondarily generalized tonic-clonic seizures) (Dikmen et al., 1977; Dodrill, 1986; Jokeit et al., 2004). Although IQ-decline may be less pronounced in patients with other seizure types, it is also reported in patients with high frequency of partial seizures (Dodrill, 2004). Whether repeated brief seizures induce neuronal damage, and whether they are related to possible cognitive deterioration is still unknown and remains to be elucidated (Sutula et al., 2003). In the past, patients were reassured that there risks for damage only existed when seizures were generalized and prolonged, as in status epilepticus (Dodrill, 1986). However, in recent years evidence is growing that localization-related epilepsy with partial seizures alone may also constitute a risk factor for cognitive impairment (Adcock et al., 2003).

Currently, no clear evidence is available which factors contribute to cognitive impairment in localization-related epilepsy. Potential factors include the location of the epileptogenic zone, the type of epileptiform activity, the duration of epilepsy, the number of partial seizures or secondarily generalized seizures, medication, or a combination of these factors. Characteristics that describe the chronicity of epilepsy, such as duration and number of seizures, are most likely related to the deterioration of the mental status.

Even less is known about the brain-behavior relationships, i.e. what neuronal mechanisms underlie the cognitive and behavioral changes. Emerging experimental studies in chronic (animal) models and human magnetic resonance imaging (MRI) and neuropsychological studies are providing new information about adverse long-term consequences of seizures (e.g. (Tasch et al., 1999; Hermann et al., 2002; Sutula et al., 2003)).

Experimental studies in rodents provide evidence that single seizures and repeated brief seizures induced by kindling indeed may produce cumulative neuronal cell damage in the epileptogenic zone (hippocampal sclerosis) (Sutula et al., 2003). MRI studies in humans already have demonstrated that reductions in brain volume occur also distant to the neural regions involved in the generation and propagation of seizures (Hermann et al., 2002). Repetitive secondarily generalized tonicoclonic seizures (SGTCS) are moreover known to provoke inflammatory reactions which may lead to neuronal cell loss (Hulkkonen et al., 2004).

To determine which neuronal correlates are identifiable for cognitive impairment in living human patients, MR techniques seem most suited. Moreover, MR techniques not only enable a non-invasive procedure to study the macrostructural effects of epilepsy on the human brain, but also provide the opportunity to investigate cerebral damage in various fundamentally different ways (Tofts, 2003). In addition to widely used structural MR imaging to detect changes in volumes of pre-defined brain regions, MR is capable to detect abnormalities at the micro-structural and metabolic level. For example, T2 relaxometry provides an objective measurement of tissue characteristics, as the transverse relaxation time (T2) is a physical property of tissue, which mainly reflects the (relatively) free water content. Micro-structural effects can be probed by diffusion MRI, which essentially relies on the quantification of random motion of water protons causing loss of signal phase coherence. Whenever micro-structural changes occur particularly in the neuronal cell environment (e.g. increase of extra-cellular space due to cell death), the motion of water protons will be affected, thereby changing the water diffusion properties and thus the MRI signal. Apart from deriving a measure for the average extent of molecular motion that is affected by cellular organization and integrity (Apparent Diffusion Coefficient, ADC), it is also possible to measure the preferred direction of molecular motion, which provides information on the degree of alignment of cellular structures within fiber tracts, as well as their structural integrity (fractional anisotropy, FA). MR spectroscopy is another technique that enables the observation of particular chemical compounds or metabolites. Four major metabolites that are commonly observed in brain tissue are: N-acetyl-aspartate (NAA), which is indicative of neuronal integrity, choline (Cho), of which increased concentrations can act as a malignancy (i.e. tumor) marker, total creatine (tCr), indicative of the energy metabolism, and myo-inositol (mI), which functions as an osmolyte and is thought to indicate ongoing myelin damage (Govindaraju et al., 2000).

Previous efforts to study cerebral effects of epilepsy have mainly used structural MRI techniques (i.e. T1-volumetry (Specht et al., 1997)) to reveal local volume reductions in white and gray matter. Significantly poorer cognitive status has been shown to be associated with larger reductions in gray-white matter volume (Hermann et al., 2002). MR Spectroscopy (MRS) studies targeting NAA have shown reductions in epilepsy patients in general, and particularly in patients with many secondarily generalized seizures (Tasch et al., 1999). However, as far as we know, no relations with cognitive functioning have been explored.

We hypothesize that MR abnormalities appear more profound in epilepsy patients with compared to patients without cognitive decline. To address this issue, in 2006 we have initiated a study, using a multi-modal MR research approach which has previously been extensively tested on healthy volunteers (chapter 3). The study aims at (i) exploring neuronal correlates as detected with quantitative MR for this cognitive morbidity, (ii) explaining the severity and nature of cognitive problems in terms of spatial location, degree, and type (microstructural and/or metabolic) of the MR abnormality, and (iii) relating this to characteristics of epilepsy. In this cross-sectional CODICE (COgnitive Deterioration In Cryptogenic Epilepsy) study, 70 patients with localization-related epilepsy with impaired and unimpaired cognitive functioning will be included. Cognitive impairment will be defined as a clinical diagnosis of either significant IQ decline or psychometrically confirmed memory impairment or mental slowing. In addition, a healthy control group of 35 subjects will be included, to provide normative brain MR data and to facilitate the detection of possible MR abnormalities in epilepsy patients who show no cognitive decline. Figure 8.1 illustrates the study design.

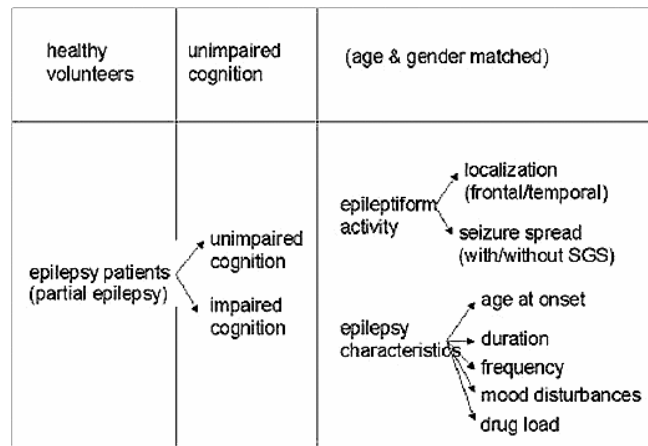


**Figure 8.1.** Study design. Three groups of subjects are defined: (i) healthy age and gender matched volunteers and (ii) partial epilepsy patients with and (iii) without cognitive impairment. All patients are characterized in terms of seizure type and epilepsy characteristics. SGS=secondarily generalized seizures

The current report discusses the preliminary results of the ongoing MR study based on data from 15 patients.

## **Materials and Methods**

### **Subjects**

The study population included 15 patients (9 women and 6 men; mean age 43 years; range 22-64). All patients were selected during their visit at the outpatient neurology department of the Maastricht University Hospital or at the Epilepsy Centre Kempenhaeghe (a tertiary epilepsy referral and care center). Data acquisition was conducted within the guidelines of the local institutional medical ethical committee overseeing human research, and every study participant provided written informed consent. Inclusion criteria for the study were: localization-related epilepsy with or without secondarily generalized seizures, no history of status epilepticus and no other underlying disease that could possibly cause cognitive decline or epilepsy, progressive neurological disorders, or symptomatic epilepsy (e.g. tumors or vascular abnormalities).

The following patient data were collected: age at onset, SGTCS seizure frequency per year, partial seizure frequency (including simple and complex seizures) per year, and seizure focus. Total number of SGTCS was calculated according to patient history and seizure diaries. No SGTCS were reported in the last two weeks before MR scanning. Patient characteristics are listed in Table 8.1.

### **Neuropsychological testing**

All subjects underwent neuropsychological testing, including tests for intelligence, attentional functions, information processing and memory function. To test intelligence, the Wechsler Adult Intelligence Scale third edition (WAIS-III) was used. Memory function was tested using the FePsy neuropsychological testbattery (Aldenkamp et al., 1992). Based on the combined results of these tests, a composite score was derived, comparing the actual level with the expected level, based on premorbid educational level. The resulting score was one of five categories: 1. no intellectual deterioration and no cognitive dysfunction, 2. no intellectual deterioration but signs of mental slowing, 3. no intellectual deterioration but signs of dysfunction in only one area of higher cognitive functioning (i.e. language or memory), 4. no intellectual deterioration and two impaired areas of higher cognitive function (i.e. impaired language and memory) with or without mental slowing, and 5. global intellectual deterioration.

Table 8.1.

Patient	Age (y)	Sex	Epilepsy duration (y)	Seizure focus*	Total number of SGTCs	Partial seizure frequency (per year)	IQ	Deterioration score
<b>Less than 10 partial seizures / v</b>								
1	31	M	-	-	0	6	89	2
3	31	M	20	ET	2	1	88	3
4	56	F	35	Fr	40	0	70	4
5	38	F	-	-	-	0	97	4
6	37	F	22	T	>1000	0	97	4
7	52	M	20	T	0	1	86	3
8	60	F	-	T	2	8	86	3
11	62	M	-	FT	2	0	111	3
15	64	M	7	FT	0	1	101	2
<b>Mean (SEM)</b>	48 (4)		21 (4)			2 (1)	92 (4)	3.1 (0.2)
<b>More than 10 partial seizures / v</b>								
2	24	F	20	Fr	2	350	70	3
9	32	F	13	T	0	100	69	4
10	35	M	30	-	-	12	108	1
12	48	F	21	T	2	36	116	1
13	22	F	12	FT	2	200	96	2
14	51	F	17	FT	0	12	95	3
<b>Mean (SEM)</b>	36 (4)		19 (2)			118 (50)	92 (7)	2.3 (0.5)

Patient demographics and characteristics

y, year; SGTCs, secondarily generalized tonicoclonic seizures; -, unknown; F, female; M, male; Fr, frontal; T, temporal; FT, frontotemporal; ET, extratemporal; SEM, standard error of the mean.

\* Based on the electroencephalogram

## MR Imaging

The patients were imaged using the protocol previously described in Chapter 3, with a 3.0-Tesla whole-body unit (Philips Achieva [software release 1.5.4.0], Philips Medical Systems, Best, The Netherlands).

## Data analysis

Data analysis was performed as described in Chapter 3. In short, image processing was performed using customized software in Matlab (The Mathworks, Natick, MA, USA), based on SPM2 software routines (Wellcome Department of Cognitive Neurology, London, UK). Spectra were analyzed using the LCModel software package (Version 6.1-4), and a metabolite basis set (PRESS, TE 30 ms, 3.0 T) kindly provided by Dr. Provencher. Metabolite concentrations were determined mmol per kg wet weight, calibrated using a 50 mmol NAA phantom.

As the effect related to cognitive decline might be different for different cerebral tissue types (e.g. neuronal and axonal tissue) (Geinisman et al., 1990),

we chose to examine grey matter (containing neurons) and white matter (containing axons) independently. To enable a separate analysis of grey matter and white matter, segmentation of the T1-weighted images into grey matter, white matter, and CSF was performed using SPM2. Statistical analysis of the T2-,  $\lambda_{\text{CSF}}$ -, FA- and ADC-maps and the  $^1\text{H-MRS}$  CSI voxels was performed on various cerebral regions, using standard masks created with WFU-Pickatlas (Maldjian et al., 2003). As effects related to cognitive decline not necessarily localize to the same microstructural regions from patient to patient, we analyzed data more globally by averaging quantitative MR outcomes over selected regions, rather than performing a pixel by pixel analysis. Since the presence of structural and functional brain asymmetry has been reported in morphological studies (Hugdahl, 2000), the left and right hemispheres were analyzed separately. Analysis of the imaging data was restricted to the temporal and frontal lobes. The mean T2,  $\lambda_{\text{CSF}}$ , FA, ADC, NAA, Cho, tCr, and mI values were calculated for the selected regions.

### Statistical analysis

All statistical calculations were performed in SPSS 12.0.1 (SPSS Inc., Chicago, IL). Quantitative MR outcomes and cognitive performance (IQ and deterioration scores) were correlated using Spearman's correlation.

Additionally, since IQ-decline has previously been reported in patients with high seizure frequency of partial seizures (Dodrill, 2004), and as the characteristics of the included patients allowed us to make two relatively small groups with different partial seizures frequency, we divided patients into one group ( $n = 9$ ) with less than 10 partial seizures per year, and one group ( $n = 6$ ) with more than 10 partial seizures per year. Clinical and neuropsychological data were compared between these two groups using the two-tailed Student's  $t$  tests, and differences in deterioration scores were analyzed using the non-parametric Wilcoxon/Mann-Whitney test. For all statistical analyses,  $p < 0.05$  was considered significant. Data are expressed as mean  $\pm$  standard error of the mean (SEM).

## Results

### Clinical and Neuropsychological assessment

Patient's characteristics are shown in Table 8.1. Correlation analysis of IQ levels and the cognitive deterioration scores, revealed a significant negative correlation (Spearman's  $\rho = -0.561$ ,  $p < 0.05$ , Figure 8.2). No other statistically significant relationships were observed. The group with less than 10 partial seizures per year was younger than the group with more than 10 partial seizures per year (approximately 12 years), although the age was not

significantly different between the groups ( $p = 0.07$ ). No other statistically significant differences were found.

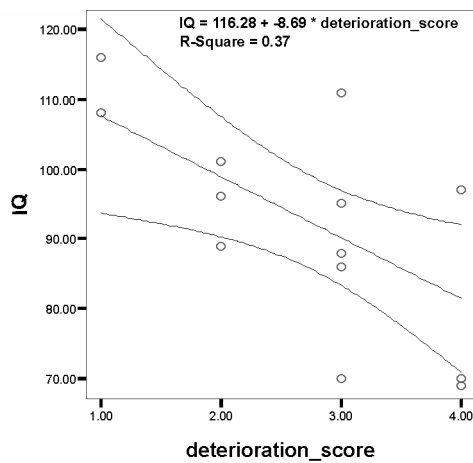


**Figure 8.2.** IQ levels of the patients with epilepsy in relation to cognitive deterioration scores. Lines indicate the 95% confidence interval.

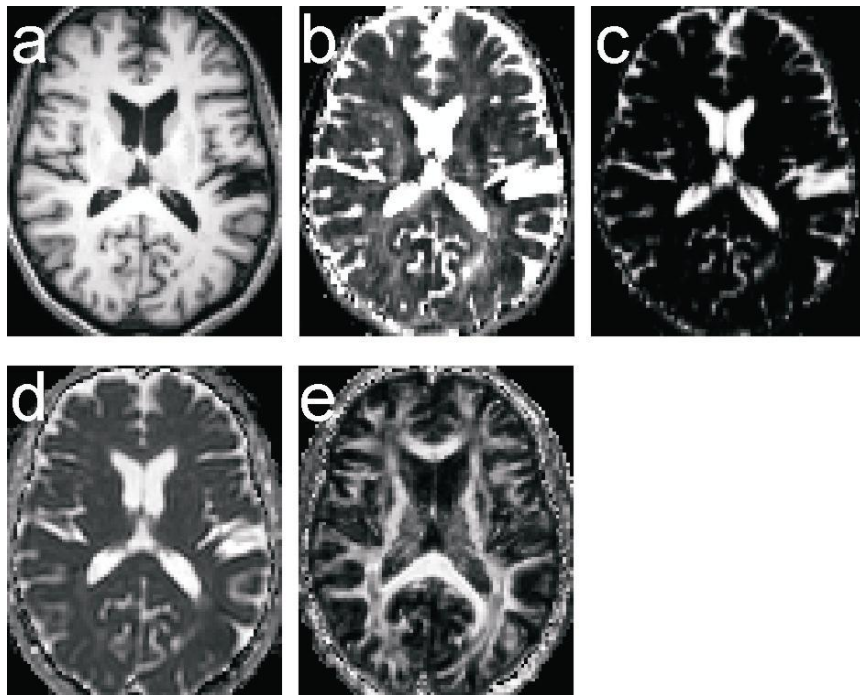


**Figure 8.3.** Spatially normalized transverse (a) T1-weighted, (b) T2-, (c)  $\lambda$ CSF-, (d) ADC-, and (e) FA maps of a patient with eight partial seizures per year. Slice position is  $z = +14$  mm in stereotaxic Talairach coordinates.

## Quality

Visual inspection of all T2-, ADC-, and FA-maps did not reveal image artifacts; therefore we were confident that the obtained maps were of good quality (Figure 8.3). For the CSI, out of a total of 720 voxels from the temporal lobe slice of all volunteers, 248 voxels were rejected based on their too high Cramer-Rao minimum variance estimate for NAA, tCr, Cho, or mI. For the frontal lobe slice, 135 out of a total of 960 voxels were discarded. Both patient groups displayed similar MR quality characteristics. Figure 8.4 shows an example of the selected spectroscopic imaging slices from one patient, and the spectral fit of two voxels.

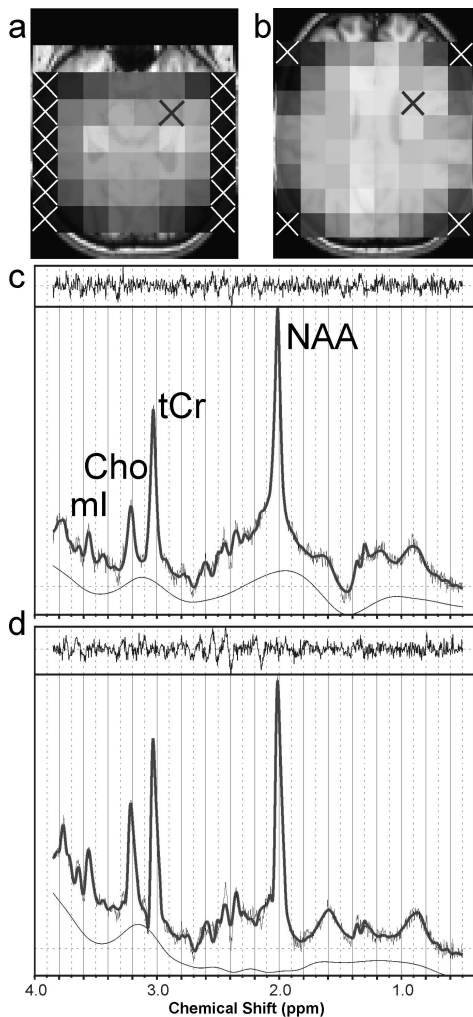


**Figure 8.4.** Spectroscopic imaging data of a patient with eight partial (simple and complex) seizures per year. The NAA map in (a) the temporal and (b) frontal slice of voxels satisfying the quality control requirements, overlaid on oblique normalized transverse T1-weighted images. Slice positions were approximately  $z = -14$  mm and  $+32$  mm, in stereotaxic Talairach coordinates, for the temporal and frontal slice, respectively. Voxels that did not fulfill the quality control criteria are marked with white crosses. (c-d) Original in vivo spectra of voxels from the (c) temporal and (d) frontal lobe slice, marked with a black cross in (a) and (b), respectively. The in vivo spectra (thin upper curves) have been estimated with the LCMoDel (Version 6.1-4) output (thick upper curves), and the difference of the spectra is plotted at the top. Underneath the in vivo spectrum, the baseline spline estimate, as determined by LCMoDel, is displayed. NAA = N-acetylaspartate, tCr, = total creatine, Cho = choline, and mI = myo-inositol.



Table 8.2.

		<10 PS / year Mean (SEM)	>10 PS / year Mean (SEM)
Regions	Quantity		
<b>left frontal</b>			
	T2 GM	197 (23)	167 (10)
	T2 WM	96 (6)	85 (1)
	$\lambda_{CSF}$	16.4 (1.4)	15.9 (1.0)
	ADC GM	994 (18)	1011 (26)
	ADC WM	791 (8)	851 (42)
	FA GM	28.8 (0.4)	29.1 (0.9)
	FA WM	38.6 (0.7)	36.6 (1.5)
	NAA	10.0 (0.4)	8.9 (0.4)
	<i>tCr</i>	6.2 (0.2) †	5.0 (0.3)
	<i>Cho</i>	1.7 (0.1)	1.4 (0.1)
	<i>mI</i>	3.5 (0.2) †	2.4 (0.3)
<b>right frontal</b>			
	T2 GM	216 (24)	209 (21)
	T2 WM	93 (4)	115 (25)
	$\lambda_{CSF}$	17.1 (1.5)	16.8 (1.0)
	ADC GM	990 (21)	994 (17)
	ADC WM	793 (9)	836 (35)
	FA GM	29.0 (0.4)	29.8 (0.9)
	FA WM	38.4 (0.6)	37.5 (1.3)
	NAA	9.6 (0.5)	8.5 (0.4)
	<i>tCr</i>	6.0 (0.3) †	4.8 (0.4)
	<i>Cho</i>	1.6 (0.1)	1.3 (0.1)
	<i>mI</i>	3.1 (0.2)	2.6 (0.2)
<b>left temporal</b>			
	T2 GM	115 (3)	130 (16)
	T2 WM	84 (2)	101 (20)
	$\lambda_{CSF}$	9.0 (0.5)	9.3 (0.9)
	ADC GM	950 (11)	963 (27)
	ADC WM	818 (4)	865 (34)
	FA GM	28.6 (0.4)	29.5 (1.0)
	FA WM	38.8 (0.5)	37.3 (1.5)
	NAA	6.1 (0.4)	6.5 (0.4)
	<i>tCr</i>	3.9 (0.5)	4.0 (0.9)
	<i>Cho</i>	1.3 (0.1)	1.3 (0.1)
	<i>mI</i>	2.8 (0.3)	4.5 (1.3)

		<10 PS / year Mean (SEM)	>10 PS / year Mean (SEM)
Regions	Quantity		
<b>right temporal</b>			
	T2 GM	120 (4)	128 (6)
	T2 WM	83 (2)	94 (9)
	$\lambda_{CSF}$	10.5 (1.0)	10.6 (0.5)
	ADC GM	944 (12)	960 (17)
	ADC WM	811 (7)	855 (28)
	FA GM	30.4 (0.7)	30.9 (1.1)
	FA WM	42.0 (0.7)	41.0 (1.8)
	NAA	6.3 (0.4)	5.0 (0.8)
	tCr	4.4 (0.3)	3.4 (0.5)
	Cho	1.2 (0.1)	1.0 (0.2)
	mI	2.4 (0.3)	3.0 (0.5)

Clinical and quantitative MR results in patients with less than 10 partial seizures (PS) per year and more than 10 partial seizures per year.

SEM, standard error of the mean; T2, transverse relaxation time (in ms); WM, white matter; GM, grey matter;  $\lambda_{CSF}$ , percentage of cerebrospinal fluid (in %); ADC, apparent diffusion coefficient (in  $10^{-6}$  mm<sup>2</sup>/s); FA, fractional anisotropy (in %); NAA, N-acetyl-aspartate; tCr, total creatine; Cho, choline; and mI, myo-inositol.

† 2-tailed P<0.05

### T2 relaxometry and Diffusion weighted imaging

No significant differences in T2,  $\lambda_{CSF}$ , ADC, and FA values were found between the patient group with less and the group with more than 10 partial seizures per year (Table 8.2).

### <sup>1</sup>H MR spectroscopy

In the left and right frontal lobe, a significantly decreased (-20%, p<0.05) tCr concentration was observed in the group with more than 10 partial seizures per year (Table 8.2). Additionally, a significantly decreased mI concentration (-30%, p <0.05) was found in the left frontal lobe. No statistically significant differences were found for NAA and Cho.

## Discussion

This report outlines the design, set up, and preliminary interim results of the cross-sectional CODICE study. This study is aimed at revealing brain abnormalities by quantitative MR related to the cognitive problems experienced by patients with localization-related epilepsy. A number of quantitative MR techniques, including T2 relaxometry, DTI, and <sup>1</sup>H-MRS, were combined to assess possible neuronal correlates for this cognitive co-morbidity on metabolic

and microstructural cerebral tissue characteristics. Unfortunately, in this preliminary report, no statistically significant relationships between MR outcomes and cognitive performance was detected yet, most likely due to the low number (22%) of included patients so far. However, an analysis based on the number of partial seizures was more fruitful.

### **Comparison of measured quantitative MR values with literature**

For all measured quantities, the obtained values (Table 8.2) were within the expected range as measured in patients with epilepsy in previous studies at 3.0T or at 1.5T. The average tissue water T2 within the frontal lobe for white matter was  $96 \pm 6$  ms (mean  $\pm$  SEM) for the patients with less than 10 partial seizures per year, which is in accordance with an average T2 derived at 3.0T from patients with hippocampal sclerosis by Briellmann et al. of  $102 \pm 5$  ms for white matter within the frontal lobe (Briellmann et al., 2004). The average ADC and FA values measured within the white matter of the temporal lobe were  $818 \pm 4 \times 10^{-6}$  mm<sup>2</sup>/s and  $38.8 \pm 0.5\%$ , respectively. The ADC values were in agreement with values obtained at 1.5T from the hippocampus in patients with medial temporal lobe epilepsy by Yu and coworkers, who found  $820 \pm 59 \times 10^{-6}$  mm<sup>2</sup>/s (Yu et al., 2006). Their FA values were slightly lower though ( $16.8 \pm 3.2\%$ ), but their assessment included only the hippocampus, whereas our assessment included the full temporal lobe. Values obtained in the present study from the temporal lobes for NAA, tCr, Cho and mI were  $6.1 \pm 0.4$ ,  $3.9 \pm 0.5$ ,  $1.3 \pm 0.1$ , and  $2.8 \pm 0.3$  mmol per kg wet weight, in accordance with values obtained for patients with idiopathic generalized epilepsy at 1.5 T by Simister et al, who reported values of  $6.8 \pm 0.4$ ,  $4.3 \pm 0.4$ ,  $1.1 \pm 0.2$ , and  $2.8 \pm 0.6$  mmol per liter, respectively (Simister et al., 2003). Therefore, all MR techniques proved to be reliable and provided sensible outcomes.

### **Clinical and neuropsychological assessment**

The fact that the IQ correlated significantly with the determined deterioration score, suggests that at the time of the IQ assessment, the cognitive deterioration of the patients had already started. Ideally one would like to know the IQ of patients before the process of deterioration initiates, as this would enable an assessment of whether patients with a certain IQ level are more likely to deteriorate. However, this would require a long-term follow up study of patients who are identified to be at risk to develop cognitive decline due to epileptic seizures, which is beyond the scope of this study.

### **<sup>1</sup>H MR spectroscopy**

We found that frontal lobe tCr and mI concentrations, obtained through absolute quantification, were significantly decreased in the group with more than 10 partial seizures (including simple and complex partial seizures) per year. Also NAA was decreased frontally, though not significant. In accordance with our results, Riederer et al. (Riederer et al., 2006) found decreased tCr and mI concentrations in hippocampi of patients with mesial temporal lobe epilepsy, using single voxel spectroscopy at 3.0T. Apparently tCr reduction in patients with epilepsy sometimes coincides with mI reduction. A decrease in tCr and NAA possibly reflects cell loss (Petroff et al., 2003). Membrane-bound mI plays a well-established role in intracellular signaling pathways whereas cytosolic mI contributes to osmoregulation of the cell (Fisher et al., 2002). There is evidence that both seizures (Nonaka et al., 1999) and antiepileptic drug treatment (Vadnal et al., 1995) lead to lower cerebral mI concentrations. More information about how mI is influenced by these factors remains to be elucidated to determine its role in epilepsy.

### **<sup>1</sup>H MR spectroscopy: methodology**

We would like to address some methodological aspects of the applied spectroscopy technique and metabolite quantification. The choice of the echo time for spectroscopic imaging requires some considerations. The close proximity of bone, sinuses, and blood vessels in the frontal and temporal regions makes it often difficult to achieve a good homogeneity of the magnetic field, and thus spectroscopy studies of the brain have often used long echo times (135-272 ms). Long echo time spectra are less prone to artifacts due to lipid contamination and incomplete water suppression. Furthermore, the limited number of metabolite peaks in spectra with long echo time of NAA, tCr, and Cho facilitates quantification. However, possible effects of pathology on T2 relaxation of metabolites are avoided in short echo time spectra (25-35 ms) than in long echo time spectra. Additionally, short echo time spectra allow the measurement of mI, which is well resolved at 3.0T, and can therefore be quantified (Mueller et al., 2003). The present study indicates that mI indeed can be a pathologically relevant metabolite in epilepsy.

Often, metabolite concentrations are expressed as ratios (relative quantification), rather than as absolute concentrations. In relative quantification, which yields concentrations expressed as ratios, one of the metabolite peaks measured (most often tCr) is used as the concentration standard, and serves as the denominator of the peak ratios. Alterations in the peak ratio (e.g. NAA/tCr) do not necessarily reflect a change in the concentration of the numerator (e.g. NAA). The alteration may be caused by changes in the concentration of either the numerator or the denominator or

both, or may merely be due to changes in relaxation behavior. The assumption that the concentration of tCr remains constant is clearly incorrect in this case, and possibly detected differences in NAA/tCr ratios would have been wrongly attributed to differences in NAA concentrations if not absolute but relative quantification was applied (Jansen et al., 2006).

### **Implications of preliminary results for full study**

It is hard to generalize the conclusions derived of this preliminary study. Several limiting factors need to be considered:

To divide patients into two groups, based on the total number of partial seizures experienced per year, might seem to make some sense in this small interim study. However, it is unknown whether this also holds for the full patient population. Also, as this report considers only 15 of the 70 to be included patients with epilepsy, the value of the clinical interpretation of the obtained results should not be overestimated.

Several patient characteristics, such as underlying etiology, and medication were not available at this moment, but are of great importance for interpreting the results. Additionally, as the two patient groups differed substantially in age, possible age-related effects should be considered.

Nevertheless, the current preliminary study showed that the quantitative MR techniques could be applied successfully, which is a prerequisite for future outcomes of the full study.

### **Conclusion**

The CODICE study is aimed at revealing brain abnormalities by quantitative MR, related to the cognitive problems experienced by patients with non-symptomatic localization-related epilepsy. Preliminary results of the cross-sectional CODICE study are discussed. A number of quantitative MR techniques, including T2 relaxometry, DTI, and <sup>1</sup>H-MRS, were combined to assess possible neuronal correlates for this cognitive co-morbidity on metabolic and microstructural cerebral tissue characteristics. The current preliminary study showed that the quantitative MR techniques could be applied successfully, which is a prerequisite for future outcomes of the full study.

## References

- Adcock, J.E., Wise, R.G., Oxbury, J.M., et al., 2003. Quantitative fMRI assessment of the differences in lateralization of language-related brain activation in patients with temporal lobe epilepsy. *Neuroimage* 18, 423-438.
- Aldenkamp, A.P., Vermeulen, J., Alpherts, W.C.J., et al. (1992) Validity of computerized testing: patient dysfunction and complaints versus measured changes. IN Dodson, W. E. & Kinsbourne, M. (Eds.) *Assessment of cognitive function*. New York, Demos.
- Briellmann, R.S., Jackson, G.D., Pell, G.S., et al., 2004. Structural abnormalities remote from the seizure focus: a study using T2 relaxometry at 3 T. *Neurology* 63, 2303-2308.
- Dikmen, S., Matthews, C.G., 1977. Effect of major motor seizure frequency upon cognitive-intellectual functions in adults. *Epilepsia* 18, 21-29.
- Dodrill, C.B., 1986. Correlates of generalized tonic-clonic seizures with intellectual, neuropsychological, emotional, and social function in patients with epilepsy. *Epilepsia* 27, 399-411.
- Dodrill, C.B., 2004. Neuropsychological effects of seizures. *Epilepsy Behav* 5 Suppl 1, S21-24.
- Fisher, S.K., Novak, J.E., Agranoff, B.W., 2002. Inositol and higher inositol phosphates in neural tissues: homeostasis, metabolism and functional significance. *J Neurochem* 82, 736-754.
- Geinisman, Y., Morrell, F., de Toledo-Morrell, L., 1990. Increase in the relative proportion of perforated axospinous synapses following hippocampal kindling is specific for the synaptic field of stimulated axons. *Brain Res* 507, 325-331.
- Govindaraju, V., Young, K., Maudsley, A.A., 2000. Proton NMR chemical shifts and coupling constants for brain metabolites. *NMR Biomed* 13, 129-153.
- Hermann, B.P., Seidenberg, M., Bell, B., 2002. The neurodevelopmental impact of childhood onset temporal lobe epilepsy on brain structure and function and the risk of progressive cognitive effects. *Prog Brain Res* 135, 429-438.
- Hugdahl, K., 2000. Lateralization of cognitive processes in the brain. *Acta Psychol (Amst)* 105, 211-235.
- Hulkkonen, J., Koskikallio, E., Rainesalo, S., et al., 2004. The balance of inhibitory and excitatory cytokines is differently regulated in vivo and in vitro among therapy resistant epilepsy patients. *Epilepsy Res* 59, 199-205.
- Jansen, J.F., Backes, W.H., Nicolay, K., et al., 2006. <sup>1</sup>H MR spectroscopy of the brain: absolute quantification of metabolites. *Radiology* 240, 318-332.
- Jokeit, H., Schacher, M., 2004. Neuropsychological aspects of type of epilepsy and etiological factors in adults. *Epilepsy Behav* 5 Suppl 1, S14-20.
- Maldjian, J.A., Laurienti, P.J., Kraft, R.A., et al., 2003. An automated method for neuroanatomic and cytoarchitectonic atlas-based interrogation of fMRI data sets. *Neuroimage* 19, 1233-1239.
- Mueller, S.G., Laxer, K.D., Suhy, J., et al., 2003. Spectroscopic metabolic abnormalities in mTLE with and without MRI evidence for mesial temporal sclerosis using hippocampal short-TE MRSI. *Epilepsia* 44, 977-980.
- Nonaka, M., Kohmura, E., Yamashita, T., et al., 1999. Kainic acid-induced seizure upregulates Na(+)/myo-inositol cotransporter mRNA in rat brain. *Brain Res Mol Brain Res* 70, 179-186.
- Oyegbile, T.O., Dow, C., Jones, J., et al., 2004. The nature and course of neuropsychological morbidity in chronic temporal lobe epilepsy. *Neurology* 62, 1736-1742.
- Petroff, O.A., Errante, L.D., Kim, J.H., et al., 2003. N-acetyl-aspartate, total creatine, and myo-inositol in the epileptogenic human hippocampus. *Neurology* 60, 1646-1651.
- Riederer, F., Bittsanksy, M., Schmidt, C., et al., 2006. <sup>1</sup>H magnetic resonance spectroscopy at 3 T in cryptogenic and mesial temporal lobe epilepsy. *NMR Biomed* 19, 544-553.

- Simister, R.J., McLean, M.A., Barker, G.J., et al., 2003. Proton MRS reveals frontal lobe metabolite abnormalities in idiopathic generalized epilepsy. *Neurology* 61, 897-902.
- Specht, U., May, T., Schulz, R., et al., 1997. Cerebellar atrophy and prognosis after temporal lobe resection. *J Neurol Neurosurg Psychiatry* 62, 501-506.
- Sutula, T.P., Hagen, J., Pitkanen, A., 2003. Do epileptic seizures damage the brain? *Curr Opin Neurol* 16, 189-195.
- Tasch, E., Cendes, F., Li, L.M., et al., 1999. Neuroimaging evidence of progressive neuronal loss and dysfunction in temporal lobe epilepsy. *Ann Neurol* 45, 568-576.
- Tofts, P. (2003) *Quantitative MRI of the brain measuring changes caused by disease*, Chichester, West Sussex; Hoboken, N.J., John Wiley & Sons Ltd.
- Vadnal, R., Parthasarathy, R., 1995. Myo-inositol monophosphatase: diverse effects of lithium, carbamazepine, and valproate. *Neuropsychopharmacology* 12, 277-285.
- Yu, A.H., Li, K.C., Yu, C.S., et al., 2006. Diffusion tensor imaging in medial temporal lobe epilepsy. *Chin Med J (Engl)* 119, 1237-1241.





# Chapter 9

**Functional MRI reveals declined prefrontal cortex activation in epilepsy patients on topiramate therapy**

**Jansen JFA, Aldenkamp AP, Majoie HJM, Reijs RP, de Krom MCTFM, Hofman PAM, Kooi ME, Nicolay K, and Backes WH**

*Published in: Epilepsy & Behavior 9 (1): 181-5, 200*

## **Abstract**

Functional magnetic resonance imaging of covert word generation was used to examine brain activation abnormalities associated with topiramate-induced cognitive language impairment in patients with epilepsy. Compared with a control epilepsy group, the topiramate group showed significantly less activation in the language-mediating regions in the prefrontal cortex together with significantly lower neuropsychological language scores. These findings suggest that topiramate has a critical effect on the cerebral neural systems that mediate expressive language.

## Introduction

Cognitive impairment induced by antiepileptic drugs is a major issue in the treatment of epilepsy (Aldenkamp et al., 2003). Many therapeutic dilemmas arise when adequate seizure control can only be achieved with medication that is associated with cognitive side effects. An example of a drug with tolerability related issues is topiramate (TPM). It is a broad-spectrum antiepileptic drug used both in adjunctive therapy and monotherapy for patients with epilepsy, which has also shown efficacy in the treatment of several other neurologic and psychiatric diseases, including migraine (Brandes et al., 2004).

Although TPM is beneficial for patients with epilepsy in terms of efficacy (Faught et al., 1996), studies based on subjective complaints have revealed a high frequency of TPM-induced cognitive adverse events (Ketter et al., 1999; Tatum et al., 2001). These cognitive side effects are an important reason for TPM discontinuation, even when the drug has a favorable effect on seizure frequency (Bootsma et al., 2004). Additionally, neuropsychological studies provide clear clinical evidence for TPM induced cognitive impairment (Martin et al., 1999; Thompson et al., 2000). It was revealed that primarily frontal lobe-associated executive functions like verbal fluency and working memory declined (Thompson et al., 2000). Secondly, non-verbal functions may be affected as well, in case they have a working memory or short term memory component (Kockelmann et al., 2004; Fritz et al., 2005). Hence, certain function-specific brain areas (i.e. prefrontal language- and memory-related areas) might be more affected by the TPM treatment than other areas.

The possible alterations on the functional neuroanatomy of language due to TPM treatment can be visualized with functional magnetic resonance imaging (fMRI) of covert word generation. This offers added value to neuropsychological testing alone, as it enables the determination of differences in sensitivity of brain regions to TPM treatment. Here we examine the effect of TPM treatment on patients with epilepsy using both methods to gain insight into the underlying cortical activation patterns, and modification thereof.

## Methods

### Study Subjects

Five epilepsy patients using TPM as add-on treatment (TPM group), and ten control epilepsy patients without TPM, but all on add-on polytherapy (control group), were selected during their visit at the outpatient neurology department of the Maastricht University Hospital or at the Epilepsy Centre Kempenhaeghe (a tertiary epilepsy referral and care center). All patients were identified with refractory epilepsies. Seizure classification and syndrome classification was based on history taking, a hetero-anamnesis, additional

interictal electroencephalography and MR imaging. Most patient demographics and characteristics (e.g. age at onset epilepsy, age at examination, and seizure frequency) are not significantly different between the two groups (Table 9.1). All TPM patients had a TPM starting dose of 25 mg, and a titration schedule of 25 mg per week. The TPM patients experienced self-reported and psychometric speech/ language dysfunction as well as attentional difficulties during the medication treatment. All patients were right-handed, as assessed by the Edinburgh inventory handedness test (Oldfield, 1971), and were at least 3 weeks seizure-free before inclusion. The study was approved by the commission on Medical Ethics of the Maastricht University Hospital, and all subjects gave written informed consent.

**Table 9.1.** Patient demographics and characteristics

	Epilepsy patients with TPM	Epilepsy patients without TPM	Statistical significance
Number of patients	5	10	
Male/female	0/5	3/7	
Age at onset epilepsy (y)*	11.0 ± 4.3	9.4 ± 3.5	<i>p</i> = 0.18
Age at examination (y)*	32.6 ± 11.6	35.3 ± 9.1	<i>p</i> = 0.17
Seizure frequency (month <sup>-1</sup> )*	4.8 ± 8.5	3.1 ± 1.5	<i>p</i> = 0.31
Pathology	1 DNET, 4 UK	8 HS, 1 Cyste, 1 UK	
Type epilepsy	5 CLRE	10 CLRE	
Seizure Focus ‡	2 LT, 1 MF, 2 BL	5 LT, 5 RT	
Duration epilepsy before TPM introduction (y)*	19.6 ± 12.0	NA	
TPM treatment time (days)*	128.8 ± 120.6	NA	
TPM dosage (mg)*	170 ± 115	NA	
TPM drug load *, †	0.7 ± 0.5	NA	
Full drug load *, †	2.0 ± 0.7	1.4 ± 0.7	<i>p</i> = 0.13
Other medication	2 LEV, 2 CBZ, 1 GBP, 1 LTG	1 LEV, 7 CBZ, 3 LTG, 1 VPA, 3 OXC	
Neuropsychological language score*	1.8 ± 0.8	4.3 ± 0.7	<i>p</i> = 0.002
Number of voxels with an activation level of >0.9 % in the language areas*	291 ± 155	1861 ± 1150	<i>p</i> = 0.01

\* mean ± standard deviation. ‡ based on the electroencephalogram

† Drug load is a quantitative assessment of total antiepileptic drug use, by standardizing the doses using the ratio of prescribed daily dose to defined daily dose (Lammers et al., 1995)

TPM, Topiramate; HS, hippocampal sclerosis; DNET, dysembryoplastic neuroepithelial tumor; UK, Unknown; HS, hippocampal sclerosis; CLRE, cryptogenic localization-related epilepsy; IGE, idiopathic generalized epilepsy; LT, left temporal; RT, right temporal; MF, multifocal; BL, bilateral; NA, not applicable; LEV, levetiracetam; OXC, oxcarbazepine; CBZ, carbamazepine; GBP, gabapentin; LTG, lamotrigine; VPA, valproate.

## Neuropsychological Tests

Language was assessed with an aphasia test battery that includes the word generation task and the naming test (Deelman et al., 1980). Using the results of these tasks, an experienced clinical neuropsychologist attributed a neuropsychological language score to each patient, with a nominal scale from 1 (severe cognitive language problems) to 5 (no problems). Differences in scores between the two groups were analyzed using the Wilcoxon Mann-Whitney test.

## Imaging Procedures

MRI was performed with a 1.5-Tesla unit (Philips Intera, Philips Medical Systems, Best, The Netherlands). Functional MRI data were acquired using a whole-brain single-shot three-dimensional (3D) blood-oxygen-level-dependent echo-planar imaging sequence, with repetition time 2 s, echo time 50 ms, flip angle 90°, voxel size 3.5×3.5×3.5 mm, matrix 64×64, 34 contiguous slices per volume, and 96 volumes per acquisition. For anatomical reference, we acquired a 3D T1-weighted fast field-echo image, repetition time 11 ms, echo time 3.5 ms, flip angle 90°, matrix 256×256, 150 contiguous slices, and 3.5×3.5×3.5 mm sized voxels.

## Cognitive language task

During fMRI, subjects performed a standard expressive language task, aimed at frontal activation (which includes naming, comprehension and repetition), as opposed to receptive language which encompasses more temporal/parietal activation. The task comprised the covert generation of words beginning with a different input letter (U-N-K-A-E-P) visually presented (McCarthy et al., 1993). The activation paradigm consisted of six word-generation condition blocks (32 s each) alternated with six baseline rest condition blocks (32 s each).

## Data analysis

Spatial data preprocessing was performed with SPM2 software (Wellcome Department of Cognitive Neurology). The number of activated voxels was determined in predefined brain regions, essential for language processing (Ojemann et al., 1989). These bilateral regions comprise the inferior and middle prefrontal cortex (Brodmann areas, BA 44-47), the superior prefrontal cortex (BA 6,9, and 10), the anterior cingulate cortex (ACC, BA 24 and 32), the anterior temporal lobe (BA 38), the posterior and inferior temporal lobe (BA 20 and 21), and the temporo-parietal junction (BA 39 and 40).

The quantitative analysis consisted of counting all voxels with an activation level, expressed as percent signal change, higher than a certain threshold with respect to baseline signal within the predefined language areas of all individual

activation maps. To eliminate the rather strong variation of the noise between subjects, activation was thresholded according to the percent signal change rather than the Student's t-statistics. The threshold should be high enough to exclude a relatively large number of false-positively activated voxels but also low enough to reduce the number of false-negatively activated voxels and to reduce the weight of the relatively strong T2\* responses (i.e. high signal increases) of draining veins. Therefore, the threshold was obtained by calculating the global mean (averaged over all patients) plus twice the standard deviation of the activation level of the brain areas, other than the predefined language areas. This method yielded a threshold of 0.9 %. Activation differences, between the TPM group and the control group were analyzed using a two-tailed Student's t-test.

To visualize which brain regions display the largest or, conversely, the smallest differences in activation level between the TPM and the control group, the average differences with corresponding standard deviation (SD) were calculated on a voxel-by-voxel basis for the whole brain. Then, from all voxels for which the absolute value of the activation difference level was larger than its SD, it was calculated how strong those voxels deviated from the global averaged activation difference level.

## Results

Neuropsychological assessment revealed that the language score was significantly lower in the TPM group than in the control group (Table 9.1).

Furthermore, fMRI demonstrated that the main region activated in both groups was an extensive area of the known expressive language network, including the left inferior prefrontal cortex (IPC, i.e. Broca's area (BA 44-45)), the medial prefrontal cortex (MPC, i.e. ACC (BA 24 and 32), and medial superior prefrontal cortex (BA 6 and 9)), and predominantly the left posterior parietal lobule (part of BA 40).

Quantitative analysis revealed that the TPM group showed significant underactivation (Table 9.1, Figure 9.1A) relative to the control group in the language areas (i.e. less voxels with an activation level higher than the threshold of 0.9 % (Figure 9.2A)). The results from the neuropsychological assessment and the fMRI analysis are combined in Figure 9.2B. A separate analysis of the female-only subsets of the two groups revealed similar results.

The TPM group displayed a significant underactivation throughout the whole brain, however to elucidate which brain regions are more sensitive to TPM, we calculated which regions had a lower or a higher than average underactivation level. This analysis revealed that the language areas (IPC and MPC) of the TPM group uniformly displayed a larger than average activation decline, whereas the occipital cortex had sub-regions with lower as well as higher than average activation decline (Figure 9.1B).

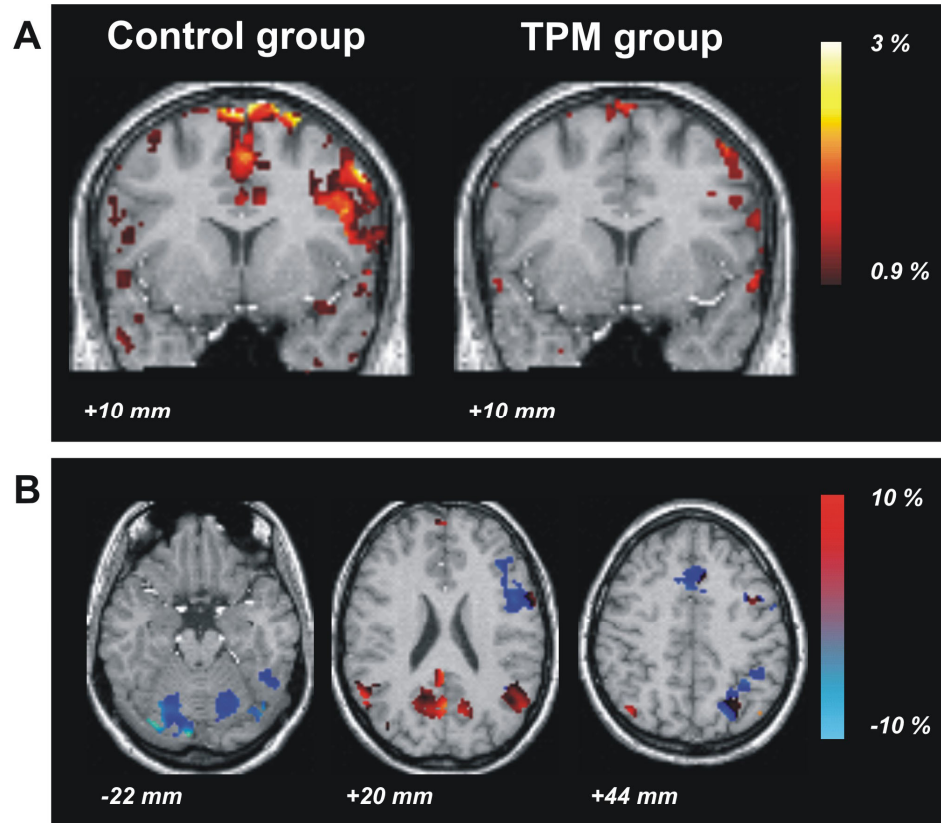


**Figure 9.1.** (A) Coronal images of group mean functional MRI activation maps, obtained for the covert word generation paradigm overlaid on a spatially normalized T1-weighted MR image, with left the control group, and right the topiramate group. The activation maps consist of all voxels within the language areas that have an activation level  $> 0.9\%$ . In the control group, the activation is clearly visible in the left inferior prefrontal cortex (IPC) and the medial prefrontal cortex (MPC), whereas the TPM group displays a significant underactivation in these regions.

(B) Transverse images of average underactivation level for the whole brain of the TPM group as compared to the control group. The prefrontal cortex (IPC & MPC) uniformly displays a higher than average underactivation, whereas the occipital cortex has sub-regions with lower as well as higher than average activation decline.

Slice positions are given in stereotaxic Talairach coordinates.

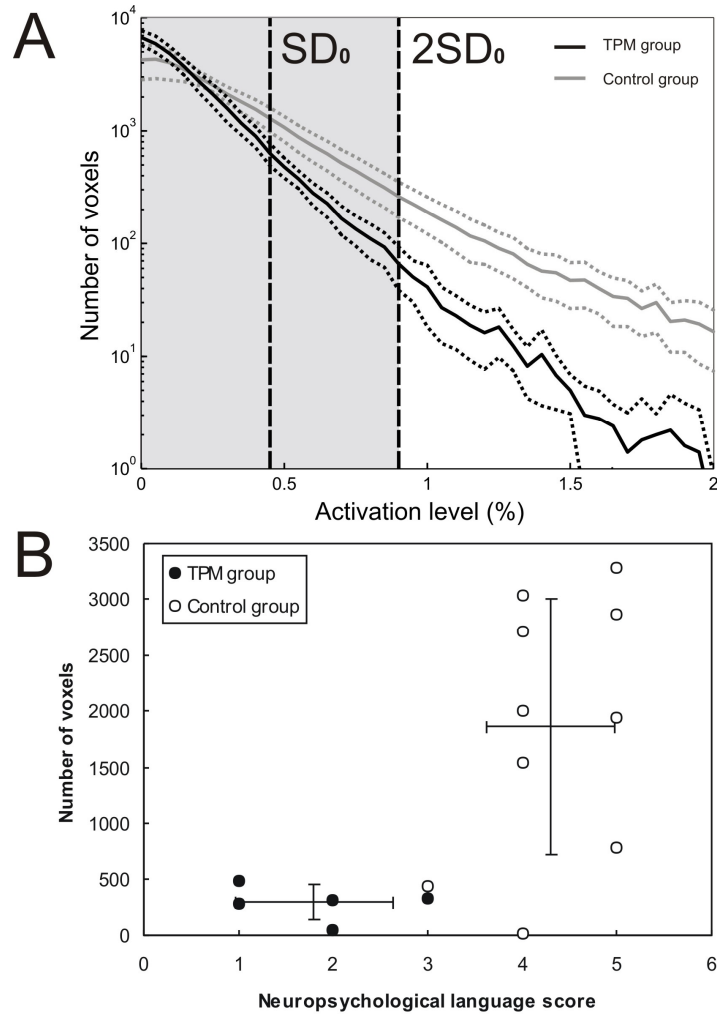


**Figure 9.2.** (A) Distribution of the voxels within the language areas as function of the activation level. The black curves correspond with the TPM group, and the grey curves correspond with the control group. The solid lines display the mean values, whereas the dotted lines display the 95% confidence interval. The dashed vertical lines indicate the global mean (averaged over all patients) plus one ( $SD_0$ ) or two times the standard deviation ( $2SD_0$ ) of the activation level of the brain areas, other than the language areas, respectively. The global mean plus twice the  $SD_0$  equals the threshold value of 0.9 % which is used for the quantitative analysis. (B) Number of suprathresholded voxels within the language areas as function of neuropsychological language score. A significant difference between the two groups is observed both for the neuropsychological language score and the number of voxels. Error bars display the standard deviation.



## Discussion

The present study was performed to expand our understanding of TPM-induced language impairment by investigating underlying cortical activation pattern changes using fMRI. The covert word generation paradigm used reveals a significant underactivation in the language areas in epilepsy patients on TPM therapy, which is in accordance with the type of neuropsychologically assessed cognitive language impairment (i.e. dysphasia). Often it is reported that most cognitive adverse events emerge especially at high doses, and increase in a dose-related fashion (Biton et al., 2001). However, this TPM group displayed cognitive language impairment using a relatively slow titration schedule, and a relatively low final dose level, which is in accordance with previous results (Aldenkamp et al., 2000).

These observations indicate that TPM induces a local dysfunction of the left prefrontal cortex. The current findings emphasize that not only the efficacy profile, but also the tolerability profile of TPM should be thoroughly considered before prescription. Especially since TPM has demonstrated its potential utility in neurological disorders other than epilepsy (Brandes et al., 2004), the importance of the tolerability profile of TPM should not only be acknowledged in epilepsy treatment.

An explanation for the generally lower activation level for the TPM group throughout the traditional expressive language areas, is that TPM likely has an effect on the entire cerebrum. However, the fact that the prefrontal language-related areas display a relatively stronger activation decline indicates that these regions have a higher sensitivity to TPM-induced activation-modifying effects. TPM has multiple mechanisms of action that have been hypothesized to contribute to its seizure control effects of which some also may be involved in the induction of cognitive impairment, including sodium and calcium channel blockade, gamma-amino butyric acid (GABA) potentiation, and glutamate receptor antagonism (Shank et al., 2000). Preclinical studies link disruptions in the neurotransmission system of GABA with disturbances in the frontal lobe (Petty, 1995). Since it has been shown that daily TPM therapy increases brain GABA concentration (Kuzniecky et al., 2002), a TPM-induced increase in the inhibiting effect of the total GABA pool, might be responsible for the cognitive language problems, as these problems originate from the frontal lobe. However, not all GABAergic antiepileptic drugs are associated with cognitive impairment. E.g. gabapentin, which is also known to increase brain GABA concentration (Kuzniecky et al., 2002) is associated with minimal cognitive effects (Martin et al., 1999). This indicates that the TPM-induced cognitive language impairment is possibly caused by a complex interaction of all mechanisms of action.

Since the present comparative groups both have epilepsy, we can only describe the effect of TPM therapy on patients with epilepsy. To study the effect of TPM alone, or the interaction effect between epilepsy and TPM, a control group without epilepsy, for instance migraine, would be required. However, at present it is difficult to obtain controls, without epilepsy, on TPM due to their limited availability. Moreover, the doses of TPM used in migraine are much lower than used in epilepsy.

The current study has some limitations that restrict generalization of TPM-induced brain function abnormalities within the cerebral language system. Due to its cross-sectional design, the lack of randomization, the lack of interpretations of the tests by blinded investigators, and the limited number of patients, the observed effect cannot be unambiguously attributed to TPM alone. As the separate female-only analysis yielded similar results, we argue for the exclusion of a gender effect. Furthermore, there is an obvious correspondence between type and severity of cognitive (i.e. language) impairment and the observed areas with declined activation (prefrontal cortex), hence TPM seems to play an important role in the origin of the observed underactivation. Another shortcoming is the absence of neuropsychological assessment of the patients before TPM administration. However, all patients were living independently in society and were at normal function levels (without aphasic disorders), as evaluated by a trained neurologist. Therefore, additional larger clinical studies may help provide additional support for cognitive language impairment induced by TPM therapy. In order to elucidate left-right hemispheric differential effects, it would be valuable to include further fMRI exams, aimed at revealing non-dominant hemispheric activation (e.g. (Staudt et al., 2002)).

Though to provide solid scientific support for our findings, ideally a randomized, double-blind, controlled study design is needed, preferably in patients randomized to TPM monotherapy.

In conclusion, by revealing brain function abnormalities within the language system and determining which regions are involved, the present findings help to visualize cognitive language impairment induced by TPM.

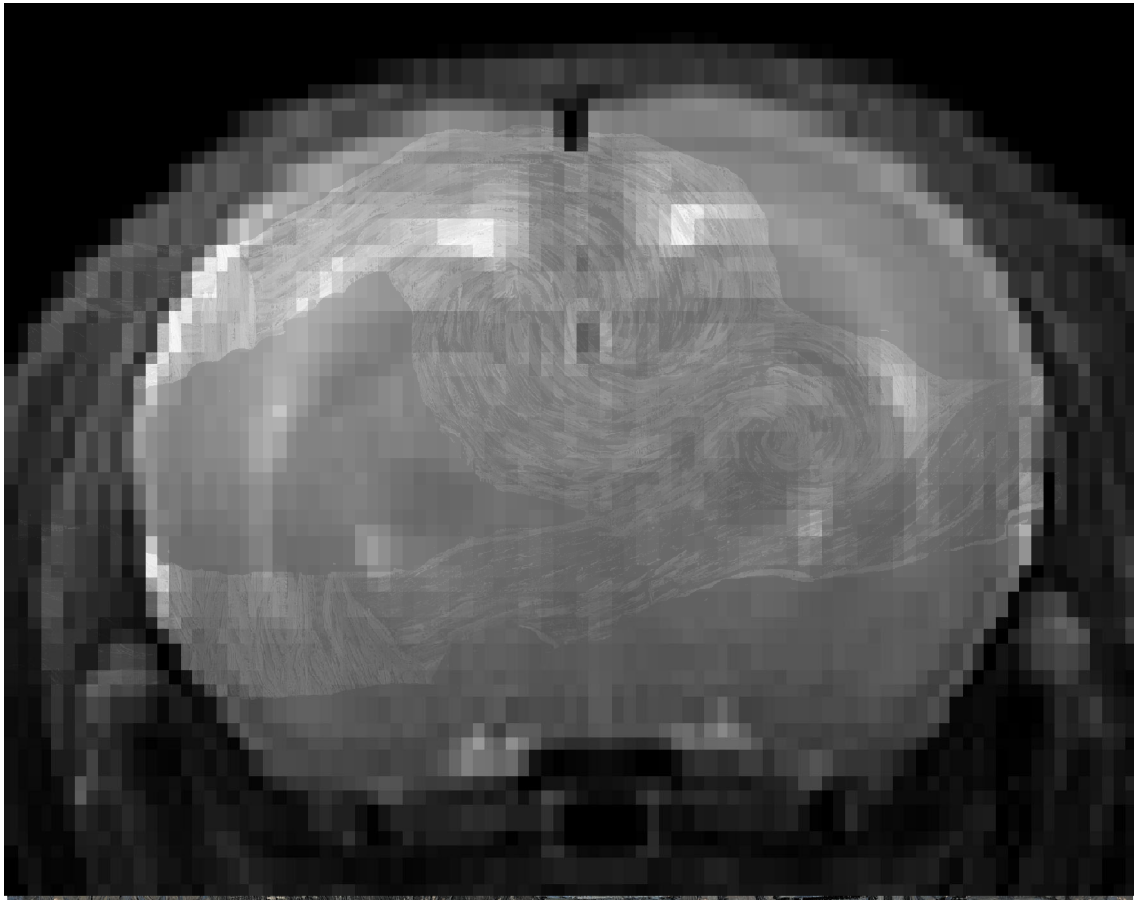
## References

- Aldenkamp, A.P., Baker, G., Mulder, O.G., et al., 2000. A multicenter, randomized clinical study to evaluate the effect on cognitive function of topiramate compared with valproate as add-on therapy to carbamazepine in patients with partial-onset seizures. *Epilepsia* 41, 1167-1178.
- Aldenkamp, A.P., De Krom, M., Reijs, R., 2003. Newer antiepileptic drugs and cognitive issues. *Epilepsia* 44 Suppl 4, 21-29.
- Biton, V., Edwards, K.R., Montouris, G.D., et al., 2001. Topiramate titration and tolerability. *Ann Pharmacother* 35, 173-179.
- Bootsma, H.P., Coolen, F., Aldenkamp, A.P., et al., 2004. Topiramate in clinical practice: long-term experience in patients with refractory epilepsy referred to a tertiary epilepsy center. *Epilepsy Behav.* 5, 380-387.
- Brandes, J.L., Saper, J.R., Diamond, M., et al., 2004. Topiramate for migraine prevention: a randomized controlled trial. *Jama* 291, 965-973.
- Deelman, B.G., Liebrand, W.B., Koning-Haanstra, M., et al., 1980. Measurements of aphasic disorders. A brief description of the SAN-battery. *Gerontologie* 11, 17-21.
- Faught, E., Wilder, B.J., Ramsay, R.E., et al., 1996. Topiramate placebo-controlled dose-ranging trial in refractory partial epilepsy using 200-, 400-, and 600-mg daily dosages. Topiramate YD Study Group. *Neurology* 46, 1684-1690.
- Fritz, N., Glogau, S., Hoffmann, J., et al., 2005. Efficacy and cognitive side effects of tiagabine and topiramate in patients with epilepsy. *Epilepsy Behav.* 6, 373-381.
- Ketter, T.A., Post, R.M., Theodore, W.H., 1999. Positive and negative psychiatric effects of antiepileptic drugs in patients with seizure disorders. *Neurology* 53, S53-67.
- Kockelmann, E., Elger, C.E., Helmstaedter, C., 2004. Cognitive profile of topiramate as compared with lamotrigine in epilepsy patients on antiepileptic drug polytherapy: relationships to blood serum levels and comedication. *Epilepsy Behav.* 5, 716-721.
- Kuzniecky, R., Ho, S., Pan, J., et al., 2002. Modulation of cerebral GABA by topiramate, lamotrigine, and gabapentin in healthy adults. *Neurology* 58, 368-372.
- Lammers, M.W., Hekster, Y.A., Keyser, A., et al., 1995. Monotherapy or polytherapy for epilepsy revisited: a quantitative assessment. *Epilepsia* 36, 440-446.
- Martin, R., Kuzniecky, R., Ho, S., et al., 1999. Cognitive effects of topiramate, gabapentin, and lamotrigine in healthy young adults. *Neurology* 52, 321-327.
- McCarthy, G., Blamire, A.M., Rothman, D.L., et al., 1993. Echo-planar magnetic resonance imaging studies of frontal cortex activation during word generation in humans. *Proc. Natl. Acad. Sci. U. S. A.* 90, 4952-4956.
- Ojemann, G., Ojemann, J., Lettich, E., et al., 1989. Cortical language localization in left, dominant hemisphere. An electrical stimulation mapping investigation in 117 patients. *J. Neurosurg.* 71, 316-326.
- Oldfield, R.C., 1971. The assessment and analysis of handedness: the Edinburgh inventory. *Neuropsychologia* 9, 97-113.
- Petty, F., 1995. GABA and mood disorders: a brief review and hypothesis. *J. Affect. Disord.* 34, 275-281.
- Shank, R.P., Gardocki, J.F., Streeter, A.J., et al., 2000. An overview of the preclinical aspects of topiramate: pharmacology, pharmacokinetics, and mechanism of action. *Epilepsia* 41 Suppl 1, S3-9.
- Staudt, M., Lidzba, K., Grodd, W., et al., 2002. Right-hemispheric organization of language following early left-sided brain lesions: functional MRI topography. *Neuroimage* 16, 954-967.

- Tatum, W.O.I., French, J.A., Faught, E., et al., 2001. Postmarketing experience with topiramate and cognition. *Epilepsia* 42, 1134-1140.
- Thompson, P.J., Baxendale, S.A., Duncan, J.S., et al., 2000. Effects of topiramate on cognitive function. *J. Neurol. Neurosurg. Psychiatry* 69, 636-641.

**Part III:**

**Preclinical application of Quantitative MR in epilepsy**





# Chapter 10

**Multimodal brain MR in a  
developmental rat model of early-life  
febrile seizures**

**Jansen JFA, Lemmens EMP, Strijkers GJ, Prompers JJ, Schijns OE,  
Kooi ME, Hoogland G, Backes WH, and Nicolay K**

**Abstract**

Experimental febrile seizures (FS) are known to cause cellular and molecular changes that promote hyperexcitability and epileptogenesis. In this study, FS were evoked in neonatal rats, to examine which MR modality may localize acute and chronic abnormalities during brain development. FS were induced by hyperthermia (HT) treatment at postnatal day (PN) 9, and brains were examined using quantitative multimodal MR at 6.3 Tesla at two time points: PN10 and 66. Full quantitative MR comprised hippocampal volumetry, cerebral T2 relaxometry, diffusion tensor imaging (DTI), and single voxel spectroscopy. Changes in cerebral MR tissue characteristics, possibly related to pathologic cellular processes linked to epileptogenesis, were determined.

A combined analysis of T2 and DTI results revealed transient alterations in the retrosplenial cortex, corpus callosum, amygdala, and piriformic cortex. Furthermore a chronic effect was observed in the hippocampus. Additionally, acutely and transiently elevated T2 values, indicative of edema, were observed in the hippocampus (+5%,  $p < 0.05$ ). A temporal decrease in N-acetyl aspartate values (-40%,  $p < 0.10$ ), indicative of decreased neuronal integrity, was observed at PN10, but not at PN66. Chronic decrease of DTI trace values, indicative of excitotoxicity, was observed in the amygdala (-10%,  $p < 0.01$ ), together with increase of fractional anisotropy (+30%,  $P < 0.05$ ), likely indicative of a chronic pathological process.

For the first time it was shown that early-life HT-induced FS give rise to both transient and foremost permanent micro-structural and metabolic changes to the limbic system (hippocampus and amygdala). Whether the detected MR abnormalities are specific for epileptogenesis or are the consequence of epileptiform activity remains to be elucidated.



## Introduction

Febrile seizures (FS) are the most common type of seizures in children, affecting 3-5 % of infants and young children between the age of 3 months and 5 years (Offringa et al., 1991). During FS, children have high fever leading to an increased body temperature which is accompanied with focal or generalized convulsions. The commonest histopathological finding in temporal lobe epilepsy (TLE) patients is mesial temporal sclerosis (MTS), which affects approximately 0.1% of the human population (Ojemann, 2001). Retrospective studies reveal that up to 50% of epilepsy patients with MTS have a history of FS during childhood. This suggests a causative role for FS in the development of MTS-associated TLE (Cendes et al., 1993).

Clinical investigations, aiming to resolve this hypothesized relationship, strongly benefit from the non-invasive capabilities of structural Magnetic Resonance Imaging (MRI). In addition to structural MRI, quantitative MRI has great clinical utility in identifying age- and disease-related abnormalities at a regional and global brain level (Tofts, 2003; Inglese et al., 2004). Quantitative Magnetic Resonance (MR) techniques such as T2 relaxometry, diffusion tensor imaging (DTI), and proton MR spectroscopy ( $^1\text{H-MRS}$ ), are sensitive to micro-structural (T2, DTI) and metabolic ( $^1\text{H-MRS}$ ) changes in brain tissue, and therefore can be used to determine changes over time in tissue characteristics possibly related to FS-induced pathologic cellular processes that promote epileptogenesis.

Longitudinal clinical studies addressing the potential link between FS and TLE are complicated, due to (i) the possibly long and variable silent period between early-life FS (occurring up to the age of 5 years) and the first onset of epileptic seizures (often starting during puberty) and (ii) the low incidence of patients displaying early-life FS later diagnosed with epilepsy. Previous MRI studies in children who suffered from FS (Scott et al., 2002; Scott et al., 2003) reported enlarged hippocampal volumes and prolonged T2 relaxation times, consistent with edema, within two days after generalized FS. This normalized thereafter within five days. The acute hippocampal edema may be the start of the pathophysiological sequence that links FS to MTS, although the exact nature of that edema remains uncertain. In a follow-up study using diffusion weighted imaging (Scott et al., 2006), it was concluded that the edema had a vasogenic nature, which reflects a temporal blood-brain barrier disruption. So far, mainly T2-weighted MR imaging was used in human studies. However, it is as yet unknown which MR contrast is most suitable to reveal relevant epileptogenic abnormalities.

For the reasons mentioned above, it is beneficial to use an animal model of FS to study the latent period between FS and epilepsy and whether early-life FS progress into MTS-associated TLE in adulthood. In the well-established hyperthermia (HT) rat model of epileptogenesis (Baram et al., 1997; Toth et al.,

1998), young rats are subjected to a hyperthermia treatment that induces FS at postnatal day (PN) 9-10. The seizures that are induced by heat in rats are comparable with fever-induced seizures in children. Another advantage of this model is that it uses rats during a brain-development age comparable to that of a human child when it is most susceptible to seizures (Avishai-Eliner et al., 2002). Furthermore, the model is highly suitable for long-term follow-up studies. It has been shown (Dube et al., 2006) that spontaneous electro-clinical seizures (as demonstrated by cortical electroencephalography (EEG) and long-term video monitoring) were observed at PN90-180 in 35% of the HT treated rats, and additionally, interictal epileptiform discharges were recorded in 88% of the rats. Using histological methods, only primarily transient alterations in neuronal structure were observed, that were no longer present at 4 weeks after the HT-induced seizures (Toth et al., 1998). The same research group (Dube et al., 2004) also collected serial T2-weighted MRI scans at 4 Tesla, before and after HT-induced FS in neonatal rats. An abnormal relative T2-weighted signal enhancement of the hippocampus and the amygdala was observed at 24 hours and 8 days after HT treatment. However, these MRI changes were not accompanied with histologically proven neuronal injury. It was therefore concluded that abnormal T2-weighted signal enhancements related to prolonged febrile seizures do not necessarily signify cell death, but might be related to processes promoting epileptogenesis.

In this study we examined rat brain after experimental HT-induced FS using a wide spectrum of quantitative MR techniques: volumetry, T2 relaxometry, DTI, and  $^1\text{H}$ -MRS, to determine microstructural and metabolic tissue changes which are possibly related to pathologic cellular processes linked to epileptogenesis. MR examinations were performed at two time points: 24 hours and 57 days after HT treatment, to enable differentiation between possible chronic, or transient alterations. Understanding the cellular mechanisms underlying these changes may provide insights into the mechanisms that link early-life FS and (late) epilepsy.

## Materials and Methods

### Animals

Sprague-Dawley rats (Harlan, The Netherlands) were housed under standard conditions ( $21\pm 2^\circ\text{C}$  ambient temperature, a 12-h light/dark schedule, background noise provided by a radio, and food and water ad libitum). In total, 42 male rats were divided into the following two groups: (a) normothermia (NT;  $n = 9$ ) and (b) hyperthermia (HT;  $n = 33$ ) rats. Based on the occurrence of FS behavior (body flexion), HT treated rats were assigned to either the HT+ (with typical FS behavior) or the HT- (without typical FS behavior) group. HT+ and NT rats were subsequently selected for MR examination. All experiments

were approved by the Animal Experiments Committee of the Maastricht University, The Netherlands.

### **Hyperthermia treatment**

HT was induced as described previously (Baram et al., 1997; Lemmens et al., 2005). In brief, PN9 rat pups were injected subcutaneously with 0.2 ml 0.9% saline to prevent dehydration and placed in a high Perspex cylinder with a diameter of 10 cm (one rat/cylinder). An adjustable stream of heated air (50–52°C) was blown into the cylinder by a commercial hair dryer, placed 50 cm above the rats, to raise the body temperature of the rat pups from a basal value of circa 35°C to 41–42.5°C. Core temperatures were measured before and every 2.5 min during the HT treatment, with a rectal probe. When the core temperature of the rats reached 39.5°C, usually after 5–10 min, the temperature and volume of the air were adjusted so that a core temperature of 41–42.5°C was maintained for 30 min. If the core temperature exceeded 42.5°C, the rat was removed from the cylinder until the temperature dropped below 42°C. The manifestation of FS was monitored behaviorally by two observers. The behavioral seizures were stereotyped and previously shown to correlate with EEG discharges in the hippocampus (Baram et al., 1997; Dube et al., 2000). Behaviorally, the seizures consisted of arrest of heat-induced hyperkinesis, followed by body flexion, and occasionally followed by clonic contractions of the limbs. The moment the rats showed body flexion was taken as the start of a seizure, whereas the end of the seizure was marked either by the end of the 30-min hyperthermia treatment or by regaining normal behavior. Immediately after the 30-min treatment, the rats were placed in water (room temperature, RT) with their heads above the surface to regain their normal body temperature, after which they were returned to their mother. Normothermia (NT) controls from the same litter as the HT rats were exposed to the same conditions, except that the stream of air was used to maintain the core temperature of the rats. At PN21, all pups were weaned and randomly housed, two to three rats per cage.

### **MR**

MRI system. The MR experiments were performed on a 6.3 Tesla horizontal bore magnet (Oxford Instruments, England) interfaced to a Bruker Biospec (Bruker, Ettlingen, Germany) MR Imaging console. A dedicated linear birdcage volume coil and a butterfly surface coil (Rapid Biomed, Rimpfing, Germany) were used for pulse transmission and signal detection, respectively. MR was performed at PN10 on 9 NT and 10 HT+ rats, and at PN66 on 9 NT and 9 HT+ rats.

Animal handling. Anesthesia was induced in PN10 rats with a mixture of 2-3% isoflurane and medicinal air, and maintained with 1-1.5% isoflurane. In PN66 rats, anesthesia was induced with 4% and maintained with 1.5-2.5% isoflurane-medicinal air. Rats were placed in a home built cradle, equipped with a mask for anesthesia gas supply and a warm water pad. Respiration and rectal temperature were monitored during the MR experiments, and the body temperature was kept at 35°C.

MR protocol. For anatomical reference, a proton density and T2-weighted (PDT2w) multi slice multi spin-echo (MSME) was used acquiring 15 coronal slices of 1 mm thickness with a repetition time (TR) of 4937 ms and echo times (TE) of 12.2 and 128.3 ms (256 x 192 matrix, field of view 4 x 4 cm, 1 average). Quantitative T2 imaging was performed using an MSME sequence with a TR of 5 s and TEs of 17.2, 43.0, 77.3, 111.7, 146.1, and 180.4 ms (15 coronal slices, 1 mm thickness, 128 x 128 matrix, field of view 4 x 4 cm, 2 averages).

T2 relaxation times were calculated on a pixel-by-pixel basis using a nonlinear monoexponential fit. For DTI, an echo planar imaging sequence was used, with 30 directions (TR = 3 s, TE = 34 ms,  $b = 0$  and 1000 s/mm<sup>2</sup>, diffusion gradient duration 4 ms, diffusion gradient strength 239.1 mT/m, 15 coronal slices, 1 mm thickness, 128x128 matrix, field of view 4 x 4 cm, 2 averages). The apparent diffusion coefficient (ADC, unit 10<sup>-6</sup> mm<sup>2</sup>/s) and fractional anisotropy (FA, unit %) maps were calculated using the diffusion software available on the MRI console. In short, using the averaged images acquired at  $b = 0$  and 1000 s/mm<sup>2</sup>, 30 images of directional sensitive ADC can be calculated, each being a linear combination of three elements of the diffusion tensor. The diffusion tensor elements were calculated and the tensor was subsequently diagonalized, yielding eigenvalues  $\lambda_1$ ,  $\lambda_2$ , and  $\lambda_3$ , as well as the three eigenvectors that define the corresponding orthogonal diffusion directions. Based on the eigenvalues from the tensor, FA and ADC were calculated on a voxel-by-voxel basis.

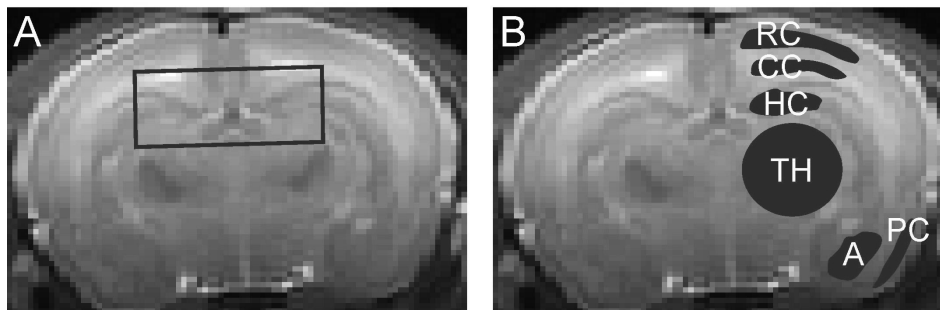


**Figure 10.1.** T2-weighted image of a hyperthermia treated rat at PN10, indicating the voxel of interest for <sup>1</sup>H-MRS (A), and the employed regions of interests for MRI analysis (B). Abbreviations: TH, thalamus; HC, hippocampus; RC, retrosplenial cortex; A, amygdala; PC, piriformic cortex; and CC, corpus callosum.

Single-voxel  $^1\text{H}$ -MRS was applied to a  $5 \times 4 \times 2 \text{ mm}^3$  (0.04 ml) voxel mainly covering the bilateral hippocampi, but also partially the retrosplenial corti, thalamus and corpus callosum (Figure 10.1A). The following parameters were used: TE 14 ms, TR 10 s, 256 averages, spectral bandwidth 4006.41 Hz, and number of points 1977. Localization and water suppression were achieved with point-resolved spatially localized spectroscopy (PRESS) and chemical shift selective suppression (CHESS), respectively. For absolute quantification of metabolite concentrations expressed in mmol/l, the calibration strategy based on the water reference signal was used (Barker et al., 1993). To this end, after the *in vivo* measurement, the signal from unsuppressed tissue water was recorded from the same voxel, which served as an endogenous concentration reference. The unsuppressed spectrum was recorded under identical conditions (16 averages) as the metabolite spectra, but with the water-suppression radiofrequency pulses switched off. Relaxation correction was performed utilizing onsite determined T2 and T1 relaxation parameters for water (averaged per group; data not shown), and previously reported relaxation times for metabolites by de Graaf et al (De Graaf et al., 2006). Absolute concentrations were determined using previously reported values of water content by Tkac et al (Tkac et al., 2003).

### MR data analysis

Image processing and analysis was performed using the software package MRICro (Rorden et al., 2000) and customized software programmed in Matlab (The Mathworks, Natick, MA, USA). Hippocampal volumetry was performed using the T2-weighted images recorded with the MSME sequence with TE =128.3 ms. A three-dimensional volume of interest was manually drawn by two independent observers blinded to the experimental status of the animals, from which the hippocampal volume was calculated. Further analysis was based on values averaged over both observers. Furthermore, on the T2-weighted coronal slice with coordinates (Bregma -3.30 mm, interaural 5.70 mm), bilateral regions of interest (ROI) were manually drawn within the thalamus (TH), hippocampus (HC), retrosplenial cortex (RC), amygdala (A), piriformic cortex (PC), and corpus callosum (CC) (Figure 10.1B), conform the Paxinos brain atlas (Paxinos et al., 1994). The mean T2, ADC and FA values were calculated for the selected structures. The agreement between observers was calculated using the Pearson correlation coefficient.

The spectra were analyzed using the LCModel software package (Version 6.1-4), which analyzes the *in vivo* MR spectra as a linear combination of the separately recorded *in vitro* spectra of the individual metabolites. The metabolite basis set (PRESS, TE 14 ms, 6.3 T) including simulated macromolecule peaks was kindly provided by Dr. Provencher. For each spectrum, the parts per million (ppm) range included for analysis was

0.2-4.2 ppm. LCModel provides estimates in mmol/kg for a total of 16 metabolites, including N-acetyl-aspartate (NAA), which is indicative of neuronal integrity, choline (Cho), which can act as a malignancy marker, total creatine (tCr), indicative of the energy metabolism, myo-inositol (mI), which functions as an osmolyte and is considered to indicate ongoing myelin damage, taurine (Tau), which is involved in osmoregulation and modulation of the action of neurotransmitters and the neurotransmitters glutamate (Glu) and gamma-aminobutyric acid (GABA). The Cramer-Rao minimum variance was calculated as an estimate of the error in metabolite quantification (Cavassila et al., 2001). Metabolite estimates were excluded from analysis, if the Cramer-Rao minimum variance exceeded the 20% range.

### Statistical analysis

Hippocampal volumetry, tissue T2, ADC, and FA of the right and left hemisphere were first compared for each ROI in each animal separately. A paired two-tailed Student's t-test revealed no significant differences between hemispheres. Data from the two hemispheres were therefore averaged for further analysis.

Multiple end point testing was controlled for by first investigating in what regions MR-detectable HT-induced alterations appeared. To this end, T2, ADC, and FA MRI outcomes were combined per ROI, since these measures are substantially affected by changes in water content. For each ROI, the global null hypothesis stating that within that region no differences between the HT+ and NT group of the included MR modalities exist was tested using the ordinary least squares test of O'Brien and Läuter (O'Brien, 1984; Läuter, 1996). For the combined analysis, statistical significance was calculated with two-tailed Student's t tests with Hochberg correction for multiple comparisons (Hochberg, 1988).

Additionally, in a subsequent analysis per modality, hippocampal volumetry, tissue T2, ADC, FA values, and spectroscopic data of HT+ rats were compared with those of control rats at PN10 and PN66. To examine a possible hyperthermia-induced effect on maturation, the differences between the values at the two time points (PN66-PN10) were also analyzed. For the separate modality analyses, statistical significance was calculated with two-tailed Student's t tests. For all statistical analyses,  $p < 0.05$  was considered significant. Data are expressed as mean  $\pm$  standard error of the mean (SEM).

Table 10.1. Quantitative MR results in hyperthermia and control rats

Region of Interest		PN10		PN66	
		HT+ Mean (SEM)	NT Mean (SEM)	HT+ Mean (SEM)	NT Mean (SEM)
Hippocampus					
	T2	106.5 (1.9) †	101.3 (1.6)	53.4 (2.3)	49.6 (2.2)
	ADC	993 (11)	1020 (14)	1240 (62) ‡	1292 (39)
	FA	19 (1)	21 (1)	34 (3)	28 (3) *
	Volume	60 (2)	64 (2)	114 (6)	115 (3)
	NAA	1.7 (0.2)	2.3 (0.3)	4.7 (0.2)	4.5 (0.2) *
	tCr	5.2 (1.0)	5.6 (0.6)	7.2 (0.2) †	6.7 (0.2)
	Cho	1.1 (0.2)	1.3 (0.2)	1.1 (0.0)	1.1 (0.1)
	GABA	2.2 (0.2)	2.3 (0.2)	2.1 (0.1)	2.4 (0.1)
	Glu	3.6 (0.3)	4.1 (0.3)	6.2 (0.2)	6.2 (0.4)
	Tau	9.4 (1.0)	11.5 (1.1)	5.9 (0.1)	5.5 (0.2)
	Ins	3.7 (0.8)	2.7 (0.3)	5.6 (0.1)	5.4 (0.2)
Retrosplenial cortex					
	T2	113.9 (2.6)	108.7 (2.2)	51.7 (2.5)	48.9 (2.6)
	ADC	946 (15) ‡	977 (15)	1180 (71)	1239 (47)
	FA	20 (1)	21 (1)	34 (3)	30 (3)
Corpus Callosum					
	T2	120.9 (4.0)	118.2 (2.3)	9.8 (1.6)	47.4 (1.6)
	ADC	1075 (13) ‡	1093 (29)	1227 (62)	1294 (31)
	FA	24 (1)	25 (1)	37 (2)	39 (3)
Thalamus					
	T2	95.9 (0.9)	93.3 (1.7)	48.1 (0.9)	47.8 (0.8)
	ADC	970 (11)	1002 (16)	1170 (55)	1250 (48)
	FA	20 (1)	22 (1)	39 (3) †	31 (2)
Amygdala					
	T2	84.5 (1.3)	85.0 (1.4)	55.4 (1.3)	55.1 (1.4)
	ADC	914 (6) † ‡	962 (11)	1163 (48) †	1320 (39)
	FA	15 (1)	16 (1)	39 (3)	32 (2)
Piriformic cortex					
	T2	80.9 (2.6)	85.0 (1.4)	56.3 (2.2)	53.6 (1.7)
	ADC	924 (10) † ‡	972 (15)	1136 (50)	1217 (45)
	FA	19 (1)	17 (1)	38 (3)	35 (2)

HT+, experimental hyperthermia group NT, normothermia control group; PN10, post natal day 10; PN66, postnatal day 66; SEM, standard error of the mean; T2, transverse relaxation time (in ms); ADC, apparent diffusion coefficient (in  $10^{-6}$  mm<sup>2</sup>/s); FA, fractional anisotropy (in %); Volume, hippocampal volume (in  $\mu$ l); NAA, N-acetyl-aspartate; tCr, total creatine; Cho, choline; GABA, gamma-aminobutyric acid; Glu, glutamate; tau, taurine; Ins, myo-inositol (all in mmol/kg)

† 2-tailed  $P < 0.05$

‡ 2-tailed  $P < 0.05$  (ordinary least squares test using Hochberg correction)

\* 2-tailed  $P < 0.05$  time course maturation effect (PN66-PN10), see Figure 10.5

## Results

### Animal model

During hyperthermia treatment, febrile seizures observed by behavioral monitoring were present in 12 of the 33 (36%) HT rats. Mortality due to the hyperthermia treatment and during the follow up MR examinations was 36% (12/33) and 17% (2/12), respectively. Mortality in the normothermia group was 0% (0/9). During the MR experiments, all control and experimental animals were stable, displaying normal body temperature and respiratory signal. No signs of seizures were observed during MR acquisition.

### Combined regional analysis

The ordinary least squares test revealed significant HT-induced MR alterations at PN10 for the retrosplenial cortex, corpus callosum, amygdala, and piriformic cortex and at PN66 for the hippocampus (Table 10.1).

#### Hippocampal volumetry

There were no significant statistical differences in hippocampal volumes between the two groups at both time points (Table 10.1).

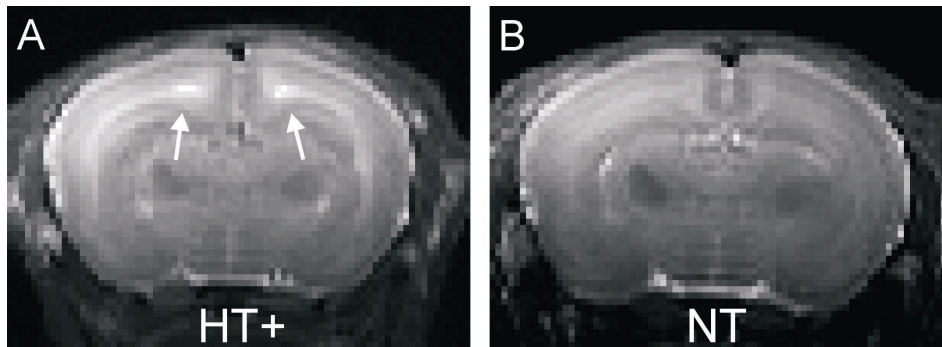


**Figure 10.2.** T2-weighted MR images of neonatal rat brains at PN10, 24 hours after hyperthermia treatment of a (A) hyperthermia (HT+) and (B) normothermia (NT) treated rat. Note the hyperintense MRI signal due prolongation (white arrows) of the tissue T2 relaxation time, indicative of edema formation in (A) proximal to the corpus callosum and hippocampus of the rat with hyperthermia-induced febrile convulsions compared to the normothermia rat (B).

### T2 relaxometry

In Figure 10.2AB, typical examples of T2-weighted MR images of neonatal rat brains 10 days after birth are shown, displaying an abnormal hyperintense signal due to T2 relaxation time prolongation in the region at and near the corpus callosum and the hippocampus in the HT+ rat. At PN10, HT+ rats had elevated T2 relaxation values in most dorsal regions (retrosplenial cortex, corpus callosum, hippocampus, and thalamus) compared to NT rats (increase of 5%). This effect



was significant in the hippocampus (HT+ compared with NT,  $p < 0.05$ ). At PN66, no differences were found in T2 relaxation times between the groups (Table 10.1).

### Diffusion Tensor Imaging

ADC values were significantly decreased at PN10 (decrease of 10%) for HT+ rats in the amygdala (HT+ compared with NT,  $p < 0.01$ ) and piriformic cortex (HT+ compared with NT,  $p < 0.05$ ). Also at PN66 ADC values were decreased in the amygdala (HT+ compared with NT,  $p < 0.05$ ). Figure 10.3AB displays an ADC map at PN66 of a typical HT+ and NT rat. For the HT+ rat a decrease in ADC values can be appreciated ventrally.

For FA, no differences were observed at PN10. However, at PN66 FA values were higher (+30%) in the thalamus (HT+ compared with NT,  $p < 0.05$ ) (Table 10.1). The analysis of a possible HT-induced effect on maturation, revealed a significantly larger FA increase in the hippocampus between PN10 and PN66 (Figure 10.5A).

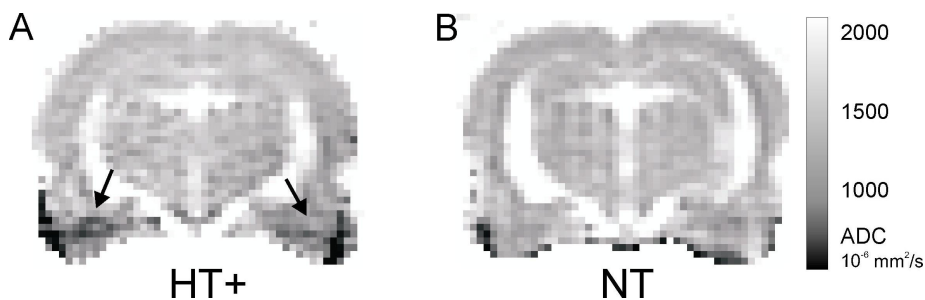


**Figure 10.3.** ADC maps at PN66 of the rat brain of a representative hyperthermia (HT+) (A) and a normothermia (NT) treated rat (B). Notice for the HT+ rat the pronounced ventral ADC decrease in the bilateral amygdala region (black arrows), which is indicative of chronic micro-structural tissue damage.

### Spectroscopy

Figure 10.4 illustrates typical  $^1\text{H}$ -MRS spectra of a control and HT+ rat at PN10 (Figure 10.4AB) and PN66 (Figure 10.4CD). While there were no changes observed in the concentrations of the neurotransmitters glutamate and GABA, a trend towards a lower concentration of the neuronal marker NAA (decrease of 40%) was observed at PN10 ( $p < 0.10$ ). Also, a significantly higher concentration of tCr (increase of 7%) was observed at PN66 for the HT+ rats ( $p < 0.05$ ). Furthermore, the rate of NAA increase (to adult values) was significantly higher in the HT+ rats at PN66 ( $p < 0.05$ ) (Figure 10.5B).

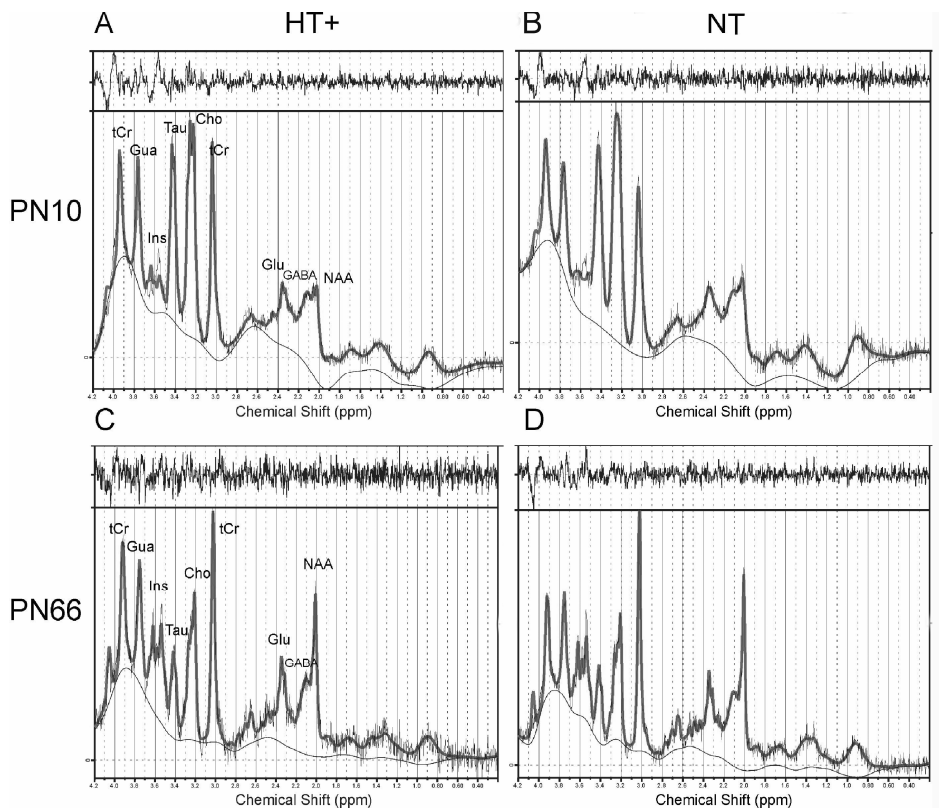


**Figure 10.4.** LCMoDel (Version 6.1-4) analysis output of a localized  $^1\text{H}$ -MRS spectra obtained at postnatal days (PN) 10 (**A, B**) and 66 (**C, D**) in the hippocampus of a hyperthermia (HT+) treated rat (**A, C**) after hyperthermia-induced febrile convulsions and a control rat (**B, D**). Note the relatively strong increase in the NAA peak at PN66, which was abnormally low at PN10 shortly after hyperthermia treatment. The *in vivo* spectrum (thin grey curve) has been estimated with the LCMoDel output (thick black curve), and the difference of these spectra is plotted at the top. The thick gray curve at the bottom indicates the fitted macromolecule baseline. The inserted table at the right displays the estimated metabolite concentrations and the Cramer Rao minimum variance bounds. NAA, N-acetylaspartate; tCr, total creatine; Cho, choline; and Ins, myo-inositol.

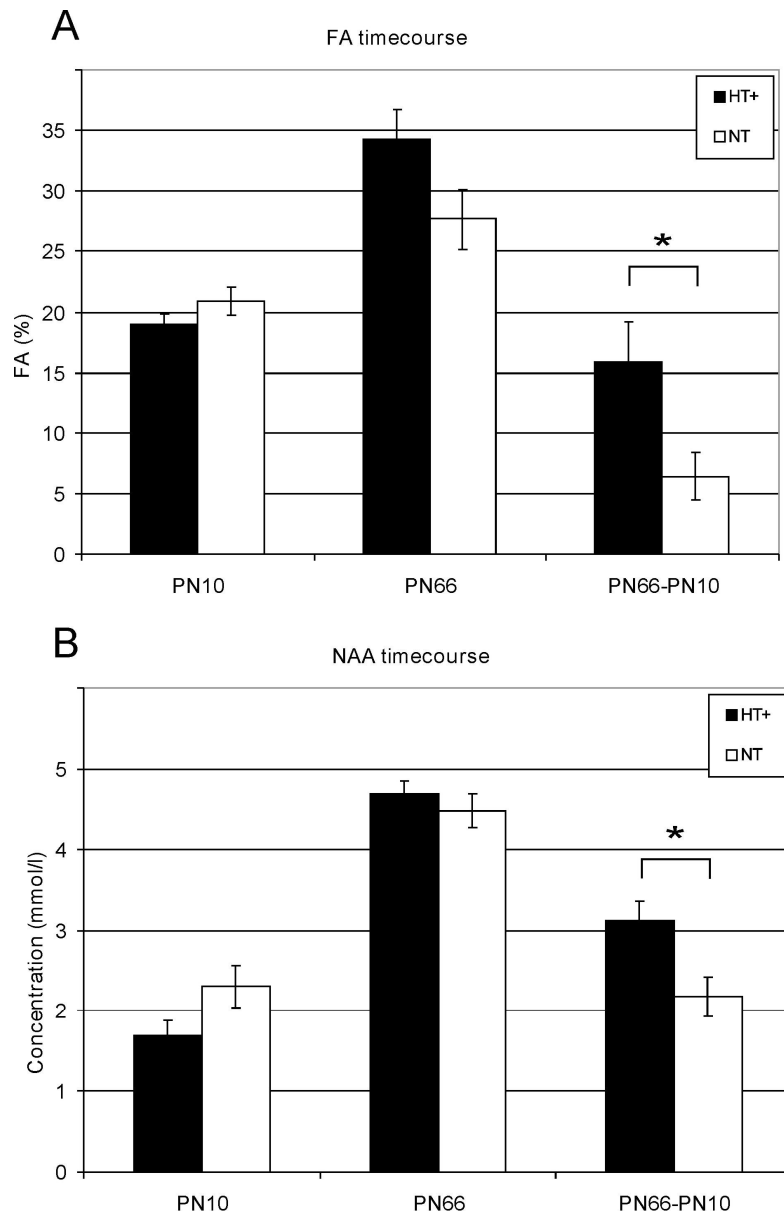


**Figure 10.5.** Time course of maturation effects within the hippocampus. **(A)** Bar diagrams displaying the FA values within the hippocampus, for the HT+ (black bars) and NT (white bars) rats, at PN10, PN66 and the difference PN66-PN10. **(B)** Bar diagrams displaying the concentration of NAA within the hippocampus, for the HT+ (black bars), and NT (white bars) neonatal rats, at PN10, PN66 and the difference PN66-PN10. Bars represent mean value  $\pm$  standard error of the mean. \* denotes  $p < 0.05$ .

## Observer agreement

The Pearson correlation coefficient between the data obtained by the two observers was 0.91, 0.96, 0.87, and 0.75, for the hippocampal volumetry, T2, ADC, and FA values, respectively.

## Discussion

In this study, quantitative multimodal MR, comprising volumetry, T2 relaxometry, DTI, and <sup>1</sup>H-MRS was combined, to monitor cerebral (patho)-physiological changes induced by FS in neonatal rats. A number of novel MR abnormalities have been observed. A combined analysis revealed significant quantitative MR changes both in the retrosplenial cortex and corpus callosum (i.e. dorsal regions) and in the amygdala and piriformic cortex (i.e. ventral regions) at PN10, and in the hippocampus at PN66. Tissue T2 relaxation times were shown to transiently increase in the hippocampus at PN10, but normalized at PN66. DTI revealed permanently decreased ADC values in the amygdala, and increased FA values in the thalamus. NAA, as determined by <sup>1</sup>H-MRS, was somewhat decreased at PN10, but displayed a higher developmental increase between PN10 and PN66 in HT+ rats.

### Hippocampal volumetry and T2 relaxometry

Quantification of hippocampal volume revealed no significant differences between the HT treated rats and the control rats at either time point. However, at PN10 T2 relaxometry revealed prolonged T2 relaxation times for HT treated rats within the hippocampus (and most other dorsal regions: thalamus, retrosplenial cortex, and corpus callosum) which was confirmed by hyperintense T2-weighted images. This effect, probably due to edema formation, was transient as values normalized at PN66. These results concur with earlier findings by Dubé et al (Dube et al., 2004), who reported hyperintense T2-weighted images in HT treated rats at 24 hours and 8 days after inducing seizures. As they observed T2 signal enhancement at 8 days after FS, we reason that the timescale of transient edema formation must be longer than 8 days, but shorter than 57 days, since we did not find any T2 relaxation time prolongation at PN66 (i.e. 57 days after hyperthermia).

In a serial MRI investigation of the rat kindling model of epileptogenesis, Jupp et al (Jupp et al., 2006) also observed prolonged T2 relaxation times that were not accompanied by differences in hippocampal volume between kindled rats and control rats. Amygdala kindling is considered to be a model of both seizure manifestation and epileptogenesis. As both kindling and hyperthermia are not associated with status epilepticus, they are relatively 'mild' models of epileptogenesis, and might share some characteristics, in contrast to models

where status epilepticus is generated by administration of either lithium-pilocarpine or kainic acid. Most epileptogenesis models inducing status epilepticus are associated with acute tissue degradation, resulting in both hippocampal volume reduction and prolonged T2 relaxation times (Nairismagi et al., 2004; Nairismagi et al., 2006a; Nairismagi et al., 2006b).

### **Diffusion Tensor Imaging**

The chronic decrease of ADC values at PN10 and PN66 in the limbic system, namely the amygdala and piriformic cortex, are similar to observations made shortly after status epilepticus in the lithium-pilocarpine model (Wall et al., 2000; Van Eijsden et al., 2004). It was hypothesized (Wall et al., 2000; Van Eijsden et al., 2004) that these changes could be attributed to several processes that are involved in the cascade leading from transient neuronal alterations to long-lasting modifications of the neuronal circuit organization. These include the activation of immediate-early genes, activation of growth factor genes within hours, alterations in glutamate receptors, glial hypertrophy, and cytoskeletal protein changes (Ben-Ari, 2001). The cascade is induced by a massive calcium influx due to hyperexcitation, resulting in neuronal damage or death. The glutamate stored intracellularly is released from damaged cells and causes additional excessive excitation. Cell swelling is most likely a manifestation of cytotoxic edema due to the long-term excitation (Handforth et al., 1995). We also observed increases of FA values at PN66 within the thalamus. An explanation for this might be cellular reorganization (i.e. sprouting), which has been observed in the thalamus after status epilepticus (Nairismagi et al., 2006b) and in the hippocampus after HT-induced seizures (Bender et al., 2003). Another explanation might be axonal growth and neosynapse formation, which are processes known to be involved in the cascade of synaptic rearrangements after seizures (Ben-Ari, 2001).

### **Spectroscopy**

At PN10, HT induced a decreased hippocampal NAA concentration, usually attributed to neuronal death or dysfunction (Maton et al., 2000), which normalized at PN66. This might be indicative of metabolic recovery (Hugg et al., 1996). Both the increase in NAA and hippocampal FA between PN10 and PN66 are larger in the HT treated group than the NT group, and the cluster analysis revealed significant MR-observable alterations at PN66. Therefore, the effects observed might be indicative of an underlying pathological process, expectedly epileptogenesis. At PN66, we observed for the HT+ group a significant increase in concentration of creatine, a commonly used reference metabolite for relative quantification. As creatine is not a constant metabolite in this case, metabolite concentrations expressed as ratios with respect to creatine

are not reliable, whereas absolute quantified concentrations are (Jansen et al., 2006).

### **Maturation**

For all quantitative MR parameters an obvious difference was detected between PN10 and PN66, which can be attributed to maturation. The general decrease of T2 values concurs with increased myelination associated with maturation in human neonates (Thornton et al., 1999). Larvaron et al (Larvaron et al., 2006) have investigated the effect of postnatal aging on ADC and FA values in mouse brains. At several time points (PN5, PN12, PN19 and PN54), they observed changes both in ADC and FA. Between PN5 and PN12, the ADC generally increases, whereas the FA decreases. After PN12, the ADC decreases whereas the FA increases. A DTI examination of maturation in early childhood revealed a general increase in FA and a decrease in ADC in the first 50 months of human life (Hermoye et al., 2006). We observed both increased ADC and FA values at PN66 compared with PN10. As mice, humans, and rats have different maturation timescales, it is not clear how to interpret mouse or human maturation data and apply it to rats. Moreover, as the ADC generally decreases as the FA increases and vice versa, it is not clear why we observe an increase in both ADC and FA. For  $^1\text{H}$ -MRS on the contrary, the most notable increase of NAA and decrease of taurine over time is completely in accordance with earlier work on developmental changes of the rat brain by Tkac et al (Tkac et al., 2003).

### **Analogies with human FS**

Previously, Vanlandingham et al observed hippocampal MRI abnormalities using volumetry and T2-weighted imaging in children with generalized FS (Vanlandingham et al., 1998). Additionally, Scott et al (Scott et al., 2002; Scott et al., 2003) found enlarged hippocampal volumes and prolonged T2 relaxation times within two days after generalized FS, which normalized already within five days. Interestingly, Scott et al (Scott et al., 2006) observed a transient increase in ADC values in children shortly after they suffered from FS, which was accompanied by an abnormal developmental changes. It was concluded that the edema had a vasogenic, rather than a cytotoxic nature, possibly due to an early blood-brain-barrier disruption. Future research aimed at investigating possible blood-brain-barrier disruptions after FS, and the possibly incomplete recovery thereof, is required to resolve this. It is very complicated to unambiguously link levels of maturation in rodents to those in humans. Based on timing of the 'growth spurt' occurring in human infants during the last few weeks of gestation and the first few months of life, Dobbing showed that human newborns have developmental similarities with PN7-PN12 rats (Dobbing, 1970). Although the current animal model study provides

qualitatively similar results (except for volumetric analysis), one should be cautious to try to relate observations in an animal model to clinical observations in humans.

**Table 10.2.** Overview of analogies between humans and animals regarding early-life febrile seizures and epilepsy during adulthood

Characteristics	Human	Animal model
<b>Etiology/Cause</b>	High fever in young children	HT+ at postnatal day 9/10
<b>Symptoms</b>	Febrile Seizures	Experimental Febrile Seizures
<b>Time scale &amp; incidence</b>	Adulthood TLE is associated with early-life FS (retrospective 40-60%); latent period (Cendes et al. 1993)	HT+ leads to epilepsy at postnatal days 90-180 in 35% of cases (Dube et al. 2006)
<b>Acute MR effects after FS</b>	Increased T2, increased hippocampal volume, vasogenic edema by diffusion MRI (Scott et al. 2002; Scott et al. 2003)	Increased T2, decreased ADC, decreased NAA (neuronal integrity marker)
<b>Chronic MR effects after FS</b>	T2 normalized, hippocampal volume normalized/asymmetric (Scott et al. 2002; Scott et al. 2003)	T2 normalized, NAA normalized, ADC decreased and anisotropy increased Groupwise analysis of hippocampal T2, ADC, and FA reveals significant differences

TLE, temporal lobe epilepsy; HT+, hyperthermia treatment followed by seizures; NT, normothermia treatment; FS, febrile seizures; NAA, N-acetylaspartate; ADC: apparent diffusion coefficient.

### Implications for human febrile seizures

Although HT-induced FS in rats is a model of FS in children, not necessarily all observed MR changes of our study can be translated to the human condition, due to inherent differences between rodents and humans. However, there are some obvious parallels. In Table 10.2, the analogies between humans and animals regarding early-life febrile seizures (FS) and epilepsy during adulthood are summarized. Both the HT-induced FS in rats and FS in humans (Scott et al., 2002; Scott et al., 2003; Scott et al., 2006) cause transient hippocampal alterations, which seem to normalize during development. However, a combined analysis of hippocampal T2, ADC, and FA displayed a chronic effect in the rat hippocampus, a subtle effect that also might be present in children, and can be an important early marker of epileptogenesis. Further research in which MR findings can be directly linked with seizure activity and pathology is required to investigate this potential early marker of epileptogenesis and its underlying working mechanism. Long-term longitudinal MR studies, using DTI and spectroscopy, in human children who

had FS are lacking up to now and should be encouraged to reveal such possible chronic MR abnormalities during development and their relation with epilepsy.

### **Limitations**

The current study has some limitations that restrict the general validity with respect to its clinical relevance. It is not possible to differentiate between hyperthermia itself and FS as underlying cause of the observed MR abnormalities. To resolve this in the future, the inclusion of an additional control group (as earlier described by Dubé et al. (Dube et al., 2006)) would control for this effect. This group of hyperthermic controls can be generated by subjecting littermates to the same HT treatment, but blocking the resulting seizures by treating the rats with the rapidly acting barbiturate pentobarbital. If this hyperthermic control group does not develop similar MR detectable abnormalities, the observed MR abnormalities in the experimental hyperthermia group must be due to FS.

Furthermore, as there was no registration of seizure activity in rats using combined EEG and video monitoring, it is not clear whether the rats with the strongest MR-observable alterations would indeed develop –or had developed– epilepsy. This problem can be solved in the future by including extensive EEG and video monitoring in the assessment.

### **Conclusion**

For the first time it was shown that early-life HT-induced FS give rise to both transient and foremost chronic micro-structural and metabolic changes to the limbic system (hippocampus and amygdala). Whether the detected MR abnormalities are specific for epileptogenesis or are the consequence of epileptiform activity remains to be elucidated.

### **Acknowledgements**

We gratefully acknowledge W. Jennekens and J. Habets for their valuable assistance.



## References

- Avishai-Eliner, S., Brunson, K.L., Sandman, C.A., et al., 2002. Stressed-out, or in (utero)? *Trends Neurosci* 25, 518-524.
- Baram, T.Z., Gerth, A., Schultz, L., 1997. Febrile seizures: an appropriate-aged model suitable for long-term studies. *Brain Res Dev Brain Res* 98, 265-270.
- Barker, P.B., Soher, B.J., Blackband, S.J., et al., 1993. Quantitation of proton NMR spectra of the human brain using tissue water as an internal concentration reference. *NMR Biomed* 6, 89-94.
- Ben-Ari, Y., 2001. Cell death and synaptic reorganizations produced by seizures. *Epilepsia* 42 Suppl 3, 5-7.
- Bender, R.A., Dube, C., Gonzalez-Vega, R., et al., 2003. Mossy fiber plasticity and enhanced hippocampal excitability, without hippocampal cell loss or altered neurogenesis, in an animal model of prolonged febrile seizures. *Hippocampus* 13, 399-412.
- Cavassila, S., Deval, S., Huegen, C., et al., 2001. Cramer-Rao bounds: an evaluation tool for quantitation. *NMR Biomed* 14, 278-283.
- Cendes, F., Andermann, F., Dubeau, F., et al., 1993. Early childhood prolonged febrile convulsions, atrophy and sclerosis of mesial structures, and temporal lobe epilepsy: an MRI volumetric study. *Neurology* 43, 1083-1087.
- de Graaf, R.A., Brown, P.B., McIntyre, S., et al., 2006. High magnetic field water and metabolite proton T1 and T2 relaxation in rat brain in vivo. *Magn Reson Med* 56, 386-394.
- Dobbing, J., 1970. Undernutrition and the developing brain. The relevance of animal models to the human problem. *Am J Dis Child* 120, 411-415.
- Dube, C., Chen, K., Eghbal-Ahmadi, M., et al., 2000. Prolonged febrile seizures in the immature rat model enhance hippocampal excitability long term. *Ann Neurol* 47, 336-344.
- Dube, C., Richichi, C., Bender, R.A., et al., 2006. Temporal lobe epilepsy after experimental prolonged febrile seizures: prospective analysis. *Brain* 129, 911-922.
- Dube, C., Yu, H., Nalcioglu, O., et al., 2004. Serial MRI after experimental febrile seizures: altered T2 signal without neuronal death. *Ann Neurol* 56, 709-714.
- Handforth, A., Treiman, D.M., 1995. Functional mapping of the early stages of status epilepticus: a <sup>14</sup>C-2-deoxyglucose study in the lithium-pilocarpine model in rat. *Neuroscience* 64, 1057-1073.
- Hermoye, L., Saint-Martin, C., Cosnard, G., et al., 2006. Pediatric diffusion tensor imaging: normal database and observation of the white matter maturation in early childhood. *Neuroimage* 29, 493-504.
- Hochberg, Y., 1988. A sharper Bonferroni procedure for multiple tests of significance. *Biometrika* 75, 800-802.
- Hugg, J.W., Kuzniecky, R.I., Gilliam, F.G., et al., 1996. Normalization of contralateral metabolic function following temporal lobectomy demonstrated by <sup>1</sup>H magnetic resonance spectroscopic imaging. *Ann Neurol* 40, 236-239.
- Inglese, M., Ge, Y., 2004. Quantitative MRI: hidden age-related changes in brain tissue. *Top Magn Reson Imaging* 15, 355-363.
- Jansen, J.F., Backes, W.H., Nicolay, K., et al., 2006. <sup>1</sup>H MR spectroscopy of the brain: absolute quantification of metabolites. *Radiology* 240, 318-332.
- Jupp, B., Williams, J.P., Tesiram, Y.A., et al., 2006. Hippocampal T2 signal change during amygdala kindling epileptogenesis. *Epilepsia* 47, 41-46.
- Larvaron, P., Boespflug-Tanguy, O., Renou, J.P., et al., 2006. In vivo analysis of the post-natal development of normal mouse brain by DTI. *NMR Biomed.*

- Läuter, J., 1996. Exact T and F tests for analyzing studies with multiple endpoints. *Biometrics* 52, 964-970.
- Lemmens, E.M., Lubbers, T., Schijns, O.E., et al., 2005. Gender differences in febrile seizure-induced proliferation and survival in the rat dentate gyrus. *Epilepsia* 46, 1603-1612.
- Maton, B.M., Kuzniecky, R.I., 2000. Proton MRS: N-acetyl aspartate, creatine, and choline. *Adv Neurol* 83, 253-259.
- Nairismagi, J., Grohn, O.H., Kettunen, M.I., et al., 2004. Progression of brain damage after status epilepticus and its association with epileptogenesis: a quantitative MRI study in a rat model of temporal lobe epilepsy. *Epilepsia* 45, 1024-1034.
- Nairismagi, J., Pitkanen, A., Kettunen, M.I., et al., 2006a. Status epilepticus in 12-day-old rats leads to temporal lobe neurodegeneration and volume reduction: a histologic and MRI study. *Epilepsia* 47, 479-488.
- Nairismagi, J., Pitkanen, A., Narkilahti, S., et al., 2006b. Manganese-enhanced magnetic resonance imaging of mossy fiber plasticity in vivo. *Neuroimage* 30, 130-135.
- O'Brien, P.C., 1984. Procedures for comparing samples with multiple endpoints. *Biometrics* 40, 1079-1087.
- Offringa, M., Hazebroek-Kampschreur, A.A., Derksen-Lubsen, G., 1991. Prevalence of febrile seizures in Dutch schoolchildren. *Paediatr Perinat Epidemiol* 5, 181-188.
- Ojemann, G.A., 2001. Temporal lobe epilepsy -current wisdom. *Stereotact Funct Neurosurg* 77, 213-215.
- Paxinos, G., Ashwell, K.W.S., Törk, I. (1994) *Atlas of the developing rat nervous system*, San Diego, Academic Press.
- Rorden, C., Brett, M., 2000. Stereotaxic display of brain lesions. *Behav. Neurol.* 12, 191-200.
- Scott, R.C., Gadian, D.G., King, M.D., et al., 2002. Magnetic resonance imaging findings within 5 days of status epilepticus in childhood. *Brain* 125, 1951-1959.
- Scott, R.C., King, M.D., Gadian, D.G., et al., 2003. Hippocampal abnormalities after prolonged febrile convulsion: a longitudinal MRI study. *Brain* 126, 2551-2557.
- Scott, R.C., King, M.D., Gadian, D.G., et al., 2006. Prolonged febrile seizures are associated with hippocampal vasogenic edema and developmental changes. *Epilepsia* 47, 1493-1498.
- Thornton, J.S., Amess, P.N., Penrice, J., et al., 1999. Cerebral tissue water spin-spin relaxation times in human neonates at 2.4 tesla: methodology and the effects of maturation. *Magn Reson Imaging* 17, 1289-1295.
- Tkac, I., Rao, R., Georgieff, M.K., et al., 2003. Developmental and regional changes in the neurochemical profile of the rat brain determined by in vivo <sup>1</sup>H NMR spectroscopy. *Magn Reson Med* 50, 24-32.
- Tofts, P. (2003) *Quantitative MRI of the brain measuring changes caused by disease*, Chichester, West Sussex; Hoboken, N.J., John Wiley & Sons Ltd.
- Toth, Z., Yan, X.X., Haftoglou, S., et al., 1998. Seizure-induced neuronal injury: vulnerability to febrile seizures in an immature rat model. *J Neurosci* 18, 4285-4294.
- van Eijsden, P., Notenboom, R.G., Wu, O., et al., 2004. In vivo <sup>1</sup>H magnetic resonance spectroscopy, T2-weighted and diffusion-weighted MRI during lithium-pilocarpine-induced status epilepticus in the rat. *Brain Res* 1030, 11-18.
- VanLandingham, K.E., Heinz, E.R., Cavazos, J.E., et al., 1998. Magnetic resonance imaging evidence of hippocampal injury after prolonged focal febrile convulsions. *Ann Neurol* 43, 413-426.
- Wall, C.J., Kendall, E.J., Obenaus, A., 2000. Rapid alterations in diffusion-weighted images with anatomic correlates in a rodent model of status epilepticus. *AJNR Am J Neuroradiol* 21, 1841-1852.

# Chapter 11

**General discussion and Conclusions**

## General discussion and Conclusions

In this thesis, a number of essential characteristics of quantitative MR were explored in detail. These quantitative magnetic resonance techniques were applied in epilepsy. In particular, cognitive adverse events of epilepsy (either due to medication or due to seizures) and epileptogenesis were examined. In the following paragraphs these characteristics will be discussed and further speculated on in relation to the results that were obtained and described in the previous chapters.

### Technological and methodological considerations

Quantitative magnetic resonance (MR) techniques possess the potential of tracing the links between tissue function, microstructure, and metabolism in both the normal and diseased brain. These new techniques provide the opportunity to investigate cerebral damage in various fundamentally different ways (Tofts, 2003).

In Chapter 2, a systematic review is provided on absolute quantification of brain metabolites using proton magnetic resonance spectroscopy ( $^1\text{H}$ -MRS). Three major metabolites that are commonly observed using  $^1\text{H}$ -MRS are: N-acetyl-aspartate (NAA), which is indicative of neuronal integrity, choline (Cho), of which increased concentrations can act as a malignancy (i.e. tumor) marker, and total creatine (tCr), a key metabolite of tissue energy metabolism. Often, metabolite concentrations are expressed as ratios (relative quantification), rather than as absolute concentrations. In relative quantification, where concentrations are expressed as ratios, one of the metabolite peaks measured (e.g. tCr) is used as the concentration standard, and serves as the denominator of the peak ratios. Alterations in the peak ratio (e.g. NAA/tCr) do not necessarily reflect a change in the concentration of the numerator (e.g. NAA). The alteration may be caused by changes in the concentration of either the numerator or the denominator or both, or may merely be due to changes in relaxation behavior. The assumption that the concentration of tCr is unaltered by a certain type of pathology has been proven incorrect, for instance in patients with localization-related epilepsy as measured at 3.0 Tesla (Chapter 8). Also, we observed in Chapter 10 that rat brains which have been subjected to a hyperthermia treatment display a significant increase in concentration of tCr as measured at 6.3 Tesla with respect to a control group. As creatine was not a constant metabolite in these studies, metabolite concentrations expressed as ratios with respect to creatine are not reliable, and possible detected differences in NAA/tCr ratios would have been wrongly attributed to alterations in NAA concentrations. It is therefore strongly advised to obtain concentrations expressed in standard units (such as mmol per kg wet

weight) by applying absolute quantification. As relative quantification of  $^1\text{H}$ -MRS at 1.5 Tesla did not reveal any significant effects of secondarily generalized tonicoclonic seizures (SGTCS) in patients with localization-related epilepsy (Chapter 5) one could speculate that absolute quantification could have detected some differences. However, there are several methodological differences related to the acquisition techniques, field strengths, and inclusion criteria between the studies described in Chapters 5, 8, and 10. Therefore these results should be considered in the light of all the different techniques used, and not just the quantification method.

Chapter 3 represents a reproducibility study of a number of quantitative MR techniques (spectroscopy, diffusion, and relaxometry) which was performed on a 3.0 Tesla MR system. These techniques were subsequently applied to patients with localization-related epilepsy in Chapter 8. It was found that the reproducibility at 3.0 Tesla seems to be better than, or at least similar to, the reproducibility at 1.5 Tesla as reported by others. However, the reproducibility study only considered 3.0 Tesla, a similar design at 1.5 Tesla was not performed. Nevertheless, both Chapter 3 and 8 indicate that the quality of the quantitative MR techniques at 3.0 Tesla is excellent.

In Chapter 4, a newly developed statistical image analysis method is presented. This method offers considerably increased sensitivity for the detection of subtle signal changes in images of several neurological MRI applications (diffusion weighted and functional MRI). In contrast to commonly used statistical methods, such as uncorrected thresholding, Bonferroni correction, or conventional false discovery rate (FDR) control, the presented method is based on regional control of the FDR to exploit the generally clustered nature (i.e. spatially correlated) of true neurophysiological effects. With respect to the signal-to-noise image properties, the discriminatory power of the method was approximately 1.4 times better than the other methods. To achieve an equivalent improvement in performance by increasing the number of image averages, the duration of experiments would roughly have to be doubled. However, its quantitative computational complexity, regarding the involved number of operations, is higher than for the other three methods, and thus more computer calculation time is needed. But, as this image analysis method enables a possible shorter effective investigation scan time for patients, and given the continuing increase in available computational power (Biswas et al., 2005), such considerations are expected to be of secondary importance in future studies.

## Quantitative MR in epilepsy

A number of factors influence the behavioral and cognitive impact of epilepsy, including the etiology of the epilepsy, the epilepsy syndrome in question, seizure-related factors, and side-effects of antiepileptic drugs (Kwan et al., 2001). Quantitative MR can have a great impact on the understanding of the cognitive and behavioral attributes of epilepsy, allowing evaluation of anatomical, microstructural, metabolic, and functional relationships between seizures and neuropsychological performance.

Additionally, the use of quantitative MR is very useful for investigations of the process involved in the development of epilepsy (Sutula et al., 2003). This process, called epileptogenesis, is dynamic and evolving, and may progressively alter neuronal excitability, establishes critical interconnections, and may require critical structural changes before the first clinical seizures appear.

### Seizures

Clinically, it has been proven difficult to substantiate that seizures can cause (permanent) brain damage that might be responsible for cognitive decline. These days, emerging data from human MRI and neuropsychological studies exist on neurodegenerative effects from epileptic seizures (reviewed in (Vingerhoets, 2006)). Consequently, patients can no longer be reassured with confidence that only prolonged seizures, as in status epilepticus, can cause brain damage and/or cognitive decline, whereas repeated brief seizures do not. The results described in Chapters 5, 6, and 7 suggest that seizure control in patients with epilepsy is of major importance, as the presence of secondarily generalized tonicoclonic seizures (SGTCS) in the human brain has an adverse and widespread neurodevelopmental impact on both brain structure and function. Furthermore, preliminary results presented in Chapter 8 suggest that also partial seizures may have an impact on metabolic brain function.

Chapters 5, 6, and 7 discuss the application at 1.5 Tesla of several quantitative MR methods, namely T2 relaxometry, diffusion weighted imaging, <sup>1</sup>H-MR-spectroscopy (Chapter 5), and functional MRI (Chapters 6 and 7) in a group of patients with localization related epilepsy and SGTCS to study cognitive deterioration. It was shown that secondarily generalized seizures in epilepsy are associated with cognitive decline. Furthermore, quantitative MR revealed frontal lobe changes in microstructural and functional brain tissue characteristics. In Chapter 5 it was found that secondarily generalized seizures are related to frontal brain microstructural changes, as determined by T2 relaxometry and diffusion weighted imaging. Chapter 6 revealed that these seizures are also associated with a relatively increased activation in prefrontal brain areas as demonstrated by fMRI using two paradigms aimed at activating

regions involved in verbal working memory and speed of mental processing. As the performance of primarily prefrontal cortex-associated executive functions (e.g. working memory) is of substantial importance for normal cognitive performance, it is most plausible to assume that the frontal lobe is involved in this cognitive decline (Dikmen et al., 1977). Therefore, the neuronal (microstructural, and functional) correlates for cognitive deterioration in patients with SGTCs is located in the frontal brain regions. This knowledge may help to obtain a better understanding and anticipatory treatment of SGTCs-related cognitive deterioration. In clinical practice, it seems necessary to prevent cognitive dysfunction by proactively preventing seizures with antiepileptic drugs or epilepsy surgery, if possible.

In the same patient group it was also found that the presence of telencephalin, a marker for neuronal damage in blood serum, correlates with relatively bad clinical characteristics (though not statistically significant) and a decreased frontotemporal activity during an fMRI memory task (Chapter 7). The relationship between quantitative MR and promising biomarkers related to possible inflammatory processes and neuronal cell loss such as telencephalin needs to be explored further.

Due to the cross-sectional study design, the small size and heterogeneous nature of the study group, the observed frontal lobe effect in Chapters 5 and 6 could not be unambiguously attributed to SGTCs alone. Other factors are age and drug load differences. Possibly, in more homogeneous and larger epilepsy populations, the effects could be more pronounced. To address whether MR abnormalities appear more profound in epilepsy patients with compared to patients without (determined) cognitive decline, in 2006 a new study was initiated, using a multi-modal MR research approach. This study aims at (i) exploring neuronal correlates as detected with quantitative MR for this cognitive morbidity, (ii) explaining the severity and kind of cognitive problems in terms of spatial location, degree, and type (microstructural, metabolic, functional or biochemical) of the MR abnormality and, (iii) relating this to characteristics of the epilepsy etiology. In this cross-sectional CODICE (COgnitive Deterioration In Cryptogenic Epilepsy) study, 70 patients with localization-related epilepsy with impaired and unimpaired cognitive functioning will be included. Cognitive impairment will be defined as a clinical diagnosis of either significant IQ decline or psychometrically confirmed memory impairment or mental slowing. In addition, a healthy volunteer group of 35 persons will be included, to facilitate the detection of possible MRI abnormalities in epilepsy patients who show no cognitive decline. Chapter 8 discusses preliminary results from the CODICE study. A number of quantitative MR techniques, including T2 relaxometry, DTI, and  $^1\text{H}$ -MRS, were combined to assess possible neuronal correlates for this cognitive morbidity on metabolic and microstructural cerebral tissue characteristics. It was shown in

Chapter 8 that the quantitative MR techniques from Chapter 3 could be applied successfully, which is a good perspective for future outcomes of the full study. In addition to microstructural and metabolic MR measurements, the study will also include functional MRI and biochemical and neuro-immunological assessments. This way, the detection of possible abnormalities at the (micro-)structural, metabolic, and functional level may lead to a better understanding of the relation between cognitive decline, epileptiform activity, and epilepsy characteristics.

### **Antiepileptic drugs**

In addition to the impact of epileptic pathologies themselves, cognitive and behavioral functions in individuals with epilepsy are also very sensitive to the effects of antiepileptic drugs (Kwan et al., 2001). These effects include slowing of central information processing, impairment of short-term (working) memory and language disturbances such as dysphasia (Thompson et al., 2000). These cognitive and behavioral side-effects of antiepileptic drugs are a source of concern to patients and appears to be an important determinant of treatment retention, which is itself a prerequisite for effective seizure control (Bootsma et al., 2004). Using fMRI it was demonstrated in Chapter 9 that patients with epilepsy using the antiepileptic drug topiramate display a decreased prefrontal activation during a cognitive language task, which was in accordance with neuropsychologically assessed cognitive impairment. Additionally, in Chapter 5 it was shown that drug load could have been a confounding factor in the quantitative MR abnormalities observed in the frontal lobe. These results suggest that patients with a more severe type of epilepsy, due to many SGTCS, are receiving more antiepileptic drugs, probably because these patients are more likely to be therapy-resistant. To be able to unambiguously attribute possible effects to an antiepileptic drug, for future research a randomized, double-blind, controlled study design is required, ideally in patients randomized to one drug in monotherapy.

### **Epileptogenesis**

Experimental febrile seizures (FS) are known to cause cellular and molecular changes that promote hyperexcitability and epileptogenesis. In chapter 10, FS were evoked using hyperthermia in neonatal rats, to examine which MR modality may localize acute and chronic abnormalities during brain development. It was shown that early-life hyperthermia-induced FS give rise to both transient and foremost chronic micro-structural and metabolic changes to the limbic system (hippocampus and amygdala). Whether the detected MR abnormalities are specific for epileptogenesis or are the consequence of epileptiform activity remains to be elucidated. The application of quantitative



MR in both experimental and clinical epilepsy may provide complementary information. MR research on epilepsy models yields knowledge on the pathophysiology, potential therapeutic strategies, and provides leads for clinical use of MR technologies.

### **Future prospects and Conclusion**

The implementation of quantitative MR in a clinical epilepsy routine has been greatly facilitated by the continuous improvement and development of techniques. Quantitative MR techniques have potential to improve diagnosis, prognosis, managing patients and treatment trials. Furthermore, the introduction of phased array coils (Pruessmann et al., 1999) and higher field strengths (>1.5 T) (Ugurbil et al., 2003) has proven to be advantageous with regard to signal-to-noise characteristics, quantification precision, reproducibility, and detection sensitivity. However, in clinical practice, quantitative measures may be less convenient because often they require more effort. In order to obtain reliable measures by quantitative MR, one has to consider potential complicating factors, both with respect to the data acquisition and data processing method. Nevertheless, most of these problems have been critically addressed and can be taken into account in a satisfying manner. Using quantitative MR, an increasing range of quantitative measures that look at different aspects of disease pathology, improved specificity, and higher sensitivity to subtle changes all become available. The biological significance of these measures is immensely important, yet still comparatively little about this subject is known. It needs to be elucidated how these quantitative MR measures relate to biological changes that take place in disease, and whether each parameter tells us something different. The understanding of the connection between MR parameters and biology is crucial, and requires interdisciplinary research by biologists, pathologists, chemists and physicists. Multi-parametric combinations of MR parameters may further improve our ability to understand the biological changes taking place in vivo (Tofts, 2003).

Quantitative MR will remain an essential tool for epilepsy research purposes, certainly considering the ongoing technological and methodological developments. Although quantitative MR is important in epilepsy diagnosis and prognosis, it should always be realized that the main goal is to improve the patient's quality of life and not the appearance of quantitative MR measures. Therefore, neurological assessment and clinical care remain of primary and crucial importance.

## References

- Biswas, J., Nelson, C.B., Runge, V.M., et al., 2005. Brain tumor enhancement in magnetic resonance imaging: comparison of signal-to-noise ratio (SNR) and contrast-to-noise ratio (CNR) at 1.5 versus 3 tesla. *Invest Radiol* 40, 792-797.
- Bootsma, H.P., Coolen, F., Aldenkamp, A.P., et al., 2004. Topiramate in clinical practice: long-term experience in patients with refractory epilepsy referred to a tertiary epilepsy center. *Epilepsy Behav.* 5, 380-387.
- Dikmen, S., Matthews, C.G., 1977. Effect of major motor seizure frequency upon cognitive-intellectual functions in adults. *Epilepsia* 18, 21-29.
- Kwan, P., Brodie, M.J., 2001. Neuropsychological effects of epilepsy and antiepileptic drugs. *Lancet* 357, 216-222.
- Pruessmann, K.P., Weiger, M., Scheidegger, M.B., et al., 1999. SENSE: sensitivity encoding for fast MRI. *Magn Reson Med* 42, 952-962.
- Sutula, T.P., Hagen, J., Pitkanen, A., 2003. Do epileptic seizures damage the brain? *Curr Opin Neurol* 16, 189-195.
- Thompson, P.J., Baxendale, S.A., Duncan, J.S., et al., 2000. Effects of topiramate on cognitive function. *J. Neurol. Neurosurg. Psychiatry* 69, 636-641.
- Tofts, P. (2003) *Quantitative MRI of the brain measuring changes caused by disease*, Chichester, West Sussex; Hoboken, N.J., John Wiley & Sons Ltd.
- Ugurbil, K., Adriany, G., Andersen, P., et al., 2003. Ultrahigh field magnetic resonance imaging and spectroscopy. *Magn Reson Imaging* 21, 1263-1281.
- Vingerhoets, G., 2006. Cognitive effects of seizures. *Seizure* 15, 221-226.

## Summary

Epilepsy is a chronic brain disorder characterized by unprovoked recurrent seizures that give rise to episodes of abnormal neuronal activity in the central nervous system. The most common application of magnetic resonance imaging (MRI) techniques in the epileptic brain is the identification of the underlying cause for a person's epilepsy, and possibly the localization of the epileptic focus. In addition, quantitative magnetic resonance (MR) techniques enable examining certain relatively subtle aspects of epilepsy within the brain that go beyond the identification of seizure focus within the brain. In this thesis a number of studies are presented that investigate the application of quantitative MR techniques to epilepsy-related abnormalities of metabolism, microstructures and brain function. The research project was aimed at developing and validating quantitative MR techniques (spectroscopy, diffusion, T2 relaxometry, and functional magnetic resonance imaging) with clinical diagnostic potential. The main focus was on data acquisition and processing, and the application of this multi-modal MR approach in both patients with epilepsy and an animal model of epileptogenesis. We explored in a clinical setting how the cognitive consequences of epilepsy (either due to medication or due to seizures) may be reflected in altered MR tissue characteristics. Furthermore, using an experimental model of febrile convulsions, it was investigated whether neurological abnormalities, possibly linked with epileptogenesis and thus with epilepsy, could be detected by quantitative MR.

A general introduction into quantitative MR techniques and epilepsy is given in **Chapter 1**.

**Chapter 2** describes a thorough review on absolute quantification of metabolites using spectroscopy, which can substantially improve the diagnostic utility of spectroscopy. Absolute quantification requires more time and expertise than relative quantification, as additional calibrations for concentration determination and spectrum analyses have to be performed. One can only benefit from absolute quantification if all additional reference steps are executed properly; otherwise unwanted additional errors may be introduced.

**Chapter 3** concerns a clinically relevant reproducibility study of several quantitative MR techniques which was performed on a 3.0 Tesla MR system. Repeated measurements in 10 healthy volunteers were used to establish the reproducibility of quantitative measures derived from different quantitative MR techniques, namely the T2 relaxation time, the apparent diffusion coefficient (ADC), the fractional anisotropy (FA), and metabolite concentrations of N-acetyl-aspartate (NAA), total creatine (tCr), choline (Cho) and myo-inositol

(mI). The reproducibility of quantitative brain MR at 3.0 T appeared to be better than, or at least comparable to the reproducibility at 1.5 T.

A newly developed statistical image analysis method, which offers considerably increased sensitivity for the detection of subtle signal changes in images of several neurological MR applications, is described in **Chapter 4**. This method, the regional false discovery rate (FDR) control, increases sensitivity by exploiting the spatially clustered nature of neuroimaging effects. The method was validated, characterized, and compared to some other commonly used methods (uncorrected thresholding, Bonferroni correction, and conventional FDR-control). It was found that the new method showed considerably higher sensitivity as compared to conventional FDR-control. Application of the method to two different neuroimaging applications, revealed substantial improvements compared to the other methods.

Quantitative MR (T2 relaxation, diffusion, spectroscopy, and functional MRI) at 1.5 T and neuropsychological assessment was performed in a group of patients with localization related epilepsy and secondarily generalized tonicoclonic seizures (SGTCS) to study cognitive deterioration.

**Chapter 5** relates to the investigation of the effect of these seizures on microstructural and metabolic changes in brain tissue characteristics. Frontal, but not temporal, MR abnormalities were found to be related to SGTCS. These findings confirm that SGTCS do have a substantial effect on frontal brain function and on the microstructural brain tissue characteristics. This knowledge may help to obtain a better understanding and anticipatory treatment of SGTCS-related cognitive deterioration.

In **Chapter 6** it was investigated using functional MRI whether a higher number of SGTCS were associated with a functional reorganization of working memory. It was found that high numbers of SGTCS resulted in a decrease in intelligence scores and altered prefrontal brain activation. A shift from frontotemporal to prefrontal activation seemed to have occurred, suggesting that a functional reorganization of working memory is induced by a high number of SGTCS. It remains uncertain if this reorganization reflected compensatory mechanisms, or the underlying pathological processes of cognitive deterioration.

In the same patient group it was found in **Chapter 7** that the presence of a certain marker for neuronal damage in blood serum (telencephalin) correlates with a decreased frontotemporal activity during an functional MRI memory task.

**Chapter 8** discusses preliminary results from a study investigating whether quantitative MR abnormalities detected at 3.0 Tesla appear more profound in epilepsy patients with than without (determined) cognitive decline. The current preliminary study showed that the quantitative MR techniques could be applied successfully, which is a prerequisite for future outcomes of the full study.

In **Chapter 9** it is investigated whether the antiepileptic drug topiramate, which is known to induce cognitive impairment, also caused changes in activation patterns on functional MRI at 1.5 Tesla during a cognitive language task. Compared with a control epilepsy group, patients with epilepsy on topiramate therapy showed significantly less activation in the language-mediating regions in the prefrontal cortex together with significantly lower neuropsychological language scores. These findings suggest that topiramate has a critical effect on the cerebral neural systems that mediate expressive language.

In **Chapter 10**, a quantitative MR study of an experimental epileptogenesis model for febrile convulsions is described. Neonatal rats were subjected to a hyperthermia treatment, which is known to be linked with the later development of epilepsy. Using quantitative MR it was investigated whether microstructural and metabolic changes in brain tissue could be found. Both transient and foremost permanent micro-structural and metabolic changes to the limbic system were observed. Whether the detected MR abnormalities are specific for epileptogenesis or are the consequence of epileptiform activity remains to be elucidated.

Finally, **Chapter 11** integrates the results of the various studies and discusses them in a broader perspective.



## Samenvatting

Epilepsie is een vaak voorkomende chronische neurologische aandoening die gekenmerkt wordt door het regelmatig optreden van plotselinge aanvallen. De meest gebruikelijke toepassing van kernspinresonantie-beeldvorming (MRI) technieken voor het epileptische brein is het opsporen van de mogelijke oorzaak en de aanvalshaard. Daarnaast is het met behulp van kwantitatieve magnetische resonantie (MR) technieken ook mogelijk om bepaalde relatief subtiele aspecten van epilepsie in de hersenen te onderzoeken, die verder gaan dan de aanvalshaard. In dit proefschrift wordt een aantal studies beschreven waarin de toepassing van kwantitatieve MR technieken op epilepsie gerelateerde afwijkingen wordt onderzocht, zoals metabolisme, microstructuren en hersenfunctie. Het onderzoeksproject was gericht op de ontwikkeling en validatie van kwantitatieve MR technieken (spectroscopie, diffusie, T2 relaxometrie en functionele MRI) die een klinisch diagnostische waarde kunnen hebben. De aandacht ging uit naar data acquisitie, kwantitatieve verwerking en de toepassing van deze multimodale MR aanpak in zowel patiënten met epilepsie als een proefdiermodel voor epilepsie. In een klinische omgeving werd onderzocht hoe de cognitieve consequenties van epilepsie (veroorzaakt door ofwel medicatie ofwel aanvallen) zich mogelijk manifesteren als veranderingen van weefseleigenschappen die met MR technieken te detecteren zijn. Aan de hand van een proefdiermodel werd verder onderzocht of neurologische afwijkingen, mogelijk horend bij epileptogenese (het ontstaan van epilepsie), gedetecteerd konden worden met behulp van kwantitatieve MR.

Een algemene introductie over epilepsie en kwantitatieve MR technieken is beschreven in **Hoofdstuk 1**.

**Hoofdstuk 2** beschrijft een grondige inventarisatie van het absoluut kwantificeren van metaboliëten met behulp van spectroscopie, hetgeen de klinische toepasbaarheid van spectroscopie substantieel kan verbeteren. Absolute kwantificatie van metaboliëten vergt meer tijd en expertise dan relatieve kwantificatie, aangezien extra kalibraties voor concentratie bepalingen en spectrale analyses voltooid moeten worden. Men kan alleen profiteren van absolute kwantificatie indien alle additionele stappen zorgvuldig worden uitgevoerd, anders kunnen fouten optreden.

**Hoofdstuk 3** beschrijft een klinisch relevante reproduceerbaarheidstudie van de kwantitatieve MR technieken spectroscopie, diffusie en T2 relaxometrie, uitgevoerd op een 3.0 Tesla MR systeem. Herhaalde metingen in 10 vrijwilligers werden gebruikt om de reproduceerbaarheid vast te stellen van kwantitatieve

uitkomsten verkregen uit verschillende kwantitatieve MR technieken, namelijk de T2 relaxatie tijd, de effectieve diffusie coëfficiënt (ADC), de fractionele anisotropie (FA), en de metaboliëconcentraties van N-acetyl-aspartaat, totaal creatine, choline en myo-inositol. Voor de reproduceerbaarheid van kwantitatieve brein MR bij 3.0 T worden waardes gevonden die beter blijken dan, of minstens zo goed zijn als, de reproduceerbaarheid bij 1.5 T.

Een algemeen neuroradiologisch probleem bij het opsporen van subtiele afwijkingen in de hersenen bij drie-dimensionale brein MRI, is het optreden van zogenaamde fout-positieve voxels (beeldpunten) door het grote aantal voxels dat in beschouwing wordt genomen, en de geringe verhoudingen tussen het signaal effect en de ruis. Een nieuw ontwikkelde statistische methode waarmee een substantiële verbetering wordt verkregen met betrekking tot de gevoeligheid van detectie van signaalafwijkingen is beschreven in **Hoofdstuk 4**. Deze methode, de regionale false discovery rate (FDR) controle, verhoogt de gevoeligheid door gebruik te maken van de ruimtelijke naburigheid (coherentie) van brein signaalwaardes. De methode is gevalideerd, gekarakteriseerd en vergeleken met enkele andere veelgebruikte methodes (ongecorrigeerd afkappunt, Bonferroni correctie en conventionele FDR). De nieuwe methode toont een substantiële verbeterde gevoeligheid, vergeleken met de traditionele FDR methode. De methode is toepasbaar voor uiteenlopende MRI technieken. Toepassing van de methode op twee verschillende in vivo brein beeldvorming technieken, toonde duidelijke verbeteringen vergeleken met conventionele methodes.

In een patiënten groep met lokalisatie-gebonden epilepsie en secundair generaliseerde tonisch clonische aanvallen (SGTCS), werden kwantitatieve MR (T2 relaxometrie, diffusie, spectroscopie en functionele MRI) bij 1.5 T en neuropsychologisch onderzoek uitgevoerd om de mogelijke relatie tussen potentiële MR afwijkingen en cognitieve deterioratie (achteruitgang) te onderzoeken.

**Hoofdstuk 5** beschrijft het onderzoek naar de effecten van deze aanvallen op het optreden van hersenweefsel afwijkingen en in het bijzonder microstructurele en metabolische karakteristieken. Frontale, maar geen temporale, brein MR afwijkingen konden gerelateerd worden aan SGTCS. Deze bevindingen bevestigen dat SGTCS een substantieel effect hebben op zowel functie als microstructurele weefsel eigenschappen van de frontale hersenkwab. Deze kennis zou kunnen helpen om een beter begrip en een betere anticiperende behandeling te bewerkstelligen van epilepsie patiënten met SGTCS om het ontstaan van cognitieve deterioratie te voorkomen.



In **Hoofdstuk 6** werd met behulp van functionele MRI en neuropsychologische testen onderzocht of een hoger aantal SGTCS geassocieerd is met een functionele reorganisatie van het werkgeheugen. Er werd gevonden dat een groot aantal SGTCS resulteert in een afname van intelligentie scores en gewijzigde prefrontale hersenactiviteit. Er lijkt een verschuiving van frontotemporale naar prefrontale activiteit op te treden, hetgeen suggereert dat een functionele reorganisatie van het werkgeheugen wordt geïnduceerd door een groter aantal SGTCS. Het is niet duidelijk of deze reorganisatie een gevolg is van een compensatiemechanisme of gevolg is van de onderliggende pathologische processen van cognitieve deterioratie.

Bij dezelfde groep patiënten is in **Hoofdstuk 7** beschreven dat de aanwezigheid van een bepaalde marker voor neuronale schade in het bloedserum (telencephaline) correleert met een afgenomen frontotemporale activiteit bij een functionele MRI geheugen taak.

**Hoofdstuk 8** beschrijft de opzet en uitvoering van een nieuwe studie waarin wordt onderzocht of kwantitatieve MR afwijkingen meer kenmerkend zijn voor epilepsie patiënten met (vastgestelde) cognitieve achteruitgang, dan patiënten zonder achteruitgang. De voorlopige resultaten van deze nog lopende studie laten zien dat de kwantitatieve MR technieken met succes toegepast kunnen worden. Dit is een voorwaarde is voor de succesvolle afronding van de gehele studie.

In **Hoofdstuk 9** is met behulp van functionele MRI aangetoond dat patiënten met epilepsie die als anti-aanvals medicatie het medicijn topiramaat gebruiken, verminderde prefrontale activiteit hebben tijdens een cognitieve taalkaak. Dit is volledig in overeenstemming met de reeds bekende karakteristieke cognitieve (spraakgerelateerde) bijwerkingen van topiramaat. Deze bevinding suggereert dat topiramaat een kritisch effect heeft op het cerebrale neurale systeem dat betrokken is bij expressieve taal functie (prefrontale gebieden).

In **Hoofdstuk 10** wordt een kwantitatieve MR studie beschreven van een model met febriële convulsies (koortsstuipen) voor de ontwikkeling van epilepsie (epileptogenese). Pasgeboren ratten werden onderworpen aan een hyperthermie behandeling, waarvan bekend is dat het op latere leeftijd epilepsie induceert. Met behulp van kwantitatieve MR technieken werd onderzocht of microstructurele en metabolische afwijkingen in het hersenweefsel aangetoond konden worden. Acute en voor het eerst chronische microstructurele en metabolische veranderingen werden waargenomen in het limbische systeem van de hersenen. Of de gedetecteerde MR afwijkingen

specifiek zijn voor epileptogenese of juist de consequentie van epileptische ontladingen is onbekend en zal verder onderzocht moeten worden.

In **Hoofdstuk 11** worden de resultaten uit de diverse studies geïntegreerd en in een breder perspectief geplaatst.

## Dankwoord

Hoewel alleen mijn naam op de kaft van dit boek prijkt, zijn er natuurlijk veel meer mensen betrokken geweest bij de totstandkoming van dit proefschrift. Niet alleen op het werk, maar ook daarbuiten hebben veel mensen mij inhoudelijk of op een andere waardevolle manier gesteund bij het afronden van mijn promotieonderzoek en het schrijven van dit manuscript. Bij voorbaat wil ik hierbij graag al deze mensen bedanken, opdat ik later geen verwijten krijg dat ik abusievelijk iemand vergeten zou zijn....

Beste Walter, ik heb uitermate kunnen profiteren van je kennis en betrokkenheid in je functie als kartrekker van alle projecten waarbij ik betrokken mocht zijn. Dit is me zelfs zo bevallen dat ik graag als postdoc een jaartje langer bij je blijf. Ik hoop alleen dat je dan niet meer 's nachts van me wakker zult liggen?

Ook Eline wil ik graag bedanken voor haar inzet. Helaas liep de GABA spectroscopie mis, maar gelukkig hebben we toch nog het Radiology artikel zodat mijn proefschrift toch nog een substantieel spectroscopie deel bevat.

Klaas, als promotor op afstand hield je toch de voortgang nauwgezet bij. Jouw kennis is een onuitputtelijke bron voor inspiratie. Ook veel dank voor de mogelijkheid om toch nog een rattenstudie te kunnen doen in Eindhoven, hetgeen een zeer welkome aanvulling voor mijn proefschrift was.

Ik wil graag ook professor van Engelshoven bedanken voor de gelegenheid die mij is geboden om bij radiologie alle klinische MRI studies te kunnen uitvoeren.

Bert, als hoogleraar epileptologie heel nauw betrokken bij mijn onderzoek, ook zeer bedankt voor het delen van je vakkennis en je persoonlijke betrokkenheid.

Niet onbelangrijk zijn al mijn collega's van de SEGAED/CODICE studie groep, betrokken bij de klinische epilepsie studies. Met name de neurologen Marian en Marc waren onmisbaar, aangezien zij de patiënten graag wilden motiveren om deel te nemen aan ons onderzoek. Ook dank aan Paul Hofman en professor Wilmink voor de neuroradiologische beoordelingen. En natuurlijk niet te vergeten mijn onmisbare collega Marielle, zonder wie het onderzoek onmogelijk zou zijn. Dat je het toch nog voor elkaar krijgt om naast je drukke opleiding tot neuroloog alle deelnemers voor de studie te bellen (en af te bellen als mijn agenda mij weer eens in de steek laat), en tijd hebt om artikelen te schrijven voor je promotie is een wonder. Het is mij ook een waar genoegen om nog een jaar langer met je te mogen samenwerken. Ook Rianne wil ik graag bedanken, vanwege haar inzet voor de patiënteninclusie aan het begin van mijn promotie. Helaas liep het een en ander niet geheel volgens plan, waardoor je voor een ander onderzoek hebt moeten kiezen, maar gelukkig was dat geen reden ons leuke contact te verbreken.

Govert en Evi, ook jullie bedankt voor onze samenwerking bij de rattenstudie. Dankzij jullie heb ik aangenaam kennis gemaakt met een heel andere (dieren) wereld met betrekking tot epilepsie onderzoek. Ook het feit dat jullie het geen enkel probleem vonden om 's ochtends vanuit België of Maastricht te vertrekken om reeds om 8:00 uur in Eindhoven mij te helpen met de experimenten kon ik zeker appreciëren.

Nou Fons, dan toch ook nog een bedankje voor jou. Ik heb voornamelijk genoten van onze (lunch) gesprekken die over van alles en ook weer niks konden gaan. En het feit dat jij zo nu en dan juist bij mij komt voor advies is eigenlijk de omgekeerde wereld, maar ja dan blijkt ook weer dat je toch niet zoveel aan me hebt. Het is mij een grote eer dat we toch nog samen een echte publicatie hebben, zonder dat we daarvoor een of andere vage website moesten misbruiken!

Van mijn azM radiologie collegae wil ik eerst Dave hartelijk bedanken voor zijn interesse en -niet onbelangrijk- bijdrage van zo'n 30 pagina's aan mijn proefschrift. Ook mijn andere AIO collega's mogen niet ontbreken: Quido, Marianne, Vera (mede spectroscopie-fanatiekeling), Vincent, Rob (zeer gewaardeerde kamergenoot, zowel in het begin als op het einde), Nils, Marc, Suzanne, Max & Sanne (ondanks de drukte toch ook zeer gezellige kamergenoten), Luc, Robbert-Jan, Karolien, Robert, Marlies en Frank (leuk dat we zelfs collega's zijn geworden!). Ook de andere radiologie collega's mogen niet ontbreken: Gerrit, Marc Geerlings (voor de ICT ondersteuning), Jos, Karin, Tim (altijd geïnteresseerd en met vele connecties) en alle secretaresses. Ook de laboranten wil ik graag bedanken, in het bijzonder Henk, Etienne, Liesbeth, Sonja, Thea en Eveline. En natuurlijk Ine Kengen hartelijk bedankt voor het verzorgen van de mooie lay-out van mijn proefschrift!

Mijn collega's uit Eindhoven mogen ook echt niet ontbreken. Aanvankelijk zag ik iedereen eigenlijk alleen tijdens de ISMRM op diverse exotische locaties, waar ik dan toch altijd als volwaardig TU/e collega werd gezien. Gelukkig ben ik door mijn experimenten in Eindhoven nu ook echt een tijdje fysiek in Eindhoven geweest, wat me zeer is bevallen. Omdat ik 'nieuw' was in Eindhoven heb ik optimaal kunnen profiteren van alle kennis en hulpvaardigheid van met name Gustav, Jeanine, Jo, Ward (nogmaals bedankt voor de prachtige insert), Henk, Geralda, Edwin, Willem, Anneriet, Nicole, Erik, Maarten, Glenda, Hein en Larry. Ook wil ik Ria en Hedwig bedanken voor alle organisatorische zaken en Leon voor de financiële zaken.

Tijdens mijn promotie heb ik het geluk gehad dat een aantal studenten bereid waren om mij wat werk uit de handen te nemen. Inge, Karin, Cathryn en Rob hartelijk bedankt, en succes met jullie verdere carrière!

A special thanks to my former colleagues from Johns Hopkins, who always showed great interest in my PhD project. I would especially like to thank Jeff, Juhana, Peter van Zijl, Hanzhang and also Peter Barker, who was very kind to help me with various spectroscopic problems. Also Stephen Provencher proved to be very helpful with his excellent service for all my LCModel issues.

Al mijn gezonde werkstress kon ik gelukkig ventileren bij de diverse muziekgezelschappen waarvan ik lid mag zijn. Als een soort van tweede familie mag ik natuurlijk harmonie Arti et Amicitiae te Oirschot niet onvermeld laten. De oprechte interesse van de leden en het bestuur in mijn studie doet mij altijd weer veel deugd, zeker als je je realiseert dat mijn studie nou niet echt bevorderlijk is voor mijn repetitie bezoek de afgelopen 10 jaar. Ik wil in het bijzonder mijn altijd trouwe hoorncollega's Bram en Jan noemen, Jan, Hans, William en Stefan van het koperkwintet, en ook Rob, Bart, Elleke, Hans vd V, Hanneke en Martien. Ook de muzikanten van de Redtband hebben de gave om mij ieder jaar weer een leuke carnaval te bezorgen. Hoe jullie het met mij uithouden zal wel altijd een raadsel blijven.

Ook iedereen van de muziekverenigingen in Maastricht, te weten de Koninklijke Harmonie van Heer en het Universiteits Orkest Maastricht wil ik graag bedanken!. Mijn hoornmaatjes en goede vrienden Frank (+Linda) en Joost (+Marlies) zal ik echt missen als ik Maastricht ooit zal verlaten. Ook de andere 'studenten' wil ik graag noemen: Nicole, Martijn, Rianne, Marlies en Dennis.

Als oud JRLers wil ik graag Ivo, Marcel en Pim noemen. Van mijn jaren in Nijmegen zijn dat Joost, Irene, Paul en Joost Zwijnenburg.

Als laatste wil ik mijn familie noemen. Eerst mijn peetoom Toon en peettante Coby en de overige ooms en tantes, die altijd geïnteresseerd zijn gebleven in mijn vorderingen. De steun van mijn ouders is altijd onvoorwaardelijk geweest, zonder hun betrokkenheid was ik niet ver gekomen. Niet voor niks kom ik nog zeer graag thuis. Ook Mieke, Willem, Frans en Annabelle heel erg bedankt. En niet te vergeten: Jasper en Tijn, dat ik jullie ome Jaap mag zijn is het mooiste wat me ooit overkomen is. Of je dit boek ooit zult lezen is niet belangrijk, zolang jullie maar de laatste pagina mooi vinden! Het grootste nadeel van mijn buitenland plannen is dat ik jullie allemaal zal moeten missen.



## List of Publications

- [1] Spronk, C.A., Tessari, M., Kaan, A.M., **Jansen, J.F.**, Vermeulen, M., Stunnenberg, H.G., and Vuister, G.W., 2000. The Mad1-Sin3B interaction involves a novel helical fold. *Nat Struct Biol* 7, 1100-1104.
- [2] Spronk, C.A., **Jansen, J.F.**, Tessari, M., Kaan, A.M., Aelen, J., Lasonder, E., Stunnenberg, H.G., and Vuister, G.W., 2001. Sequence-specific assignment of the PAH2 domain of Sin3B free and bound to Mad1. *J Biomol NMR* 19, 377-378.
- [3] van Ingen, H., Lasonder, E., **Jansen, J.F.**, Kaan, A.M., Spronk, C.A., Stunnenberg, H.G., and Vuister, G.W., 2004. Extension of the binding motif of the Sin3 interacting domain of the Mad family proteins. *Biochemistry* 43, 46-54.
- [4] **Jansen, J.F.**, Backes, W.H., Nicolay, K., and Kooi, M.E., 2006. <sup>1</sup>H MR spectroscopy of the brain: absolute quantification of metabolites. *Radiology* 240, 318-332.
- [5] **Jansen, J.F.**, Shablott, M.J., van Zijl, P.C., Lehtimäki, K.K., Bulte, J.W., Gearhart, J.D., and Hakumäki, J.M., 2006. Stem cell profiling by nuclear magnetic resonance spectroscopy. *Magn Reson Med* 56, 666-670.
- [6] **Jansen, J.F.**, Aldenkamp, A.P., Majoie, H.J., Reijs, R.P., de Krom, M.C., Hofman, P.A., Kooi, M.E., Nicolay, K., and Backes, W.H., 2006. Functional MRI reveals declined prefrontal cortex activation in patients with epilepsy on topiramate therapy. *Epilepsy Behav* 9, 181-185.
- [7] **Jansen, J.F.**, Kooi, M.E., Kessels, A.G., Nicolay, K., and Backes, W.H., 2007. Reproducibility of quantitative cerebral T2 relaxometry, diffusion tensor imaging, and <sup>1</sup>H magnetic resonance spectroscopy at 3.0 Tesla. *Investigative Radiology* 42, In press.
- [8] Langers, D.R., **Jansen, J.F.**, and Backes, W.H., 2007. Enhanced signal detection in neuroimaging by means of regional control of the false discovery rate. *Neuroimage*, provisionally accepted.
- [9] **Jansen, J.F.**, Vlooswijk, M.C., de Baets, M.H., de Krom, M.C., Rieckmann, P., Backes, W.H., and Aldenkamp, A.P., Soluble telencephalin is a marker for frontotemporal dysfunction in epilepsy as revealed by fMRI. Submitted.
- [10] Vlooswijk, M.C., **Jansen, J.F.**, Reijs, R.P., de Krom, M.C., Kooi, M.E., Majoie, H.M., Hofman, P.A., Backes, W.H., and Aldenkamp, A.P., Seizure related cognitive deterioration is associated with increased prefrontal fMRI activation. Submitted.
- [11] **Jansen, J.F.**, Kooi, M.E., Vlooswijk, M.C., Majoie, H.J., Reijs, R.P., Hofman, P.A., Nicolay, K., de Krom, M.C., Aldenkamp, A.P., and Backes, W.H., Multimodal MR reveals secondarily generalized seizure related abnormalities at 1.5 T. Submitted.

## Abstracts at Scientific Meetings

- [1] Renema, W.K., Janssen, E.E., **Jansen, J.F.**, Oerlemans, F., Wieringa, B., and Heerschap, A., 2002. <sup>31</sup>P MRS reveals a compromised phosphoryl transfer system in mice lacking both cytosolic CK and AK. *Proc Int Soc Mag Reson Med* 10, 1869, Honolulu, Hawaii, USA.
- [2] **Jansen, J.F.**, Hakumäki, J.M., Ifeanyi, L., Shablott, M.J., Gearhart, J.D., and van Zijl, P.C., 2002. <sup>1</sup>H-NMR spectroscopy of stem cells in vitro demonstrates high proliferation state. *Proc Int Soc Mag Reson Med* 10, 131, Honolulu, Hawaii, USA.
- [3] **Jansen, J.F.**, Reijs, R.P., Kooi, M.E., de Krom, M.C., Aldenkamp, A.P., Nicolay, K., and Backes, W.H., 2003. Neuronal working mechanisms responsible for cognitive side-effects of the anti-epileptic drug topiramate: an investigation with functional MRI and MR spectroscopy. 25th International Epilepsy Congress, 53, Lisbon, Portugal.
- [4] **Jansen, J.F.**, Kooi, M.E., Reijs, R.P., de Krom, M.C., Hofman, P.A., Aldenkamp, A.P., Nicolay, K., and Backes, W.H., 2005. Multi-modal MRI of epilepsy patients with secondary generalized seizures. 26th International Epilepsy Congress, 170, Paris, France.

- [5] de Krom, M.C., Backes, W.H., Reijs, R.P., Aldenkamp, A.P., Majoie, H.J., Kooi, M.E., and **Jansen, J.F.**, 2005. Functional MRI reveals deactivation of prefrontal (Broca) function in epilepsy patients in topiramate therapy. 57th Annual Meeting of the American Academy of Neurology, A219, Miami Beach, Florida, USA.
- [6] Westmijse, I.A., **Jansen, J.F.**, Reijs, R.P., de Krom, M.C., Hofman, P.A., Aldenkamp, A.P., Nicolay, K., and Backes, W.H., 2005. Quantitative analysis of T2 and diffusion weighted images in epilepsy patients with secondary generalized seizures. Proc Int Soc Mag Reson Med 13, 1377, Miami Beach, Florida, USA.
- [7] **Jansen, J.F.**, Backes, W.H., Lamberts, K.W., Reijs, R.P., de Krom, M.C., Hofman, P.A., Aldenkamp, A.P., Nicolay, K., and Kooi, M.E., 2005. Spectroscopic imaging reveals reduced NAA/Cr ratios in epilepsy patients with secondary generalized seizures. Proc Int Soc Mag Reson Med 13, 1208, Miami Beach, Florida, USA.
- [8] **Jansen, J.F.**, Aldenkamp, A.P., Majoie, H.J., Reijs, R.P., de Krom, M.C., Hofman, P.A., Kooi, M.E., Nicolay, K., and Backes, W.H., 2006. fMRI reveals declined prefrontal cortex activation in epilepsy patients on topiramate therapy. 7th European Congress on Epileptology, 48, Helsinki, Finland.
- [9] **Jansen, J.F.**, Aldenkamp, A.P., Majoie, H.J., Reijs, R.P., de Krom, M.C., Hofman, P.A., Kooi, M.E., Nicolay, K., and Backes, W.H., 2006. fMRI reveals declined prefrontal cortex activation in epilepsy patients on topiramate therapy. Proc Int Soc Mag Reson Med 14, 312, Seattle, Washington, USA.
- [10] **Jansen, J.F.**, Kooi, M.E., Aldenkamp, A.P., Majoie, H.J., Reijs, R.P., de Krom, M.C., Hofman, P.A., Nicolay, K., and Backes, W.H., 2006. ROC analysis based visualization of pathological brain regions in patients with epilepsy using multi-modal MR Imaging (DWI, T2 and CSI). Proc Int Soc Mag Reson Med 14, 3417, Seattle, USA.
- [11] **Jansen, J.F.**, Vlooswijk, M.C., de Baets, M.H., de Krom, M.C., Rieckmann, P., Backes, W.H., and Aldenkamp, A.P., 2007. Soluble telencephalin is a marker for frontotemporal dysfunction in epilepsy as revealed by fMRI. Proc Int Soc Mag Reson Med 15, 2231, Berlin, Germany.
- [12] **Jansen, J.F.**, Vlooswijk, M.C., Kooi, M.E., Aldenkamp, A.P., Majoie, H.J., Reijs, R.P., de Krom, M.C., Hofman, P.A., Nicolay, K., and Backes, W.H., 2007. Secondarily generalized seizures induce a functional reorganization of working memory, as demonstrated by fMRI. Proc Int Soc Mag Reson Med 15, 2232, Berlin, Germany.
- [13] **Jansen, J.F.**, Kooi, M.E., Kessels, A.G., Nicolay, K., and Backes, W.H., 2007. Reproducibility of quantitative cerebral T2 relaxometry, diffusion tensor imaging, and <sup>1</sup>H magnetic resonance spectroscopy at 3.0 Tesla. Proc Int Soc Mag Reson Med 15, 790, Berlin, Germany.
- [14] **Jansen, J.F.**, Kooi, M.E., Kessels, A.G., Nicolay, K., and Backes, W.H., 2007. Iron in basal ganglia causes weak reproducibility of T2-weighted images at 3.0 Tesla. Proc Int Soc Mag Reson Med 15, 2174, Berlin, Germany.
- [15] **Jansen, J.F.**, Lemmens, E.M., Hoogland, G., Schijns, O.E., Jennekens, W., Strijkers, G.J., Prompers, J.J., Habets, J.W., Kooi, M.E., Backes, W.H., and Nicolay, K., 2007. Prospective brain T2 relaxometry, diffusion tensor imaging, and spectroscopy in a rat model of early life febrile convulsions. Proc Int Soc Mag Reson Med 15, 2419, Berlin, Germany.
- [16] **Jansen, J.F.**, Lemmens, E.M., Hoogland, G., Schijns, O.E., Jennekens, W., Strijkers, G.J., Prompers, J.J., Habets, J.W., Kooi, M.E., Backes, W.H., and Nicolay, K., 2007. Prospective brain T2 relaxometry, diffusion tensor imaging, and spectroscopy in a rat model of early life febrile convulsions. 27th International Epilepsy Congress, Singapore.
- [17] Vlooswijk, M.C., **Jansen, J.F.**, Reijs, R.P., de Krom, M.C., Kooi, M.E., Majoie, H.M., Hofman, P.A., Backes, W.H., and Aldenkamp, A.P., 2007. Seizure related cognitive deterioration is associated with increased prefrontal fMRI activation. 27th International Epilepsy Congress, Singapore.



## Curriculum Vitae



Jacobus (Jaap) Franciscus Antonius Jansen was born on July 4th 1979 in Oirschot, The Netherlands. After graduating secondary school in 1997 at the Jacob Roelands Lyceum in Boxtel, he studied Chemistry at the Radboud University Nijmegen, where he obtained his M.Sc. degree in Chemistry in 2002. He did his major in Biophysical Chemistry at the Laboratory of Biophysical Chemistry of the Radboud University Nijmegen, under the supervision of Dr. G.W. Vuister and Prof. Dr. C.W. Hilbers on the study of the structure, mobility, and function of proteins using high resolution nuclear magnetic resonance (NMR) spectroscopy. His minor in Biomedical NMR was done at two institutes. In the department of Radiology, Radboud University Nijmegen Medical Centre, he was involved in the elucidation of murine muscle energy metabolism using phosphorous NMR spectroscopy, under the supervision of Prof. Dr. A. Heerschap. At the department of Radiology, School of Medicine, Johns Hopkins University, Baltimore, USA, he used NMR techniques to study stem cells, which was supervised by Dr. J.M. Hakumäki, Dr. J.W.M. Bulte, and Prof. Dr. P.C.M. van Zijl. In September 2002 he started his Ph.D. project in the group Biomedical NMR of the department of Biomedical Engineering of the Technical University of Eindhoven (TU/e) and at the department of Radiology at the Maastricht University Hospital (azM). This research project concerned quantitative MR techniques in epilepsy, and was under supervision of Prof. Dr. K. Nicolay (TU/e), Dr. W.H. Backes (azM), and Dr. M.E. Kooi (azM). Presently, he is appointed as a Postdoc within the epilepsy center Kempenhaeghe and the departments of Radiology and Neurology in the Maastricht University Hospital. Within the framework of the collaboration of these institutes he is currently working on the development and application of quantitative MR techniques in epilepsy research.



Statler: Boo! Boo! That was terrible!  
Waldorf: Yeah, it was awful! Boo!  
Statler: Worst thing I've ever seen!  
Waldorf: It was horrendous.  
Statler: I hated it!  
Waldorf: Well, it wasn't that bad.

Statler: Oh yeah?  
Waldorf: There were parts of it I liked.  
Statler: Yeah, I liked a lot of it.  
Waldorf: I thought it was great, actually.  
Statler: Yeah, it was terrific!  
Both: We really loved it!!! Hurray!  
More! More!